The University

of Liverpool

The Interfacial Fracture Toughness Characterisation of Sandwich Structures

This thesis is submitted in accordance with the requirements of the University of Liverpool for the degree of Doctor in Philosophy by:

J G A Ratcliffe

September 2001

Publications

Cantwell W.J., Scudamore R., Ratcliffe J. and Davies P., Interfacial Fracture in Sandwich Laminates, Composites Science and Technology, Vol.59, 1999, pp2079-2085.

Gower M.R.L., Sims G.D., Ratcliffe J. and Cantwell W.J., Development of Test Method for Determining the Skin-to-Core Bond Strength of Thick-Skinned Sandwich Constructions, Institute of Mechanical Engineers, UK, Paper C548/015/99, 1999, pp99-110.

Ratcliffe J. and Cantwell W.J., Journal of Materials Science Letters, A New Test Geometry for Characterising Skin-Core Adhesion in Thin-Skinned Sandwich Structures, Vol.19, 2000, pp1365-1367.

Ratcliffe J. and Cantwell W.J., The Centre Notch Flexure Sandwich Geometry for Characterising Skin-Core Adhesion in Thin-Skinned Sandwich Structures, Journal of Reinforced Plastics and Composites, Vol.20, 2001, pp945-970.

Ratcliffe J. and Cantwell W.J., Characterisation of Mixed-Mode Fracture in Sandwich Constructions, *in preparation.*

Acknowledgements

First and foremost I would like to acknowledge Professor W. J. Cantwell for his excellent guidance and supervision.

Additionally I wish to express my gratitude to Dr F.W. Noble for his advice on issues concerning fracture mechanics. My thanks are also due to the following: Rob Scudamore, Paul Grant, Tim Nixon, Daniel Morrice, Pierre Hymas, Dawn Devonald, Liverpool University Ski and Snowboard Club and all others without whom my time at Liverpool would not have been the same. Also, I would like to thank the technical staff Dave Whitehurst and Chris Jackson, my thanks for your continual assistance.
Thanks to Mum, Dad and big brother Simon, you guys are the best. Finally, my thanks to Mary, who has provided me with sufficient love and patience to last anyone a lifetime.

Abstract

The aim of this study was to characterise the interfacial fracture toughness of a wide range of sandwich structures, including those based on very thin face-sheets. However, existing face-sheet peel tests are not suited to testing thin-skinned sandwich structures. Consequently, a test configuration was designed during the preliminary stages of this research programme. Initially, specimen sizing tests were performed using the new test configuration, whereby specimens of various widths were tested. This confirmed that the fracture toughness data obtained following this new test were intrinsic properties of the sandwich specimen interface. Due to the geometry of the new test and the disparity in mechanical properties between the facings and the core of a sandwich structure, the test was thought likely to provide a mixed-mode form of loading at the crack-tip. Therefore, a detailed finite element analysis was conducted. The analyses showed that for crack propagation within a low-modulus core material, parallel to the face-sheet/core interface, the new test exhibits a Mode I dominated loading condition at the crack-tip. Further analyses were conducted to determine the effect of specimen crack length and crack location on the mixed-mode ratio. The findings from the analyses suggested that the mode ratio would not vary significantly over the crack length range suggested for the tests. The fracture tests were used to determine the interfacial fracture toughness of a range of sandwich systems. Furthermore, the effect of crosshead-displacement rate and temperature on the fracture toughness of a PVC foam-based system was identified. Finally, the J integral was used as a fracture criterion for specimens that exhibited a significant amount of yielding during a test.

Glossary of Terms and Acronyms

Term	Symbol	Units
Crack length extension factor	Δ	m
Critical strain energy release rate (Toughness)	G_c	J/m^2
Compliance	C	m/N
J-Integral	*J*	J/m^2
Mode I strain energy release rate	G_I	J/m^2
Mode II strain energy release rate	G_{II}	J/m^2
Poisson's Ratio	ν	-
Shear modulus	G	N/m^2
Shear strength	τ	N/m^2
Stored elastic strain energy	U	Nm
Tensile strength	σ	N/m^2
Thermal conductivity	K	W/m°C
Young's Modulus	E	N/m^2

Finite Element Analysis	FEA
Linear Elastic Fracture Mechanics	LEFM
Modified Virtual Crack Closure Technique	MVCCT
Multi-Point Constraint	MPC

Asymmetric Sandwich Peel Test	ASPT
Centre Notch Flexure Specimen	CNFS
End Notch Flexure Specimen	ENFS
Mixed-Mode Flexure Specimen	MMFS
Modified Three-Point Bend Specimen	MTPBS
Single Cantilever Sandwich Beam	SCSB
Three-Point Bend Specimen	TPBS

Contents

1. INTRODUCTION

1.1 The Sandwich Construction 1

1.2 Sandwich Structure Core Materials 2

1.2.1 Honeycomb Structures 3

1.2.2 Balsa Wood 7

1.2.3 Cellular Foams 7

1.2.4 Summary of Core Materials 11

1.3 Face-Sheet Materials 11

1.4 Face-Sheet/Core Adhesive Materials 14

1.5 Manufacturing Techniques 16

1.5.1 Sandwich Structure Fabrication 16

1.5.2 Techniques for Curing Sandwich Structures 17

1.6 Typical Applications of Sandwich Structures 21

1.6.1 Marine Applications 21

1.6.2 Aerospace Applications 22

1.6.3 Application to Ground-Based Transport 22

1.6.4 Sporting Equipment 23

1.7 Flexural Behaviour of Sandwich Beams 23

1.7.1 The Sandwich Effect 25

1.8 Failure Modes of Sandwich Structures 26

1.9 References 28

2. LITERATURE REVIEW

2.1 Introduction 30

2.2 Interfacial Debonding of Sandwich Structures In Service 31

2.3 Characterisation of the Fracture Behaviour of Sandwich Structures 33

2.3.1 Techniques for Simulating Face-Sheet/Core Crack Growth 33

2.3.2 Comparison of Face-Sheet/Core Fracture Test Configurations 44

2.3.3 Fracture Criterion for Non-Linear Plastic Crack Growth 46

2.3.4 Effect of Loading Rate on Fracture Toughness of Sandwich Panels and Their Constituent Materials 48

2.3.5 Effect of Temperature on Fracture Toughness of the Constituent MaterialsUsed in a Sandwich Structure 50

2.4 Determination of the Crack-Tip Loading Conditions in Mixed-Mode Fracture Specimens 52

2.4.1 Crack-Tip Loading Conditions in Composite Materials 52

2.4.2 Techniques for Determining Crack-Tip Loading Conditions 52

2.4.3 Determination of Crack-Tip Loading Conditions at the Face-Sheet/Core Interface in Sandwich Structures 53

2.5 Issues Requiring Study/Aims and Objectives 55

2.6 References 57

3. NUMERICAL PROCEDURE

3.1 Introduction 61

3.2 Sandwich Structures Modelled 62

3.3 Interfacial Fracture Test Specimens 64

3.4 Finite Element Analysis Procedure 66

3.4.1 Load Application 71

3.4.2 Model Rotation – Transfer of Coordinate System 72

3.5 Determination of Strain Energy Release Rates 73

3.5.1 Modified Virtual Crack Closure Integral 73

3.5.2 Global Energy Methods 74

3.5.3 Finite Element Analysis Verification 77

3.6 Parametric Studies 78

3.6.1 Effect of Face-Sheet Thickness on The Crack-Tip Mode Ratio of the Three Test Geometries 78

3.6.2 Effect of Crack Location on the Crack-Tip Mode Ratio of the Three Test Geometries 79

3.6.3 Sensitivity of the Crack-Tip Mode Ratio to the Mechanical Properties of the Core and Face-Sheet Materials 80

3.6.4 Summary of Finite Element Analysis 80

3.7 References 81

4. EXPERIMENTAL PROCEDURE

4.1 Introduction 84

4.2 Sandwich Structures Investigated During the Research Programme 85

4.2.1 Aerospace-Grade Sandwich Structures 86

4.2.2 Shipyard-Grade Sandwich Structures 87

4.3 Configurations for Characterising Crack Growth at the Face-Sheet/Core Interface of Sandwich Structures 91

4.3.1 Development of a Fracture Test for Face-Sheet/Core Debonding in Sandwich Structures with Thin Face-Sheets 91

4.3.2 Selection of Test Technique for Performing Fracture Tests on Sandwich Structures Based on Thin Facings 95

4.3.3 The Modified Three-Point Bend Sandwich Specimen 96

4.3.4 Data Reduction Methods 98

4.3.5 Specimen Reinforcement 102

4.3.6 Summary of Procedure for Conducting CNFS and MTPB Tests 104

4.4 Influence of Displacement Rate and Temperature on Interfacial Fracture Toughness 105

4.4.1 Effect of Crosshead-Displacement Rate 105

4.4.2 Effect of Temperature 105

4.5 *J* Integral Testing of Specimens Exhibiting Non-Linear Plastic Crack Growth 106

4.6 References 110

5. NUMERICAL RESULTS/DISCUSSION

5.1 Introduction 111

5.2 Model Verification 111

5.2.1 Optimisation of Finite Element Mesh 111

5.2.2 Comparison of Finite Element Models with Experiment 113

5.3 Effect of Specimen Crack Length on the Crack-Tip Loading Conditions in the CNFS, MTPB and SCSB Geometries 116

5.3.1 Effect of Crack Length on Crack-Tip Loading Conditions in CNFS Specimen 117

5.3.2 Effect of Crack Length on Crack-Tip Loading Conditions in MTPB Specimen 119

5.3.3 Effect of Crack Length on Crack-Tip Loading Conditions in SCSB Specimen 121

5.3.4 Comparison of Crack-Tip Loading Conditions Between the CNFS, MTPB and SCSB Geometries 122

5.3.5 Summary 124

5.4 Effect of Crack-Tip Location on the Mode Ration in the CNFS, MTPB and SCSB Geometries 124

5.4.1 Effect of Crack Location on the Mode Ratio in a CNFS Specimen 126

5.4.2 Effect of Crack Location on the Mode Ratio in a MTPB Specimen 127

5.4.3 Effect of Crack Location on the Mode Ratio in a SCSB Specimen 129

5.4.4 Summary 132

5.5 The Effect of Core and Face-Sheet Mechanical Properties on the Mode Ratio in the Three Specimen Geometries 133

5.5.1 The Effect of Core and Face-Sheet Properties on the Mode Ratio in a CNFS Specimen Containing a Core Crack 134

5.5.2 The Effect of Core and Face-Sheet Properties on the Mode Ratio in a CNFS Specimen Containing a Face-Sheet Crack 137

5.5.3 Summary 140

5.6 The Influence of Face-Sheet Thickness on the Crack Length Extension Factor 141

5.7 Summary 144

5.8 References 145

6. EXPERIMENTAL RESULTS/DISCUSSION

6.1 Introduction 146

6.2 Development of a New Test method for Characterising the Interfacial Fracture Toughness os Sandwich Structures With Thin Face-Sheets 146

6.2.1 Selection of Test Configuration 146

6.2.2 Comparison of Fracture Toughness Data Calculated Using Different Data Reduction Methods 149

6.2.3 Effect of Specimen Width on the Interfacial Fracture Toughness 150

6.2.4 Comparison of Interfacial Fracture Toughness Values Obtained Using the CNFS and MTPB Geometries 152

6.2.5 Summary of Test Development 155

6.3 CNFS Interfacial Fracture Toughness Tests – Sandwich Systems A to P 156

6.3.1 Load-Displacement Response 156

6.3.2 Variation of the CNFS Specimen Compliance with Crack Length 161

6.3.3 Interfacial Fracture Toughness of Structures A to F 166

6.3.4 Interfacial Fracture Toughness of Structures G to K 167

6.3.5 Interfacial Fracture Toughness of Structures L to P 172

6.3.6 Summary of the Interfacial Fracture Toughness Characteristics of Structures A to P 176

6.4 MTPB Interfacial Fracture Toughness Tests – Sandwich Systems A to F and L to R 178

6.4.1 Load-Displacement Response 179

6.4.2 Variation of Specimen Compliance with Crack Length 181

6.4.3 Interfacial Fracture Toughness of Structures A to F 185

6.4.4 Interfacial Fracture Toughness of Structures L to O 185

6.4.5 Interfacial Fracture Toughness of Structures P to R 188

6.4.6 Summary of the Interfacial Fracture Toughness Characteristics of Structures A to F and Structures L to R 189

6.5 Effect of Temperature and Crosshead-Displacement Rate on the Interfacial Fracture Toughness of PVC Foam-Based Systems 192

6.5.1 Effect of Crosshead-Displacement Rate on Interfacial Fracture Toughness 192

6.5.2 Effect of Temperature on Interfacial Fracture Toughness 194

6.6 *J* Integral Estimation 197

6.6.1 Equivalence of J_c to G_c 197

6.6.2 *J* Integral Estimation – CNFS Tests on Structure J 201

6.6.3 Summary of *J* Integral Testing 203

6.7 Summary of Experimental Findings 204

6.8 References 205

7. CONCLUSIONS

7.1 General Summary 207

7.2 Further Work 211

APPENDIX A 214

1. INTRODUCTION

1.1 The Sandwich Construction

The ASTM definition of a structural sandwich component is '*a construction comprising a combination of dissimilar simple or composite materials, assembled and intimately fixed in relation to each other so as to use the properties of each specific material to the best structural advantage for the whole assembly*' [1].

Thus, a sandwich structure consists of three main elements, as illustrated in Fig. 1.1.1. Typically, thin, stiff face-sheets are either adhesively-bonded or co-cured to both sides of a low-density core material. The primary role of the core material is to carry the majority of shear loading through the thickness of the sandwich panel and to stabilise the face-sheets, such that the intended distance between them is kept constant. The main function of the face-sheets is to provide bending and in-plane stiffness, in addition to carrying the axial, bending and in-plane shear loads applied to the panel [2].

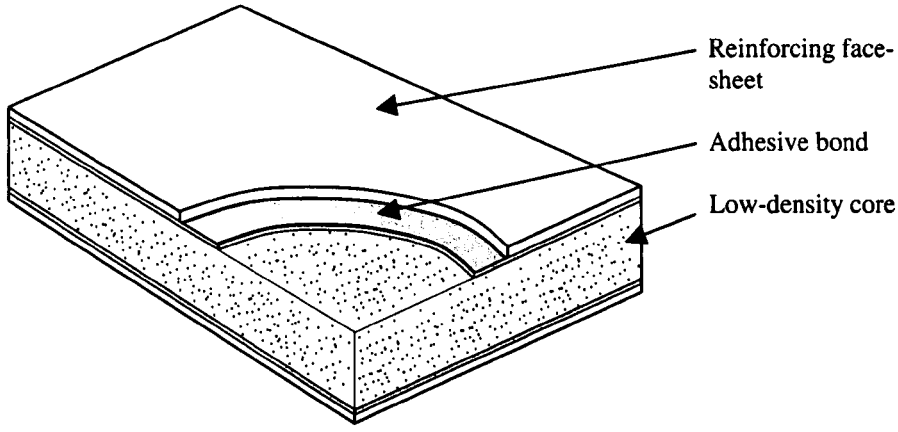

Figure 1.1.1 Sandwich panel construction, comprising of a low-density core reinforced by two thin, stiff face-sheets.

Essentially, the concept of a sandwich construction is to provide a panel with a high stiffness to weight ratio, by placing the stiff face-sheet materials at the maximum possible distance from the neutral axis of the panel. This is achieved by bonding the faces to both sides of the low-density core material, as illustrated in Fig. 1.1.1. Thus, an increase in core thickness effectively places the face-sheets further from the neutral axis of the panel, resulting in a higher stiffness to weight ratio. This is referred to as the 'sandwich-effect', and will be discussed further in Section 1.7.1.

1.2 Sandwich Structure Core Materials

The materials currently used in the core section of sandwich panels are numerous. Two main groups of core material are used in the marine and aerospace industries, namely

honeycomb-based structures, commonly used in the aerospace industry and polymeric foams and balsa woods, mainly employed in the marine industry. Each group of materials is available in a variety of forms, each of which will be discussed briefly in the following sections.

1.2.1 Honeycomb Structures

Owing to their low density and favourable acoustic properties, honeycomb-based structures have become commonly used in aircraft components ranging from fuselage sections and flooring, to noise-reducing panels in nacelle structures [3,4]. The most frequent type of honeycomb structure is the hexagonal arrangement illustrated in Fig. 1.2.1a. Other arrangements are available, such as the square (Fig. 1.2.1b), the over-expanded hexagonal (Fig. 1.2.1c) and the flex-core configuration (Fig. 1.2.1d). The over expanded and the flex core structures are frequently used when the honeycomb is required to adapt to the profile of a curved component, such as the torsion box used in a thrust reverser or in a cylindrical nacelle structure. Additionally, a notch is cut into one side of the cells to facilitate bleeding of any moisture that may be produced during the manufacturing process or operational service.

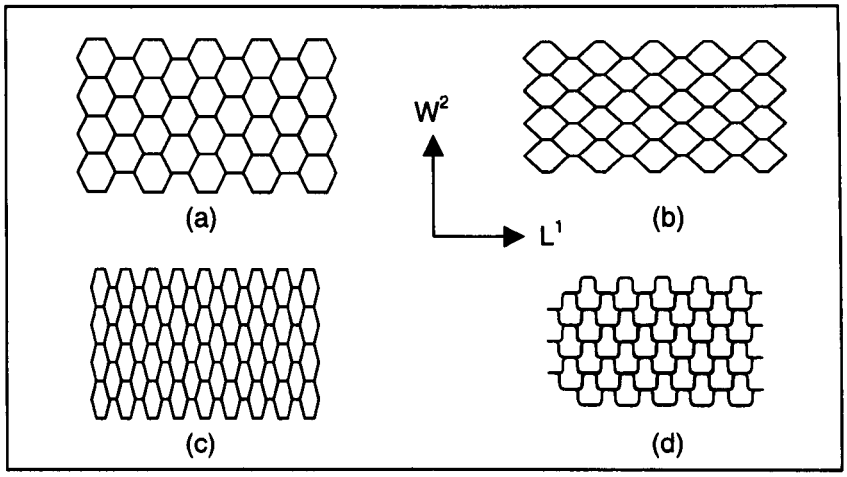

1 Length direction, 2 width direction

Figure 1.2.1 Examples of honeycomb structures used in sandwich construction. (a) hexagonal arrangement, (b) square honeycomb, (c) over-expanded hexagonal. (d) flex-core [5].

Typically, honeycomb structures can be manufactured using one of two different methods. The first, known as the corrugating process, is mainly used for the manufacture of high density honeycomb materials, where pre-corrugated sheets are bonded together and stacked into blocks. The second process begins by stacking thin plates of the honeycomb material containing an adhesive print, until a certain thickness is achieved. After the adhesive has been cured, the bonded plates are pulled in the width direction (Fig. 1.2.1) until the desired honeycomb shape is created. This process is known as expansion. The majority of honeycomb structures are employed in the aerospace industry with exception to the paper honeycomb, which is used in the manufacture of low cost housing. In addition, aluminium honeycomb is used within both the aerospace and marine industries. The following section gives a brief description of some of the commonly-used honeycomb materials.

- *Aluminium honeycomb.* These core structures are typically manufactured from 5052, 5056 and 2024-grade aluminium, to which a corrosion-resistant coating is applied in order to prevent attack from moisture and chemicals during operational service. The 5056-grade aluminium is a high strength version of the 5052-grade, both of which can be used up to temperatures of 180°C, the 2024-grade can be used at the higher temperature of 210°C.

- *Glass fibre reinforced (GFR) honeycomb.* GFR honeycomb structures are typically used with two types of matrix material. This first is a phenolic resin, which is intended for use at temperatures of up to 177°C, and the second is a polyimide resin, which can be used at temperatures up to 260°C.

- *Aramid fibre paper honeycomb (Nomex®).* This honeycomb structure is intended for use at temperatures of up to 177°C, and is available in the flex-core arrangement (Fig. 1.1.2d). This structure is suitable for highly curved aircraft components, where the honeycomb is required to adapt to the profile of complex structures.

A selection of the key properties of the honeycomb structures discussed above is presented in Table 1.2.1, where G^L, G^W τ^L and τ^W are the shear moduli and shear strength of the honeycomb structures in the length and width direction respectively (Fig. 1.2.1). K is the thermal conductivity of the honeycomb structures.

Honeycomb Material	Density (kg/m^3)	G^L (MPa)	G^W (MPa)	τ^L (MPa)	τ^W (MPa)	K (W/m °C)
Paper	23	33	10	0.24	0.09	0.066-0.114[1]
	56	141	38	1.30	0.48	0.066-0.114
Al (5025-grade)	32	186	99	0.83	0.48	3.9
	50	311	152	1.45	0.86	5.4
	71	469	207	2.28	1.48	5.4
	92	621	266	3.17	2.07	8.8
	112	787	320	4.07	2.59	14.4
	131	932	373	5.00	3.31	14.4
GFR Phenolic	65	90	45	2.14	1.10	0.066-0.114
	89	131	76	3.38	1.83	0.066-0.114
	113	207	97	4.76	2.55	0.066-0.114
	130	255	131	5.18	3.17	0.066-0.114
	194	331	193	6.80	4.66	0.066-0.114
GFR Polyimide	65	166	69	1.93	0.90	0.066-0.114
	73	228	76	2.21	1.04	0.066-0.114
	81	255	83	2.55	1.24	0.066-0.114
	97	311	104	3.17	1.59	0.066-0.114
	130	380	152	4.83	2.90	0.066-0.114
Nomex®	29	26	14	0.56	0.34	0.066-0.114
	48	42	28	1.20	0.68	0.066-0.114
	80	69	44	2.20	1.00	0.066-0.114

[1]Termal conductivity varies with cell size.

Table 1.2.1 Typical properties of some commonly-used honeycomb materials [5].

1.2.2 Balsa Wood

Load-bearing components in boat structures such as hulls, are frequently constructed from balsa wood-based sandwich panels. Owing to the fibrous nature of balsa, the mechanical properties are strongly orthotropic, with the highest strength and stiffness of the material coinciding with the direction of the fibres. However, the mechanical properties of this material are prone to degradation from seawater attack. In an attempt to combat this effect, balsa cores are usually fabricated from individual blocks, bonded together and positioned in the sandwich such that the fibre direction is perpendicular to the plane of the panel. This type of fabrication is known as 'end-grain' balsa.

1.2.3 Cellular Foams

The recent developments in cellular foams have enabled these systems to compete with end-grain balsa for use in structural sandwich components employed in the marine industry. The majority of foams are based on a closed cell structure, making them attractive for use in the marine and aerospace industries since they have good buoyancy characteristics, moisture resistance and radar transparency. Furthermore, the superior thermal properties of polymeric foams render them suitable for use in insulating components.

Although the strength to weight ratio of these materials is inferior to honeycomb structures, cellular foams are less expensive to manufacture. Furthermore, relative to honeycomb structures cellular foams are essentially solid on the scale of components such as boat hulls. This simplifies the bonding process of the face-sheets, reducing manufacturing times and easing the production of a uniform interfacial bond strength.

In general, foam materials are manufactured by mixing the appropriate polymer with a blowing agent, which either expands or vaporises when heated, resulting in the formation of a cellular foam structure. A number of polymers are used to manufacture foams, which are typically available with densities ranging from 15 to 400 kg/m^3.

- *Polyurethane foam (PUR)*

  This foam is manufactured by reacting iso-cyanates with polyol. Triclor-fluor-methane is used as the blowing agent, which is vaporised by the heat released during the exothermic reaction. The foam can be produced in a range of structures, from a soft, open cell-type to more rigid closed cell systems. The foam can also be made fire resistant by incorporating phosphorus additives, and is mainly used for insulating components due to the low thermal conductivity of this cellular system.

- *Polystyrene foam (PS)*

  This foam is manufactured by expansion or extrusion in closed moulds. In both cases, the blowing agent is mixed and expands at room temperature. The foam generally exhibits a closed cell structure, offering intermediate mechanical properties and is relatively inexpensive to produce. Again this foam is generally used for thermal insulating components.

- *Polyvinyl chloride foam (PVC)*

  This foam is available in a linear form and a crosslinked form. Linear PVC is more ductile, but has lower mechanical properties than the crosslinked version. However, both types offer superior mechanical properties compared to those offered by PUR and PS foams. Both types of PVC are non-flammable, however the linear version softens at elevated temperatures. These foams are the most widely used of all the types available, typically finding use in the aerospace, transport, thermal-insulation and marine industries. Furthermore, this material can be mixed with PUR resulting in a hybrid foam of the two systems.

- *Poly-methacryl-imide foam (PMI)*

  This foam is manufactured by expanding imide-modified polyacrylates, to yield a closed cell structure. PMI foam offers the most impressive mechanical properties of the foams available, although this system is expensive to manufacture. The foam is brittle, but the mechanical properties do not suffer significant degradation at elevated temperatures, making this foam suitable for use in the aerospace industry.

Table 1.2.2 presents a summary of a number of the key properties of the balsa and foam materials discussed, where the symbols have the same meaning to those in the previous table. In general, the foams are slightly anisotropic, with the in-plane properties being similar in all directions and the out of plane properties varying with direction. Furthermore, the data available for the Poisson's ratio of individual foams is not

completely reliable, but these values are known to be in the range of 0.2-0.4 for the materials discussed here [6].

Material	Density (kg/m^3)	G (MPa)	τ (MPa)	K (W/m °C)
Balsa	96	108	1.85	0.0509
	130	134	2.49	0.0588
	180	188	3.46	0.071
PUR foam	30	3	0.2	0.025
	40	4	0.25	0.025
PS foam	30	8	0.25	0.035
	60	20	0.6	0.035
Linear PVC foam	60	11	0.5	0.034
	90	21	1.0	0.037
	140	37	1.85	0.039
Crosslinked PVC foam	40	13	0.45	0.031
	60	22	0.8	0.031
	80	30	1.2	0.033
	100	38	1.6	0.035
	130	50	2.3	0.039
	200	75	3.5	0.048
PMI foam	52	19	0.8	-[1]
	75	29	1.3	-
	110	50	2.4	-
	205	150	5.0	-

[1]Data was not available.

Table 1.2.2 Typical properties of some commonly used solid core materials [7-11].

1.2.4 Summary of Core Materials

Honeycomb core materials offer a superior performance compared to that exhibited by cellular foam or balsa wood alternatives. This improved response is, however, offset by the increased cost involved in manufacturing sandwich laminates based on honeycomb cores, owing to the initial expense of the core materials themselves, and the time-consuming procedures necessary to ensure a good bond across the face-sheet/core interface. The mechanical properties of balsa wood are superior to those of the cellular foam alternatives, although the strength to weight ratio is lower than that offered by cellular foam structures. Finally, the foam materials discussed previously exhibit mechanical properties that are inferior to those offered by many honeycomb structures. However, foams are generally less expensive to manufacture and can be more readily integrated into sandwich structures.

1.3 Face-sheet Materials

As stated in Section 1.1, the main function of the face-sheets in a sandwich structure is to provide bending and in-plane stiffness, and carry the axial, bending and in-plane shear loading subjected to the panel. Therefore, the required properties of a face-sheet are:

- High flexural rigidity.
- High in-plane tensile strength.
- High resistance to impact loading.
- Superior corrosion and erosion resistance, including water resistance.

Traditionally, face-sheet materials were based on metals such as aluminium, titanium and steels, including mild carbon steel and corrosion-resistant stainless steel. The introduction of fibre reinforced composites has had a significant impact on sandwich panel technology. Fibre reinforced composites offer many advantages over their metallic counterparts, including high strength to weight and high stiffness to weight ratios, a superior resistance to corrosion and erosion and the ability to be formed into complex shapes. Through careful design, the properties of a composite can be tailored according to the loading conditions applied to the component. The most commonly used matrix materials are epoxies, polyesters and vinyl esters, phenolics and polyimides and common-place fibres include glass, carbon and aramid.

Furthermore, the architecture of the reinforcing fibres is available in many different designs. Traditional aerospace-grade composites were generally comprised from plastics reinforced with unidirectional carbon fibres, however, the increasing need to improve the impact performance (and thus damage tolerance) of these structures has led to the use of many types of woven fabrics, including three-dimensional composites, designed to improve the out-of-plane properties of the material [12, 13]. The amount of fibres used in the composite face-sheets can also be varied to achieve the desired stiffness and strength. It is usual to quote the amount of fibres used in terms of the fibre volume fraction, which is determined either by burning off or chemically dissolving the matrix material. The fibre volume fraction of a unidirectional composite is typically in the range of 55 to 70%, and that of a woven fibre composite is 30 to 60%.

Steel-based face-sheets offer a higher stiffness and strength than most fibre-reinforced composites, although in general they are significantly heavier than fibre reinforced

systems. Table 1.3.1 summarises the strength and modulus values of a range of commonly-used face-sheet materials, where E and σ denote Youngs modulus and tensile strength respectively.

Material	**Density (kg/m^3)**	**E_1 [1] (GPa)**	**E_2 [2] (GPa)**	**σ_1 (MPa)**	**σ_2 (MPa)**
Aluminium Alloys					
2024-T3	2700	70	-	270	-
5251-H24	2700	70	-	150	-
6061-T6	2700	70	-	240	-
Carbon Steels					
1006	7800	205	-	285	-
1017	7800	205	-	340	-
Unidirectional Continuous Fibre Composites (v_f = 60-70%)					
Carbon/Epoxy	1600	180	10	1500	40
Glass/Epoxy	1800	39	8	1060	30
Kevlar®/Epoxy	1300	76	6	1400	12
Woven Fabric Fibre Composites (v_f = 30-40%)					
Kevlar®/Polyester	1300	17.5	17.5	375	375
Glass/Polyester	1700	16	16	250	250
Glass Woven Roving/Polyester	1600	12	12	215	215
Randomly Orientated Fibre Composites (v_f = 15-25%)					
Chopped Strand Mat	1500	6.5	6.5	85	85

[1] The property in the main fibre direction of the composite face-sheets, [2] The property perpendicular to the main fibre direction.

Table 1.3.1 Typical properties of some commonly-used face-sheet materials [6,14].

1.4 Face-sheet/Core Adhesive Materials

A fundamental issue concerning adhesives used in sandwich constructions is the preparation of the face-sheet and core material prior to bonding, to ensure an optimum adhesion between these components. Face-sheet materials can be cleaned, either mechanically or through the use of a chemical pre-treatment. The aim of this procedure is to ensure that debris is removed from the surface to be bonded, particularly contaminants such as oil, grease and other such substances. Honeycomb structures and face-sheets are typically degreased using a solvent bath, the vapour from which quickly evaporates after removal from the bath. Dust and other solid debris can be removed using compressed air. Foam and balsa-based materials are prepared by mechanical machining, a process which involves cutting a layer from the surfaces to be bonded. Here, care is taken to ensure loose balsa grains or cellular lids are not retained on the bond surface after the cutting process.

The range of adhesive materials available are numerous, with many manufacturers of specialised core materials providing adhesives designed to achieve an optimum bond strength. For example, Hexcel composites provide an adhesive product, Redux®, designed specifically for bonding face-sheets to honeycomb core materials. This phenolic-based resin system is provided in film form, which is applied to the honeycomb and heated prior to curing. This product ensures a strong mechanical bond between the face-sheets and the honeycomb [14]. The most commonly used adhesives are as follows:

- *Epoxy Resins.* Epoxies cure at low temperatures, making them suitable for most core materials. They offer moderate mechanical properties and are available in a range of forms, such as pastes, powders and films.

- *Modified Epoxy Resins.* Here, epoxy resins are toughened by the addition of elastomeric materials, resulting in an improved peel toughness relative to the unmodified systems. Toughened epoxies are frequently used to bond honeycomb sandwich panels.

- *Phenolics.* These adhesives offer good mechanical properties, especially at high temperatures. However, owing to water being released during the curing process, these systems are limited to honeycomb sandwich structures, which allow moisture to be vented.

- *Polyurethanes.* These systems are widely used as a result of their good adhesion to most materials, their fire retardant properties and the wide range of cure times available.

Other common adhesive systems include urethane acrylates, polyester and vinyl ester resins. These systems are typically used for bonding face-sheets based on polyester resins, owing to their compatibility with polyesters. Polyester and vinyl ester resins are generally employed as adhesives when the matrix of the face-sheet material is based on the same system. Here, a wet lay-up technique is used, during which the adhesive is

applied to the core material, followed by an application of reinforcing fibres and matrix material. Pre-cured face-sheets can also be bonded to core materials, which have been treated by the adhesive system prior to bonding.

1.5 Manufacturing Techniques

1.5.1 Sandwich Structure Fabrication

Prior to the curing cycle necessary to form the bond between the face-sheets and the core material, the face-sheets are positioned on the core. In general, three different techniques are used:

- *Co-bonding*. In this technique, either a pre-cured composite or metallic face-sheet is bonded to the core material using an adhesive resin, which is then cured to create the face-sheet/core bond.

- *Co-curing*. This technique is used for sandwich structures based on composite face-sheets, in which the resin material is pre-impregnated with reinforcing fibres (commonly known as pre-preg composites). Here, the uncured pre-preg face-sheets are placed on to the core material and the cure cycle is used to simultaneously cure the face-sheets and the face-sheet/core bond adhesive.

- *Wet lay-up.* Here, alternating layers of resin and fibres are hand laid onto the core faces until the desired thickness of face-sheet is achieved, after which the sandwich structure is cured.

1.5.2 Techniques for Curing Sandwich Structures

In general there are three necessary conditions for the successful manufacture of a sandwich structure [2]; the application of pressure, the application of temperature and the procurement of tooling necessary to prevent movement of the curing sandwich and to ensure the component retains its desired shape. The most common methods used to manufacture sandwich structures are:

- *Heated Press.* This is the simplest method for applying simultaneous pressure and temperature to the curing sandwich component. Typically, the sandwich lay-up is positioned between two heated press-plates, as illustrated in Fig. 1.5.1. The required pressure is applied by displacing one of the press-plates toward the other and a temperature is applied to the plates. The good thermal conductivity of the metallic plates ensures heat transfer through to the sandwich component. This is the most cost-effective curing technique available, although it does suffer some limitations. Firstly, being conducted in an open environment, the curing temperature along the plane of the sandwich panel is likely to change from the periphery of the press through to the mid-section, resulting in a non-uniform face-sheet/core bond strength. Furthermore, this technique is suitable mainly for flat panels, due to the nature of the flat press-plates.

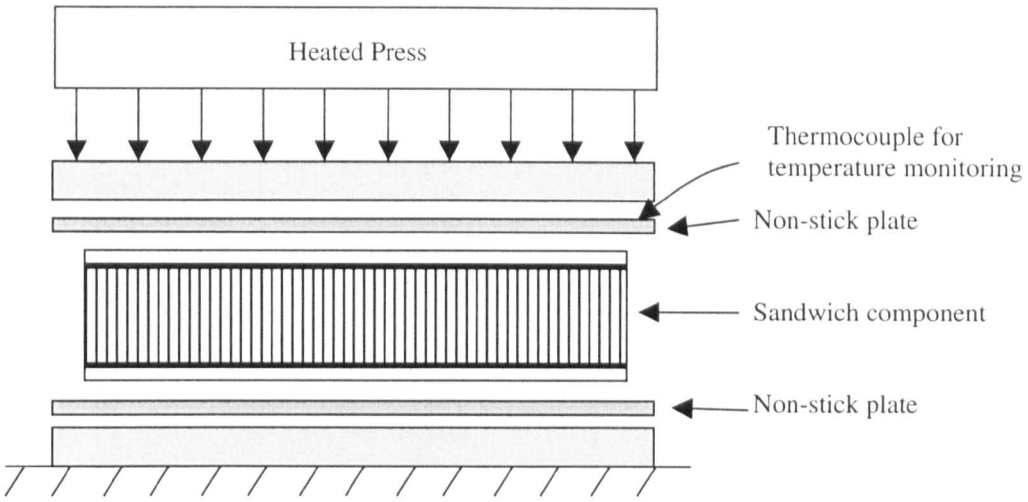

Figure 1.5.1 Heated press method for curing sandwich components.

- *Match Mould Processing.* This method is similar to the heated press technique. Here, the press-plates are machined to the desired profile of the sandwich component (Fig. 1.5.2) prior to the curing process, which is the same as that described above.

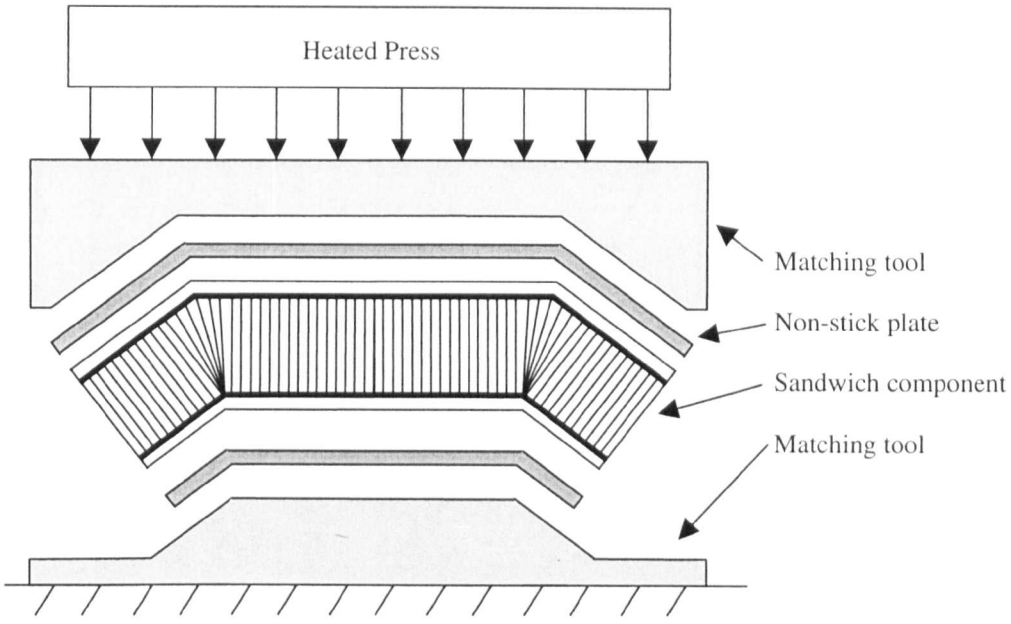

Figure 1.5.2 Match mould press method for curing sandwich components.

- *Vacuum Bag Curing*. Although this technique is the most complex of the three procedures discussed here, vacuum bagging can provide very good consolidation (pre-cure pressure application, ensuring sandwich component materials are in the correct position) for very complex shapes. This technique is favoured in the aerospace industry, where efficient curing of complicated, curved sandwich structures is required. In brief, the procedure begins by laying the sandwich panel on the tool surface. A sponge cloth is then draped over the component, which serves to distribute the pressure loading uniformly over the entire surface during the cure process (this is especially useful for components with complex profiles and sudden changes in shape, such as composite stringers and joggles). A

thermosetting film bag is then laid on the top of the component, which is sealed along the periphery of the tool. The air contained in the bag is then evacuated (via a valve positioned through the bag prior to sealing), resulting in a pressure loading by the bag onto the sandwich component. Once consolidated, the sandwich is cured in an autoclave for the required pressure, time and temperature, Fig. 1.5.3.

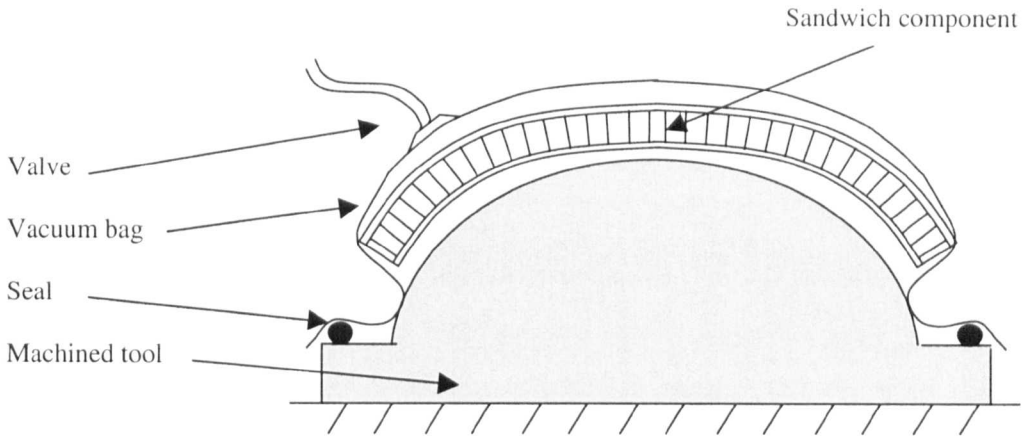

Figure 1.5.3 Vacuum bag technique for curing sandwich components. This illustration shows the bagged specimen prior to consolidation.

Irrespective of the method chosen to cure the sandwich component, the temperature, pressure and curing time will be dependent upon the face-sheet, core and adhesive resin materials. However, care has to be taken to ensure that the low-modulus core materials are not damaged by excessive pressures during the cure cycle.

1.6 Typical Applications of Sandwich Structures

Sandwich constructions are currently used in a wide range of industries, including the aerospace, marine, automotive, insulation and civil engineering sectors, in addition to increased use in the manufacture of sports equipment.

1.6.1 Marine Applications

Since the development of non-corrosive composite face-sheets and foam core materials that offer a superior resistance to moisture absorption, GFRP/foam-based sandwich structures have been used for hull sections in high performance ferries and military ships. Minesweepers designed for the Danish Navy [15] employed hull sections comprised of a rigid PVC foam core reinforced with GFRP face-sheets. These structures were cheap to manufacture and provided a good resistance to shock loading. Additionally, damage induced when the minesweeper ran aground resulted in face-sheet/core delamination. Although this affected the structural integrity of the panels, the remaining structure was able to be shipped to the repair docking area where the repairs were relatively simple.

High speed ferries, such as the Super Sea Cat with the requirement for weight optimisation are obvious applications for sandwich constructions. However, service conditions have shown that dynamic loading from waves slamming against the hull result in the face-sheets peeling from the core [16].

1.6.2 Aerospace Applications

Due to the requirement for weight reduction, sandwich constructions have been used in many aircraft components. The Boeing 747 fleet of aircraft employ sandwich structures in the flooring, side panels and the ceiling of the fuselage [3]. Furthermore, stiffened structures such as wing access panels use Nomex® honeycomb reinforced with carbon fibre reinforced plastic (CFRP) face-sheets [4].

The centre engine air inlet duct of the McDonnell Douglass MD 11 wide-body aircraft is made entirely from a CFRP/PMI-foam sandwich [17]. A thirty percent reduction in weight was achieved for this structure relative to the previous metallic design. Further, the cost of manufacturing the air inlet was reduced in addition to the operational costs (owing to the improved corrosion resistance of the sandwich materials). Sandwich constructions comprising Divinycell foam cores are used in the radome structure of the Boeing 737 aircraft [18]. These foams where chosen as a result of their superior moisture resistance, impact resistance and radar transparency of the foam materials.

1.6.3 Application to Ground-Based Transport

The outer structure of a locomotive commissioned by the by Swiss Federal Railways, was based entirely on GFRP/linear PVC foam sandwich constructions [19]. The benefits from the reduced weight saving and manufacturing costs were augmented by the ability to form aerodynamic geometries using the sandwich construction materials.

Continuing requirements for the design of lightweight buses has led to the use of aluminium/foam sandwich structures in the roof and intermediate floor of a number of vehicles [20]. The associated weight saving with the use of sandwich structures was

effective in reducing the operational costs of the bus, especially in countries with high taxes on the purchase of fossil fuels.

1.6.4 Sporting Equipment

Composite materials are used in the manufacture of a variety of sports equipment, including racquets, fishing rods, skiing boots and racing cars. In particular, recent developments in ski designs have resulted in a monoquoque structure based on a sandwich construction to provide the required flexural rigidity.

Recent concerns over the impact and compression performance of protective helmets resulted in a helmet based on a sandwich structure design [21]. Subsequent testing has shown that the overall compression performance of a helmet based on a CFRP/foam sandwich was superior to that of existing helmet designs [21].

1.7 Flexural Behaviour of Sandwich Beams

The experimental investigations conducted as part of this research will focus on the use of beam-type sandwich specimens. Therefore, an overview of the bending of sandwich beams is given below, followed by an example to illustrate the so-called sandwich effect.

Applying beam theory to sandwich beams enables the deflection of a sandwich beam under a specific loading condition to be determined. Consider a sandwich beam with the cross-section given in Fig. 1.7.1.

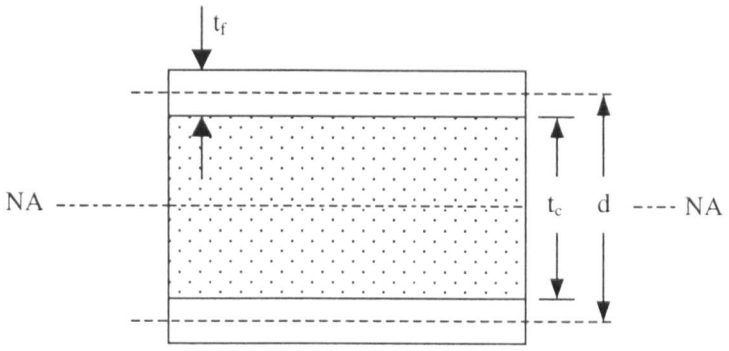

Figure 1.7.1 Cross-section of a sandwich beam.

Since the mechanical properties of the stiff face-sheets differ from the low-density core material, the moment of inertia of a sandwich beam with the cross-section illustrated in Fig. 1.7.1 cannot be expressed using only the cross-section dimensions. Instead, the sandwich beam is treated in three parts, expressed as the flexural stiffness, D. For the sandwich beam cross-section given in Fig. 1.7.1, the flexural stiffness is expressed as [1].

$$D = k\frac{P}{\delta} = \frac{E_f t_f^3 b}{6} + \frac{E_f t_f d^2 b}{2} + \frac{E_c t_c^3 b}{12} \tag{1.7.1}$$

Where P and δ are the applied load and resulting displacement respectively, E_f and E_c are the flexural moduli of the face-sheets and the core respectively, t_f and t_c are the thicknesses of the face-sheets and core respectively and b is the beam width.

The first term on the left hand side of Eqn.1.7.1 expresses the bending of the face-sheets about their respective mid-planes. The second term expresses the bending of the face-sheets about the neutral axis of the sandwich beam, and the third term expresses the bending of the core material about the neutral axis of the beam. For sandwich beams with facings that are thin in comparison to the core, the first term is negligible and the third term is negligible when the core flexural modulus is small in comparison to the

face-sheet flexural modulus. Thus, for a typical structural sandwich panel, the flexural rigidity of a sandwich beam is expressed by the second term on the left-hand side of Eqn.1.7.1.

1.7.1 The Sandwich Effect

Consider a beam comprised of two 6 mm thick perfectly-bonded beams. By placing a low-density core material between the beams, the stiffness of the resulting sandwich (calculated from Eqn.1.7.1) is significantly increased with relatively little increase in weight, as illustrated by Fig. 1.7.2. This example is based on an aluminium face-sheet (density = 2700 kg/m^3, Young's modulus = 70 GPa) and a foam core (density = 130 kg/m^3 and a shear modulus of 50 MPa).

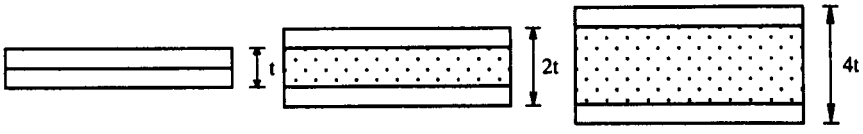

Relative Stiffness	1	15.50	75.52
Relative Weight	1	1.05	1.14
Stiffness to weight ratio	1	15	66

Figure 1.7.2 Relative increase in flexural stiffness with increasing core depth. Based on a sandwich structure with aluminium face-sheets (6mm thick) and a PVC foam core.

This example demonstrates that a significant increase in stiffness is gained for a relatively small weight penalty, where a 14% weight increase corresponds to a 750% increase in

flexural rigidity. It is this significant increase in stiffness for a relatively small increase in weight which makes sandwich laminates suitable for applications where weight is a primary design factor. Furthermore, the introduction of composite structures based on polymeric materials has resulted in the development of a wide range of sandwich constructions.

1.8 Failure Modes of Sandwich Structures

A schematic representation of the most common failure modes observed in sandwich constructions is given in Fig. 1.8.1. A bending moment applied to a panel can lead to face-sheet yielding, Fig. 1.8.1a, whereas a shear load can cause core failure, Fig. 1.8.1b. The presence of such damage will clearly reduce the ability of the sandwich to carry the subsequent loads. Combined compression and bending loads on a panel can cause face-sheet wrinkling, leading to face-sheet/core debonding and a reduction in the panel's flexural rigidity, Fig. 1.8.1c. Buckling of a sandwich panel is caused by excessive compression loading, Fig. 1.8.1d. Although this does not necessarily cause damage, it can result in the panel being distorted from its desired shape. This type of loading may also lead to dimpling of the face-sheets, Fig. 1.8.1e, in which case, the resulting compressive strength of the panel is severely reduced. Impact events, such as those associated with falling tools, can cause the core material local to the point of impact to be crushed. This may lead to face-sheet/core debonding and/or core splitting. Finally, face-

sheet debonding (Fig. 1.8.1g) is a recognised failure mode in sandwich structures, which can result from dynamic loading conditions such as wave slamming.

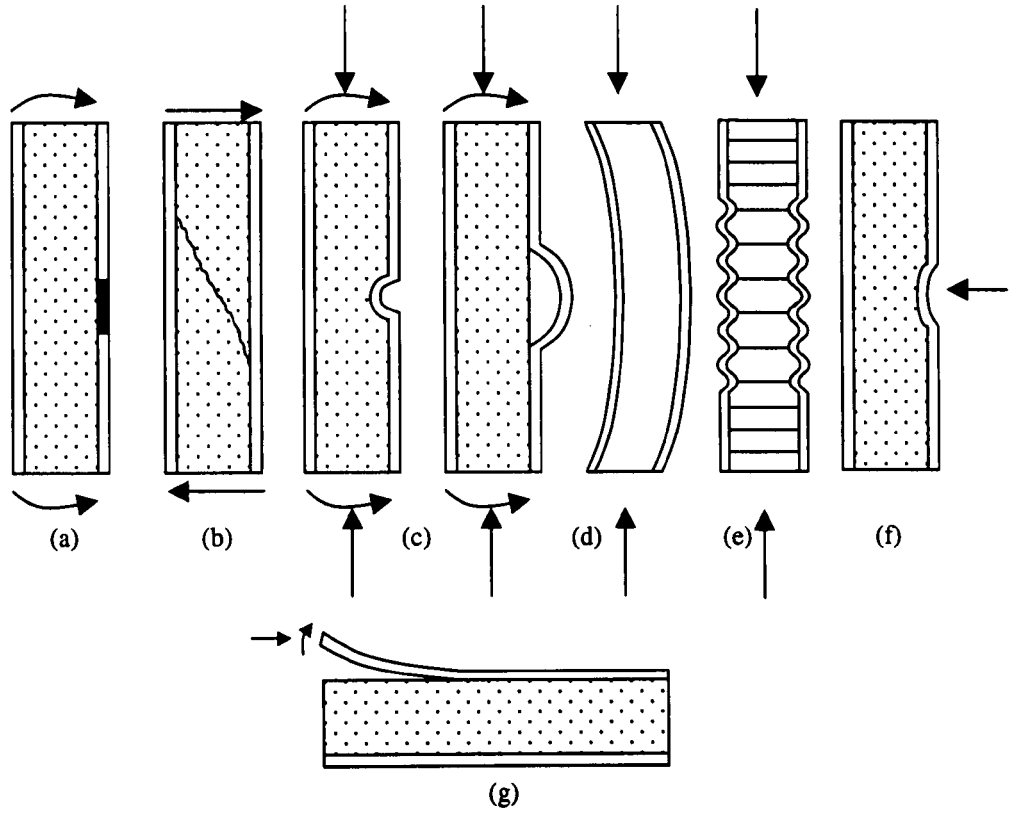

Figure 1.8.1 Typical failure modes observed in sandwich structures. (a) face-sheet yielding, (b) core shear failure, (c) face-sheet wrinkling, (d) sandwich buckling, (e) face-sheet dimpling, (f) local core crushing, (g) face-sheet/core debonding.

The majority of these failure modes have been analysed to provide design allowables for the structural engineers [6]. However, little attention has been paid to the debond resistance of the face-sheet/core interface, a failure mode which has been shown to be an important design consideration in the use of sandwich constructions [16,22-26]. In

particular, no attempt has been made to characterise the toughness of the face-sheet/core interface in sandwich structures comprised of very thin face-sheets.

1.9 References

[1]. Allen G.H., Analysis and Design of Structural Sandwich Panels, Permagon Press, 1969.

[2]. Marshall A., Handbook of Composites, Ed. Lubin G., Von Nostrand Reinhold, 1982, pp558-603.

[3]. Bitzer T.N., Proc. Second International Conference on Sandwich Construction, Florida, U.S.A., Vol.2, Engineering Materials Advisory Service,1992, pp681-693.

[4]. Watmough T., Hurel-Hispano UK., Private communication.

[5]. Hexcel Composites Data Sheet, HexWeb Honeycomb Attributes and Properties, Duxford, Cambridge.

[6]. Zenkert D., An Introduction to Sandwich Construction, Engineering Materials Advisory Service, 1995.

[7]. Jansson J.-F., Olsson K.-A. and Sorelius S.-E., Fibre reinforced Plastics 1, Swedish Tech Books, 1979.

[8]. Baltek Corporation Technical Data Sheets, 10 Fairway Court, P.O. Box 195, Northvale, NJ 07647, USA.

[9]. Airex, Technical Data Sheet, Airex Ltd, Speciality Foams, CH-5643 Sins, Switzerland.

[10]. Divinycell, Design Manual, Divinycell International AB, Box 201, S-312 22, Laholm, Sweden.

[11]. Rohacell and Rohacell WF, Technical Data Sheet, Rohm, Postfach 4242, Kirschenallee, D-6100 Darmstadt 1, Germany.

[12]. Bibo G.A. and Hogg P.J., Journal of Materials Science, Vol.31, 1996, pp1115-1137.

[13]. Cox B., Massabo R. and Rugg K.L., Proc. Sixth International Conference – Deformation and Fracture of Composites, Institute of Materials Science, 2001, pp3-12.

[14]. Hexcel Composites Data Sheet, HexWeb Honeycomb Sandwich Design Technology, Duxford, Cambridge.

[15]. Hellbratt S.-E. and Gullberg O., Proc. First International Conference on Sandwich Constructions, Engineering Materials Advisory Service, 1989, pp425-442.

[16]. Olsson K-A., and Lönnö., Proc. Second International Conference on Sandwich Constructions, Vol.2, Engineering Materials Advisory Service, 1992, pp807-823.

[17]. Seibert H., Proc. Third International Conference on Sandwich Construction, Vol.1, Engineering Materials Advisory Service, 1996, pp117-128.

[18]. Braziel K.R. and Cartwright C.L., Proc. Second International Conference on Sandwich Constructions, Engineering Materials Advisory Service, 1992, Vol.2, pp825-841.

[19]. Kalbermatten Th. de. and Reif G., Proc. Second International Conference on Sandwich Constructions, Engineering Materials Advisory Service, 1992, Vol.2, pp873-886.

[20]. Starlinger A. and Reif G., Third International Conference on Sandwich Construction, Engineering Materials Advisory Service, 1996, Vol.1, pp103-115.

[21]. Foreman A. and Curtis P., Proc. Sixth International Conference – Deformation and Fracture of Composites, Institute of Materials Science, 2001, pp225-232.

[22]. Lönnö A. and Hellbratt S-E., Proc. Third International Conference on Sandwich Construction, Engineering Materials Advisory Service, 1996, Vol.1, pp3-13.

[23]. Lönnö A. and Hakanson P., Proc. Third International Conference on Sandwich Construction, Engineering Materials Advisory Service, 1996, Vol.1, pp15-26.

[24]. Norwood L.S., Proc. First International Conference on Sandwich Constructions, Engineering Materials Advisory Service, 1989, pp279-290.

[25]. Brevik A.F., Proc. Third International Conference on Sandwich Construction, Engineering Materials Advisory Service, 1996, Vol.1, pp27-35.

[26]. Olsson K-A. and Lönnö A., Proc. Third International Conference on Marine Applications of Composite Materials, Institute of Marine Engineers, 1990, report No.90-4.

2. LITERATURE REVIEW

2.1 Introduction

As discussed briefly in the previous chapter, face-sheet/core debonding in sandwich laminates can result from severe loading conditions during service, which in turn can lead to a reduction in the flexural rigidity of the panel. This chapter discusses the different studies that have been conducted to investigate the face-sheet/core (interfacial) fracture toughness of sandwich structures.

Initially, evidence of face-sheet/core debonding during service and the type of loading conditions experienced by sandwich structures is presented. The test techniques that have been developed to simulate this type of failure are reviewed, to assess their suitability for determining the interfacial fracture toughness of sandwich structures. Investigations into environmental effects on the interfacial fracture toughness of sandwich structures are reviewed, including the influence of temperature and loading rate on fracture toughness. Finally, the numerical procedures undertaken to determine the crack-tip loading conditions in an interfacial fracture sandwich specimen are briefly reviewed.

2.2 Interfacial Debonding of Sandwich Structures In Service

The possible causes of debonding of the face-sheet/core interface in sandwich structures that are employed in the marine, space, and aerospace industries are well documented in the literature [1-13]. While discussing the use of carbon fibre reinforced plastic (CFRP)/PVC foam sandwich structures containing large amounts of carbon fibre for a high performance stealth surface vessel, Lönnö *et al* [1,2] highlighted a number of loading scenarios that must be considered during the design process. Here, wave-induced local loads, localised impact and point loads and shock loads from underwater explosions were highlighted as necessary considerations during design. All of these loading conditions have the ability to cause face-sheet/core delamination of the sandwich laminate. Norwood [3] investigated the use of tough resin systems to improve the peel resistance of a stiffener/hull interface, where the stiffener was based on a glass fibre reinforced polyester/PVC sandwich. The investigation was based on the observation that stiffener failure occurred as a consequence of peeling forces initiated on the inside of the stiffeners, leading to delamination between the face-sheet and the foam core. Brevik [4] discussed the loading conditions experienced by a GFRP/PVC wellhead protection structure (WPS) employed on an offshore oil rig. Following impact tests designed to simulate the shock loading and wave slamming conditions experienced by the operational structure, it was concluded that the bond between the facing and the core was an important design parameter. Olsson and Lönnö [5-6] concluded that large hydrostatic pressures applied to the hull comprised of a GFRP/PVC foam sandwich panel could cause the face-sheet covering the entire side of the hull to debond.

Another critical loading condition experienced by sandwich laminates in aerospace and space applications is rapid depressurisation. In the case of honeycomb sandwich laminates used for expendable rockets such as ARIAN 4, ATLAS, PROTON etc., the structures have to withstand significant vibrations while undergoing rapid depressurisation. Once again, such loading conditions can lead either to the initiation of face-sheet/core debonding or the propagation of existing delaminations at this interface. Furthermore, for sandwich structures used in re-usable spacecraft such as the space shuttle, re-pressurisation becomes an issue [7]. Additionally, structures employed for space applications will also have to withstand extremes of radiation and temperature, with the later in the range of -185°C to 121°C [8]. Bitzer [9] stated that the fuselage of aircraft such as the Boeing 747 contain a number of Nomex® honeycomb sandwich structures, such as flooring, side panels and ceiling. Abrate [10] stated that rapid depressurisation in structures such as an aircraft fuselage may lead to face-sheet/core debonding of the sandwich structure. Smidt [11] observed face-sheet/core debonding whilst determining design criteria for curved GFRP/PVC foam sandwich structures. Here, an opening bending moment was applied to a curved beam type panel, resulting in interfacial debonding.

Thus far, the discussion has focused on the causes of face-sheet/core delamination in sandwich structures. It is important to note that in the marine industry, face-sheet/core delamination may be a more desirable mode of failure than crushing or fracture within the core material [12]. This is because the reinforcing faces can be more easily replaced than the entire sandwich laminate [13]. The implications of this are twofold; firstly the repair time is short and therefore more cost-effective if only face-sheet/core delamination

has occurred. Furthermore, it is less expensive to replace the face-sheets than the entire sandwich structure.

In summary, the literature highlights the significant use of sandwich structures within the marine, aerospace and space industries. In addition, face-sheet/core debonding has been recognised as a common failure mode in these structures. In response to this, a number of techniques have been developed to characterise the face-sheet/core bond toughness of these sandwich structures and these are reviewed in the following section.

2.3 Characterisation of the Fracture Behaviour of Sandwich Structures

2.3.1 Techniques for Simulating Face-sheet/core Crack Growth

In light of the fact the that loading conditions experienced during the operational service of sandwich components may lead to debonding of the face-sheet/core interface, a number of workers have attempted to characterise the toughness of this interface. Originally, the traditional method employed by investigators was the ASTM B1781-93 climbing drum peel test (CDPT) [14]. Here, the facing is peeled from the core by wrapping it around a rotating cylinder as illustrated in Fig. 2.3.1. During the test, the load and crosshead displacement response of the specimen are obtained and this record is then used to calculate the peeling resistance of the bond between the facing and core material. However, the CDPT has several limitations, these being:

- To ensure the face-sheet is sufficiently flexible to rotate around the cylinder, only sandwich structures based on thin facings can be tested.
- The test rig is complex.
- The technique can only be used at low crosshead displacement rates. It is therefore incapable of simulating higher strain rates that are frequently observed in operational service, for example as those associated with rapid depressurisation or underwater shock loading.
- Since the torque resistance of the peeled face-sheet is used to characterise the interface, only qualitative measurements of the quality of the face-sheet/core can be made.
- The force required to roll the cylinder without a specimen must be calculated and a correction must be made to determine the peel resistance of the adhesive of the sandwich specimen.

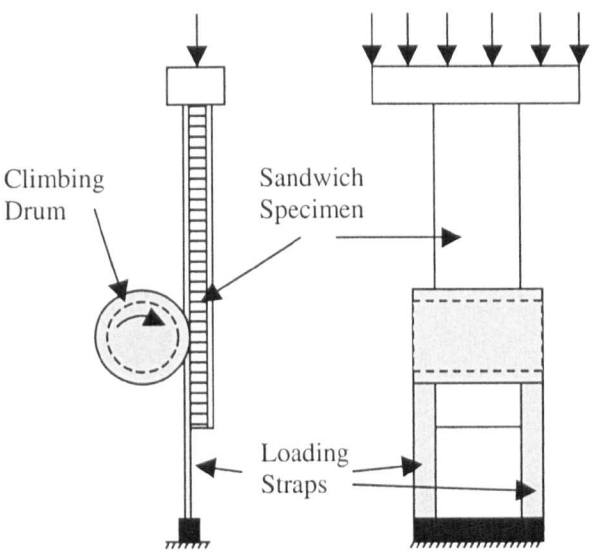

Figure 2.3.1 Schematic of the climbing drum peel test.

In light of these limitations, investigations into the characterisation of the face-sheet/core bond strength have concentrated on testing sandwich laminates with thick face-sheets. Additionally, the tests were engineered to enable a material property of the face-sheet/core interface to be used to characterise the bond quality. Consequently, flexural, beam-type fracture specimens evolved, the data from which were analysed using fracture mechanics principles. Thus, stress intensity factors and fracture toughness values were adopted to determine the face-sheet/core bond characteristics [16-25, 27-31].

Figs. 2.3.2 and 2.3.3 show a selection of the test geometries that have been developed for characterising the interfacial fracture toughness of sandwich structures. During all of the test procedures, a pre-crack is introduced at the face-sheet/core interface, either manually or during the manufacture of the specimen. The specimen is then loaded and the pre-crack is forced to propagate. A load versus displacement plot is recorded during the test and load and displacement values are recorded at known crack lengths. In most cases, fracture mechanics techniques are then used to calculate the critical strain energy release rate, G_c, known as the fracture toughness or stress intensity factors of the face-sheet/core interface.

During the 1960s, Houwink and Salomon [15] developed the bending peel test shown in Fig. 2.3.2a, to characterise the peel resistance of the face-sheet/core interface of a sandwich structure. Here, the peel resistance was monitored using a peel-load displacement record, from which a mean peel load was calculated. This technique has since been adapted to yield the wide range of interfacial fracture test methods that are currently available.

Carlsson *et al* [16, 17] developed the cracked sandwich beam (CSB) test to simulate interfacial crack propagation in sandwich structures, Fig. 2.3.2b. Here, the Mode II interfacial fracture toughness of a glass fibre reinforced polyester (GFRP)/balsa sandwich structure was determined using an experimental compliance calibration technique coupled with linear elastic fracture mechanics (LEFM). Additionally, the interfacial fracture toughness values were estimated following a theoretical approach involving shear deformation theory. Typical Mode II fracture toughness values for the GFRP/balsa interface were approximately 1000 J/m^2. Zenkert [18] later modified the CSB geometry, to determine the effect of interfacial debonds on the load-bearing capacity of PVC foam-based sandwich beams. Additionally, a four-point bend sandwich specimen (Fig. 2.3.2c) was used to determine the Mode II interfacial fracture toughness of sandwich panels manufactured from a range of foam core materials. Again an experimental compliance calibration technique coupled with LEFM was used to determine the fracture toughness values, which were reported to be in the range of 385 to 1920 J/m^2 for the sandwich systems tested. Additionally, it was found that the presence of interfacial debonds significantly reduced the load-bearing capacity of the sandwich beams [18].

During an investigation into the toughness of a foam-core sandwich system, Falk [19] employed two types of square panel to assess the effect of face-sheet/core debonds on the load-bearing capacity of the panels. These were based on the same basic geometry, with one type containing a circular debond at the panel centre, and the other containing semi-circular debonds at the edges, as illustrated in Fig. 2.3.2d. A pressure load was applied to the specimens and the failure load was recorded. It was concluded that the load-bearing capacity of the panels was more sensitive to the location of the debond than the debond

size itself. Falk [19] also conducted CSB tests on the sandwich structures following the same procedure as Carlsson *et al* [16, 17], to determine the interfacial fracture toughness of these structures. Fracture toughness values for sandwich beams based on four different foam-core materials were reported to be in the range of 115 to 223 J/m^2.

Papanicolaou and Bakos [20] adapted the double cantilever beam (DCB) [21, 22] to investigate the effect of surface treating the face-sheets on Mode I face-sheet/core fracture toughness of a glass fibre reinforced epoxy sandwich with aluminium facings, Fig. 2.3.2e. The corrected crack length technique coupled with LEFM was employed to determine the Mode I interfacial fracture toughness properties of the structures. Sandwich structures based on aluminium facings which had been abraded with an emery cloth prior to bonding to the core material, were reported to offer the highest fracture toughness. In a later study, Papanicolaou and Bakos [23] performed Mode I fracture tests on the same sandwich structures, with cracks positioned at the neutral axis of the sandwich beams, as shown in Fig. 2.3.2f. Fracture toughness values were found to be 900 J/m^2 for the sandwich structures based on a glass fibre reinforced epoxy core system.

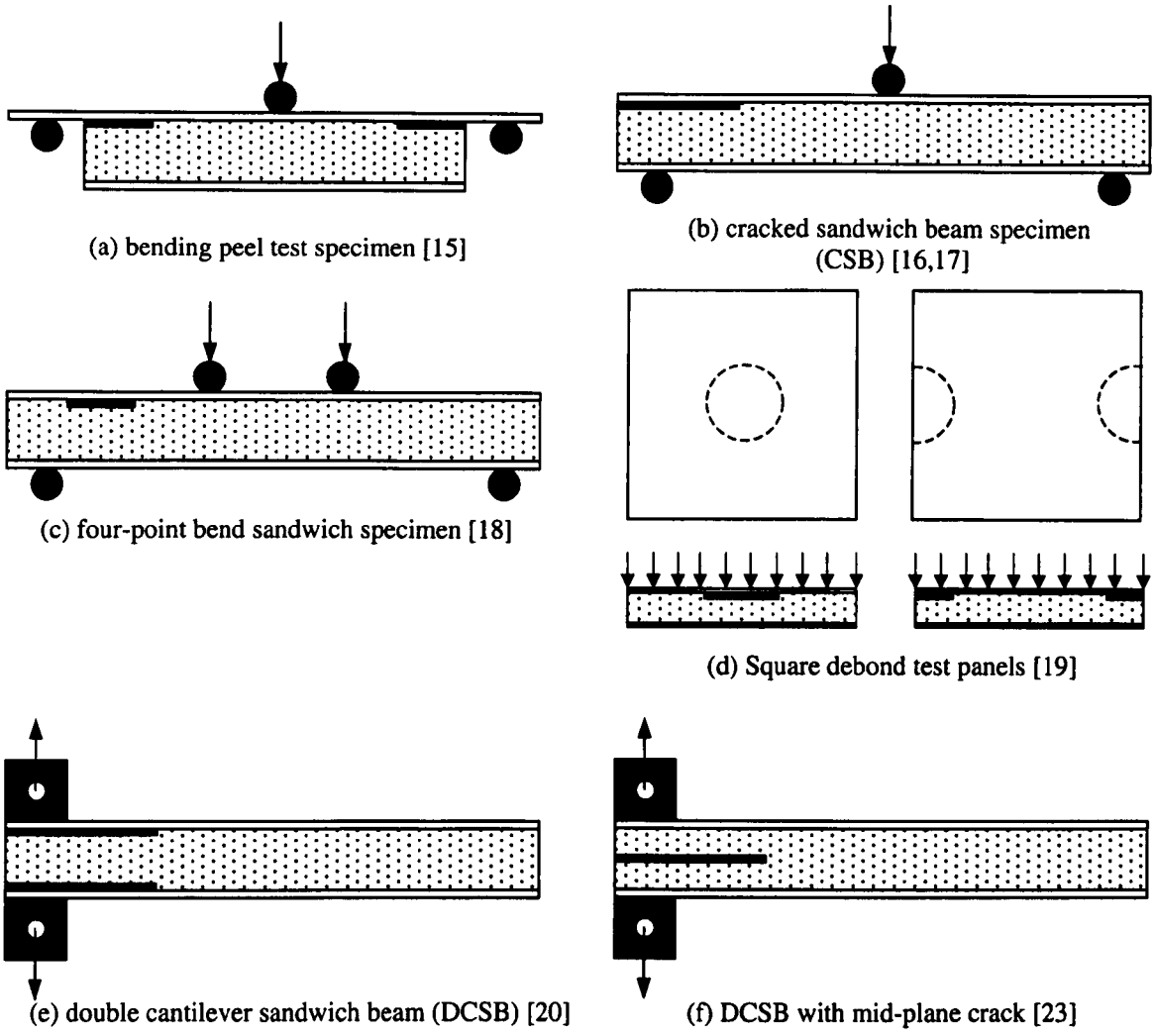

Figure 2.3.2 Face-sheet/core delamination test geometries (thick lines denote pre-cracks).

Prasad and Carlsson [24, 25] introduced a new Mode I fracture specimen to determine the interfacial fracture toughness of sandwich structures comprised of aluminium facings bonded to PVC and PMI foams, as shown in Fig. 2.3.3a. An experimental compliance calibration technique combined with LEFM was used to determine the interfacial fracture toughness values, these were reported to be in the range of 300 to 400 J/m^2. Furthermore,

by adapting the ASTM block shear test [26], a Mode II fracture test was developed for the sandwich structures as illustrated in Fig. 2.3.3b. However, instead of propagating a crack along the face-sheet/core interface, the adapted shear tests caused the pre-cracks to kink into the core material.

Echtermeyer and McGeorge [27] employed a fracture specimen similar to that developed by Prasad and Carlsson [24, 25]. Here, sandwich panels comprised of glass fibre/polyester face-sheets bonded to PVC and balsa core materials were tested. Due to specimen yielding, the areas method was used to compute the interfacial fracture toughness values of the two sandwich systems. The balsa-based sandwich panels were reported to offer a fracture toughness of approximately 1150 J/m^2.

While discussing face-sheet/core adhesion in sandwich laminates for marine applications, Cantwell and Davies [28] highlighted the limitations of the climbing drum peel test and proposed an alternative method to determine the interfacial fracture toughness. Here, GFRP/balsa and GFRP/PVC foam sandwich specimens were bonded at one end to a steel block, which in turn were bolted to a moveable carriage and loaded as shown in Fig. 2.3.3c. The interfacial fracture toughness was determined using a compliance calibration technique coupled with LEFM. The sandwich structures based on a linear PVC foam core material were found to offer the highest values of fracture toughness, those being in the range of 2770 J/m^2, whereas those offered by the balsa-based sandwich constructions varied from 900 to 1300 J/m^2. In a further study, Cantwell *et al* [29] proposed a modified version of the moveable carriage test method to investigate the influence of water immersion on the interfacial fracture behaviour of GFRP/balsa sandwich structures. In this case, the single cantilever sandwich beam specimen (SCSB) was developed, Fig.

2.3.3d. Here, interfacial fracture toughness values of the balsa-based structures investigated in an earlier study [28] were determined using an experimental compliance calibration technique and LEFM. From the investigation, it was shown that specimens which had been immersed in seawater offered higher interfacial fracture toughness than the untreated specimens [29].

Cantwell *et al* [30] later developed a modified three-point bend specimen (MTPB) as shown in Fig. 2.3.3e. Here, sandwich beam specimens similar to the SCSB were prepared and tested. Instead of clamping one end of the specimen, a three-point bend configuration was used to load the specimen, Fig. 2.3.3e. Again, an experimental compliance calibration procedure coupled with LEFM was employed to determine the interfacial fracture toughness of a number of balsa-based structures.

A mixed-mode specimen, the tilted sandwich debond specimen (TSD), designed to encourage crack propagation along the face-sheet/core interface was developed by Li and Carlsson [31], Fig. 2.3.3f. A range of sandwich panels consisting of glass/vinyl ester face-sheets bonded to PVC foam core materials with different densities were investigated. The fracture toughness values offered by the different sandwich systems were reported to range from 190 J/m^2 for the structure based on the lowest density core, to 1300 J/m^2 for the structure based on the highest density core material.

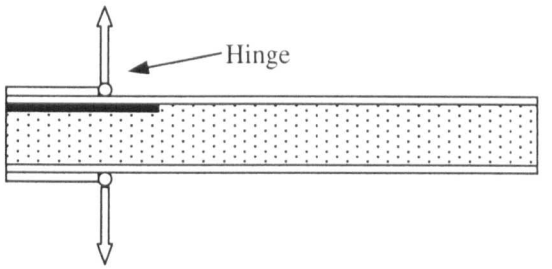

(a) modified double cantilever beam [24,25]

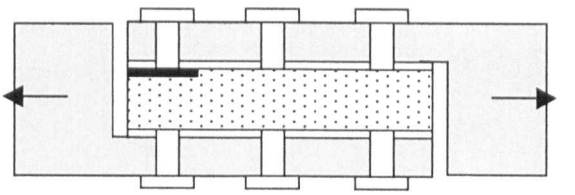

(b) shear sandwich fracture specimen [24,25]

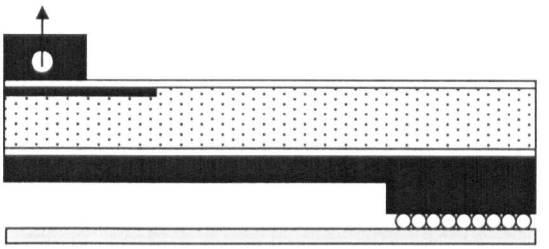

(c) movable carriage peel test [28]

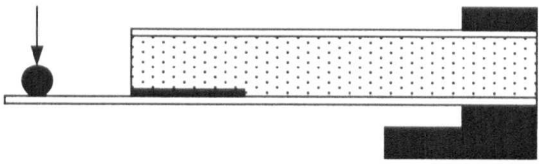

(d) single cantilever beam specimen (SCB) [29]

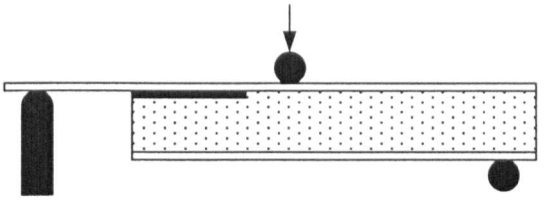

(e) modified three point bend specimen (MTPB) [30]

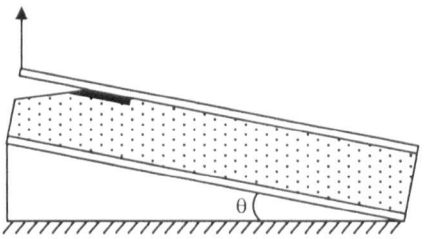

(f) Tilted debond sandwich specimen [31]

Figure 2.3.3 Face-sheet/core delamination test configurations (thick lines denote pre-cracks).

Table 2.3.1 summarises the interfacial fracture toughness data available from the literature. With values close to 3000 J/m^2, it is clear that the linear PVC foam-based sandwich structures offer the highest fracture toughness. This value is similar to that of composite materials containing through-thickness reinforcement [32]. However, this result should be viewed with caution as only one type of linear PVC foam structure is quoted here. The second highest interfacial fracture toughness values are offered by the balsa-based structures. Here, fibre bridging was reported to be present in many of the

samples [28-30]. Sandwich structures based on other foam materials were reported to offer interfacial fracture toughness values in the range of 115 to 1300 J/m^2, with the crosslinked PVC foams offering the lowest values. Here, the data suggest that an increase in core density for a given foam type will result in an increase in the interfacial fracture toughness [31]. Finally, in some cases interfacial crack growth was observed to occur within the core material, as well as at the face-sheet/core interface.

Reference	Materials	Crack location	Fracture Toughness G_c	Crosshead Displacement rate	Mode
	Face-sheet/core		J/m2	mm/min	
[16-17]	GFRP/Balsa	Interface	1070 (127)[5]	1.25	II
[18]	Al/H60	Interface	385	2	II
[18]	Al/H100	Interface	665	2	II
[18]	GFRP/H100	Interface	789	2	II
[18]	Al/H200	Interface	1918	2	II
[19]	H60	Core	115	-	II
[19]	H100	Core	223	-	II
[19]	PMI51	Core	141	-	II
[19]	PMI71	Core	169	-	II
[20]	Al (2024-T6)/Epoxy	Interface	318 (7.4)	2	I
[20]	Al (2024-T6)/Epoxy	Interface	244 (29.2)	2	I
[20]	Al (2024-T6)/Epoxy	Interface	384 (18.1)	2	I
[23]	Al (2024-T6)/GFRE	Core	930	2	I
[24-25]	Al/R90.400	Interface	340 (40)	2	I
[24-25]	Al/C50.60	Interface	341 (40)	2	I
[27]	GFRP/H200	Core	937 (280)	1-10	I
[27]	GFRP/Balsa	Core, interface, facing	1146 (180)	1-10	I
[28]	GFRP/Balsa (A)[1]	Interface (F-B)[4]	1300 (250)	5	I/II
[28]	GFRP/Balsa (B)[2]	Interface (F-B)	1100 (200)	5	I/II
[28]	GFRP/Balsa (C)[3]	Interface	900 (170)	5	I/II
[28]	GFRE/Clinked PVC	Core	520 (10)	5	I/II
[28]	GFRE/Linear PVC	Core	2770	5	I/II
[29]	GFRP/Balsa (A)	Interface (F-B)	875 (100)	10	I/II
[29]	GFRP/Balsa (B)	Interface (F-B)	1065 (180)	10	I/II
[29]	GFRP/Balsa (C)	Interface	810 (90)	10	I/II
[30]	GFRP/Balsa (A)	Interface (F-B)	900 (400)	-	I/II
[30]	GFRP/Balsa (B)	Interface (F-B)	500 (200)	-	I/II
[30]	GFRP/Balsa (C)	Interface	1000 (150)	-	I/II
[31]	GFRP/H30	Core	190	-	I/II
[31]	GVE/R75	Core	300	-	I/II
[31]	GVE/H100	Core	380	-	I/II
[31]	GVE/H200	Core	1200	-	I/II
[31]	GVE/R400	Core	1300	-	I/II

[1] GFRP skins bonded directly to balsa core, [2] Balsa core sealed with polyester prior to bonding with skins, [3] Layer of chopped strand mat situated at the skin/core interface, [4] Fibre bridging accompanied crack growth [5]Numbers in parenthesis denote standard deviation.

Table 2.3.1 Summary of face-sheet/core fracture toughness data reported in the literature.

2.3.2 Comparison of Face-sheet/Core Fracture Test Configurations

In order to offer a clearer comparison of the methods discussed herein, Table 2.3.2 summarises a number of their key attributes and limitations. From the table, it is clear that a number of the test methods exhibit some limitations, for example an inability to test sandwich laminates with thin face-sheets or to simulate operational-service loading conditions such as high strain rates; the climbing drum peel test and the moveable carriage technique are good examples. Furthermore, many of the configurations require loading blocks to be bonded to the face-sheets (e.g. the DCB sandwich specimen, the modified DCB specimen and the moveable carriage peel test), therefore, adjustments have to be made to the fracture toughness calculations to accommodate for their consequent stiffening effects. However, a small number of simple test configurations have been designed, such as the single cantilever beam and the modified three-point bend test, although these tests are unsuitable for thin-skinned sandwich specimens Additionally, the majority of the specimens are based on flexural, beam-type configurations and the test data can be analysed using a fracture mechanics approach to yield stress intensity factors or fracture toughness.

Face-sheet/core fracture test	Testing of thin face-sheets	Testing of thick face-sheets	High load rate/impact		Number of crack fronts	Simple test rig
Climbing drum [14]	✔	✘	✘	No	1	✘
Bending peel test [15]	✘	✔	✔	Yes	2	✔
CSB specimen [16,17]	✘	✔	✔	Yes	1	✔
Four-point bend [18]	✘	✔	✔	Yes	2	✔
Square debond test[19]	✔	✔	✔	No	1 / 2	✘
DCB sandwich specimen [20]	✔	✔	✔	No	1	✘
DCB – mid plane crack [23]	✘	✔	✔	No	1	✘
Modified DCB specimen [24,25]	✔	✔	✔	No	1	✘
Shear sandwich fracture specimen [26]	✘	✔	✘	No	1	✘
Moveable carriage peel test [27]	✘	✔	✔	No	1	✘
SCB sandwich specimen [28]	✘	✔	✔	Yes	1	✔
Modified TPB specimen [29]	✘	✔	✔	Yes	1	✔
NSSB [30]	✔	✔	✔	No	1	✔
TDS [31]	✔	✔	✔	No	1	✔

Table 2.3.2. Comparison of Face-sheet/core Fracture test methods.

The review thus far has shown that fracture mechanics can be applied with some success to investigate face-sheet/core debonding in a range of sandwich structures. The investigations conducted on the balsa sandwich structures [27-30] have shown that consistent fracture toughness data can be obtained from the different test configurations.

However, few of the investigations considered in this section have considered honeycomb-based structures. This may be due to the existing certification techniques demanded by industrial monitoring bodies, particularly with respect to the aerospace industry. For example, the Joint Aviation Regulation body (JAR) stipulates the use of the climbing drum peel test to monitor the quality of bonding between CFRP and Nomex honeycomb laminates. However, attention is focusing on the use of composite materials as damage-tolerant structures in an attempt to improve their in-service performance. In order to achieve this, sandwich structures employed in the aerospace industry need to be characterised in a more quantitative fashion, using techniques similar to those discussed above.

2.3.3 Fracture Criterion for Non-linear Plastic Crack Growth

The techniques reviewed in Section 2.3.1 were designed such that LEFM could be used to analyse the data obtained from the fracture tests, to yield either the stress intensity factors or the fracture toughness of the face-sheet/core interface. However, other fracture criteria have been developed that enable the characterisation of the fracture toughness of materials which do not exhibit linear elastic crack propagation. Such a criterion was introduced by Begley and Landes [33]. Here, the J integral, introduced by Rice [34] was used as the fracture criterion for a range of steels that displayed non-linear elastic and elastic-plastic behaviour. The J integral is defined as the potential energy difference between two identical specimens loaded in the same manner but with crack lengths infinitesimally different in length, expressed as [34]:

$$J = -\frac{1}{B}\frac{dU}{da} \tag{2.3.1}$$

Where U is the potential energy stored in a cracked specimen, B is the specimen width, and a is the crack length.

A review of the literature has shown that the adaptation of the J integral as a fracture criterion for delaminated composite and sandwich specimens is uncommon. This is mainly due to that fact that fracture test methods are tailored to enable the delaminated specimens to behave in a linear elastic fashion. Since the J integral is equivalent to the critical strain energy release rate or driving force for crack growth under such circumstances, there has been no need for the use of this fracture criterion. However, a small number of investigations have been conducted, where the J integral was employed as a criterion for crack growth in composite materials.

Rhee and Ernst [35] used an elastic work factor to compute the energy release rate of cracked lap shear specimens of graphite epoxy laminates. Here, the J integral expressed for pure bending was generalised to account for the tensile component of the load in the cracked lap shear specimen, which enabled the J integral to be computed from one specimen. The specimens were assumed to behave in a linear elastic manner, thus the generalised expression for J which includes the 'elastic work factor', was equated to the energy release rate, G, enabling a computation of the fracture toughness.

During an investigation into the validity of the elastic work factor approach for estimating the energy release rate in a DCB fibre composite specimen, Rhee [36] found that the elastic work factor provided values of G_{Ic} comparable to the values obtained via an experimental compliance calibration method. Therefore energy release rates were obtained using a single DCB specimen.

Thus far, the *J* integral has been applied to fractured composite specimens to enable the energy release rate to be computed from a single specimen. However, no investigation has been undertaken to determine the suitability of the *J* integral technique for characterising the face-sheet/core fracture toughness of sandwich specimens that exhibit non-linear plastic crack propagation. In these cases, the tests are usually discarded or the fracture toughness values are estimated using an areas method technique.

2.3.4 Effect of Loading Rate on Fracture Toughness of Sandwich Panels and Their Constituent Materials

Many sandwich structures are based on polymeric foam materials that are likely to exhibit a high degree of rate sensitivity due to the viscoelastic properties of these materials, consequently investigations have been conducted to characterise the extent of the rate sensitivity.

During an investigation into the Mode I fracture toughness behaviour of a crosslinked PVC foam (Divinycell H200), Zenkert and Backlund [37] showed that the fracture toughness of the material decreases with increasing load rate, although the differences between the low and high rate data were not sufficient to draw any precise conclusions regarding the observed rate effect.

While presenting a novel inter-penetrating polymer network (IPN) foam system, based upon a PVC matrix, Danielsson and Olsson [38] conducted tensile tests at high loading rates and at static rates of load. Here, the energy absorption was found to decrease dramatically by more than 66%, between a displacement rate of 5 mm/min to 28000

mm/min. Though, a further increase in displacement rate (137000 mm/min) resulted in an energy absorption similar to that measured for the intermediate displacement rate.

Papanicolaou and Bakos [23] suggested that an increase of displacement rate on fracture specimens, which exhibit fibre bridging, will lead to an increase in fracture toughness. They argued that an increase in displacement rate leads to matrix splitting ahead of the crack-tip, leading to further fibre bridging, which acts to stiffen the specimen and therefore increase the fracture toughness.

Investigations by Cantwell *et al* [39] made the opposite observation to that discussed previously [23]. Here, observation of the fracture surfaces suggested that fibre bridging was reduced with increasing displacement rate, therefore leading to a reduction in fracture toughness. During an investigation into the rate sensitivity of the interfacial fracture toughness of GFRP/balsa sandwich laminates, Scudamore [40] found that the fibre bridging which accompanied the interfacial crack growth caused the interface toughness of this sandwich system to be insensitive to crosshead-displacement rate. Here, it was argued that the properties of the glass fibres which bridged the crack were the cause of the observed rate insensitivity.

This review has shown that the rate sensitivity of the face-sheet/core fracture toughness is dependent upon the properties of the material in which crack growth occurs. The fracture toughness of polymeric materials has been shown to be strain rate sensitive, although conflicting observations as to the nature of this effect have been reported when fibre bridging accompanies crack growth [23, 39, 40].

2.3.5 Effect of Temperature on Fracture Toughness of the Materials used in a Sandwich Structure

Although a number of workers have shown that the interlaminar properties of composite materials are highly sensitive to temperature, investigations concerning the influence of temperature on the face-sheet/core fracture toughness of sandwich laminates are sparse. Frassine *et al* [41] investigated the rate sensitivity of the interlaminar fracture behaviour of CF/PEEK over a temperature range of –50 to 130°C. Following the investigation, they concluded that the Mode I interlaminar fracture toughness, G_{Ic}, of this composite increased with increasing temperature. Moreover, Mode I tests on the neat PEEK resin system showed a positive relationship between G_{Ic} and temperature. In a similar study on the interlaminar fracture properties of a unidirectional carbon fibre/PEI composite, Frassine and Pavan [42] again observed an increase in Mode I fracture toughness for the PEI resin matrix as temperature increased

Bibo *et al* studied the impact performance of a T800H/toughened epoxy composite and a number of thermoplastic-matrix composites over a range of temperatures [43]. Here, they observed that the fracture toughness of a Radel 8300 composite decreases with temperature due to an increased level of plastic deformation within the material. A similar relationship between fracture toughness and temperature was observed for a thermosetting-matrix composite (Fibredux 924C). However, in this case, the reduction in fracture toughness at elevated temperatures was attributed to an increase in the size of the damage zone over a range of temperatures for a fixed amount of energy absorption, and not plastic deformation as may be expected for a thermosetting polymer.

The Mode I interlaminar fracture behaviour of toughened resin matrix composite systems has been shown to exhibit a positive relationship with temperature [44]. This was attributed to an increase in 'plastic flow' in the vicinity of the crack-tip at elevated temperatures [44].

Investigations into the influence of temperature on the Mode II interlaminar fracture behaviour composite systems have shown the opposite effect to that observed under Mode I loading conditions [45,46]. During an investigation into the effect of moisture and temperature on the fracture behaviour of unidirectional carbon fibre/epoxy composites, Russell and Street [45] observed a decrease in the Mode II fracture toughness at elevated temperatures, a similar observation to that made by Fischer and Arendts [46]. The causes of this effect are unclear, however Cantwell and Blyton [47] suggested that increased damage zones at higher temperatures lead to the decrease in the shear fracture toughness. Recently, Liechti and Marton used the modified double cantilever sandwich beam, Fig. 2.3.3a, to study the effect of temperature on the fracture toughness of a titanium honeycomb-based sandwich structure [48]. The interlaminar toughness was determined following tests conducted at 23°C and 180°C and was found to be marginally higher at room temperature. The mode of fracture was observed to change from interlaminar within the face-sheet material at low temperature, to interfacial fracture at the higher temperature, which may explain the reduction in toughness at the elevated temperature.

2.4 Determination of the Crack-Tip Loading Conditions in Mixed-Mode Fracture Specimens

2.4.1 Crack-Tip Loading Conditions in Composite Materials

Charalambides *et al* [49] demonstrated that crack propagation within orthotropic materials such as those used in sandwich constructions will not be purely of one load type, irrespective of the loading applied to the specimen. It was found that an opening form of loading of a crack situated in such a material will induce shear stresses at the crack-tip and vice versa [49]. In addition, Leach *et al* [50] and Bradley and Cohen [51], have shown the Mode I fracture toughness to be smaller than the Mode II fracture toughness of fibre reinforced composite materials. As a result of these findings, a number of investigations have been undertaken to determine the crack-tip loading conditions of fracture specimens based on composite materials, which are reviewed in the proceeding section.

2.4.2 Techniques for Determining Crack-tip Loading Conditions

During an investigation into a mixed-mode flexure (MMF) specimen used to determine the fracture toughness of fibre reinforced composite materials, Williams [52] proposed a beam theory analysis whereby the Mode I and Mode II strain energy release rate components of the total fracture toughness were calculated from the bending moments and shear forces in the upper and lower sections of the MMF specimen. However, the most common approaches developed for determining the crack-tip loading conditions in composite materials have focused on the use of finite element analysis (FEA). The first

of these techniques, known as the modified virtual crack closure technique (MVCCT) was developed by Rybicki and Kanninen [53]. The approach is based on Irwin's interpretation of crack growth [54], where the strain energy released by an infinitesimally small crack extension is equivalent to the work done required to close the crack to it's original length. The method enables the individual strain energy release rate components during mixed-mode crack extension to be determined by calculating the displacements and forces of the crack-tip nodes. However, Raju *et al* [55] found that the individual strain energy release rate components calculated using the MVCCT depend on the length of the crack-tip elements when the crack was situated at a bi-material interface. Therefore, the MVCCT method is limited to calculating the individual strain energy release rate components in cases where the crack is situated within a homogeneous material. Thus, Smelser [56] developed the crack-flank displacement technique, to enable the individual stress intensity factor components of a mixed-mode crack to be determined, for cracks situated at a bi-material interface. The technique employed an extension of the J integral to derive expressions for the stress intensity factors, which were calculated from the displacements of the crack-tip flank nodes.

2.4.3 Determination of Crack-Tip Loading Conditions at the Face-sheet/Core Interface in Sandwich Structures

In response to the findings from Charalambides *et al* [49] that crack growth in an orthotropic material or at a bi-material interface will be of a mixed mode, investigators have attempted to determine the crack-tip loading conditions in a number of the sandwich beam fracture specimens reviewed in Section 2.3.1. Zenkert [19,57] employed the crack-

flank displacement technique to determine the Mode I and Mode II stress intensity factors in the four-point bend sandwich specimen, Fig. 2.3.2c. Here, the cracks were assumed to be situated at the face-sheet/core interface, and the Mode I stress intensity factor was predicted to represent 10% of the total stress intensity factor.

Prasad and Carlsson [24,25] modelled the modified double cantilever beam sandwich specimen, Fig. 2.3.3a, and calculated the Mode I and II stress intensity factors using the crack-flank displacement method. Here, the face-sheet/core crack was assumed to lie either between the facing and the resin layer or between the resin layer and the core material. For the crack modelled at the facing/resin layer interface, the Mode I stress intensity factor was predicted to represent 80% of the total stress intensity factor. In the case of the crack positioned at the resin layer/core interface, the Mode II stress intensity factor was shown to be insignificant in magnitude. Furthermore, Prasad and Carlsson modelled the shear sandwich specimen, shown in Fig. 2.3.3b [24,25], with the crack situated at the same locations as in their previous analysis. For both crack locations, the Mode II stress intensity factor was shown to be 75% of the total stress intensity factor.

Cantwell *et al* conducted a brief analyse of the SCSB sandwich beam specimen shown in Fig. 2.3.3d, using the MVCCT technique [29]. Here, the strain energy release rate components, G_I and G_{II}, were calculated. The Mode II strain energy release rate was calculated to be 12% of the total strain energy release rate.

2.5 Issues Requiring Study/Aims and Objectives

This review of the literature has discussed the investigations conducted into the characterisation of face-sheet/core debonding in sandwich constructions. The current work concerning this mode of failure, in general, uses quite complex testing configurations, which inhibit their use to static rates of strain and makes studies such as the effect of temperature difficult to perform. These difficulties are augmented by the requirement in many cases to bond end blocks to the face-sheets, from which the peel loads are applied. Thus, the experimental data require analyses to adjust for the effect of such loading methods on the compliance of the fracture sandwich specimens. Furthermore, little attention has been paid to honeycomb sandwich structures, owing to existing manufacturing constraints regarding the qualification of the face-sheet/core interface in such structures. Currently, the climbing drum peel test is the only method available for this task, which is cumbersome and only provides qualitative information, regarding the quality of the face-sheet/core interface. This leads to a further gap in this area of research, being the face-sheet/core fracture toughness characterisation of sandwich laminates containing thin face-sheets, where the current test configurations available are unsuited to this task. In the case of the three and four-point bend configurations, a minimum flexural rigidity of the loaded face-sheet is required to enable the propagation of an interfacial crack. Attempts to grow face-sheet/core cracks with these configurations would simply lead to bending of the thin face-sheets. The modified DCB type configurations are thought likely to produce too much non-linear response

from the specimens, due to the high strains that would be developed in the thin face-sheets and the large displacements that would be involved.

Furthermore, the effects of loading rate and temperature on face-sheet/core fracture toughness have received little attention. These parametric studies are essential if the interfacial fracture behaviour is to be fully understood for typical service conditions.

Of the test configurations available which do utilise simple testing rigs (the single cantilever sandwich beam [29] and the modified three-point bend sandwich [30]), little efforts have been made to determine the crack-tip loading conditions provided by these tests.

Lastly, investigations into analysing data from sandwich fracture specimens, which do not adhere to LEFM are limited. Owing to the numerous combinations of sandwich structure materials available, it is likely that some structures will display non-linear behaviour from a sandwich fracture test. Clearly, the characterisation of the face-sheet/core interface of these structures would be useful.

In view of these considerations the aim here is to develop and optimise appropriate test geometries that can be used to characterise a wide range of sandwich structures, including those based on thin face-sheets. Additionally, the tests must be suitable for use over a range of loading rates and must be simple enough to be used in a temperature chamber. However, these sandwich structures have different face-sheet and core thicknesses, different properties and this is likely to affect the loading conditions at the crack-tip in a sandwich face-sheet peel test. Therefore, to fully understand the fracture behaviour of these sandwich structures and make appropriate comparisons, a detailed finite element

analysis must be conducted in which all the key parameters (geometry, mechanical properties, etc) are varied.

2.6 References

[1]. Lönnö A. and Hellbratt S-E., Proc. Third International Conference on Sandwich Construction, Vol.1, Engineering Materials Advisory Service, 1996, pp3-13.

[2]. Lönnö A. And Hakanson P., Proc. Third International Conference on Sandwich Construction, Vol.1, Engineering Materials Advisory Service, 1996, pp15-26.

[3]. Norwood L.S., Proc. First International Conference on Sandwich Constructions, Engineering Materials Advisory Service, 1989, pp279-290.

[4]. Brevik A.F., Proc. Third International Conference on Sandwich Construction, Vol.1, Engineering Materials Advisory Service, 1996, pp27-35.

[5]. Olsson K-A., and Lönnö A., Proc. Third International Conference on Marine Applications of Composite Materials, Institute of Marine Engineers, 1990, report No.90-4.

[6]. Olsson K-A., and Lönnö., Proc. Second International Conference on Sandwich Constructions, Vol.2, Engineering Materials Advisory Service, 1992, pp807-823.

[7]. Graham R., Proc. Third International Conference on Sandwich Construction, Vol.1, Engineering Materials Advisory Service, 1996, pp129-138.

[8]. Patrick R., Structural Adhesives, Treatise on Adehesion and Adhesives, Vol.4, Marcel Dekker Inc, 1976.

[9]. Bitzer T.N., Proc. Second International Conference on Sandwich Constructions, Vol.2, Engineering Materials Advisory Service, 1992, pp681-693.

[10]. Abrate S., Applied Mechanics Review, Vol.50, 1997, pp69-82.

[11]. Smidt S., Second International Conference on Sandwich Constructions, Vol.2, Engineering Materials Advisory Service, 1992, pp665-680.

[12]. Hellbratt S-E. and Gullberge O., Proc. First International Conference on Sandwich Constructions, Engineering Materials Advisory Service, 1989, pp425-442.

[13]. Hildebrand M., Proc. Third International Conference on Sandwich Construction, Vol.2, Engineering Materials Advisory Service, 1996, pp635-646.

[14]. ASTM Testing Standard D1781-93.

[15]. Houwink R. and Salomon G., Adhesion and Adhesives, Vol.2, 1965, pp512-513.

[16]. Carlsson L.A., Sendlein L.S. and Merry S.L., First International Conference on Sandwich Construction, Engineering Materials Advisory Service, 1989, pp571-575.

[17]. Carlsson L.A., Sendlein L.S. and Merry S.L., Journal of Composite Materials, Vol.25, 1991, pp101-116.

[18]. Zenkert D., Composite Structures, Vol.17, 1991, pp331-350.

[19]. Falk L., Proc. Second International Conference on Sandwich Construction, Florida, U.S.A., Vol.2, Engineering Materials Advisory Service, 1992, pp645-661.

[20]. Papanicolaou G.C. and Bakos D., Journal of Composite Materials, Vol.29, 1995, pp2295-2317.

[21]. O'Brien T.K. and Martin R.H., Journal of Composites Technology and Research, Vol.15, 1993, pp269-281.

[22]. ASTM Testing Standard D5528-94a, 1994.

[23]. Papanicolaou G.G. and Bakos D., Composites Part A, Vol.27A, 1996, pp165-173.

[24]. Prasad S., and Carlsson L.A., Engineering Fracture Mechanics, Vol.47, 1994, pp813-824.

[25]. Prasad S., and Carlsson L.A., Engineering Fracture Mechanics, Vol.47, 1994, pp825-841.

[26]. ASTM Testing Standard CC273-61, 1991.

[27]. Echtermeyer A.T., and McGeorge D., Proc. Fourth International Conference on Sandwich Construction, Engineering Materials Advisory Service, 1998, pp634-647.

[28]. Cantwell W.J., and Davies P., Proc. Applied Composite Materials, Vol.3, 1996, pp407-420.

[29]. Cantwell W.J., Broster G. and Davies P., Journal of Reinforced Plastics and Composites, Vol.15, 1996, pp1161-1172.

[30]. Cantwell W.J., Scudamore R.J., Davies P. and Ferrer J-B., Proc. Eleventh International Conference on Composite Materials, Woodhead, 1997, pp905-914.

[31]. Li X., and Carlsson L.A., Journal of Sandwich Structures and Materials, Vol.1, 1999, pp60-75.

[32]. Cartie D.D.R. and Partridge I.K., Proc. Sixth International Conference - Deformation and Fracture of Composites, Institute of Materials Science, 2001, pp49-55.

[33]. Begley J.A., Landes J.D., Proc. Symposium on Fracture Mechanics, Part II, ASTM STP 514, American Society for Testing and Materials, 1972, pp1-20.

[34]. Rice J.R., Journal of Applied Mechanics. Transactions of the ASME, Vol.35, 1968, pp379-386.

[35]. Rhee K.Y. and Ernst H.A., Journal of Composite Materials, Vol.26, 1992, pp2028-2044.

[36]. Rhee K.Y., Composite Structures, Vol.37, 1997, pp57-63.

[37]. Zenkert D. and Backlund J., Composites Science and Technology, Vol.34, 1989, pp225-242.

[38]. Danielsson M., and Olsson, K-A., Proc. Third International Conference on Sandwich Construction, Engineering Materials Advisory Service, Vol.2, 1995, pp535-544.

[39]. Cantwell W.J., Scudamore R., Ratcliffe J. and Davies P., Composites Science and Technology, Vol.59, 1999, pp2079-2085.

[40]. Scudamore R., Ph.D Thesis, University of Liverpool, UK, 2000.

[41]. Frassine R., Rink M. and Pavan A., Composites Science and Technology, Vol.56, 1996, pp1253-1276.

[42]. Frassine R. and Pavan A., Composites Science and Technology, Vol.54, 1995, pp193-212.

[43]. Bibo G., Leicy D., Hogg P.J. and Kemp M., Composites, Vol.25, 1994, pp414-424.

[44]. Davies P. and de Charentenay F.X., Proc. International Conference on Composite Materials, Vol.3, Woodhead, 1987, pp284-294.

[45]. Russell A.J. and Street K.N., ASTM STP 876, American Society for Testing and Materials, 1985, pp349-370.

[46]. Fischer C. and Arendts F.J., Proc. Ninth International Conference on Composite Materials, Vol.5, Woodhead, 1993, pp350-357.

[47]. Cantwell W.J. and Blyton M., Applied Mechanics Review, Vol.52, 1999, pp199-212.

[48] Liechti K.M. and Marton B., Submitted to experimental mechanics, 2001.

[49]. Charalambides, M., Kinloch, A.J., Wang, Y. and Wlliams, J.G., International Journal of Fracture, Vol.54, 1992, pp269-291.

[50]. Leach D.C., Curtis D.C. and Tamblin D.R., ASTM Symposium, Toughened Composites, 1985.

[51]. Bradley W.L. and Cohen R.N., ASTM STP 876, 1985, pp389-410.

[52]. Williams J.G., International Journal of Fracture, Vol.36, 1988, pp101-119.

[53]. Rybicki E.F. and Kanninen M.F., Engineering Fracture Mechanics, Vol.9, 1977, pp931-938.

[54]. Irwin G.R., Fracture, Handbuch der Phisik, Vol.6, 1958, p551.

[55]. Raju I.S., Crews J.H. and Aminpour M.A., Engineering Fracture Mechanics, Vol.30, 1988, pp383-396.

[56]. Smelser R.E. and Gurtin M.E., International Journal of Fracture, Vol.13, 1977, pp382-384.

[57]. Zenkert D., and Falk L., International Conference on Composite Materials, Vol.8, Woodhead, 1991, 3-H.

3. NUMERICAL PROCEDURE

3.1 Introduction

The two test geomtries which were used to determine the interfacial fracture toughness of the sandwich structures investigated during the course of this research programme, were analysed to determine the crack-tip loading conditions exhibited by these test configurations. Additionally, the single cantilever beam sandwich specimen (SCBS) was analysed to provide a comparison of the crack-tip loading conditions offered by this configuration with those encountered in the other two specimen geometries. The three test configurations were analysed by using finite element analysis (FEA). Each specimen was assumed to be under plane strain conditions, therefore the Mode I and Mode II components, G_I and G_{II}, of the total strain energy release rate, G_T, were calculated following these analyses. Verification of the analyses was achieved by comparing the strain energy release rates calculated from the analyses with those determined following actual tests. A number of parametric studies were conducted to predict the influence of specimen crack length, core Young's modulus and face-sheet stiffness on the ratio of G_I and G_{II} offered by each specimen type. Furthermore, the effect of positioning the crack either within the face-sheet material and the core on this mode ratio was investigated. In summary, the aims of the numerical analyses were as follows:

- To determine the ratio of G_I and G_{II} exhibited by each specimen type, in order to establish any differences in the mixed-mode ratio between the three test geometries.
- To determine the effect of crack length on G_I and G_{II} in the three specimen geometries.
- To investigate the influence of a crack positioned either within the face-sheet material or within the core on the mixed-mode ratio exhibited by the three specimens.
- To determine the effect of the face-sheet stiffness and core shear modulus on the ratio of G_I and G_{II} offered by the three specimen types. This will enable the designers to understand the crack-tip loading conditions in a wider range of sandwich structures.

3.2 Sandwich Structures Modelled

Three sandwich constructions were modelled during the course of this research programme. These systems (Structures P to R) were all based on the same crosslinked PVC foam core (density 75 kg/m^3) reinforced by woven fabric glass/polyester face-sheets. The face-sheets of Structures P to R were comprised of a different number of composite plies. Further details of the three sandwich structures are given in Section 4.2.2.

The mechanical properties assigned to Structures P to R are given in Table 3.2.1. Here, the orthotropic mechanical properties used to define the mechanical properties of the face-sheets of all the structures were estimated using the Laminator software code [1] which used laminate theory to calculate the orthogonal properties [2]. Figure 3.2.1 illustrates the coordinate system adopted to define the orientation of the mechanical properties used.

Material	**Properties**								
	E_x GPa	E_y GPa	E_z GPa	ν_{xz}	ν_{xy}	ν_{yz}	G_{xz} GPa	G_{xy} GPa	G_{yz} GPa
GFRP	11	11	4.14	0.26	0.26	0.24	4	4.14	4.14
Polyester	E = 2 GPa, ν = 0.3 (assumed isotropic) [3]								
Crosslinked PVC Foam	E = 0.05 GPa, ν = 0.3 (assumed isotropic) [4]								

Table 3.2.1 Mechanical properties of the constituent materials in Structures P to R.

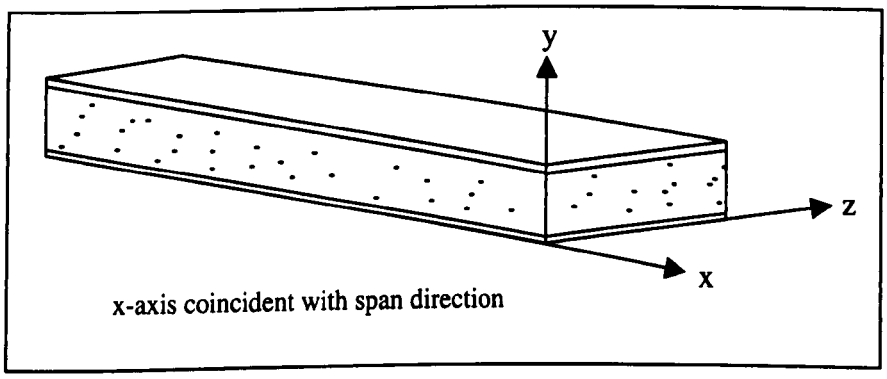

Figure 3.2.1 Coordinate system used in the FEA.

3.3 Interfacial Fracture Test Specimens

The three fracture test specimens analysed in this study were all designed to enable the face-sheet material to be peeled from the core using beam-type specimens. These geometries were the centre notch flexure sandwich specimen (CNFS) [5,6], the modified three-point bend sandwich specimen (MTPB) [7] and the single cantilever sandwich beam (SCSB) [8] details of which are given in Fig. 3.3.1. Further details of the procedures for conducting the CNFS and MTPB tests are given in Section 4.3.

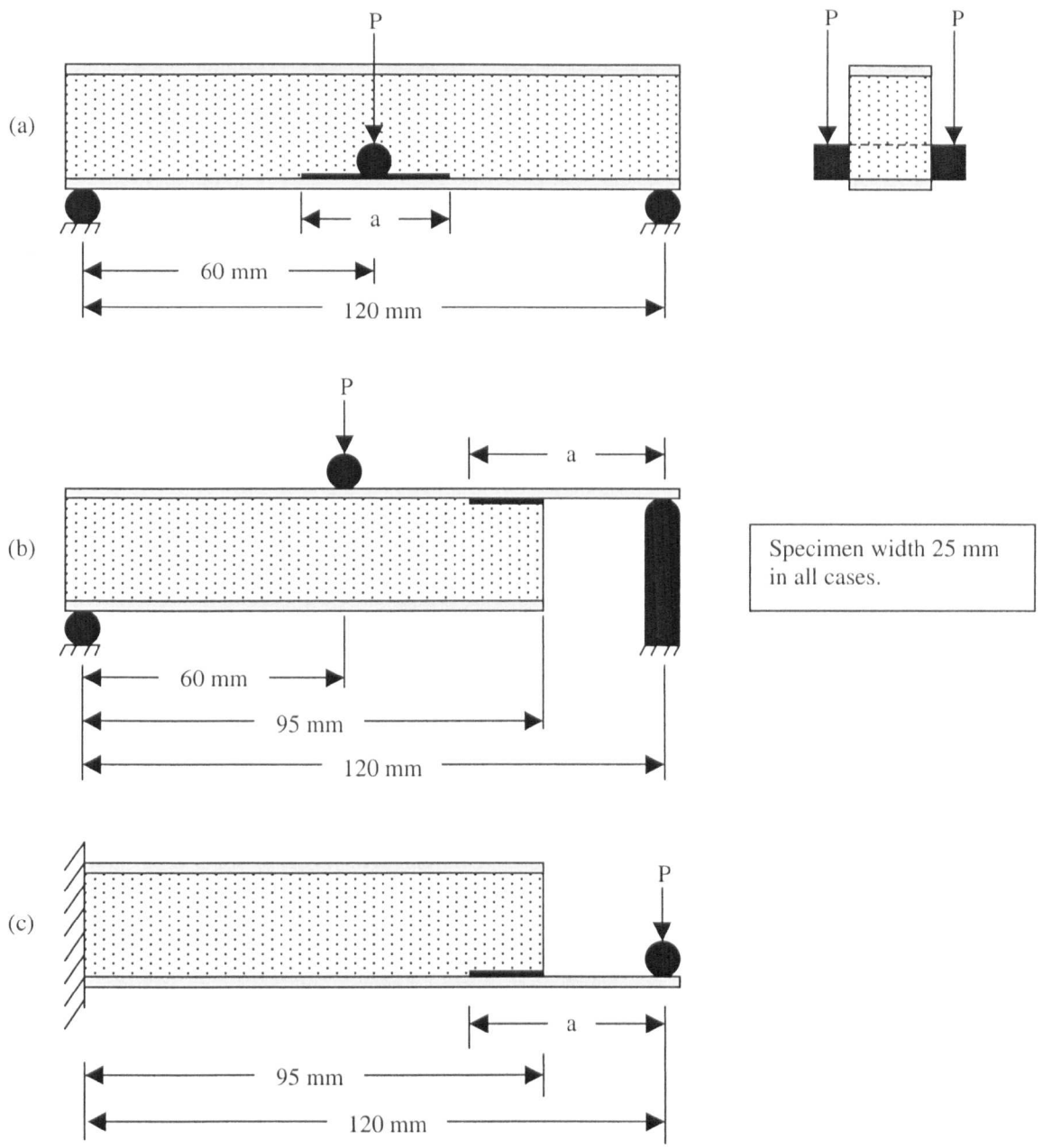

Figure 3.3.1 Geometry of the fracture specimens, (a) centre notch flexure sandwich specimen (CNFS), (b) modified three-point bend sandwich specimen (MTPB), (c) single cantilever sandwich beam (SCSB).

3.4 Finite Element Analysis Procedure

Initially, pre-processing of the finite element models was conducted manually, but later models were pre-processed using the NASTRAN® for Windows (Ver.4.6) commercial code [9]. Here, the information necessary to generate the element meshes was exported from NASTRAN® to ABAQUS®, via an exporting subroutine available with NASTRAN®. The commercial FEA code ABAQUS® (Ver.5.6) was used to perform the analysis and undertake subsequent post-processing [10].

Two-dimensional, plane strain models of all test specimens were constructed. Eight-noded isoparametric, linear strain elements (reduced integration 'CPE8R') [10] were used to represent the face-sheets and the core material. The resin layer forming the bond between the face-sheets and core was also modelled using the eight-noded elements. These elements were chosen for their relatively cost-effective accuracy (owing to a reduced number of integration points being used for each element), and more importantly the capability of the element to undergo shear, which was essential for modelling the low-density materials, such as PVC foams. This shear capability of the elements ensured that the model was capable of calculating the deflection of the core material due to shear effects. Following a method used by other workers [11,12], a fine array of 8-node isoparametric elements was used to accommodate the rapid change in the strain field approaching the crack-tip. This array was surrounded by a focusing mesh of self-similar elements, yielding a fine graduation of element length from the crack tip to the surrounding mesh, Fig. 3.4.1.

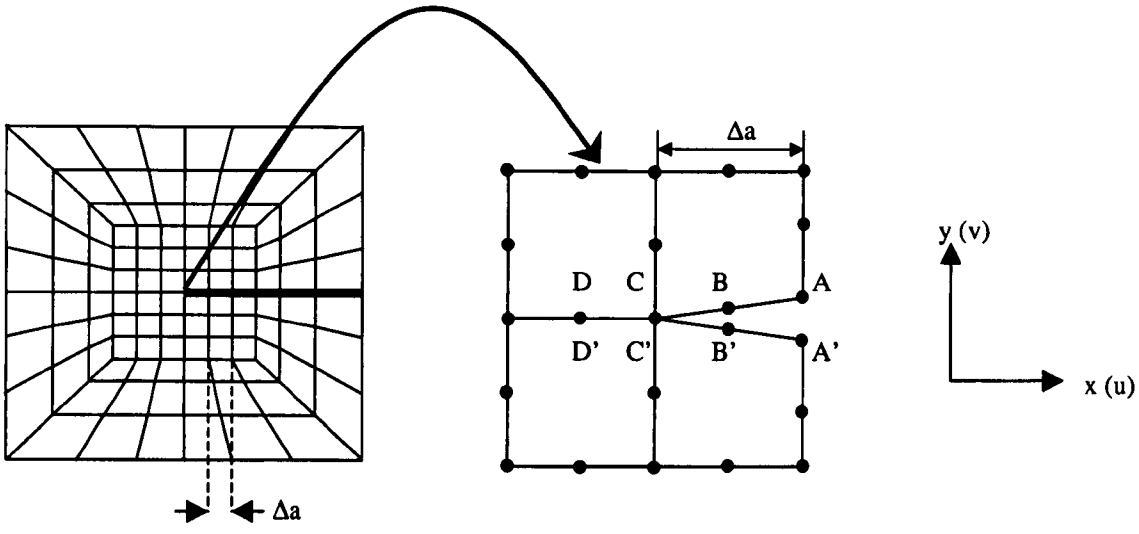

Figure 3.4.1 Self-focusing elements surrounding the crack-tip element mesh.

To improve the accuracy of the model solutions, the largest aspect ratio of an element (ratio of width to height) in the mesh geometries was five. Geometrically non-linear analyses were performed in all cases to ensure that an accurate representation of the square root singularity at the crack-tip was achieved [13].

Experimentally, crack propagation in the test specimens was observed to grow within the core material (Structures P, Q and R), therefore the cracks in the finite element models were positioned within the core. To determine the exact location of the crack-tip in these cases, the distance of the crack plane from the face-sheet/core interface was measured using a low power microscope. Other analyses were conducted in which the crack was positioned within the face-sheet material. In this case, following an approach used by Dattaguru *et al* [14] the crack was modelled in a matrix-rich region between the composite plies. The two crack locations represented in the finite element models are illustrated in Fig. 3.4.2.

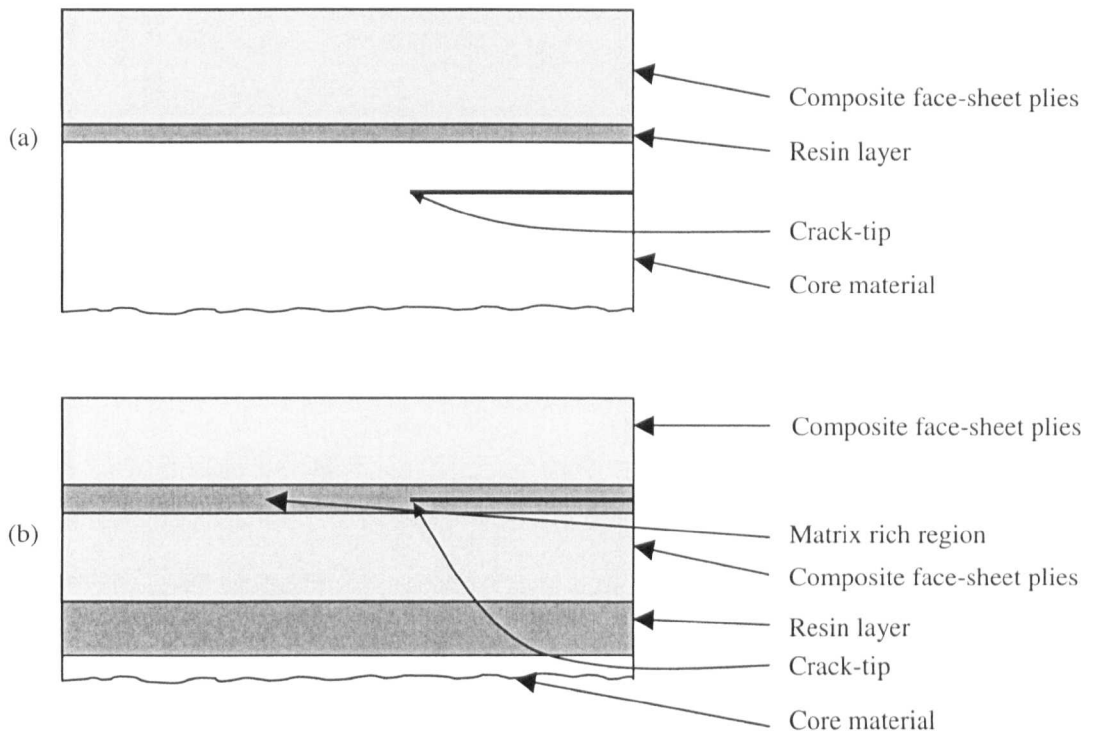

Figure 3.4.2 Crack-tip locations considered in the finite element models. (a) crack-tip located within the core material, (b) crack-tip located within the face-sheet.

In all cases, the loading pin and the other specimen supports were modelled using two-dimensional rigid 'R2D2' elements [13]. The diameter of the loading pin used in the CNFS test was 6 mm and the diameters of the loading and support pins used in the MTPB and SCSB tests were 10 mm. The pins were modelled by constructing circular segments of rigid elements. During the experimental tests, less than a quarter of the pin surfaces came into contact with the test specimen, therefore, a quadrant of each pin was modelled in the numerical analysis. A contact model [13] was employed to allow contact between the pins and the neighbouring elements in the three test specimens. This was

achieved by constructing a 'master' contact surface defined by that of the rigid pin elements, and a 'slave' contact surface lying on the surface of the 8-noded elements expected to make contact with the pins. This is illustrated in the case of the SCSB model in Fig. 3.4.3. The surface of the pins used in the experimental tests was smooth and, therefore, contact between the 'slave' and 'master' surfaces in the analyses was assumed to be frictionless. Very fine meshes were used for all the analyses conducted; a typical model comprised of approximately 7500 elements, 36000 nodes, and approximately 225000 degrees of freedom.

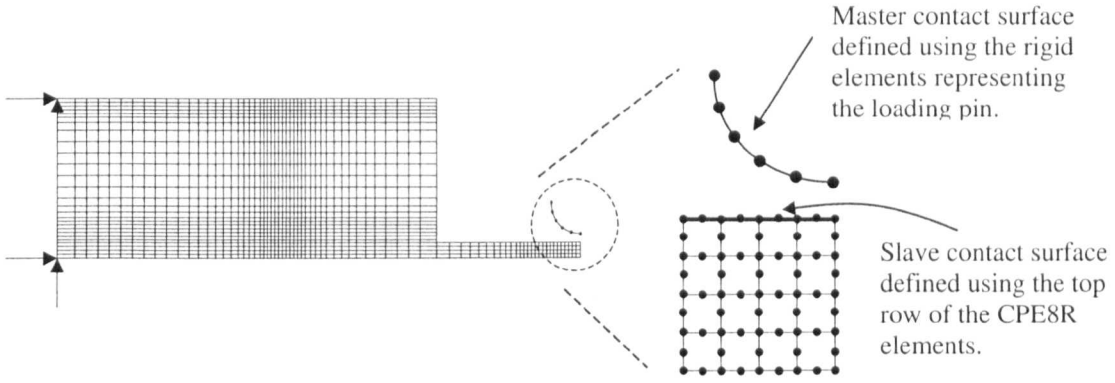

Figure 3.4.3 Illustration of the contact surfaces used to model contact between the rigid 'loading pin' elements and the face-sheet elements.

The symmetry of the CNFS test about the central loading point allowed half the specimen to be modelled. Here, the x-axis translational and z-axis rotational degrees of freedom of those nodes positioned along the axis of symmetry were constrained. The nodes of the loading pin rigid body and the support-pin rigid body were fully constrained, Fig. 3.4.4.

The clamped end of the SCSB specimens was modelled by applying fully fixed constraints to the nodes at the upper and lower corners of the end of the specimen. In addition, the support-pin nodes were fully constrained, Fig. 3.4.5.

The support-pin nodes were fully constrained when modelling the MTPB geometry. Additionally, one boundary node of the MTPB model was attached to one end of a two-node spring 'SPRNG12' element whilst the other node was fully constrained and positioned away from the model, Fig. 3.4.6. A small stiffness was assigned to the spring in order to prevent numerical difficulties caused by rigid body motion of the mesh. The density of the meshes illustrated in Figs. 3.4.4 to 3.4.6 have been reduced to aid the illustration.

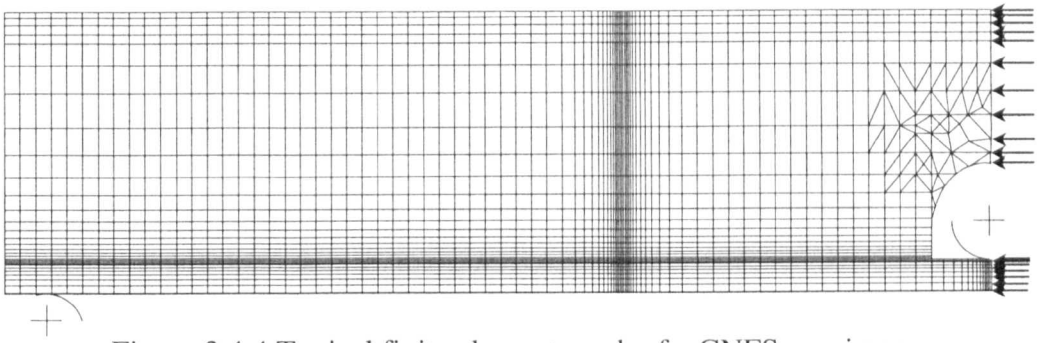

Figure 3.4.4 Typical finite element mesh of a CNFS specimen.

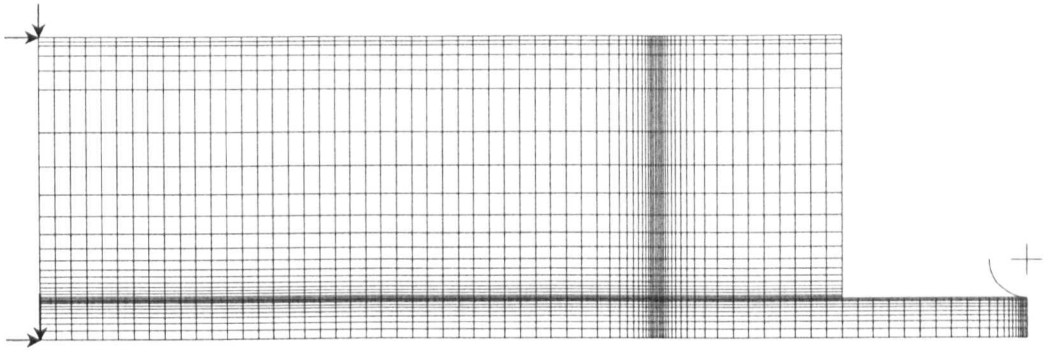

Figure 3.4.5 Typical finite element mesh of a SCSB specimen.

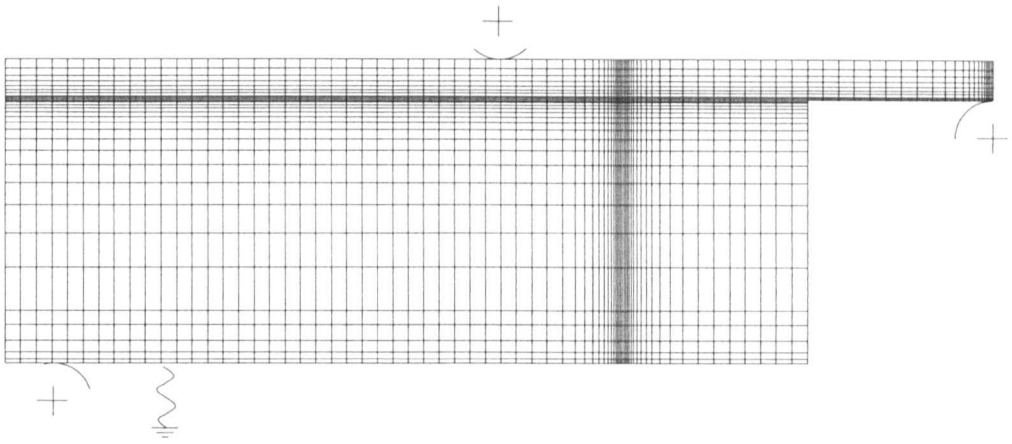

Figure 3.4.6 Typical finite element mesh of a MTPB specimen.

3.4.1 Load Application

Initially, the loading pins in each model were positioned 1 mm above the contact surface of the specimen mesh. Each analysis was then performed in two steps. The first was used to prescribe a displacement to the load-pins of 1.1 mm. This was done to gradually bring the 'master' and 'slave' surfaces into contact, thereby eliminating any numerical difficulties in terms of solution convergence. The second step was used to apply a point-load to the dummy node assigned to the rigid elements in the loading pin meshes. Here, the rigid elements were given identical degrees of freedom to the dummy node, such that any prescribed loading or displacement to this node resulted in the same load or displacement being applied to the rigid element mesh. To simulate the gradual application of the load to the specimens, the load-displacement response of each test modelled herein was obtained experimentally. This data was then used to ramp the load in the corresponding analyses with respect to the solution time, until the required magnitude of load was applied, as illustrated in Fig. 3.4.7.

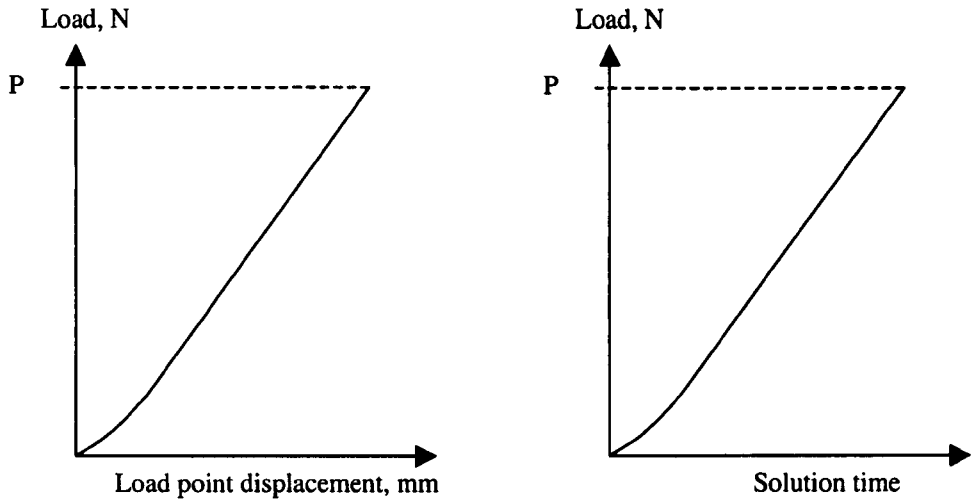

Figure 3.4.7 Use of experimental load-displacement response to simulate gradual load application in the finite element analyses.

In all cases, the magnitude of the applied load was limited to a value below that required for crack propagation. This ensured that the modelling procedure was accurate in assuming an elastic response from the constituent materials of the sandwich specimens.

3.4.2 Model Rotation – Transfer of Coordinate System

Large load-point displacements and significant rotation of the crack tip plane about the global x,y coordinate system were observed when modelling sandwich specimens based on low stiffness face-sheets. Moreover, as the ABAQUS® code only gives nodal variables (forces and displacements) with respect to the global co-ordinate system, it was necessary to transfer these values into a coordinate system that was coincident with the rotated crack-tip plane. To achieve this, the angle of rotation was calculated by measuring the gradient of the line passing through node pairs CC', DD', and node E

(assuming a straight line), Fig. 3.4.8, which was horizontal before the load application. Wherever necessary, appropriate transformations were conducted to calculate the nodal displacements and forces in the local co-ordinate system [15].

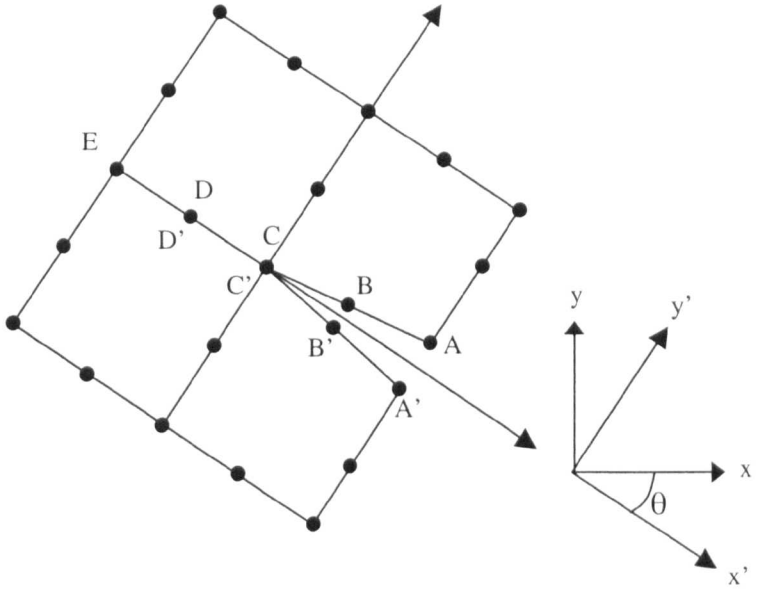

Figure 3.4.8 Rotation of crack tip plane about the x,y global co-ordinate system.

3.5 Determination of Strain Energy Release Rates

3.5.1 Modified Virtual Crack Closure Technique

The modified virtual crack closure technique (MVCCT) [16] was employed to calculate the total strain energy release rate, G_T, and the Mode I and Mode II components of G_T. For the crack tip region in Fig. 3.4.1, the mode I strain energy release rate G_I is given by:

$$G_I = \frac{1}{2B\Delta a}\left[F_A^y\left(v_A - v_{A'}\right) + F_B^y\left(v_B - v_{B'}\right)\right] \qquad (3.5.1)$$

and the Mode II strain energy release rate by:

$$G_{II} = \frac{1}{2B\Delta a}\left[F_A^x(u_A - u_{A'}) + F_B^x(u_B - u_{B'})\right] \tag{3.5.2}$$

where F^y_A, F^x_A, F^y_B, and F^x_B are the forces required to hold the node pairs A-A' and B-B' together respectively and v_i and u_i are the nodal displacements in the y and x directions respectively. The subscript i denotes the node. During each analysis, multi-point constraint equations (MPC) were used to prevent the coincident nodes C, C' and D, D' from undergoing relative displacement, thus effectively linking together node C to node C' and node D to D'. Subsequently, the reaction loads calculated to constrain node C to C' and node D to D' in the analyses were equated to the forces F^y_A, F^x_A and F^y_B, and F^x_B respectively. These load values, in addition to the calculated displacements of nodes A, A', B, and B' were used to determine the Mode I and Mode II strain energy release rates. Furthermore, the total strain energy release rate, G_T, was calculated by summing the Mode I and Mode II strain energy release rates, such that:

$$G_T = G_I + G_{II} \tag{3.5.3}$$

.

3.5.2 Global Energy Methods

The total strain energy release rate, G_T, was calculated using a compliance calibration technique [17] and from a crack length extension factor technique [18].

Both methods are based on the change in compliance with respect to crack length and rely on the following equation [19]:

$$G_T = \frac{P^2}{2B}\frac{dC}{da} \tag{3.5.4}$$

where P is the applied load, B is the specimen width, C is the compliance ($C = \delta/P$, where δ is the load-point displacement) and a is the crack length.

Here, a series of analyses were performed on each specimen type for a range of crack lengths and the resulting load and load-point displacement values were used to calculate the specimen compliance from each analysis. Subsequently, the following two methods were used to calculate the total strain energy release rate from the models.

To calculate G_T from the compliance calibration technique, the specimen compliance was assumed to take the following form [17]:

$$C = C_o + ka^3 \tag{3.5.5}$$

where C_o is the compliance of the specimen between the end of the pre-crack and the support pins and k is a constant for a given specimen. The constants C_o and k, were determined by plotting the compliance versus the cube of the crack length as illustrated in Fig. 3.5.1. Having determined these constants, Eqn. 3.5.5 was differentiated and substituted into Eqn. 3.5.4 yielding the following expression for the total strain energy release rate:

$$G_T = \frac{3P^2(C - C_o)}{2Ba} \tag{3.5.6}$$

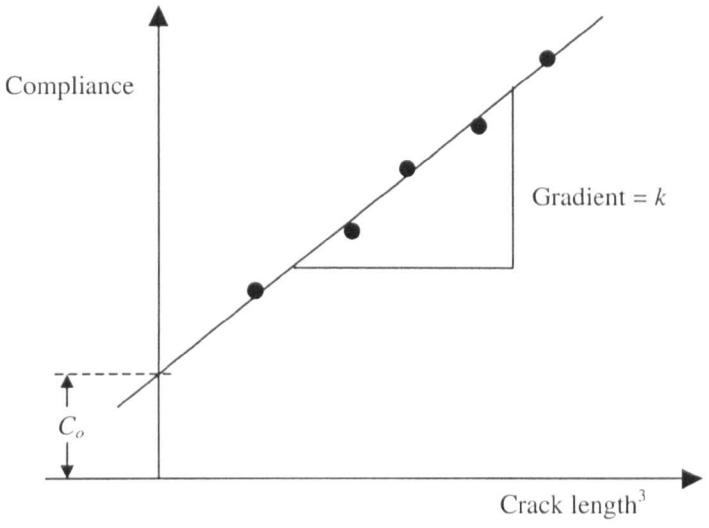

Figure 3.5.1 Generalised plot of compliance versus the cube of the crack length for determining the constants C_o and k.

The crack length extension factor was the second method used to calculate G_T. This technique assumes the specimen compliance to take the following form [18]:

$$C = m(a + \Delta)^3 \tag{3.5.7}$$

where m and Δ are constants for a given specimen. The crack length extension factor Δ was calculated from plotting the cube root of the compliance versus crack length, as illustrated in Fig. 3.5.2. Having determined Δ, Eqn. 3.5.7 was differentiated and substituted into Eqn. 3.5.4 yielding the following expression for the total strain energy release rate:

$$G_T = \frac{3P\delta}{2B(a + \Delta)} \tag{3.5.8}$$

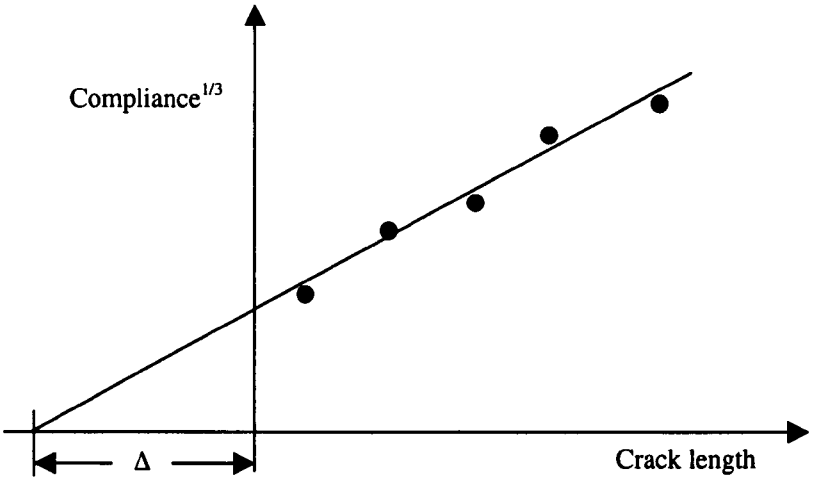

Figure 3.5.2 Generalised plot of the cube root of compliance versus crack length for determining the crack length extension factor Δ.

To provide a check of the accuracy of the total strain energy release rate values calculated using the MVCCT technique, the values of G_T calculated from the two global energy approaches were used as a comparison.

3.5.3 Finite Element Model Verification

Two techniques were used to validate the solutions obtained from the finite element analyses. These are summarised below:

- *Finite Element Mesh Optimisation.* The appropriate mesh density used to represent the crack-tip region of the specimens was determined by performing an analysis of a specimen for which a beam theory solution was available. Here, the

mixed-mode ratio was calculated using the MVCCT from a series of models with different crack-tip element mesh densities. The calculated mixed-mode ratios were compared with that obtained from beam theory.

- *Comparison with Experiment.* The strain energy release rates calculated from the analyses and experiment were compared.

3.6 Parametric Studies

A series of finite element analyses were conducted to simulate CNFS, MTPBS and SCSB tests on specimens taken from Structures P to R. Here, the effect of specimen crack length on the ratio of the Mode I and Mode II strain energy release rate components was investigated. Each specimen geometry was modelled using six to ten different crack lengths and the corresponding values of the mixed-mode ratio, G_I/G_T, were calculated. Furthermore, the analyses conducted on Structures P to R were used to perform a series of parametric studies as outlined in the following sections.

3.6.1 Effect of Face-Sheet Thickness on the Crack-Tip Mode Ratio of the Three Test Geometries

The analyses of Structures P to R were used to determine the influence of the face-sheet thickness on the mode ratio in all three test geometries. The object of this study was to determine the sensitivity of the crack-tip loading conditions to the flexural rigidity of the face-sheets. Furthermore, this study was used to establish the effect of the rigidity of the

face-sheets on the constants used in the compliance calibration method and the crack length extension factor technique detailed in Section 3.5.2.

3.6.2 Effect of Crack Location on The Crack-Tip Mode Ratio of the Three Test Geometries

During the FE analysis of CNFS, MTPB and SCSB geometries based on Structure P, the crack was positioned either within the core material (following experimental observation) or at the mid-plane of the face-sheet material, as illustrated in Fig. 3.6.1. Subsequently, the effect of crack location on the mixed-mode ratio offered in all three specimen geometries was determined.

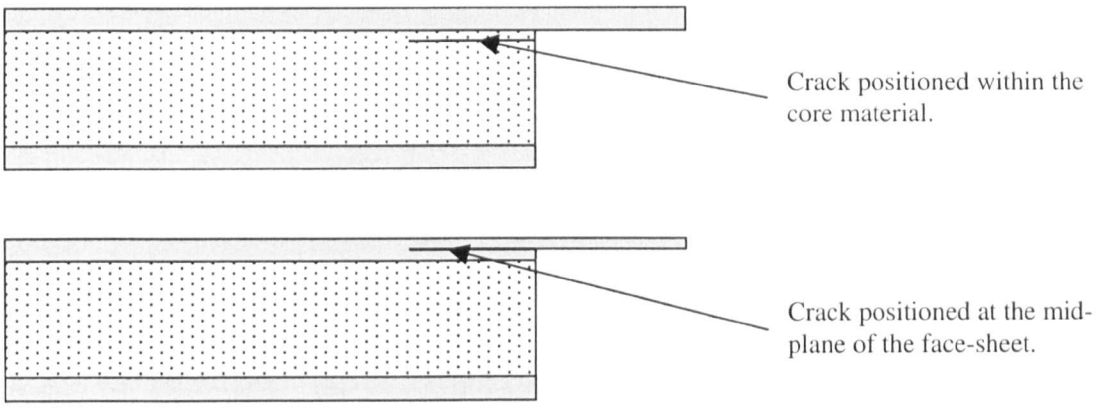

Figure 3.6.1 The two crack locations modelled in the analyses of the CNFS, MTPB and SCSB specimens of Structure P.

3.6.3 Sensitivity of the Crack-Tip Mode Ratio to the Mechanical Properties of the Core and Face-Sheet Materials

A series of analyses of CNFS, MTPB and SCSB geometries based on Structure P was conducted in which the core Young's modulus values were varied from 25 N/mm^2 to 800 N/mm^2. In addition, a range of face-sheet mechanical properties was considered which are summarised in Table 3.6.1. These studies were also conducted for cases in which the crack was situated either within the core material or within the face-sheet. In all cases, the properties of the upper and lower face-sheets were varied.

E_x GPa	E_y GPa	E_z GPa	ν_{xz}	ν_{xy}	ν_{yz}	G_{xz} GPa	G_{xy} GPa	G_{yz} GPa
5.5	5.5	2.07	0.26	0.26	0.24	2	2.07	2.07
11	11	4.14	0.26	0.26	0.24	4	4.14	4.14
16.5	16.5	6.21	0.26	0.26	0.24	6	6.21	6.21
22	22	8.28	0.26	0.26	0.24	8	8.28	8.28
44	44	16.56	0.26	0.26	0.24	16	16.56	16.56
88	88	33.12	0.26	0.26	0.24	32	33.12	33.12

Table 3.6.1 Orthotropic mechanical properties of the face-sheets used to determine the sensitivity of the crack-tip mixed-mode ratio to these properties.

3.6.4 Summary of Finite Element Analyses

Table 3.6.2 summarises the analyses conducted during the course of this research programme.

Structure	Test	Crack Location	Δa mm	Parameter Varied	
P	CNFS	Core	0.001-0.1	Δa	
P	CNFS	Core	0.001	Load	
P	CNFS	Core	0.01	Crack length	
P	MTPB	Core	0.01	Crack length	
P	SCSB	Core	0.01	Crack length	
Q	CNFS	Core	0.01	Crack length	
Q	MTPB	Core	0.01	Crack length	
Q	SCSB	Core	0.01	Crack length	
R	CNFS	Core	0.01	Crack length	
R	MTPB	Core	0.01	Crack length	
R	SCSB	Core	0.01	Crack length	
P	CNFS	Face-sheet	0.005	Crack length	
P	MTPB	Face-sheet	0.005	Crack length	
P	SCSB	Face-sheet	0.005	Crack length	
[1]P	CNFS	Core	0.02	Core shear modulus	Face-sheet properties[4]
[1]P	CNFS	Face-sheet	0.001	Core shear modulus	Face-sheet properties
[2]P	MTPB	Core	0.01	Core shear modulus	Face-sheet properties
[2]P	MTPB	Face-sheet	0.001	Core shear modulus	Face-sheet properties
[3]P	SCSB	Core	0.01	Core shear modulus	Face-sheet properties
[3]P	SCSB	Face-sheet	0.001	Core shear modulus	Face-sheet properties

[1] crack length = 90 mm, [2] crack length = 45 mm, [3] crack length = 70 mm, [4] See Table 3.6.1.

Table 3.6.2 Summary of finite element analyses conducted in the duration of the research programme.

3.7 References

[1]. Lindell M.C., Laminator Version 2.01, http://tni.net/~mlindell/laminator.html, 1997.

[2]. Jones R.M., Mechanics of Composite Materials, Scripta Book Company, 1975.

[3]. Marshall A., Handbook of Composites, Ed. Lubin G., Von Nostrand Reinhold, 1982, pp558-603.

[4]. Divinycell, Design Manual, Divinycell International AB, Sweden.

[5]. Ratcliffe J. and Cantwell W.J., Journal of Materials Science Letters, Vol.19, 2000. pp1365-1367.

[6]. Ratcliffe J. and Cantwell W.J., Journal of Reinforced Plastics and Composites, Vol.20, 2001, pp945-970.

[7]. Cantwell W.J., Scudamore R.J., Davies P. and Ferrer J-B., Proc. Eleventh International Conference on Composite Materials, Woodhead, 1997, pp905-914.

[8]. Cantwell W.J., Broster G. and Davies P., Journal of Reinforced Plastics and Composites, Vol.15, 1996, pp1161-1172.

[9]. MSC NASTRAN for Windows version 4.6 Command Reference Manual, MacNeal-Schwendler Corporation, 1997.

[10]. ABAQUS/Standard version 5.6 Users Manual, Hibbitt, Karlsson and Sorensen Incorporated, Vol.1, 1996.

[11]. Sun C.T. and Manoharan M.G., Journal of Composite Materials, Vol.23, 1989, pp460-478.

[12]. Shim J.Y. and Hong C.S., Journal of Reinforced Plastics and Composites, Vol.12, 1993, pp1295-1310.

[13]. ABAQUS/Standard version 5.6 Users Manual, Hibbitt, Karlsson and Sorensen Incorporated, Vol.2, 1996.

[14]. Dattaguru B., Venkatesha K.S., Ramamurthy T.S. and Buchholz F.G., Engineering Fracture Mechanics, Vol.49, 1994, pp451-463.

[15]. Spiegel M.R., Mathematical Handbook of Formulas and Tables, McGraw-Hill, 1968.

[16]. Rybicki, E.F. and Kanninen, M.F., Engineering Fracture Mechanics, Vol.9, 1977, pp931-938.

[17]. Cantwell W.J., Scudamore R., Ratcliffe, J. and Davies P., Composites Science and Technology, Vol.59, 1999, pp2079-2085.

[18]. Hashemi S., Kinloch A.J. and Williams J.G., Composites Science and Technology, Vol.37, 1990, pp429-462.

[19]. Broek D., Elementary Engineering Fracture Mechanics, Fourth Ed., Martinus Nijhoff, Dordrecht, 1986.

4. EXPERIMENTAL PROCEDURE

4.1 Introduction

Initially, a range of sandwich structures representative of those employed in the marine and aerospace industries was selected for the investigations proposed during the course of this research programme. Subsequently, attention focused on the design of a test method capable of simulating crack growth at the face-sheet/core interface in sandwich structures based on thin facings. Two preliminary test geometries were designed and used to conduct interfacial fracture tests on a sandwich structure based on thin face-sheets. The design that proved to be the most suitable method for characterising the fracture properties of the face-sheet/core interface of this type of sandwich structure was selected for use in the remainder of the research. This test method, in addition to a further interfacial fracture sandwich test technique selected from the literature, was used to investigate face-sheet/core interfacial crack propagation in the wide range of sandwich structures using quasi-static crosshead displacement rates. Here, appropriate data reduction schemes were selected to determine the fracture toughness of the face-sheet/core interface in each of the sandwich structures. Furthermore, one of the fracture tests was employed to investigate the influence of temperature and crosshead displacement rate on the interfacial fracture toughness of a GFRP/crosslinked PVC foam sandwich structure. Finally, an additional fracture criterion was employed to characterise the interfacial fracture behaviour of fracture sandwich specimens that exhibited

significant non-linearity during a test. Thus, the aims of conducting the experimental procedures are as follows:

- To develop a test configuration which can be used to conduct face-sheet peel tests on sandwich structures based on thin facings.
- Use the developed test geometry to characterise the face-sheet/core fracture behaviour of a range of sandwich systems.
- Study the effects of crosshead-displacement rate and temperature on the interfacial fracture toughness of sandwich structures.
- Apply a fracture criterion suitable for specimens which cannot be analysed using linear elastic fracture mechanics.

4.2 Sandwich Structures Investigated During the Research Programme

The capability of a sandwich structure to offer a high flexural rigidity for a low weight has attracted much interest from the aerospace and marine industries. These benefits have led to the development of a wide range of sandwich panels, comprised of many different materials tailored to suit a specific application. The investigations detailed herein will focus on sandwich panels designed specifically for these two industries.

4.2.1 Aerospace-Grade Sandwich Structures

Seven sandwich panels used in the manufacture of aircraft components were investigated, Structures A to G. The materials used for the face-sheets and core of Structures A to G and their nominal dimensions are presented in Table 4.2.1 and Fig. 4.2.1 respectively. In brief, Structures A to F were based on a hexagonal Nomex® honeycomb core (density 80 kg/m^3), to which the face-sheets were bonded using a film Redux® adhesive. These structures were manufactured using the vacuum bag technique and co-cured within an autoclave at approximately 150°C. Structure G was based on a hexagonal glass-fibre reinforced polyimide honeycomb core (density 96 kg/m^3). Here, a Redux® adhesive film was used to bond the components of the sandwich structure, and the vacuum bag technique used to manufacture Structures A to F was employed to fabricate this structure.

Structure	Face-sheet details		Core details	
	[Lay-up] Ply material	V_f, %	Type	Cell Size[1], mm
A	$[0°/90°]_s$ UD Glass/epoxy	55	Nomex	3.18
B	$[0°/90°]_s$ UD Glass/epoxy	55	Nomex	3.18
C	$[0°/90°]_s$ UD Glass/epoxy	55	Nomex	3.18
D	$[0°/90°]_s$ UD Carbon/epoxy	60	Nomex	3.18
E	$[0°/90°]_s$ UD Carbon/epoxy	60	Nomex	3.18
F	$[0°/90°]_s$ UD Carbon/epoxy	60	Nomex	3.18
G	$[0°/90°]_s$ UD Glass/epoxy	55	Glass/polyimide	4.76

[1]Cell dimensions measured in the length direction of the honeycomb, Fig. 1.2.1a.

Table 4.2.1 Details of the aerospace-grade sandwich structures investigated during the course of this research programme.

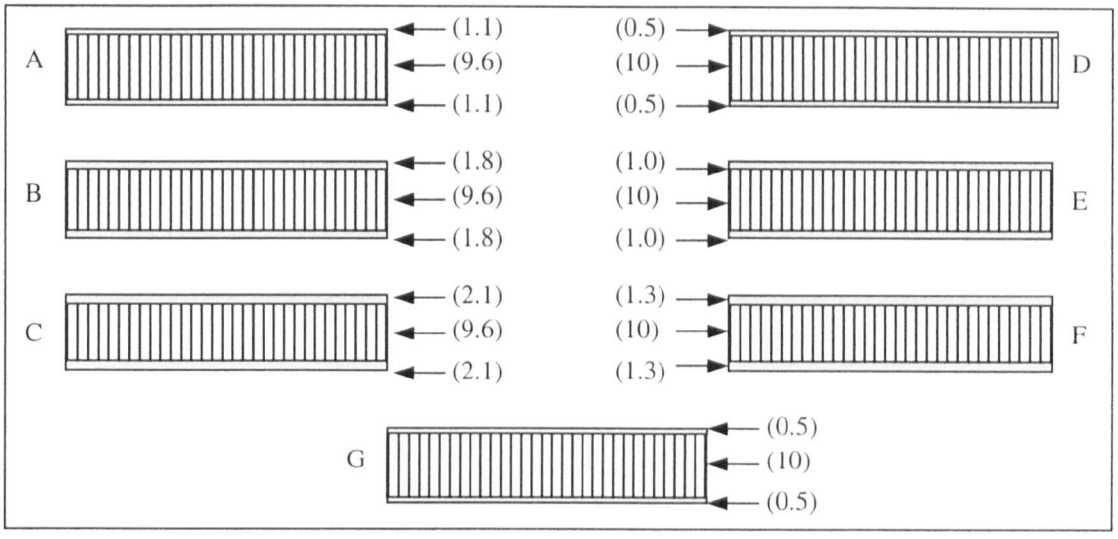

Figure 4.2.1 Dimensions of the aerospace-grade sandwich structures investigated during the course of this research programme (Numbers in parenthesis denote thickness in mm).

4.2.2 Shipyard-Grade Sandwich Structures

Eleven sandwich panels used in the manufacture of high performance marine equipment were investigated. Table 4.2.2 presents the details of the face-sheet materials used in Structures H to R, and Table 4.2.3 gives details of the core materials used in the structures. The nominal dimensions of the face-sheet and core materials used in these structures are given in Fig. 4.2.2. Structure H was manufactured by applying alternating layers of resin and fibres to the core which was pre-sealed with a polyester resin, until the desired face-sheet thickness was achieved. The face-sheets of Structures I to K were fabricated using a wet lay-up technique, in which the fibres and resin were placed directly on the core. As before, a hand lay-up technique was used to apply the face-sheet materials directly on the core materials to manufacture Structures J and K. Structures H to K were all co-cured at room temperature in a press similar to that illustrated in Fig.

1.5.1. Structures L to O were based on the same foam core material and were manufactured by hand laying the plies directly on the core material. The structures were then co-cured in a vacuum bag at room temperature. The same component materials were used in Structures P to R, which were manufactured by bonding the pre-preg face-sheets to the core using an epoxy adhesive and co-curing the structures in a press at room temperature.

Structure	Face-sheet details	
	[Lay-up]	$V_{f,}$ %
H	$[0°/+45°/-45°]_s$ UD glass/polyester	49
I	$[0°/90°]_s$ woven glass/polyester	71
J	[0°/90°] 1 ply, 2 CSM, 1 ply 2 CSM	50
K	[0°/90°] 1 ply, 2 CSM, 1 ply 2 CSM	60
L (upper)[1]	[0°/90°] 1 ply woven carbon fabric,4 plies UD Kevlar/epoxy	65
L	[0°/90°] 1 ply glass fabric, 1 ply woven carbon fabric/epoxy	55
M (upper)	[0°/90°] 1 ply woven carbon fabric, 2 plies UD Kevlar/epoxy	65
M	[0°/90°] 1 ply glass fabric, 1 ply woven carbon fabric/epoxy	55
N (upper)	[0°/90°] 5 plies woven carbon fabric/epoxy	55
N	[0°/90°] 1 ply glass fabric, 1 ply woven carbon fabric/epoxy	55
O (upper)	[0°/90°] 3 plies woven carbon fabric/epoxy	55
O	[0°/90°] 1 ply glass fabric, 1 ply woven carbon fabric/epoxy	55
P	$[\pm 45°]_s$ 2 plies woven glass/polyester	30
Q	$[\pm 45°]_s$ 4 plies woven glass/polyester	30
R	$[\pm 45°]_s$ 8 plies woven glass/polyester	30

[1] Upper refers to the face-sheet indicated in Fig. 4.2.2.

Table 4.2.2 Details of the composite skins used in Structures H to R.

Structure	Core material	Density (kg/m^3)
H	End grain balsa	175
I	Hexagonal aluminium honeycomb (cell size 8mm)[1]	92
J	Linear PVC	90
K	Crosslinked PVC	80
L to O	PVC/PUR	140
P to R	Crosslinked	75

[1] Cell size measured in the length direction, Fig. 1.2.1a.

Table 4.2.3 Details of the core materials used in Structures H to R.

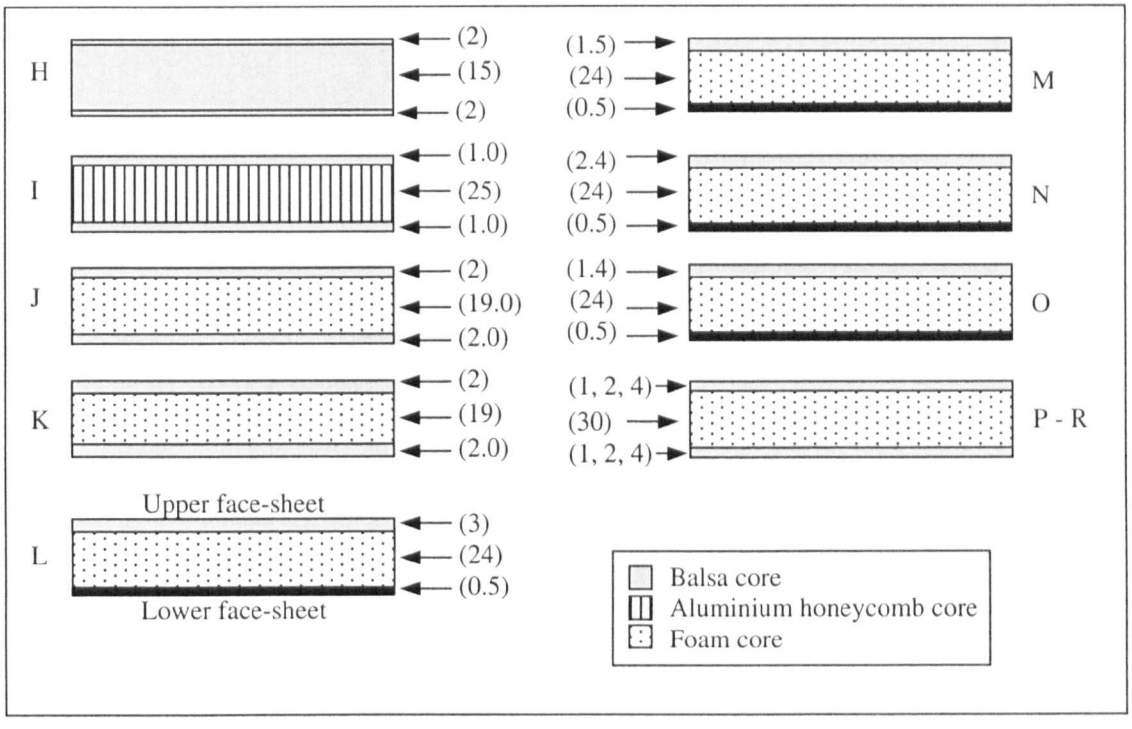

Figure 4.2.2 Dimensions of the shipyard-grade sandwich structures investigated during the course of this research programme (Numbers in parenthesis denote thickness in mm).

4.3 Configurations for Characterising Crack Growth at the Face-sheet/Core Interface of Sandwich Structures

4.3.1 Development of a Fracture Test for Face-sheet/Core Debonding in Sandwich Panels with Thin Face-sheets

During the initial part of the research programme, a number of test configurations for characterising the interfacial fracture properties of sandwich structures based on thin face-sheets were considered. Subsequently, two preliminary test configurations were developed following the design brief given below and one of these was selected for use throughout the duration of this research programme.

Design Brief:

- The test must be capable of peeling thin face-sheets from the core of the sandwich structure.
- The test rig must be simple, enabling fracture tests on laboratory-sized specimens to be conducted with ease and without the need for expensive tooling.
- The configuration must promote linear elastic crack growth in the specimens, to enable existing fracture mechanics approaches to be employed in determining fracture toughness data.
- The test configuration must be designed to enable testing to be undertaken over a range of displacement rates.
- The rig should be sufficiently small to fit into a temperature chamber.

The following gives details the test geometries that were designed and evaluated.

The Asymmetric Sandwich Peel Test

The ASPT was the first of two test methods designed for characterising the interfacial fracture toughness of sandwich structures based on thin face-sheets. The asymmetric sandwich peel test (ASPT) is a hybrid of the modified double cantilever beam introduced by Prasad and Carlsson [1, 2] and the single cantilever sandwich beam developed by Cantwell *et al* [3].

Preparation of an ASPT specimen was undertaken by removing one end of a 180 mm long (20 mm wide) sandwich beam, leaving a section of the face-sheet material to protrude from the remaining structure. A hole was drilled near to the end of this face-sheet tongue through which an end block was attached, Fig. 4.3.1. The specimen was then loaded as shown in Fig. 4.3.1 using an Instron 4505 test machine and a 30mm long pre-crack was initiated along the face-sheet/core interface. Following this, the load was removed and the pre-crack dimensions were measured. White correction fluid was then applied to the expected path of crack growth, onto which a calibrated scale of 2 mm increments was printed. The specimen was then reloaded until the pre-crack had propagated to a length of approximately 70 mm, after which the load was removed. A load versus crosshead-displacement plot was recorded for each test conducted. A crosshead-displacement rate of 2 mm/min was used during all tests and load and displacement values were recorded at regular increments of crack extension.

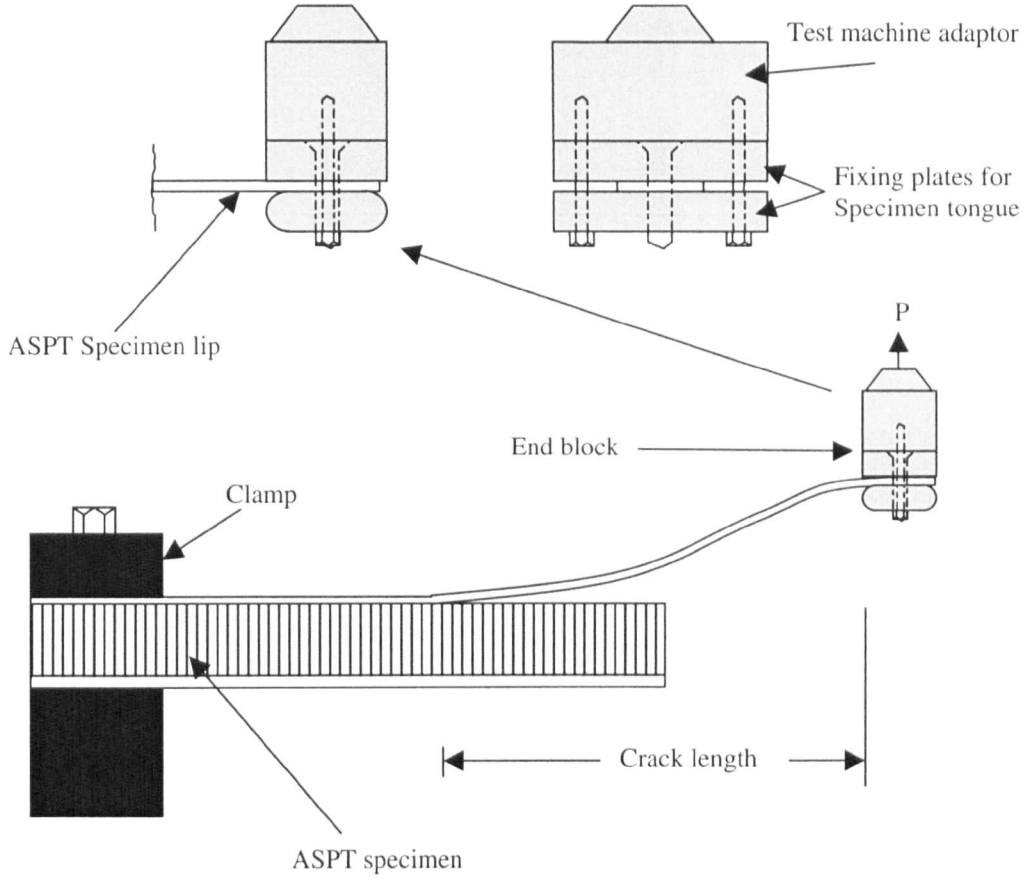

Figure 4.3.1 Schematic of the asymmetric sandwich peel test (ASPT) for sandwich structures based on thin face-sheets, including an illustration of the end block assembly.

The Centre Notched Flexure Sandwich Beam

The centre notched flexure sandwich (CNFS) specimen was the second design considered, and is based on the end notched flexure specimen introduced by Carlsson *et al* [4]. A CNFS specimen was prepared by carefully drilling a 7 mm diameter hole immediately above the lower face-sheet in a 140 mm long (20 mm wide) sandwich beam. Notches were cut into the specimen using a thin razor blade to encourage crack growth along the face-sheet/core interface, as shown in Fig. 4.3.2. A 6 mm diameter steel bar

was then placed through the hole and the assembly was positioned on 10 mm diameter rollers placed 120 mm apart. A simple frame was designed to load the steel bar in a vertical plane as shown in Fig. 4.3.3. The load was applied until a 30 mm long pre-crack was initiated along the face-sheet/core interface, after which the load was removed and the dimensions of the pre-crack were measured. Again, a calibrated scale was used to highlight the position of the crack-tip during the test. The specimen was then reloaded until the pre-crack had propagated to approximately 70 mm in length, after which the load was removed. A crosshead-displacement rate of 2 mm/min was used during all tests. The load-displacement response of the specimen was recorded for each test, and values of load and displacement were noted at regular increments of crack extension.

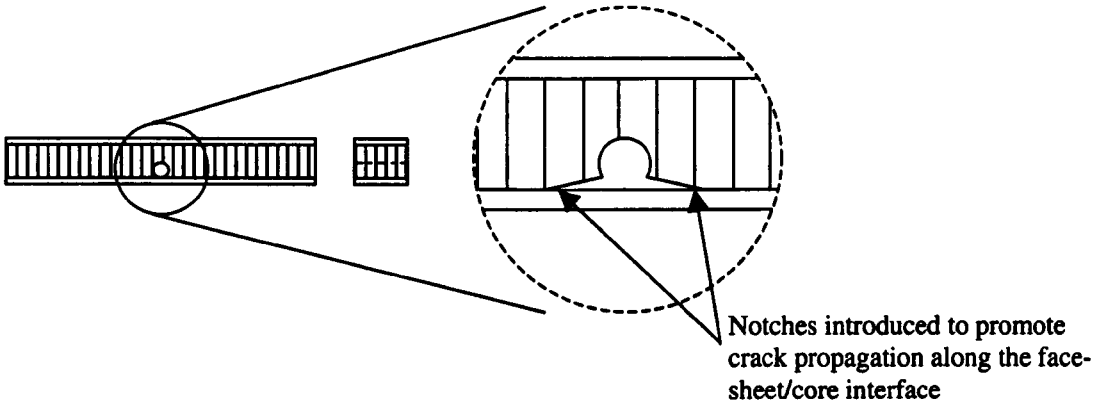

Figure 4.3.2 Illustration of the central hole drilled into a CNFS specimen, showing the notches introduced to promote crack growth along the face-sheet/core interface.

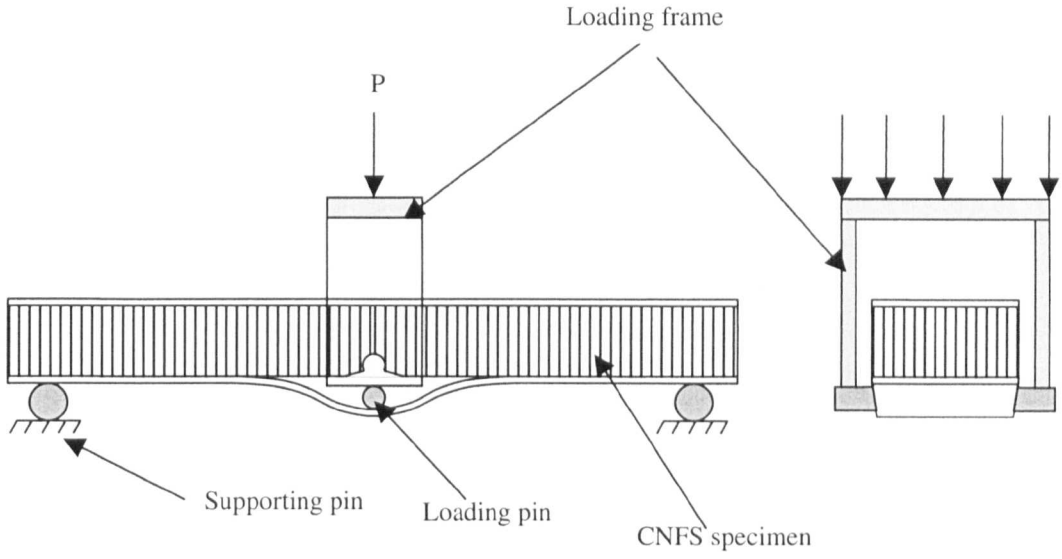

Figure 4.3.3 Schematic of the centre notch flexure sandwich specimen for testing sandwich structures based on thin face-sheets.

4.3.2 Selection of Test Technique for Performing Fracture Tests on Sandwich Structures Based on Thin Facings

Following the design of the ASPT and the CNFS tests, the two geometries were used to characterise the interfacial fracture properties of Structure G. The suitability of these methods for testing sandwich structures based on thin facings was evaluated by examining the load displacement response following the tests. Here, the test specimen that exhibited the most linear elastic response was selected for use in the research programme. In this case, the CNFS test was observed to be the most suitable of the two methods. Further details of this selection process are provided in Section 6.2.

4.3.3 The Modified Three-point Bend Sandwich Specimen

The modified three-point bend specimen (MTPB) developed by Cantwell *et al* [5] was also used to characterise the interfacial fracture toughness of the sandwich structures investigated herein. The fracture toughness values obtained following this procedure were compared to those obtained using the CNFS specimen, in order to validate the data obtained following tests using the latter geometry. Furthermore, the MTPB specimen was required for testing structures with very thick facings, for which the CNFS geometry was unsuitable.

The geometry of the MTPB specimen is illustrated in Fig. 4.3.4. Here, 25 mm wide beams, 140 mm in length were prepared and one section of the panel was removed, leaving a section of the face-sheet material to protrude from the remaining sandwich specimen, Fig. 4.3.4. The specimen was then positioned on 10 mm diameter rollers positioned 120 mm apart and the tongue was loaded as shown in the figure until a pre-crack of approximately 30 mm was produced at the face-sheet/core interface. The specimen was then unloaded and a calibrated scale was applied to the anticipated path of crack growth. The specimen was reloaded until the pre-crack had propagated to approximately 50 mm, after which the load was removed. A croshead-displacement rate of 2mm/min was used during all tests. During each test, values of load and displacement were recorded for known increments of crack extension.

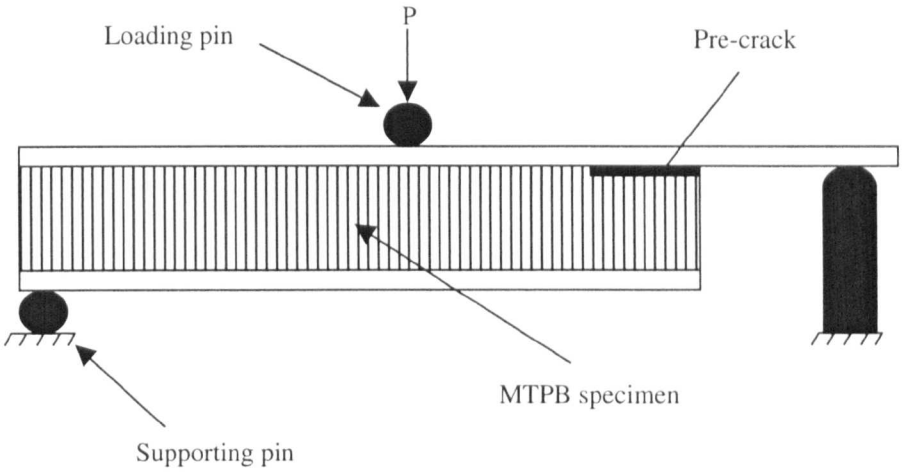

Figure 4.3.4 Schematic of the modified three-point bend (MTPB) sandwich specimen.

A typical load versus crosshead-displacement record obtained from the ASPT, CNFS and MTPB tests is illustrated in Fig. 4.3.5.

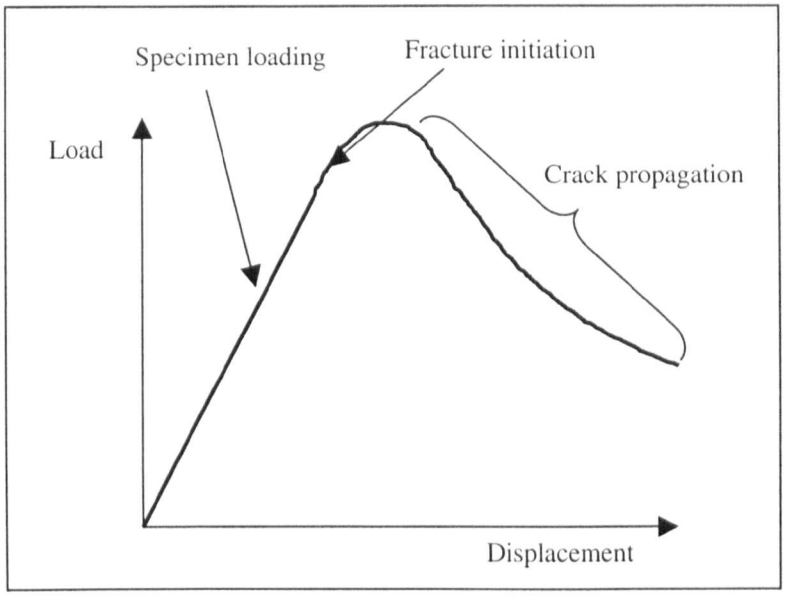

Figure 4.3.5 Generalised load vs. crosshead-displacement record obtained from the ASPT, CNFS and MTPB tests.

4.3.4 Data Reduction Methods

In this study, an ASTM procedure [6] was used to determine if the linear elastic fracture mechanics (LEFM) techniques used to calculate the fracture toughness values following CNFS and MTPB tests were valid. Here, a line with a gradient 5% less than the initial load displacement slope was drawn, such that it intersected the load-displacement record at a load, $P_{5\%}$, as shown in Fig. 4.3.6.

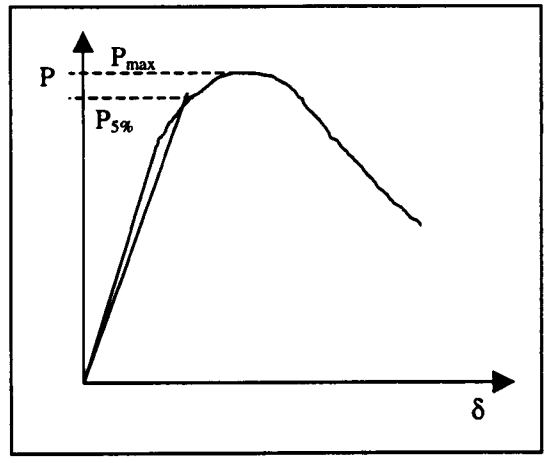

Figure 4.3.6 ASTM procedure for estimating the extent of non-linearity exhibited by a specimen during the loading stage of a fracture test.

In accordance with the ASTM standard, the ratio of the maximum load applied to the specimen, P_{max}, to the value of $P_{5\%}$ was calculated, and the following inequality was used to determine the suitability of the load-displacement data for analysis by LEFM:

$$\frac{P_{max}}{P_{5\%}} < 1.1 \qquad (4.3.1)$$

LEFM was deemed applicable when $P_{max}/P_{5\%}$ was equal to or less than 1.1. In cases where the above ratio was greater than 1.1, an alternative fracture criterion was employed, details of which are given in Section 4.5.

In cases where specimens exhibited linear elastic crack growth, the two techniques outlined in Section 3.5.2 were used to calculate the interfacial fracture toughness values. Here, the specimen compliance values used to determine the constants of the compliance calibration technique and the crack length extension factor method were determined by recording a series of load and displacement values as the specimen crack propagated, as illustrated in Fig. 4.3.7. Subsequently, Eqns. 3.5.6 and 3.5.8 were used to calculate the critical strain energy release rate, known as the fracture toughness.

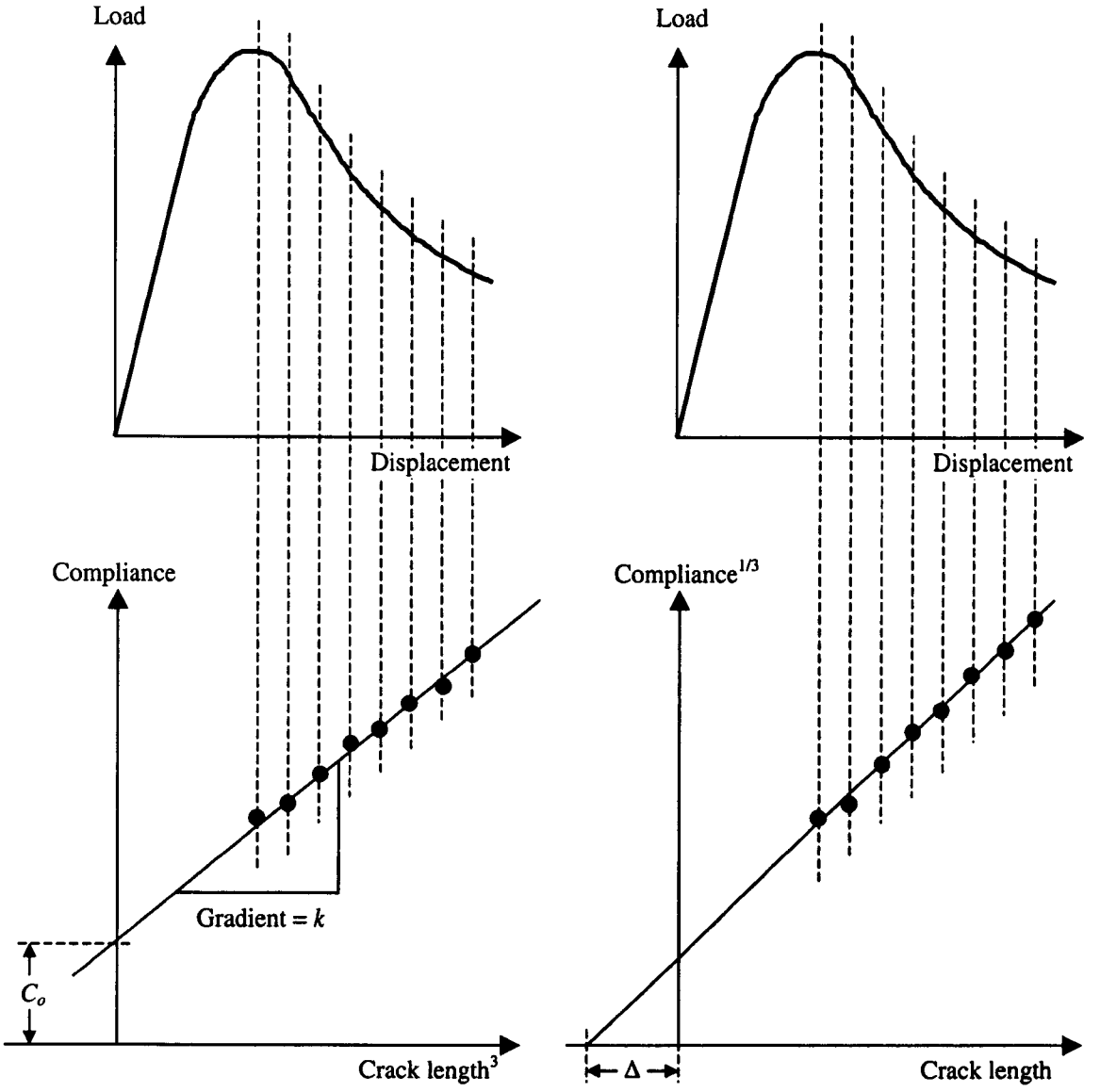

Figure 4.3.7 Examples of the methods used to generate compliance data for calculating fracture toughness values.

In cases when crack growth was unstable, the peak load values were used to generate the compliance data necessary to carry out the global energy approaches, as illustrated in Fig. 4.3.8.

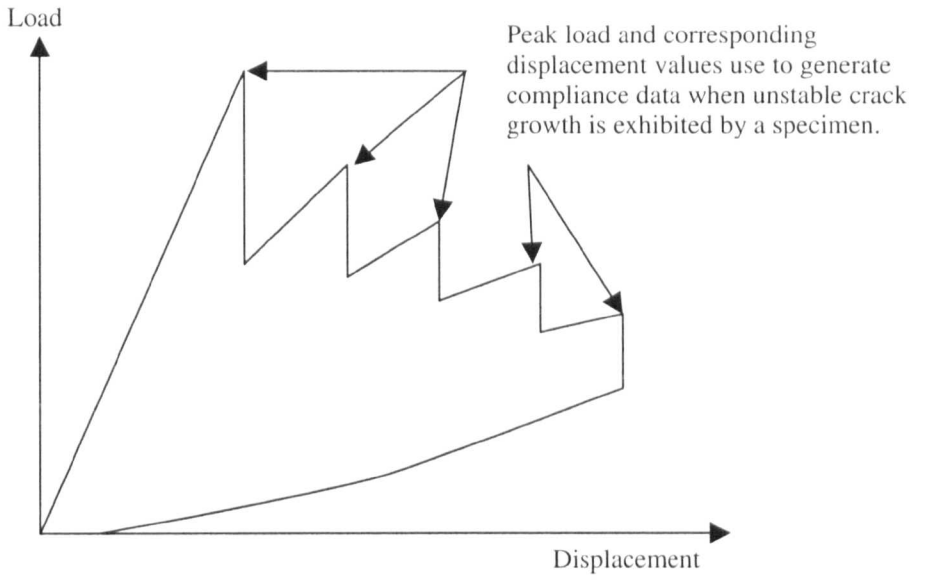

Figure 4.3.8 The technique used to generate compliance data when unstable crack propagation was exhibited by a specimen.

In addition, an areas method was employed to calculate the fracture toughness of a number of CNFS and MTPB samples. Here, the area enclosed by the load-displacement record (indicated by the shaded area, U, in Fig. 4.3.9) was normalised by the resulting crack area to provide an average fracture toughness value for the particular test. This method was used in cases where it was not possible to monitor crack extension.

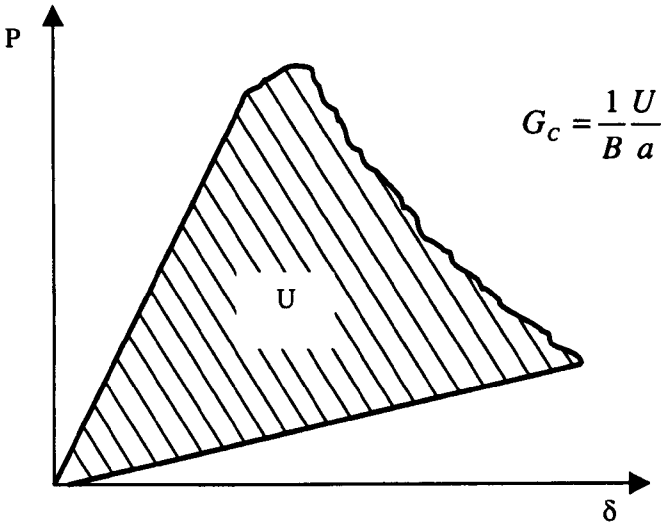

Figure 4.3.9 The areas method to calculate the average fracture toughness from a test.

4.3.5 Specimen Reinforcement

In a number of cases, it was necessary to reinforce the CNFS and MTPB specimens in order to reduce excessive flexural displacements during the test. Specimens taken from Structures A to G required reinforcement. In each case, 4 mm thick woven glass/polyester laminates were adhesively-bonded to the appropriate surface of the specimen using a two part epoxy resin. Curing was undertaken in a heated press at a temperature of 60°C. Three reinforcement configurations were used as illustrated in Fig. 4.3.10.

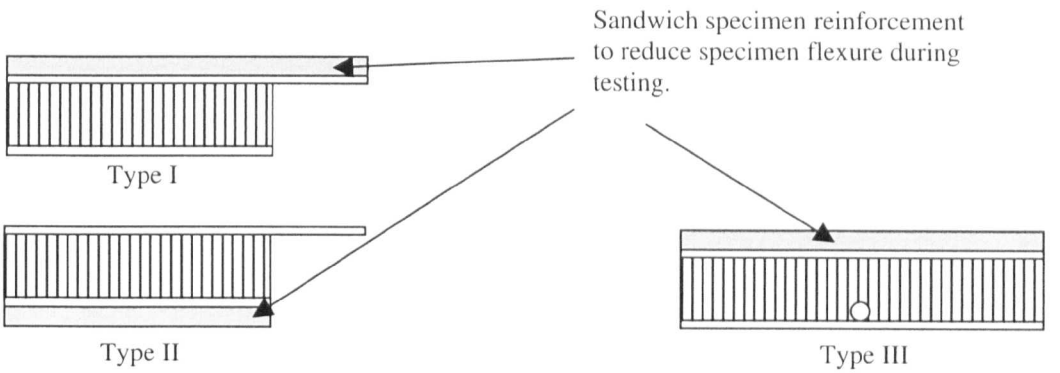

Figure 4.3.10 Reinforcement methods used for the CNFS and MTPB specimens. Type I – upper face-sheet reinforcement of the MTPB specimens, Type II – lower face-sheet reinforcement of the MTPB specimens, Type III – upper face-sheet reinforcement of the CNFS specimens.

Type I reinforcement was used in cases where the flexural rigidity of the tongue was too low and Type II reinforcement was used in cases where the flexural rigidity of the entire sandwich specimen was too low. In the latter case, the entire sandwich beam would undergo bending without propagation of the pre-crack. Similarly, in cases where the flexural rigidity of CNFS specimens was too low, the specimens would undergo significant bending without crack growth occurring. This was prevented by using reinforcement Type III. A summary of the tests specimens that needed reinforcing is presented in Table 4.3.1.

Structure	MTPB Reinforcement	CNFS Reinforcement
A	I, II	III
B	I, II	III
C	II	III
D	I, II	III
E	II	III
F	II	III
G	-	III

Table 4.3.1 Summary of tests for which it was necessary to reinforce the specimens..

4.3.6 Summary of the Procedure for Conducting the CNFS and MTPB Tests

Table 4.3.2 summarises the procedure used to conduct the CNFS and MTPB tests and to calculate the corresponding interfacial fracture toughness.

1	Prepare 4 or 5 specimens and measure the dimensions of each. If necessary, apply an appropriate reinforcement.
2	Introduce a pre-crack approximately 30 mm long into the specimen.
3	Apply a calibrated scale to the path of anticipated crack growth.
4	Reload the specimen until the pre-crack has extended approximately 70 mm (CNFS) or 50 mm (MTPB), recording the load displacement response. Record values of load and displacement for at least five crack length intervals.
5	Use the compliance calibration and crack length correction methods, to calculate the fracture toughness at each crack length. If crack monitoring is not possible, employ the areas method to calculate an average fracture toughness.
6	Plot the appropriate crack growth resistance curves.

Table 4.3.2 Summary of procedure for conducting the CNFS and MTPB tests.

4.4 Influence of Displacement Rate and Temperature on Interfacial Fracture Toughness

4.4.1 Effect of Crosshead-Displacement Rate

As discussed in the literature review, many sandwich panels employed in the marine and aerospace industries are likely to encounter a range of loading scenarios during their service lifetime. In response to this, the MTPB technique was used to study the effect of crosshead-displacement rate on face-sheet/core fracture toughness.

Structure Q was selected for this study, since the core and face-sheet materials comprising this sandwich (GFRP face-sheets and a crosslinked PVC foam core) are typical of those used in the marine industry. Here, MTPB tests were conducted at crosshead-displacement rates of 1, 10, 100, 500 and 1000 mm/min. Crack monitoring was not possible during the tests conducted at the higher displacement rates, therefore the areas method was used to calculate the fracture toughness of each specimen.

4.4.2 Effect of Temperature

Structure R was tested at different temperatures using the MTPB configuration. Here, tests were conducted using a temperature chamber at -10, 0, 25, 30 and 40°C. To achieve sub-ambient temperatures, vapour from a liquid nitrogen tank was pumped into the chamber. The speed of the pump was connected to a thermally-controlled switch enabling control of the chamber temperature within a tolerance of ±2°C. Similarly, a heated fan connected to the thermal switch was used to control the elevated temperatures.

A wire thermocouple was positioned approximately 5 mm into the foam core of the specimens, and positioned within the temperature chamber as shown in Fig 4.4.1. Before conducting the tests the specimens were left for approximately one hour to ensure the correct temperature was reached. Again, crack monitoring was not possible, therefore the areas method was used to calculate the fracture toughness values.

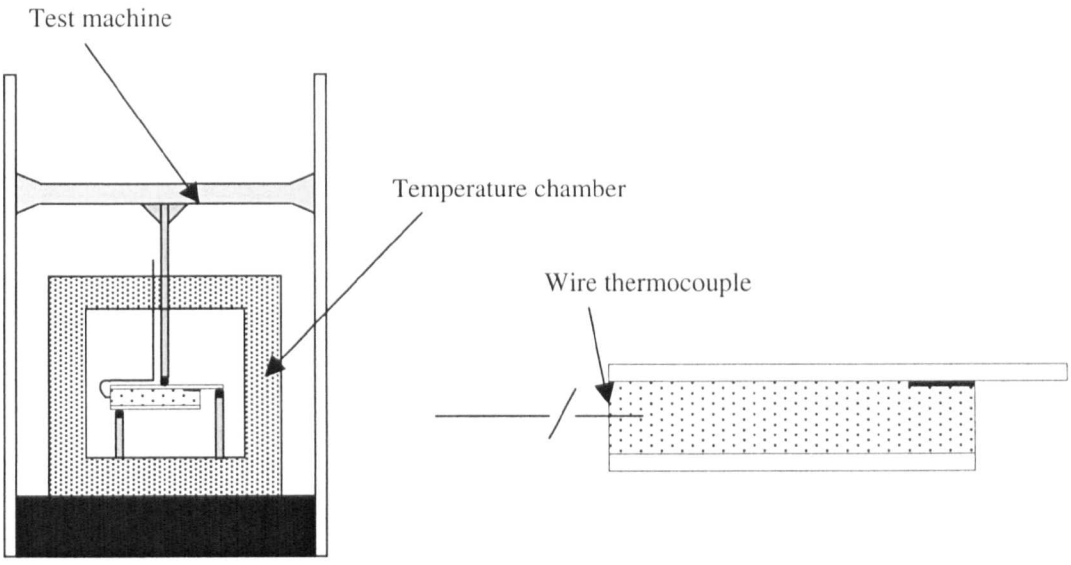

Figure 4.4.1 Schematic of test rig used for conducting MTPB tests at different temperatures

4.5 *J*-Integral Testing of Specimens Exhibiting Non-linear Plastic Crack Growth

The *J*-integral was used as an alternative fracture criterion to LEFM for characterising the interfacial fracture toughness of sandwich fracture specimens in which crack propagation was accompanied by large scale yielding within the core material. The *J*-integral

introduced by Rice [7], is based on the potential energy difference between two identical specimens loaded in the same manner with neighbouring crack lengths, and expressed as:

$$J = -\frac{1}{B}\frac{dU}{da} \tag{4.5.1}$$

where U is the potential energy of a loaded specimen containing a crack, B is the specimen width and a is the crack length.

The J-integral was used to analyse the CNFS data using the method detailed below.

- Five identical specimens were prepared and face-sheet/core interfacial cracks of different lengths were introduced, taking care not to load the specimens. Here, a hacksaw was used to introduce the pre-cracks at the face-sheet/core interface and the tips of the cracks were sharpened using a razor blade.
- A force sufficiently small to prevent yielding and propagation of the pre-crack was applied to each specimen and the corresponding load-displacement response was recorded.
- From each load-displacement record, the stored elastic strain energy (area under the load-displacement record), U, was measured at five load values.
- For each load value, the stored elastic strain energy normalised by specimen width, U/b, was plotted as a function of crack length, as shown in Fig. 4.5.1.
- The J value for each load was determined by calculating the gradient of the lines in Fig. 4.5.1.
- The calculated J values were then plotted as a function of load, Fig. 4.5.2.

- The critical load to initiate propagation, P_c, of the pre-crack was determined for each specimen.
- The critical value of the J integral needed to initiate fracture, J_c, was then determined by extrapolating the plot to the measured values of P_c, as illustrated in Fig. 4.5.2

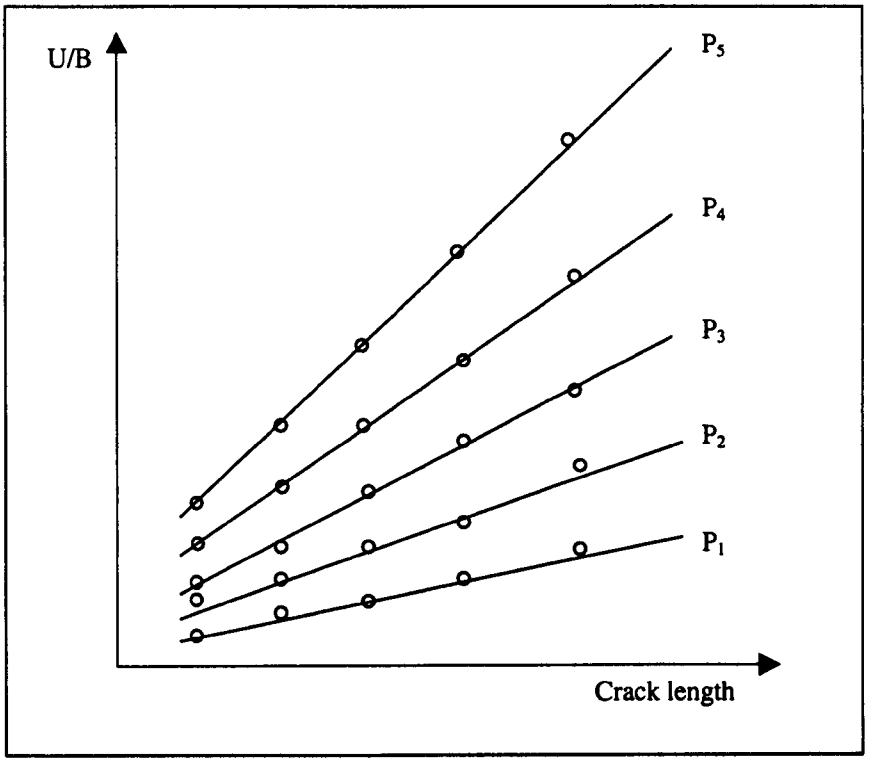

Figure 4.5.1 Energy absorbed per unit thickness as a function of crack length for a range of load values ($P_1 < P_2 \ldots . < P_5$).

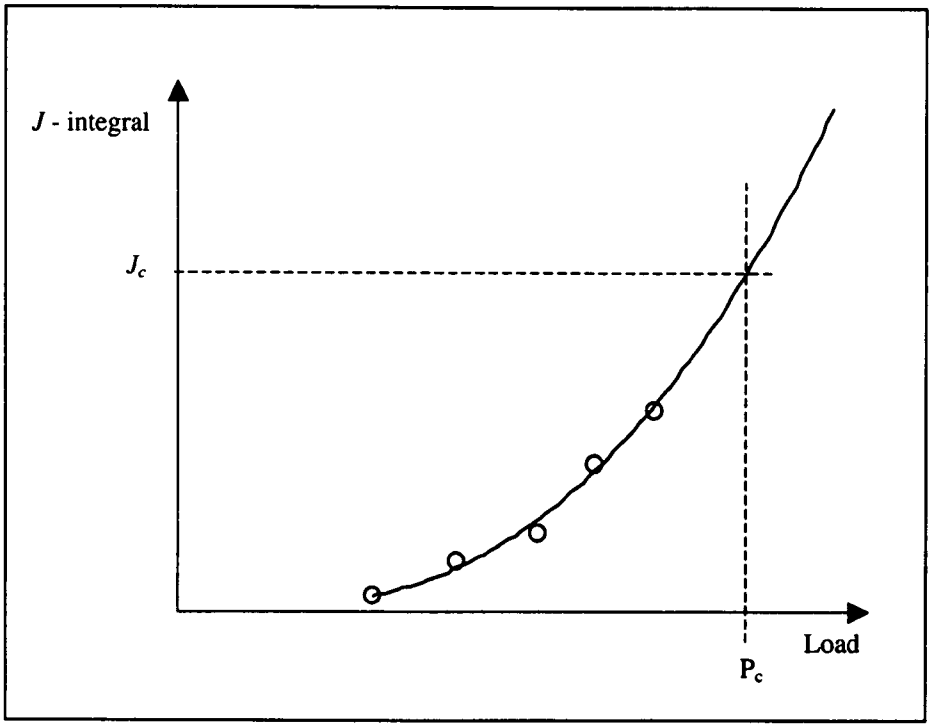

Figure 4.5.2 Generalised plot of the J values as a function of applied load.

In order to validate this method the following studies were conducted.

- The interfacial fracture toughness, G_c, of Structures I and P were calculated using the CNFS geometry and the procedure above was also undertaken on these samples to determine J_c and the two values were compared. As these specimens exhibited a linear response, the values of J_c and G_c were expected to be equal.
- CNFS tests were conducted to determine the J_c integral of Structure J, in which crack growth occurred in an elastic-plastic manner. This value was compared with the values of G_c, measured using the MTPB test, a condition in which the material behaved in a linear-elastic manner.

4.6 References

[1]. Prasad S., and Carlsson L.A., Engineering Fracture Mechanics, Vol.47, 1994, pp813-824.

[2]. Prasad S., and Carlsson L.A., Engineering Fracture Mechanics, Vol.47, 1994, pp825-841.

[3]. Cantwell W.J., Broster G. and Davies P., Journal of Reinforced Plastics and Composites, Vol.15, 1996, pp1161-1172.

[4]. Carlsson L.A., Gillespie, Jr J.W. and Pipes R.B., Journal of Composite Materials, Vol.20, 1986, pp594-605.

[5]. Cantwell W.J., Scudamore R.J., Davies P. and Ferrer J-B., Proc. Eleventh International Conference on Composite Materials, Woodhead, 1997, pp905-914.

[6]. ASTM Testing Standard E-399, 1978.

[7]. Rice J.R., Journal of Applied Mechanics, Transactions of the American Society of Mechanical Engineers, June 1968, pp379-386.

5. NUMERICAL RESULTS/DISCUSSION

5.1 Introduction

This chapter presents the findings from the finite element (FE) analyses conducted to determine the crack-tip loading conditions experienced by the CNFS, SCSB and MTPB specimens, according to the procedures detailed in Chapter 3.

5.2 Model Verification

5.2.1 Optimisation of the Finite Element Mesh Density

In order to verify that the mesh densities chosen to model the CNFS, MTPB and SCSB configurations were of the correct size, a geometry with a known crack-tip mode ratio was modelled. This geometry, the mixed-mode flexure specimen [1] is illustrated in Fig. 5.2.1. Using a simple beam theory analysis to partition the total strain energy release rate of this geometry into the Mode I and Mode II components (G_I and G_{II} respectively) [2], it can be shown that the mode ratio, G_I/G_T, is equal to 0.575 for an MMF specimen with arms of equal thickness, as shown in Fig. 5.2.1. Although, a previous investigation demonstrated that this is only true when the upper and lower arms of the MMF specimen are equal [3].

Briefly, six two-dimensional, plane strain, geometrically non-linear analyses of the MMF specimen detailed in Fig. 5.2.1 were conducted and the modified virtual crack closure technique (MVCCT) was used to determine the Mode I and Mode II strain energy release rates. In each case, the size of the crack-tip elements was varied to determine their effect on the mode ratio, G_I/G_T. The material was assumed to be isotropic, with a Young's modulus of 73 GPa and a Poisson's ratio of 0.3. The results from this investigation are presented in Table 5.2.1.

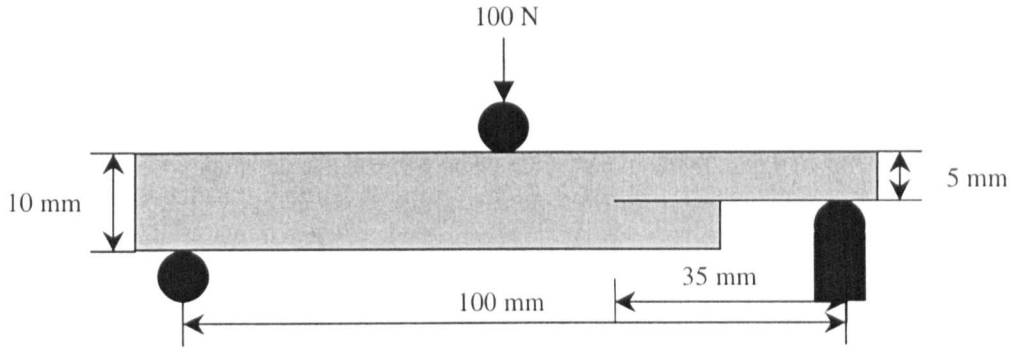

Figure 5.2.1 The mixed-mode flexure specimen. The mode ratio, G_I/G_T, of this specimen is approximately 0.575.

Crack-tip element length, mm	**G_I/G_T**	**% error compared to beam theory result [2]**
0.001	0.547	-4.9
0.005	0.558	-3.0
0.01	0.572	-1.2
0.02	0.582	0.5
0.05	0.597	2.1
0.1	0.615	7.0

Table 5.2.1 The effect of crack-tip element length on the MMF mode ratio, calculated using the MCCT.

The results from the analysis show that for the range of crack-tip element lengths used in this study, the resulting numerical solutions agree with beam theory to within 5%. The reasons for the deviation between the mixed-mode ratio calculated by the finite element analysis and the value calculated by beam theory are likely to be due to the numerical procedures used by the FE code (in this case the commercial code ABAQUS version 5.6 was employed) to solve the equations governing the stress-strain relations of the finite element mesh. For example, if the mesh density is too low, the initial 'guesses' used in the Newton/Raphson-based solving procedure will result either in a final solution which is in error or the iteration procedure will diverge. Conversely, an extremely high-density mesh will cause the crack-tip elements to significantly distort, resulting again in an erroneous solution. This scenario is reflected by the results given in Table 5.2.1, which show the most accurate FE solution is obtained for an intermediate crack-tip element length.

On the basis of the findings from this study, a crack-tip element length of 0.01 mm was chosen. However, a crack-tip element length of 0.005 mm was used for the 'face-sheet crack' models due to the required configuration of the FE mesh. The accuracy of the mesh is still reasonable, as it corresponded only to a 3% deviation from the beam theory result in the above study.

5.2.2 Comparison of Finite Element Models with Experiment

A series of CNFS and MTPB specimens was prepared from Structure P and pre-cracks of different lengths were introduced into the specimens. A 50 N load was then applied to

each specimen and the corresponding compliance was measured. One CNFS specimen and one MTPB specimen was then loaded until the pre-crack had propagated at least 10 mm. The location of the propagated crack was then noted. In each case here, crack growth occurred within the core material, parallel to the face-sheet/core interface. Also, the distance of the crack from the interface was found to be approximately 1 mm. The data reduction methods described in Section 3.5.2 were then used to calculate a strain energy release rate following the CNFS and TPBS tests conducted on Structure P. Corresponding finite element models of the CNFS and MTPB tests were conducted, following the procedures outlined in Chapter 3. The modified crack closure technique and the global-energy data reduction methods detailed in Section 3.5 were used to calculate the strain energy release rates from the models. Figure 5.2.2a presents a comparison of the strain energy release rates following the CNFS tests on Structure P with the strain energy release rates determined from the finite element analyses. Here, the crack length is normalised by the specimen span. This result shows that there is good agreement between the experimental and numerically-determined values of the strain energy release rate. This agreement is echoed by the results obtained following the MTPB tests on Structure P. This reasonable agreement between experiment and analysis suggests that the finite element analysis procedures used herein accurately represent the specimens being modelled.

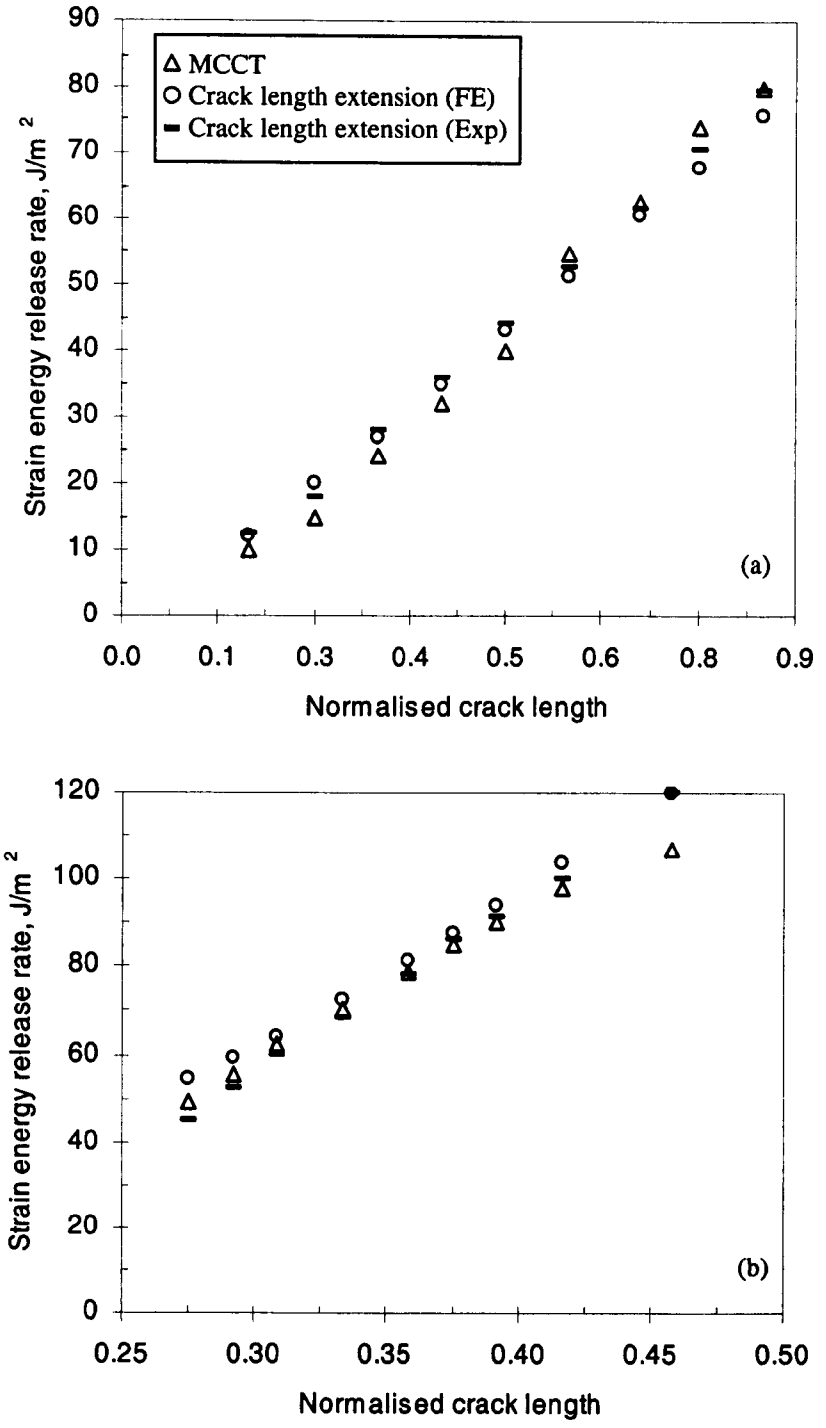

Figure 5.2.2 Comparison of the strain energy release rates calculated from experiment and finite element analysis on Structure P, (a) CNFS tests, (b) MTPB tests.

5.3 Effect of Specimen Crack Length on the Crack-Tip Loading Conditions in the CNFS, MTPB and SCSB Geometries

It has been well documented that the loading of a crack situated at a bi-material interface results in a mixed-mode loading at the crack-tip [4-8]. A purely Mode I loading applied to a bi-material crack will induce shear stresses at the crack-tip and vice versa, as the dissimilar materials try to maintain compatibility. Furthermore, the geometry of a cracked body can result in a mixed-mode loading at the crack-tip [9]. Thus, due to their dissimilar component materials and geometries, the CNFS, MTPB and SCSB sandwich specimens are likely to experience a mixed-mode loading at the crack-tip. An immediate concern is that the degree of mode-mixity may vary with the crack length of the specimens. Consequently, the finite element analyses of the three test geometries were initially used to establish the sensitivity of the crack-tip loading conditions to crack length. Here, the cracks were positioned in the core material, in accordance with the experimental observations following the CNFS and MTPB tests on Structures P to R. The results from these investigations are presented in the following sections. In each case, the crack-tip loading conditions are represented as the ratio of the Mode I strain energy release rate to the total strain energy release rate, G_I/G_T and the crack length is normalised by the specimen span. Furthermore, the G_I/G_T versus crack length analyses were also conducted on Structures Q and R, which have thicker face-sheets than Structure P.

5.3.1 The Effect of Crack Length on Crack-Tip Loading Conditions in the CNFS Specimen

The influence of crack length on the mode ratio, G_I/G_T, of the CNFS specimen is presented in Fig. 5.3.1a, where the results for Structures P to R are presented. Additionally, the predicted changes in the Mode I and Mode II strain energy release rates from the analyses of Structure P are presented, Fig. 5.3.1b, which were similar to those predicted for Structures Q and R. The results show that the crack-tip loading conditions in the CNFS specimen are highly Mode I dominated. Furthermore, an increase in crack length results in the Mode II strain energy release rate, G_{II}, becoming more dominant, until the crack length increases to 70% of the span length, after which G_{II} decreases. As the face-sheet of a CNFS specimen is loaded, membrane strains are generated which result in an axial strain being developed in the facing as indicated by the arrows in Fig. 5.3.2. This will generate forward shear conditions at the crack-tip as the adjacent core material tries to maintain compatibility with the facing. Furthermore, because this occurs symmetrically about the loading point, the core material in the vicinity of the crack-tip will be forced to displace away from the face-sheet, as indicated in the figure, resulting in the Mode I loading. The reason for the increase in G_I/G_T for a normalised crack length of greater than 70% is probably due to the Mode II causing shear conditions becoming lower, as indicated by the reduction in G_{II} for the longer crack lengths, Fig. 5.3.1b. Similar predictions have also been observed following an analysis of a blister specimen used to estimate the fracture toughness of thin films bonded to an elastic substrate [10]. Moreover, the Mode I strain energy release rate, G_I, was predicted to become more

dominant as the thickness of the specimen face-sheets is increased, although the difference in G_I/G_T between the three structures is less than 2.5%.

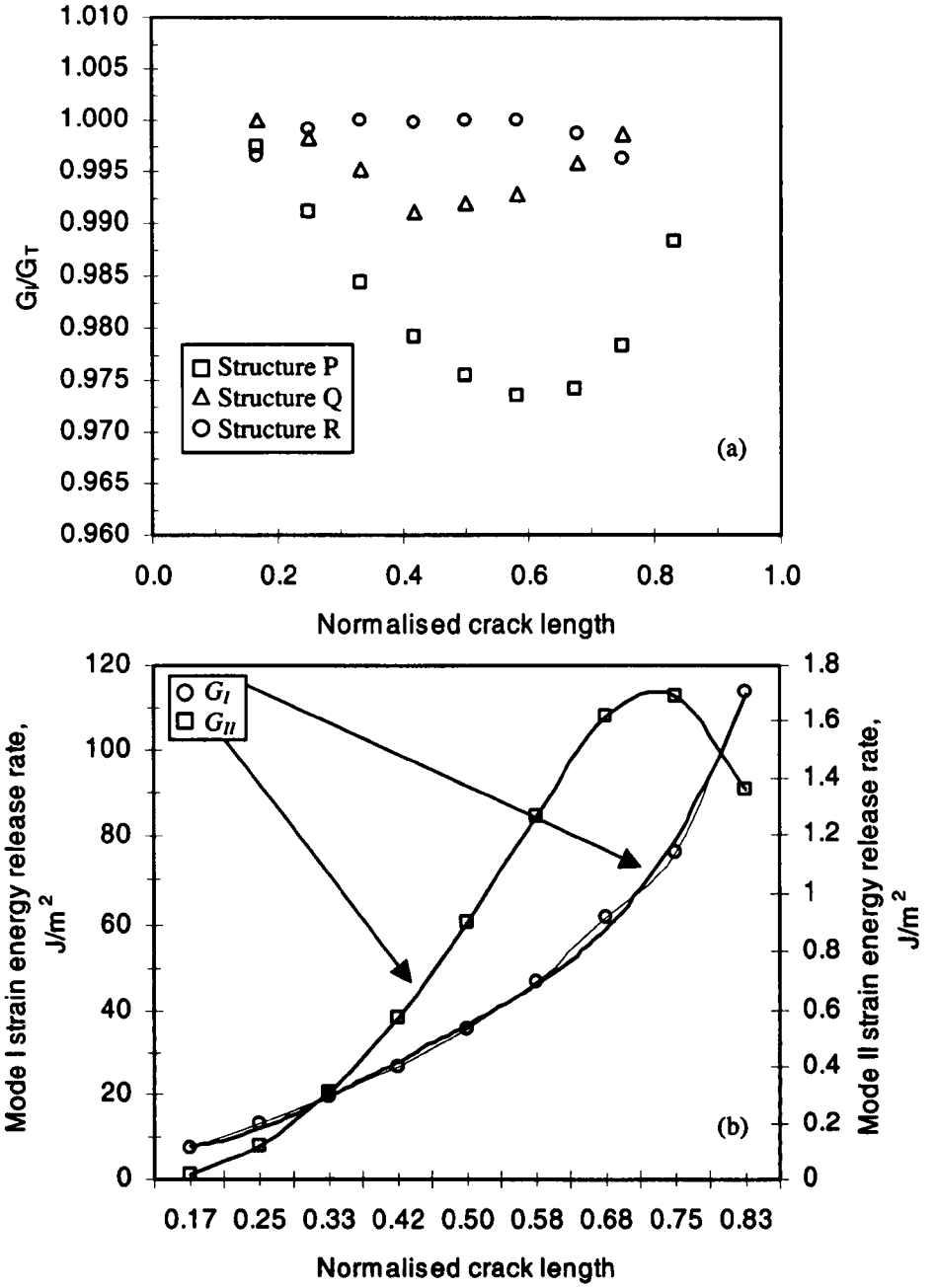

Figure 5.3.1 The effect of crack length on the mode ratio in the CNFS specimens, (a) The effect of crack length on G_I/G_T for all three structures, (b) The effect of crack length on G_I and G_{II} in the CNFS specimen of Structure P.

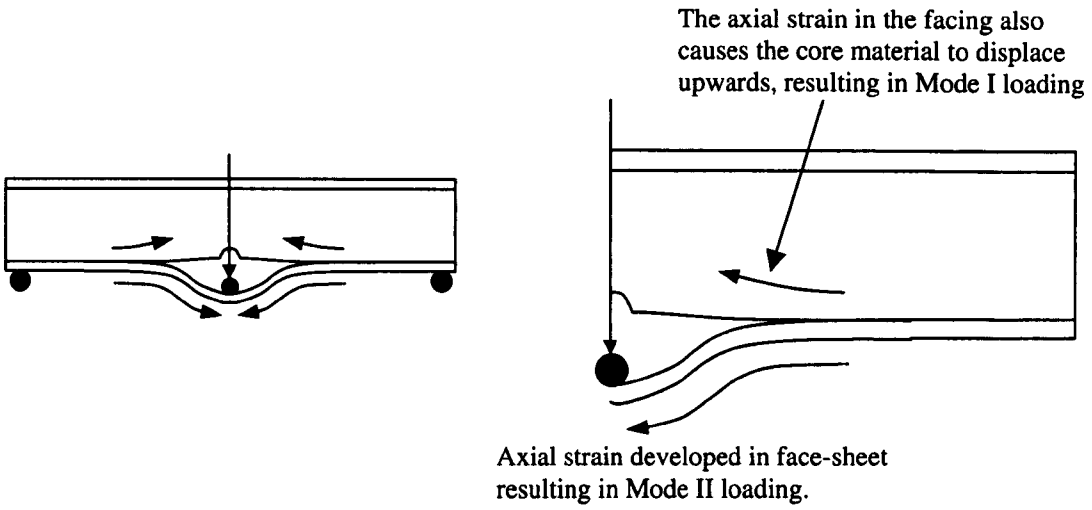

Figure 5.3.2 Illustration of the axial strain developed in the face-sheet of a CNFS specimen. It is likely that this strain contributes both to the Mode I and Mode II loading at the crack-tip of the specimen.

5.3.2 Effect of Crack Length on the Crack-Tip Loading Conditions in the MTPB Specimen

The MTPB geometry offered the most significant variation of the mode ratio with crack length, although this still corresponds to only a 3.5% decrease in the Mode I strain energy release rate, Fig. 5.3.3a. This corresponds to a more rapid increase in G_I than G_{II}, as indicated in Fig. 5.3.3b. As with the CNFS geometry, the value of G_{II} was found to become more predominant with increasing crack-length, which may be due to the increased rotation of the MTPB specimen as the crack advances, Fig. 5.3.4. Again, the relative amount of G_{II} was found to decrease as the face-sheet thickness of the MTPB specimen increased.

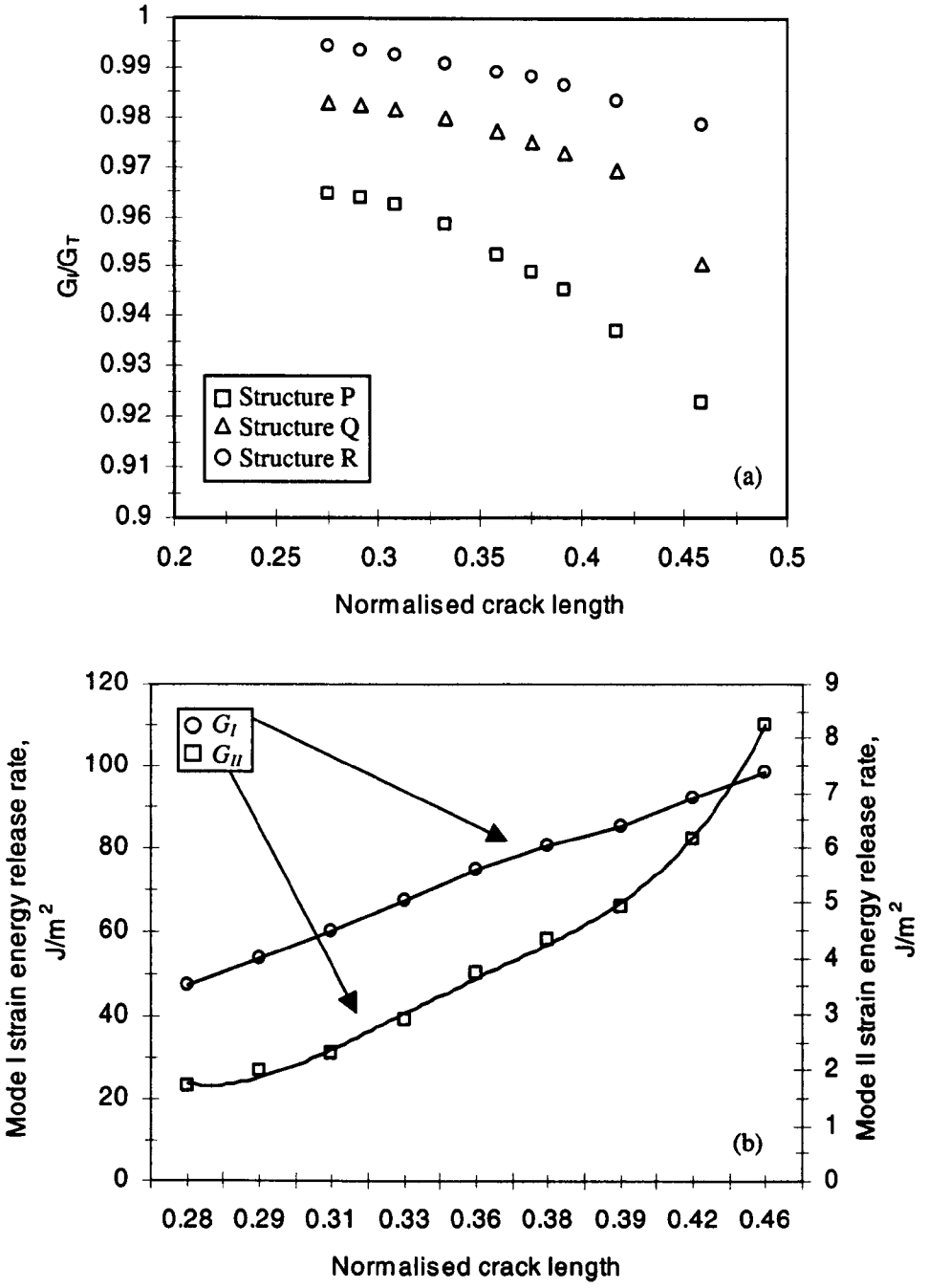

Figure 5.3.3 The effect of crack length on the mode ratio in the MTPB specimens, (a) the effect of crack length on G_I/G_T for all three Structures, (b) the effect of crack length on G_I and G_{II} in the MTPB specimen of Structure P.

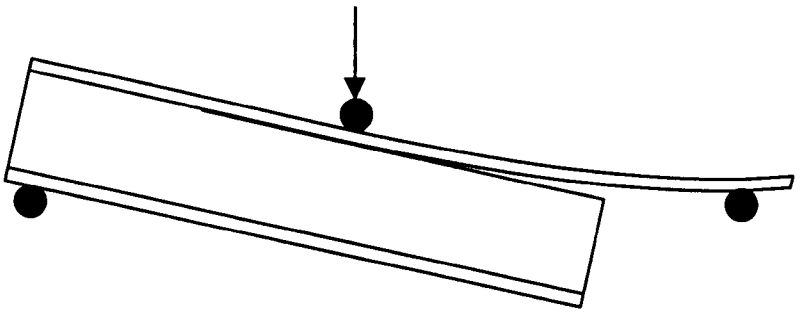

Figure 5.3.4 Illustration of the rotation exhibited by an MTPB specimen, which may lead to an increased Mode II loading at the crack-tip.

5.3.3 Effect of Crack Length on the Crack-Tip Loading Conditions of the SCSB Specimen

The mode ratios determined from the models of the SCSB tests were virtually insensitive to specimen crack length. The mode ratio was highly Mode I dominated and again, an increase in specimen face-sheet thickness resulted in a further increase in the Mode I component, as shown in Fig. 5.3.5. Unlike the previous two geometries, the SCSB does not undergo any significant rotation and the loaded face-sheet is not subjected to membrane effects as in the case of the CNFS specimen. This explains the apparent insensitivity of the mode ratio to the crack length in this case.

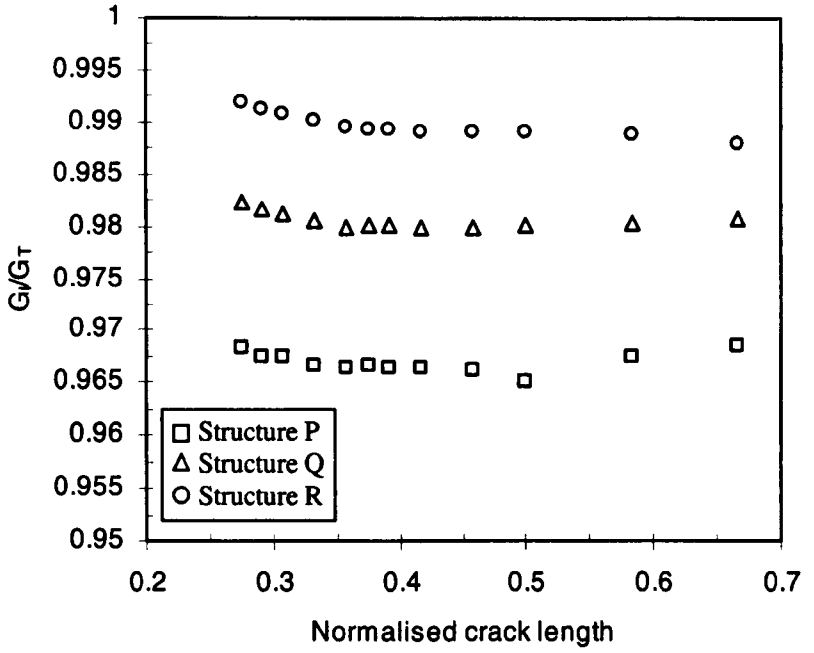

Figure 5.3.5 The effect of crack length on the mode ratio in SCSB specimens

5.3.4 Comparison of Crack-Tip Loading Conditions Between the CNFS, the MTPB and the SCSB Geometries

The mode ratio in the three specimen geometries was Mode I dominated in each case, with the CNFS geometry apparently exhibiting the largest Mode I dominance and the MTPB specimen offering the lowest degree of Mode I loading at the crack-tip. The mode ratios in the CNFS and the MTPB specimens appear to be the most sensitive to crack length, the SCSB specimen seemingly shows little dependence on crack length, Fig. 5.3.6. As discussed previously, the loaded face-sheet of the CNFS specimen is subject to a membrane effect, which appears to alter as the crack length increases. Furthermore, the MTPB specimen undergoes some rotation as the crack length increases. These are thought to be the causes of the predicted sensitivity of the mode ratio to crack length in

these two specimens. The SCSB specimen on the other hand does not encounter these effects, which is thought to be the reason for the predicted insensitivity of the mode ratio to crack length. The dominance of G_I in the three geometries was not expected, since earlier analyses on similar sandwich specimens have predicted much greater levels of Mode II loading [5,11]. However, in this case the crack was modelled in the low modulus core material (G = 50 MPa) and this is thought to be the cause of the high levels of Mode I loading. This will be discussed further in the proceeding section.

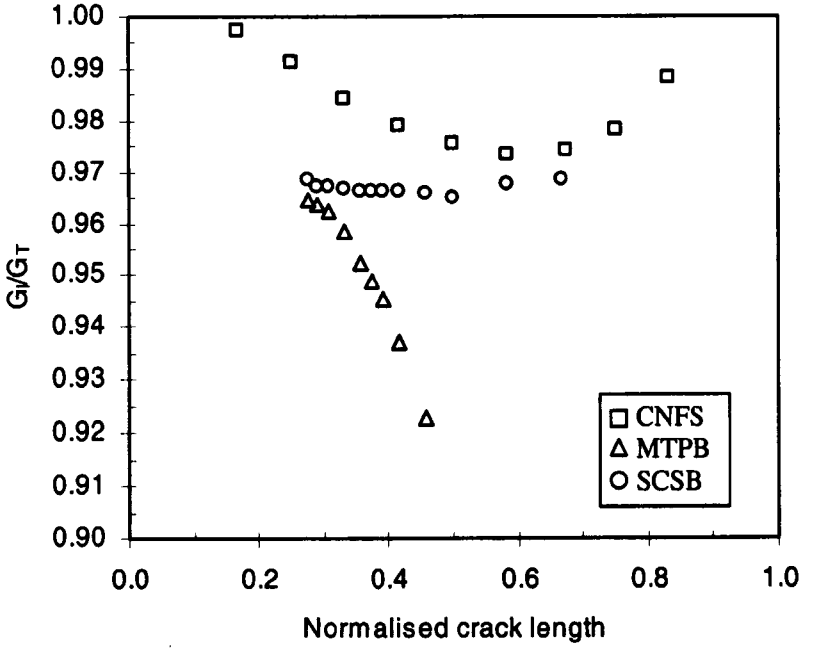

Figure 5.3.6 Comparison of the crack-tip mode ratios in the CNFS, the MTPB and the SCSB geometries of Structure P.

5.3.5 Summary

The analyses discussed above have indicated that the mode ratio in all three test specimens will be highly Mode I dominated if the crack is situated within a low-density material, such as the low density PVC foam modelled in the analyses here.

The predicted influence of crack length on the mode ratio in the CNFS specimen is likely to be due to the behaviour of the face-sheet as the crack length increases. The increase in rotation of the MTPB specimen as the crack length increases is thought to be the cause of the predicted denpendence of G_I/G_T in this instance. However, the variation in the mode ratio in each case was small (less than 3%). The mode ratio of the SCSB specimen was virtually independent of crack length. These results suggest that since these changes in mode ratio were so small, the fracture toughness values calculated over the range of crack lengths studied here for each geometry will not be affected by the changes in the mode ratio.

5.4 Effect of Crack-Tip Location on the Mode Ratio in the CNFS, MTPB and SCSB Geometries

The most common locations of crack growth observed following CNFS and MTPB tests on a number of sandwich structures were either in the low-density core material or within the face-sheet material. It is likely that the mode ratio exhibited by the three specimen types will be sensitive to the location of the crack. Consequently, the previous analyses conducted for Structure P were repeated with the crack positioned through the mid-plane

of the face-sheets, as illustrated in Fig. 5.4.1. Following a previous analysis [12], the crack was positioned in an isotropic resin layer which was assumed to be 0.02 mm thick. The crack was positioned in a resin-rich layer because the individual components of the strain energy release rate calculated using the MVCCT method become dependent on the crack-tip element length when the crack is positioned at a bi-material interface or within an orthotropic material [13].

Lastly, this investigation enabled the issues regarding the Mode I dominance in the 'core-crack' models to be discussed.

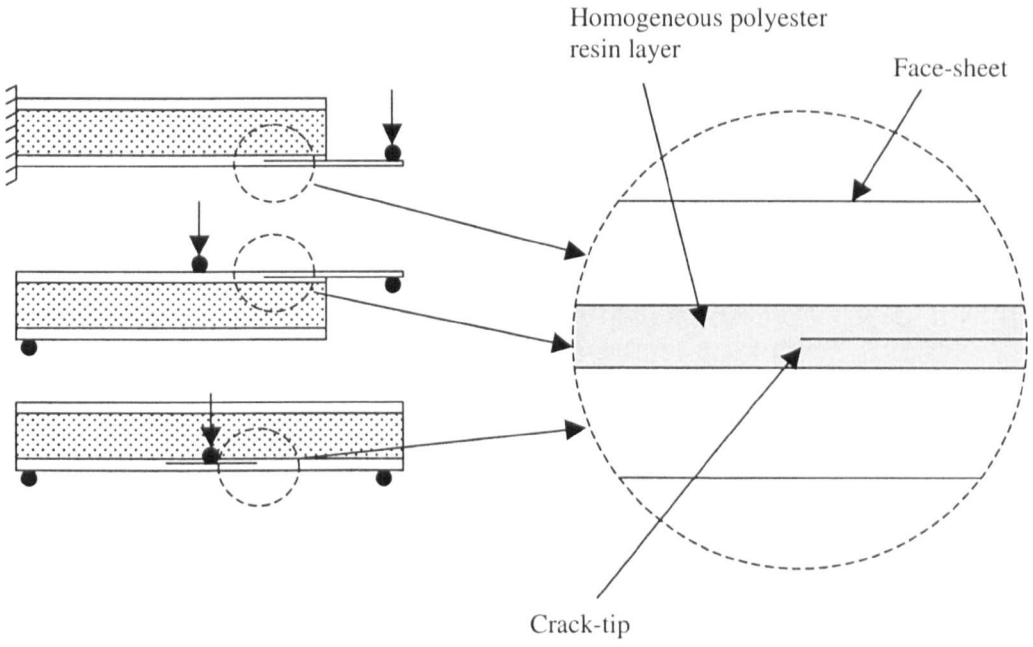

Figure 5.4.1 CNFS, MTPBS and SCSB geometries with the crack positioned in the face-sheet.

5.4.1 Effect of Crack Location on the Mode Ratio in a CNFS Specimen

Figure 5.4.2 shows that the mode ratio, G_I/G_T, decreases significantly when the crack is positioned within the face-sheet material in comparison to the mode ratios determined for the crack positioned in the core. This is likely to be due to the low compliance of the face-sheet compared to that of the core. The tendency of the face-sheet material above the crack to displace away from the crack plane will be less than that of the core material as illustrated in Fig. 5.4.3. Subsequently, the forward shear conditions generated by the membrane effect on the loaded face-sheet will become more dominant than in the case of the crack positioned in the more compliant core material, which will lead to an increase in the Mode II strain energy release rate.

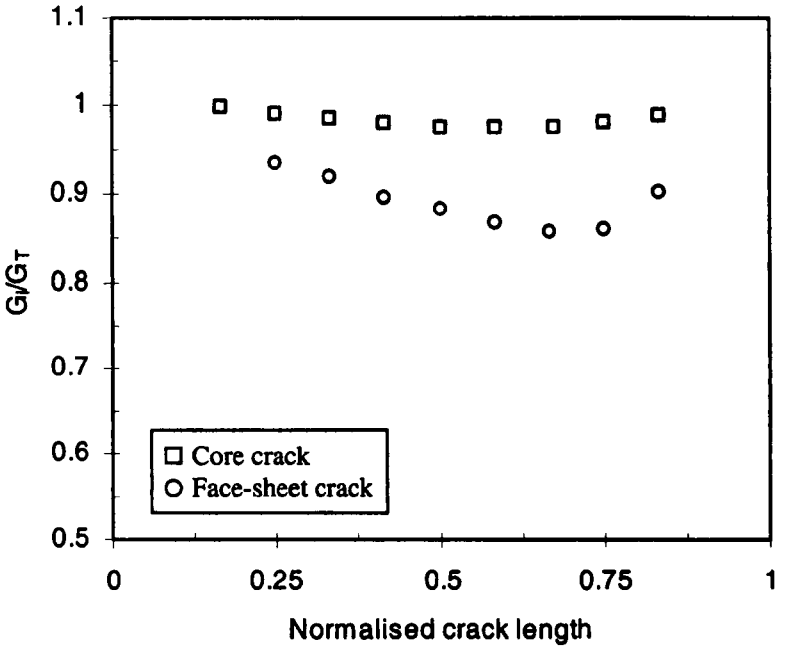

Figure 5.4.2 Effect of crack location on the mode ratio in a CNFS specimen.

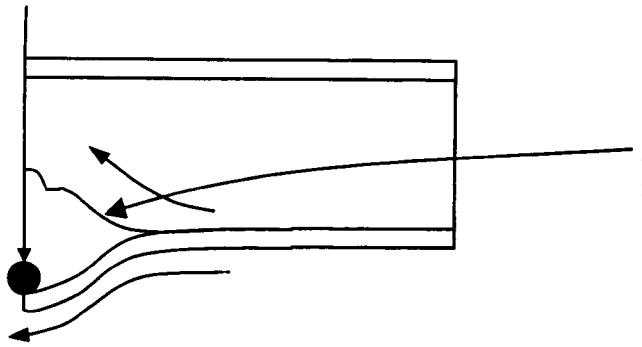

With the crack positioned within the core, the material above the crack will displace away from the crack plane as indicated.

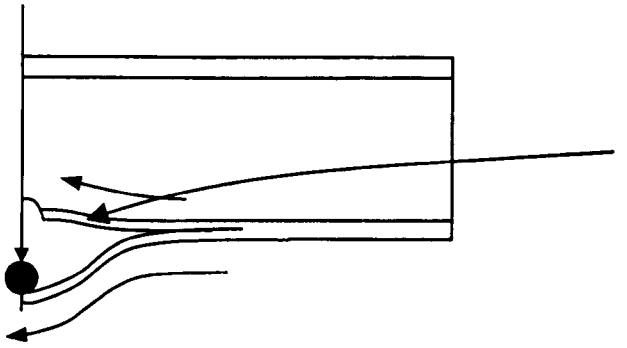

With the crack in the face-sheet, the displacement of the material above the crack away from the crack plane will be reduced in comparison to the example above.

Figure 5.4.3 The resulting difference in the compliance of the material above the crack in a CNFS specimen when the crack is positioned in the core and in the face-sheet material.

5.4.2 Effect of Crack Location on the Mode Ratio in an MTPB Specimen

Figure 5.4.4 shows the influence of crack location on the mode ratio for the MTPB geometry. Again, locating the crack within the face-sheet material results in a decrease G_I/G_T. This large reduction in the mode ratio for the crack positioned in the face-sheet is expected. This is because the MTPB configuration containing a face-sheet crack is similar to an Mixed Mode Flexure (MMF) specimen with a sandwich panel core and bottom face-sheet bonded to the upper arm of the specimen. As mentioned, the MMF specimen yields a mode ratio, G_I/G_T, of 57% when the upper and lower arms of the

specimen are equal [2]. The results presented here give similar values when the crack is positioned within the face-sheet-material. Additionally, it has been demonstrated that the mode ratio for MMF specimens will be greater than 57% when the upper arm is thinner than the lower arm [3]. This provided a means with which to tests the validity of the analyses conducted within. To achieve this, the 'core crack' MTPB models of Structure P were repeated with the core and face-sheet mechanical properties assumed to be the same isotropic material (Young's modulus 70 GPa and Poisson's ratio 0.3). Under these circumstances, the MTPB specimen approximates to the MMF specimen with $h_1/2h$ = 0.09, as illustrated in Fig. 5.4.5. The resulting FE solutions, Fig. 5.4.6, predicted that the mode ratio remains reasonably constant with crack length, at a value of approximately 0.67. This compares to a mode ratio of 0.65 predicted during a detailed study of the MMF specimen [3]. The FE solutions are therefore in good agreement (3% difference) with previous findings, lending weight to the accuracy of the present work.

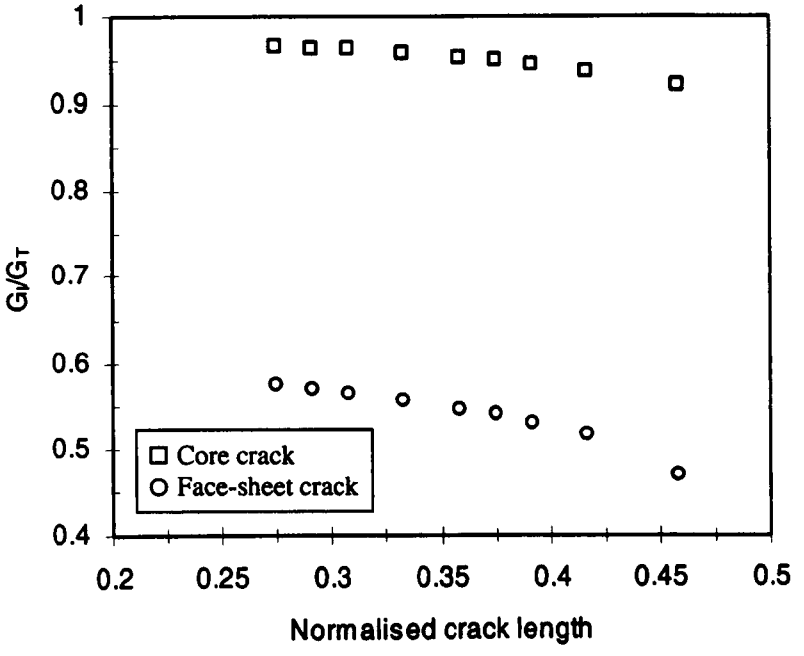

Figure 5.4.4 Effect of crack location on mode ratio in the MTPB specimen of Structure P.

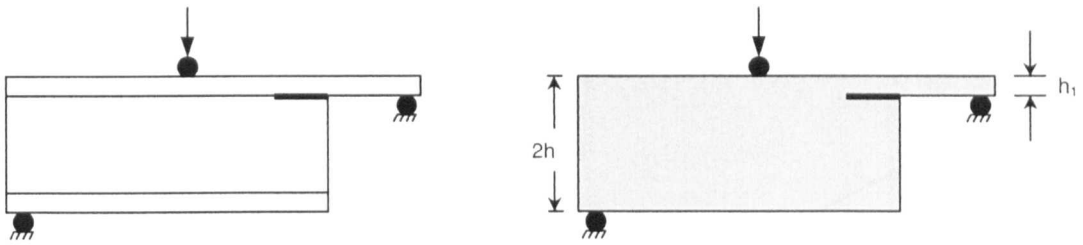

Figure 5.4.5 The MTPB specimen becomes equivalent to the MMF specimen when the core properties equal the facing properties $E_C=E_F$.

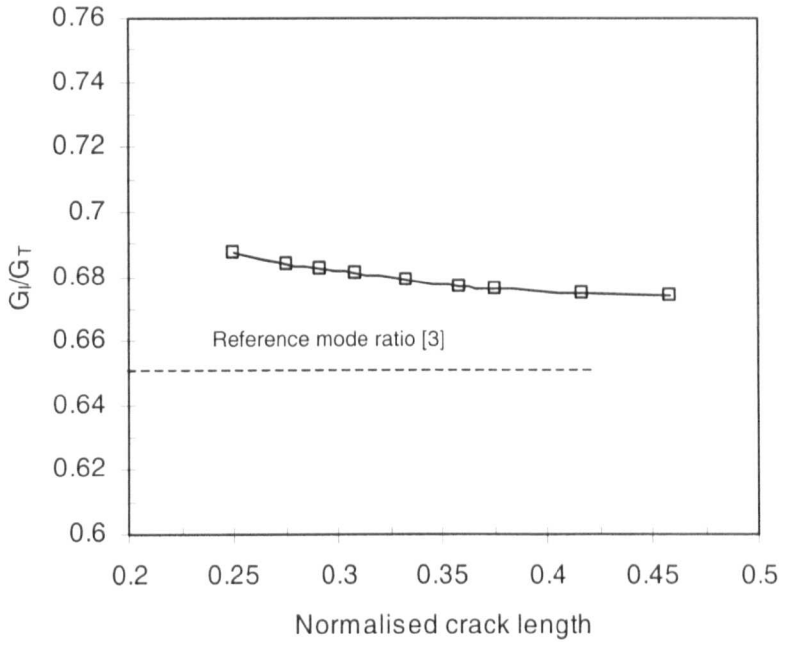

Figure 5.4.6 Predicted mode ratio in the MTPB geometry when $E_C=E_F$.

5.4.3 Effect of Crack Location on the Mode Ratio in a SCSB Specimen

Again, the FE solutions predicted a significant increase in the Mode II component when the crack is located within the skin material, Fig. 5.4.7. Previous work predicted similar values for the mode ratio for an asymmetric beam specimen [4], to which the SCSB

specimen approximates when crack growth is located within the face-sheet as illustrated in Fig. 5.4.8. In the previous study, G_I/G_T was estimated to be 57% when the upper and lower arms of the specimen were equal in thickness [4]. Additionally, G_I/G_T was shown to increase up to a limit of 62.4% as the ratio of the upper to lower arm thicknesses increased, [4]. This is lower than the value predicted by the FE solutions here, which estimated G_I/G_T to be equal to 79%. One reason for this disparity is that, the reference work assumed that the asymmetric beam specimen to be comprised of the same material throughout, which is not the case here. It is likely again that the core material is the reason for high mode ratio value calculated here, compared to the values calculated for the asymmetric beam specimen. To test this hypothesis, the SCSB 'face-sheet crack' model of Structure P was repeated with the properties of the core and the face-sheets both assumed isotropic (Young's modulus 70 GPa and Poisson's ratio 0.3), thereby emulating an asymmetric beam specimen in which $h_2/(h_1+h_2)=0.023$, Fig. 5.4.8. The results from this study are presented in Fig. 5.4.9 and agree closely (within 5%) with the mode ratios calculated for this specimen previously [4].

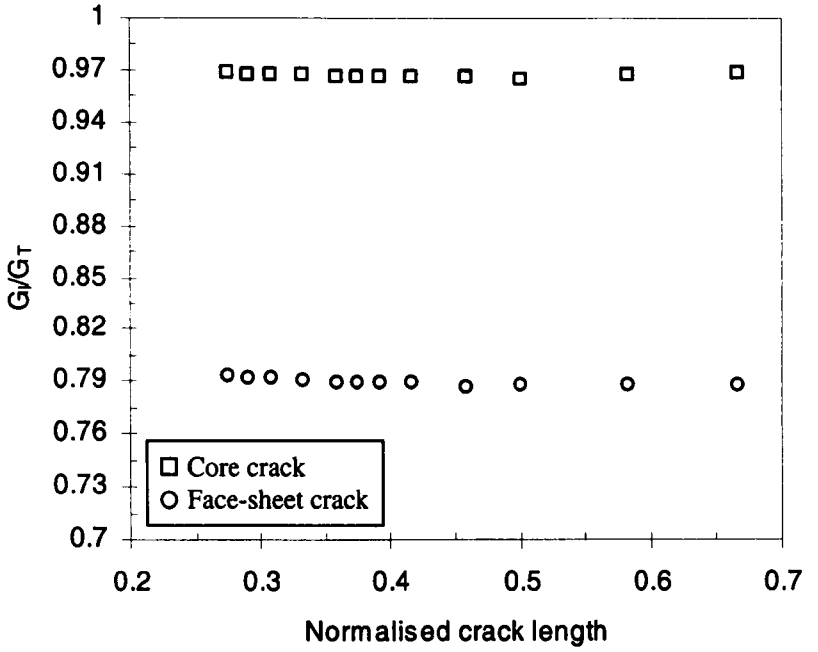

Figure 5.4.7 Effect of crack location on the mode ratio in a SCSB specimen of Structure P.

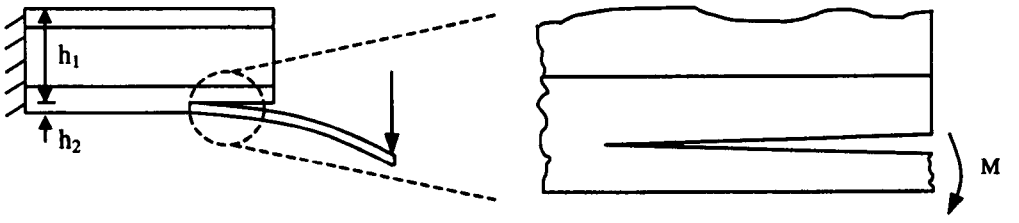

Figure 5.4.8 The SCSB specimen approximates to the asymmetric beam when the SCSB crack is positioned within the face-sheet material.

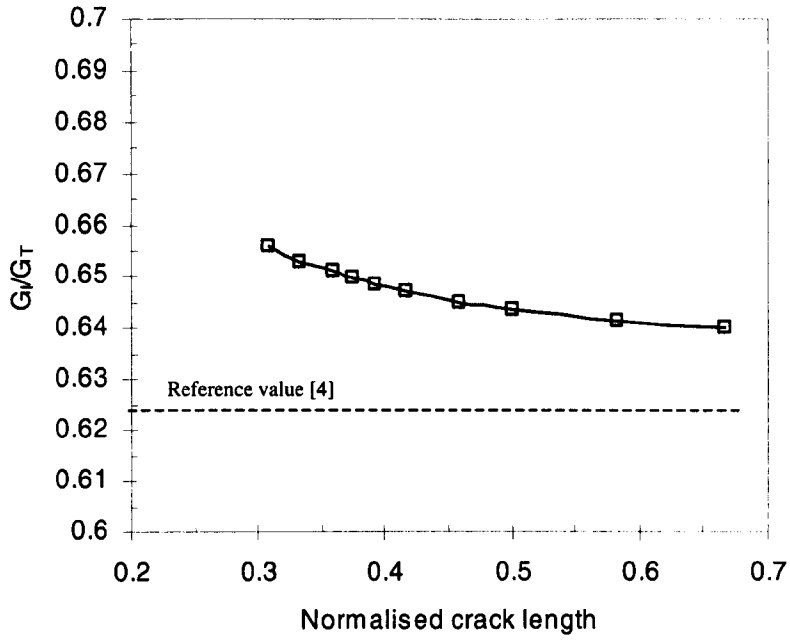

Figure 5.4.9 Variation of mode ratio with crack length for a SCSB specimen when the properties of the core and facing are the same.

The high level of agreement between this analysis and previous calculations supports the accuracy of the mode ratios calculated for the SCSB specimen.

5.4.4 Summary

The results discussed in this section indicated that the three test configurations offer highly Mode I dominated loading where crack propagation occurs within a low-modulus core material. Furthermore, the FE solutions predict a large increase in Mode II loading when the crack is positioned within the face-sheet material. The validity of these results has been established through comparisons with previous work, giving confidence to the accuracy of the results presented herein and supporting the contention that the low

modulus core material is responsible for the low values of G_{II} calculated here. Table 5.4.1 summarises the findings from these analyses.

Effect of crack location on G_I/G_{II}		
Geomerty	**G_I/G_{II} (Core crack)**	**G_I/G_{II} (Face-sheet crack)**
CNFS	0.98	0.80
MTPB	0.95	0.55
SCSB	0.97	0.79

Table 5.4.1 The influence of crack location on the mode ratio in the three specimen geometries.

From the table, it is clear that crack growth in all three specimen geometries will remain Mode I dominated when the crack is located in both the positions indicated, although the MTPB geometry is predicted to exhibit the most significant decrease in G_I/G_{II}.

5.5 The Effect of Core and Face-sheet Mechanical Properties on the Mode Ratio in the Three Specimen Geometries

Here, a series of finite element analyses of CNFS specimens based on Structure P were conducted using a range of core and face-sheet mechanical properties as outlined in Section 3.6.3. The aim of this investigation was to determine the sensitivity of the mode ratio in the CNFS specimens to the changes in the core and face-sheet mechanical

properties. Both the 'face-sheet crack' and 'core crack' models were used in this investigation.

5.5.1 The Effect of Core and Face-sheet Properties on the Mode Ratio in a CNFS Specimen Containing a Core Crack

Figures 5.5.1 and 5.5.2 show the effect of increasing the core modulus on the mode ratio. Here, the core modulus has been normalised by the modulus of the face-sheet in the span direction, E_{11} and is denoted by E_C/E_F. This result shows that the mode ratio is most sensitive to a change in the core modulus for the smaller values of the ratio, E_C/E_F. Whereas, the mode ratio becomes less sensitive to changes in the core modulus at higher values of this property. The result also confirms that the Mode II strain energy release rate diminishes with decreasing core modulus. As the core modulus increases, the Mode I strain energy release rate decreases as expected, because the crack opening displacement will decrease as the core modulus increases. However, the Mode II component is predicted to increase to a limiting value as shown in the figure below. The reasons for this are unclear, although it may be possible that the axial strains developed in the face-sheet remain virtually unaltered as the core modulus increases. Therefore, as the core modulus increases, the work done required to close the crack-tip in shear would increase and assuming the shear displacements at the crack-tip are unaltered this would lead to an increase in G_{II}. Furthermore, this decrease in the mode ratio appears to have a limiting value of approximately 0.6.

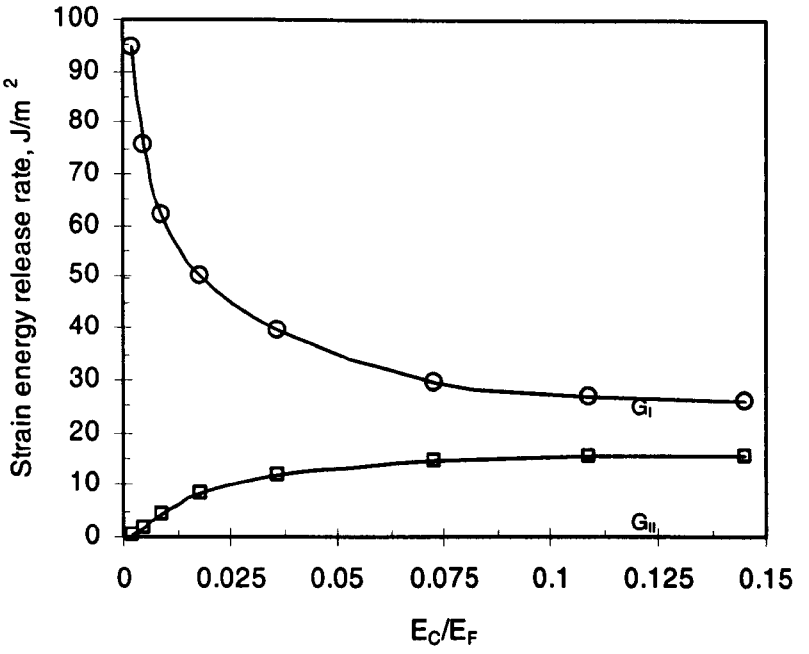

Figure 5.5.1 Effect of core modulus on the mode ratio of a CNFS specimen (Structure P) when the crack is located in the core material.

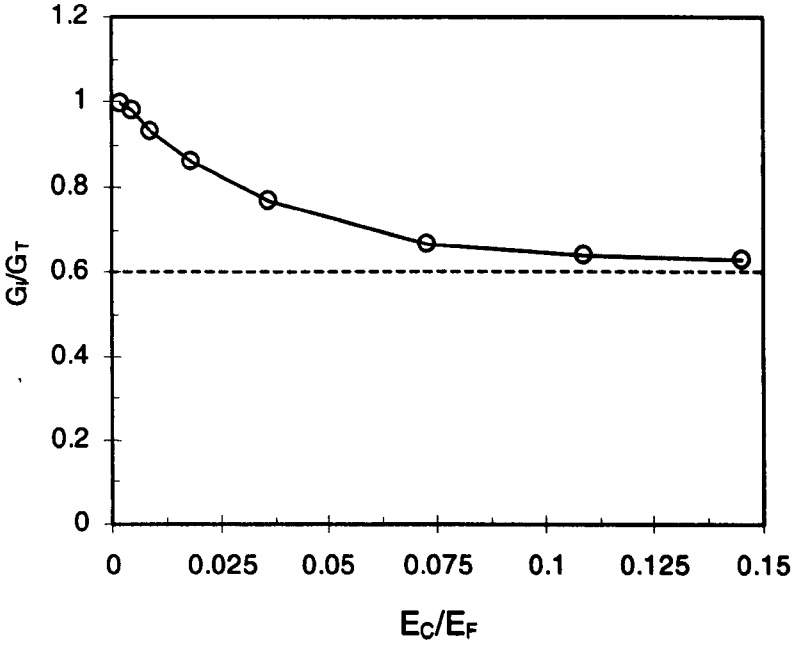

Figure 5.5.2 Effect of core modulus on the mode ratio of a CNFS specimen (Structure P) when the crack is located in the core material.

The influence of the mechanical properties of the face-sheets on the mode ratio of this CNFS specimen is shown in Fig. 5.5.3. Here, the face-sheet modulus, E_{11}, is normalised by the core modulus and denoted as E_F/E_C. These results concur with those above, in that a decrease in E_F/E_C leads to a reduction in the mode ratio and vice versa. The result also predicts that the Mode II component tends towards a limiting value for very high ratios of E_F/E_C. Figure 5.5.3 shows that an increase in the face-sheet stiffness reduces both the Mode I and Mode II strain energy release rate components. This is possibly explained by the fact that the crack opening and crack shear displacements will decrease as the face-sheet stiffness increases.

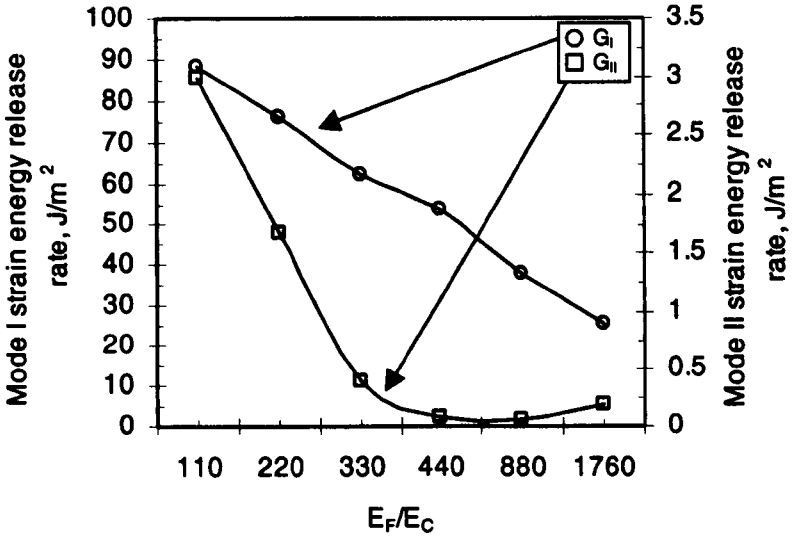

Figure 5.5.3 The effect of face-sheet mechanical properties on the mode ratio in a CNFS specimen with a crack located in the core material.

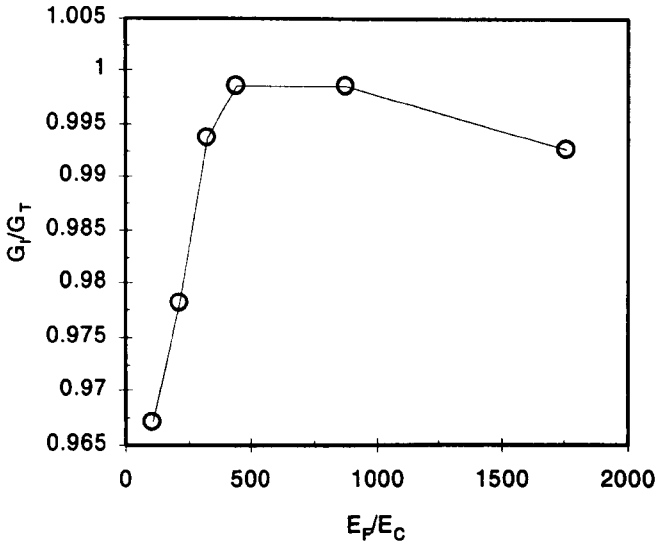

Figure 5.5.4 The effect of face-sheet mechanical properties on the mode ratio in a CNFS specimen with a crack located in the core material.

5.5.2 Effect of Core and Face-sheet Properties on the Mode Ratio of a CNFS Specimen Containing a Face-sheet Crack

In a manner similar to the 'core crack' CNFS model of Panel P, the FE solution here predicts an increase in the mode II component and a corresponding decrease in G_I, as E_C increases, Fig. 5.5.5. Here, the mode ratio tends towards a value of 0.36 as the core modulus is increased.

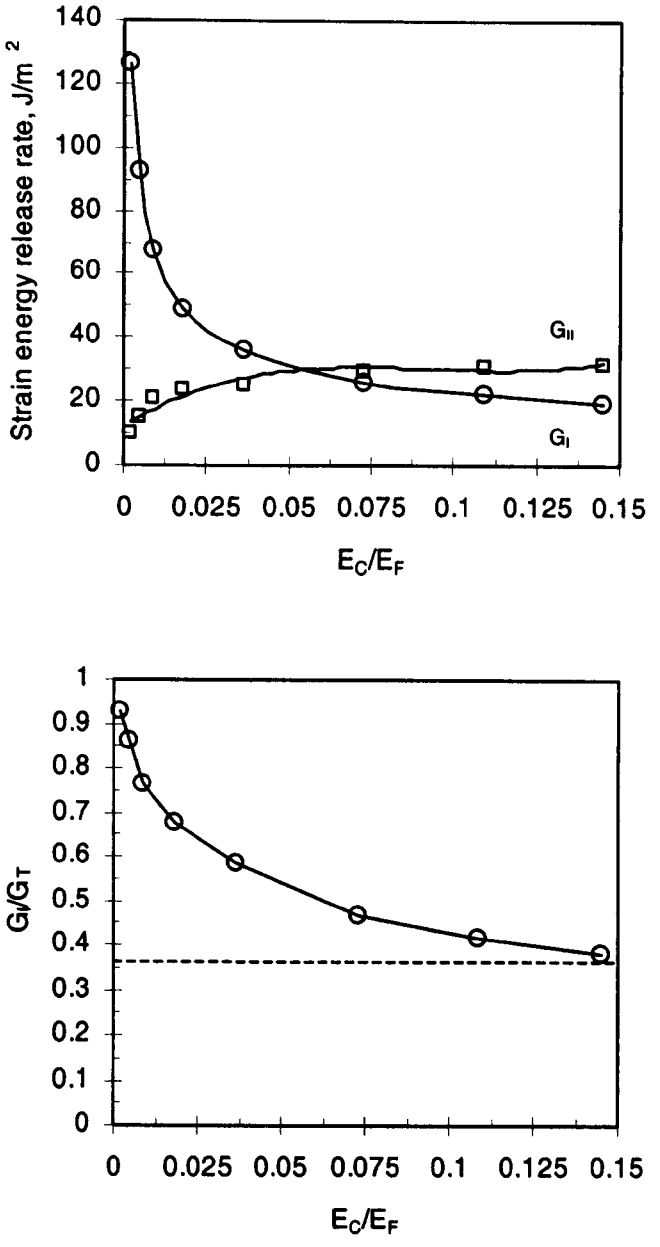

Figure 5.5.5 The effect of core modulus on the mode ratio in a CNFS specimen containing a face-sheet crack.

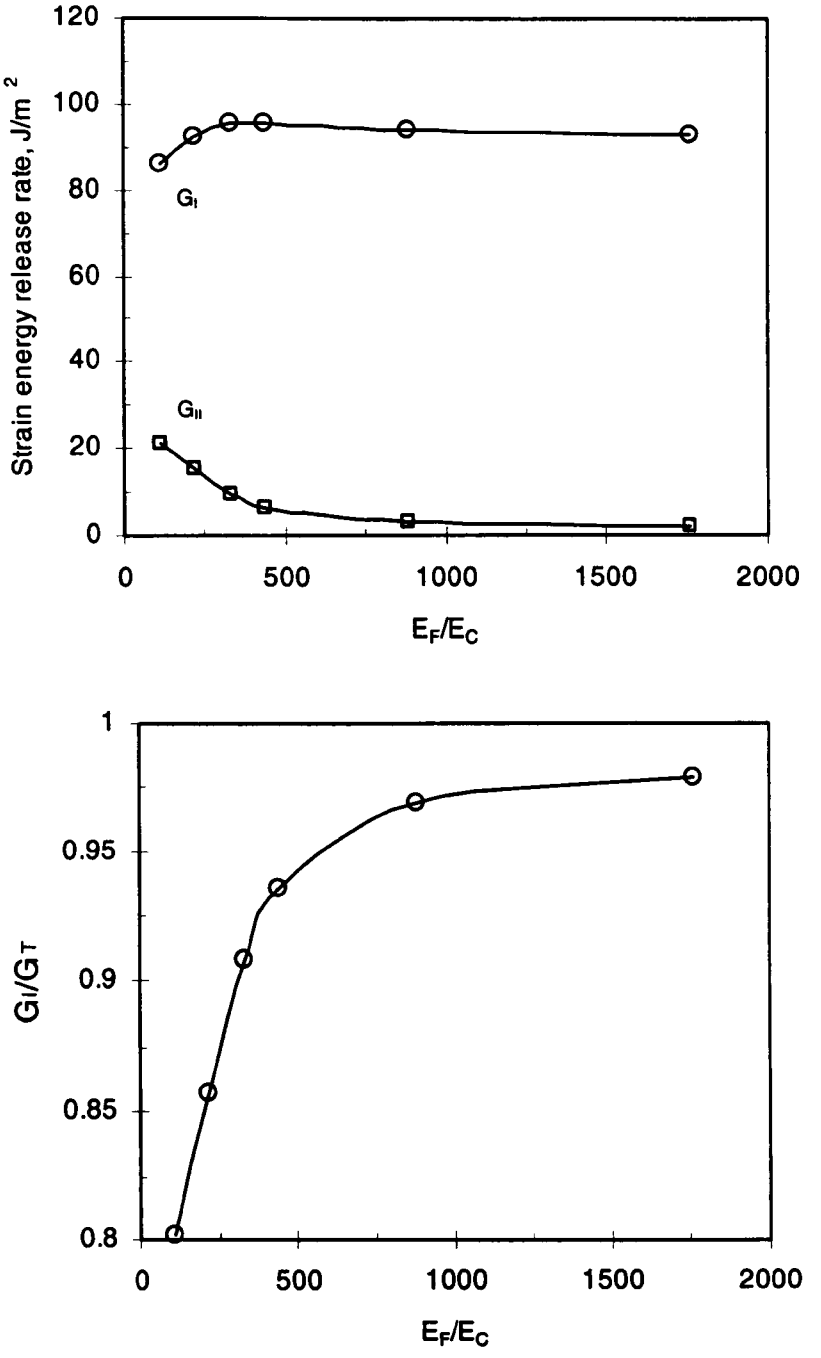

Figure 5.5.6 The effect of face-sheet mechanical properties the mode ratio in a CNFS specimen containing a face-sheet crack.

An increase in the stiffness of the face-sheets in the CNFS specimen containing a crack in the facing caused a significant reduction in the Mode II strain energy release rate, as shown in Fig. 5.5.6, where again the mode ratio tended towards a limiting value as the face-sheet stiffness was increased.

5.5.3 Summary

The parametric studies discussed in this section were also carried out for the MTPB and the SCSB configurations. The results from these two sets of investigations echoed the findings discussed in this section and, therefore, the results are not presented. In general, four key conclusions were drawn from the investigations, which are true for all three specimen geometries:

- The mode ratio, G_I/G_T decreases as the ratio of the core modulus to the facing modulus, E_C/E_F increases and vice versa. For all three specimen geometries, the mode ratio was found to be Mode I dominated for a core material with an intermediate or low-modulus core.
- The sensitivity of the mode ratio, G_I/G_T, to the core modulus, E_C, increases with decreasing values of E_C/E_F and vice versa.
- The sensitivity of the mode ratio, G_I/G_T, to the facing modulus, E_F, increases with decreasing values of E_F/E_C and vice versa.
- The mode ratio is most sensitive to changes in core modulus than the stiffness properties of the face-sheets.

5.6 The Influence of Face-sheet Thickness on the Crack Length Extension Factor

The solutions from the FE analyses were used to investigate the effect of face-sheet thickness on the crack length correction factor, Δ, used in both the finite element analyses and the fracture toughness calculations following the experimental fracture tests. Compliance calibration curves for Structures P to R were plotted for the CNFS, MTPB, and SCSB geometries using the FE predictions. The subsequent cube root of compliance versus crack length curves for the CNFS, MTPB and SCSB models are presented in Figures 5.6.1-5.6.3 respectively. The right hand graph in each figure is an enlargement of the left hand plot, to aid the illustration.

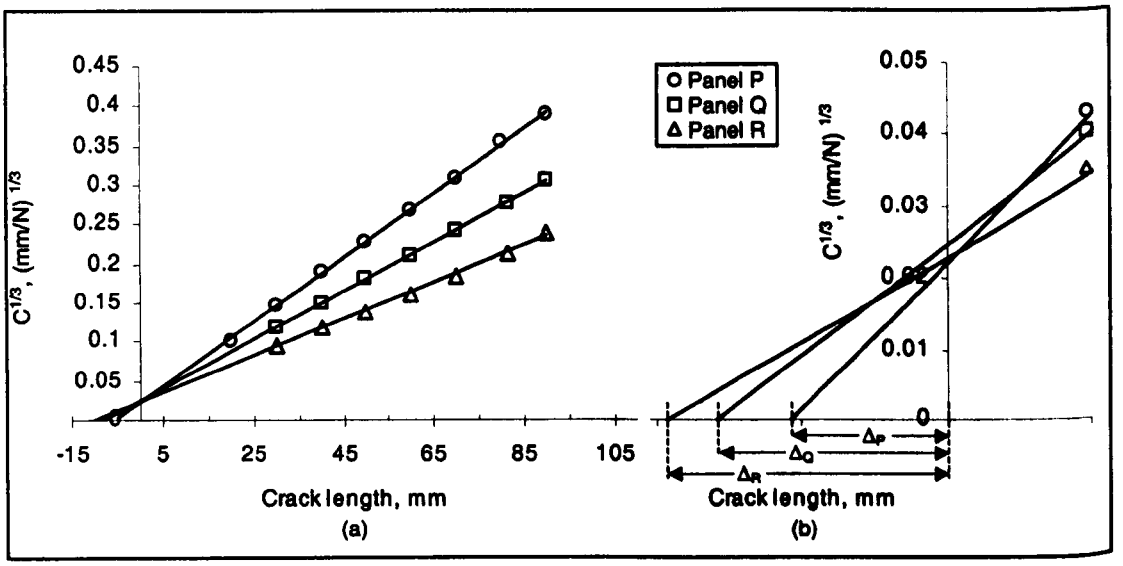

Figure 5.6.1 The effect of face-sheet thickness on Δ – CNFS geometry.

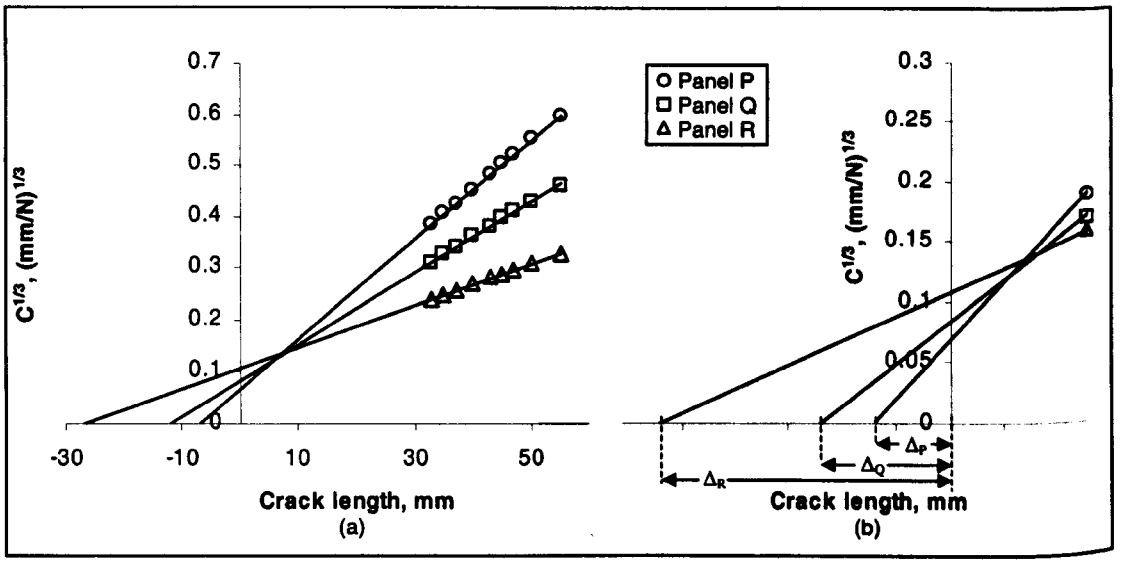

Figure 5.6.2 The effect of face-sheet thickness on Δ – MTPB geometry.

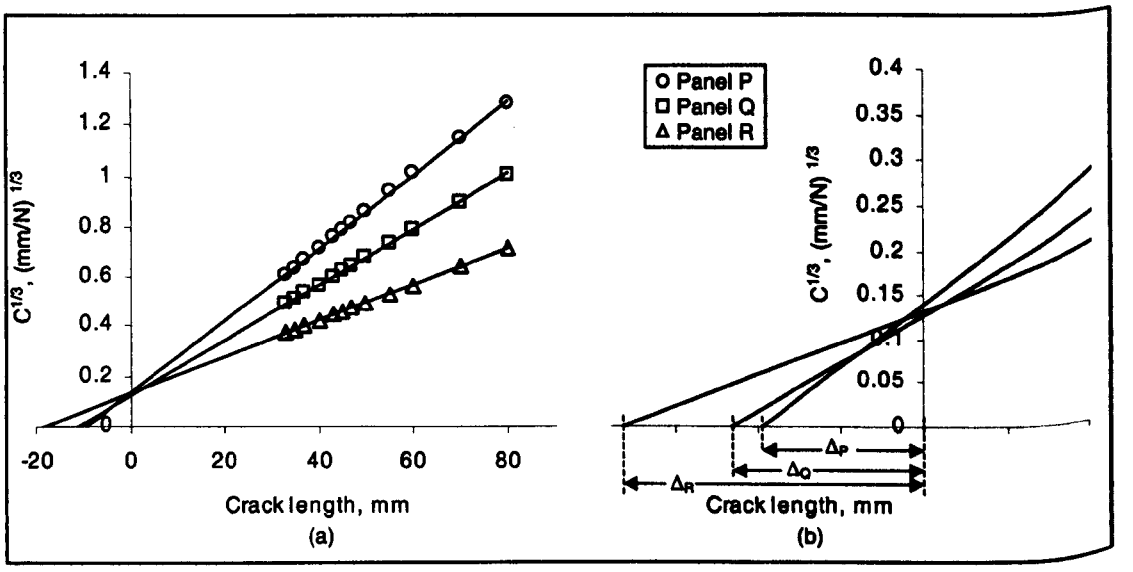

Figure 5.6.3 The effect of face-sheet thickness on Δ – SCSB geometry.

Here, the FE solutions for the CNFS, MTPB, and SCBS specimens based on Structures P to R predict an increase in the crack length correction factor, Δ, as the face-sheet thickness increases. This result agrees with the experimental data, which demonstrated the same trend, Fig. 6.4.4. The equation used in the crack length extension factor to express the change in specimen compliance with crack length, Eqn. 3.5.7, is based on the beam theory expression for the deflection of a beam where the constant, m, is inversely proportional to the flexural rigidity of the beam. As the gradient of the lines in Figs. 5.6.1 – 5.6.3 is equal to m, this value is expected to decrease with increasing face-sheet thickness and, therefore result in a larger value of Δ. Table 5.6.1 summarises the effect of face-sheet thickness on the two correction factors for the three test configurations. Here, the FE predictions for the TPBS specimens are compared with the corresponding experimental data, which are given in parenthesis.

Face-sheet thickness	**CNFS**	**MTPB**	**SCBS**
mm	**Δ, mm**	**Δ, mm**	**Δ, mm**
1	5.4	7.1 (6.6)	9.7
2	7.9	12.1 (13.5)	11.4
4	9.5	26.9 (27.1)	18.0

Table 5.6.1 The effect of face-sheet thickness on the crack length extension factor, Δ. FE model data from analysis of Structures P to R. Numbers in parenthesis denote experimentally determined values.

5.7 Summary

The finite element analyses conducted herein suggested that in the test configurations studied, crack propagation will be Mode I dominated when crack growth occurs in a low-modulus core material. The CNFS configuration was predicted to offer the highest percentage of Mode I loading, followed by the SCBS specimen, with the MTPB specimen predicted to offer the most amount of Mode II loading. Further investigations revealed that the Mode II component is significantly increased to values expected from the literature, for crack propagation in stiffer core materials. These findings have been verified by comparing the prediction of the present analyses with previous FE studies [3,4], in addition to close agreement of the preliminary models with experimental data. Crack propagation within the face-sheet material was observed to increase the Mode II component of loading for all three test configurations. An increase in face-sheet stiffness was predicted to diminish the amount of Mode II loading, irrespective of the location of the crack growth, although this effect was small. This was supported by the prediction that an increase in the face-sheet/core stiffness ratio will result in a lower amount of Mode II loading.

The investigations into the effect of sandwich panel mechanical properties on the mode ratio of each test configuration predicted a larger amount of Mode II loading as the core stiffness is increased. This corresponded to the same trend being predicted for decreasing face-sheet stiffness. The FE models were also used to study the effect of face-sheet thickness on the crack length extension factor. Again, experimental data was shown to corroborate these predictions.

5.8 References

[1]. Russell, A.J. and Street, K.N., ASTM STP 876, 1985, pp349-370.

[2]. Williams, J.G., International Journal of. Fracture, Vol.36, 1988, pp101-119.

[3]. Shim J.Y. and Hong C.S., Journal of Reinforced Plastics and Composites, Vol.12, 1993, pp1295-1310.

[4]. Charalambides M., Kinloch A.J., Wang Y. and Williams J.G., International Journal of Fracture, Vol.54, 1992, pp269-291.

[5]. Prasad S. and Carlsson L.A., Engineering Fracture Mechanics, Vol.47, 1994, pp813-824.

[6]. Sun C.T. and Manoharan M.G., Journal of Composite Materials, Vol.23, 1989, pp460-478.

[7]. Comninou M., Engineering Fracture Mechanics, Vol.37, 1990, pp197-208.

[8]. Kinloch A.J., Adhesion and Adhesives, Science and Technology, Chapman and Hall, London, 1983, p274.

[9]. Ratcliffe J. and Cantwell W.J., Journal of Materials Science Letters, Vol.19, 2000, pp1365-1367.

[10]. Andrews E.H., Stevenson A., Journal of Materials Science, Vol.13, 1978, pp1680-1688.

[11]. Cantwell W.J., Scudamore R.J., Davies P. and Ferrer J-B., Proc. Eleventh International Conference on Composite Materials, Woodhead, 1997, pp905-914.

[12]. Dattaguru B., Venkatesha K.S., Ramamurthy T.S. and Buchholz F.G., Engineering Fracture Mechanics, Vol.49, 1994, pp451-463.

[13]. Raju I.S., Crews J.H. and Aminpour M.A., Engineering Fracture Mechanics, Vol.30, 1988, pp383-396.

6. EXPERIMENTAL RESULTS/DISCUSSION

6.1 Introduction

This chapter presents the results from CNFS and MTPBS tests on the honeycomb, balsa and the PVC foam-based sandwich structures according to the procedures detailed in Chapter 4. Furthermore, the results are accompanied by corresponding discussions.

6.2 Development of a New Test Method for Characterising the Interfacial Fracture Toughness of Sandwich Structures with Thin Face-Sheets

The findings of the investigations conducted in order to develop a new fracture test method are presented in this section.

6.2.1 Selection of Test Method from Two Specimen Configurations Designed for Testing Thin-skinned Sandwich Laminates

As detailed in Section 4.3.1, two specimen geometries were designed to conduct interfacial fracture tests on sandwich laminates based on thin face-sheets, namely the asymmetric sandwich peel test (ASPT) and the centre notch flexure sandwich specimen test (CNFS). Both of the test geometries were used to perform fracture tests on Structure G, in order to highlight the most appropriate method for characterising the interfacial fracture properties of sandwich specimens containing thin face-sheets. Structure G was

chosen for this investigation, since it is based on thin (0.5 mm thickness) unidirectional glass/epoxy face-sheets. Here, 20 mm wide specimens were used for both test methods and pre-cracks of approximately 30 mm were introduced into each specimen. Figure 6.2.1 presents the typical load-displacement traces following ASPT and CNFS tests on Structure G.

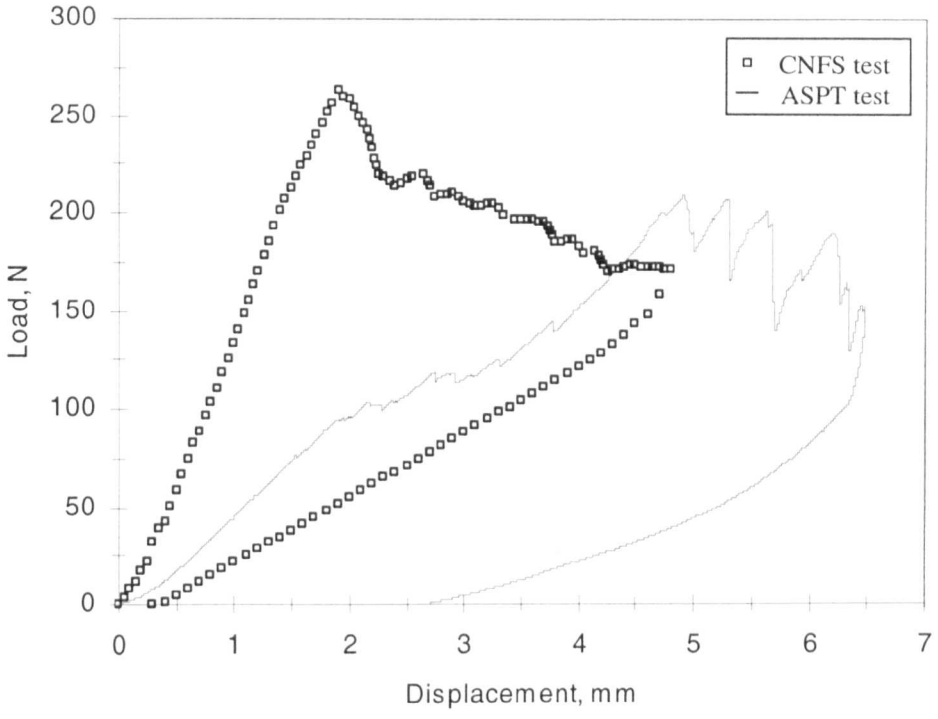

Figure 6.2.1 Load-displacement response from ASPT and CNFS tests on Structure G.

The load-displacement response of the ASPT test differs significantly from that of the CNFS test. The initial loading curve of the ASPT test was linear up to fracture initiation which occurred at approximately 100 N. Further loading resulted in a small amount of crack growth, corresponding to the jagged portion of the loading curve shown in Fig.

6.2.1. At approximately 130 N the crack growth was arrested and was proceeded by further specimen loading. Finally at 200 N the crack propagation restarted in a highly unstable manner, involving crack growth between the 0° and 90° plies of the face-sheet material. This unstable form of crack growth is likely to be a consequence of the crack-tip loading conditions within the ASPT specimen. In this geometry, the applied load introduces a large axial strain in the face-sheet, resulting in a significant component of Mode II loading at the crack-tip. It is this Mode II loading that is considered to result in the unstable crack propagation observed during the ASPT test. At the end of the test, the ASPT specimen was unloaded, resulting in a non-linear unloading curve and a residual displacement of 2.5 mm after the complete removal of the load. An inspection of this specimen revealed that the core material exhibited plastic deformation during the test, which is thought to be the reason for the non-linear unloading curve and the residual displacement. In contrast, the loading curve for the CNFS specimen was linear up to the point of fracture initiation, after which crack growth occurred in a more stable manner than that observed in the ASPT specimen. This increased stability of the crack growth was attributed to the crack-tip loading conditions experienced by the CNFS specimens. A finite element analysis of a CNFS specimen containing a crack within the face-sheet material, indicated that the crack-tip loading conditions are Mode I dominated when the ratio of the face-sheet stiffness to the core modulus is less than 0.025, as is the case here. This is a loading condition that is expected to result in a more stable form of crack propagation. Additionally, the unloading curve of the CNFS specimen was linear and a small residual displacement of approximately 0.5 mm remained after complete removal

of the load. On the basis of these findings, the CNFS configuration was selected for the fracture tests conducted in the duration of this research programme.

6.2.2 Comparison of the Interfacial Fracture Toughness Calculated Using Different Data Reduction Methods – CNFS tests on Structure G

Following CNFS tests on Structure G, the compliance calibration and the crack length extension factor methods were used to calculate the interfacial fracture toughness. Figure 6.2.2 presents the fracture toughness values of the face-sheet/core interface obtained using the two data reduction techniques.

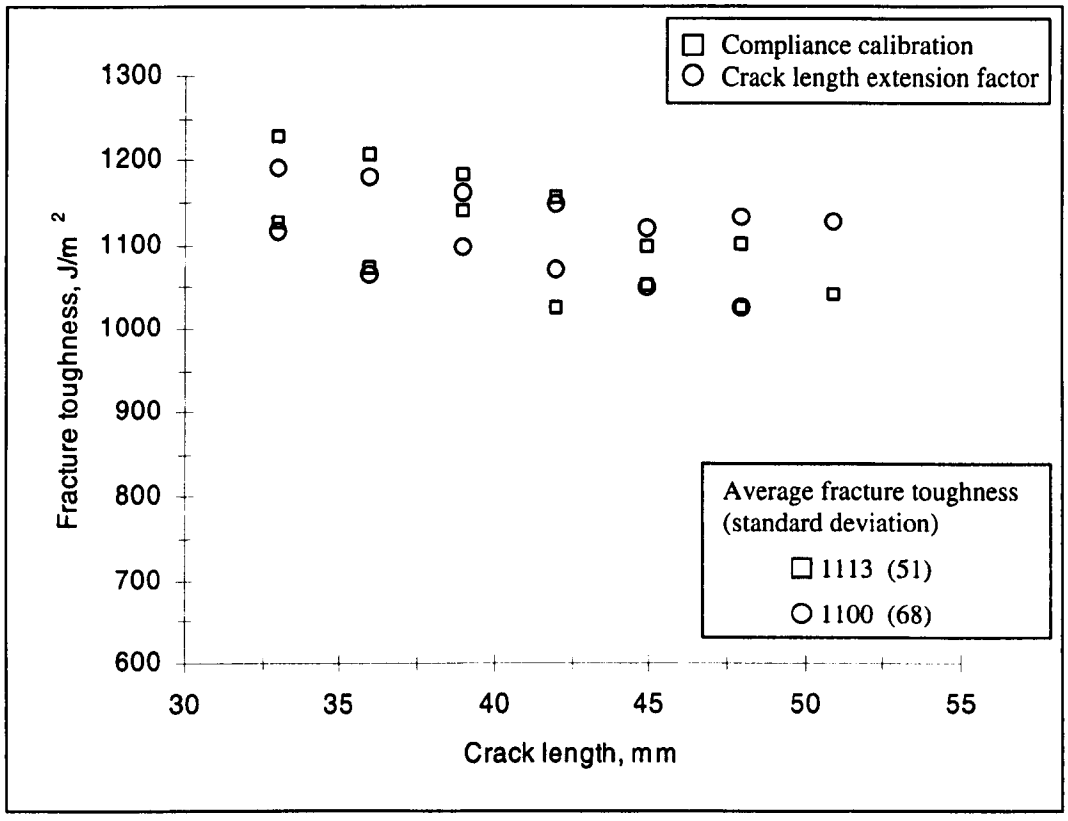

Figure 6.2.2 Interfacial fracture toughness data following CNFS tests on Structure G.

Figure 6.2.2 demonstrates that the interfacial fracture toughness values calculated from the two data reduction methods are in good agreement. Furthermore, the fracture toughness values appear to decrease slightly with increasing crack length. This may be due to stiffening effects of the loading pin on the debonded face-sheet. The relative contact area between the loading pin and the debonded face-sheet will decrease as the debond length increases. Therefore, the loading pin will have a more pronounced effect on the flexural rigidity of the face-sheet at smaller crack lengths, an effect which could lead to an increase of the interfacial fracture toughness at smaller crack lengths. Furthermore, the finite element analysis predicted the Mode II strain energy release rate component to decrease with increasing crack length for a crack situated in the face-sheet material, as is the case here. This may also explain the reduced fracture toughness values with crack length for this example. A decrease in fracture toughness with increasing crack length has also been noted by Liechti and Marton [1] following modified DCB tests on a sandwich system based on a titanium honeycomb with IM7/PETI-5 face-sheets. This decrease in fracture toughness was thought to be due to specimen end effects which are likely to diminish with increasing crack advancement.

6.2.3 Effect of CNFS Specimen Width on the Interfacial Fracture Toughness

Further CNFS tests were conducted on Structure G using specimens with different widths. Here, a series of tests were conducted on specimens with widths in the range of 10 mm to 25mm. Examples of typical the load-displacement curves following CNFS tests on specimens with different widths are presented in Fig. 6.2.3.

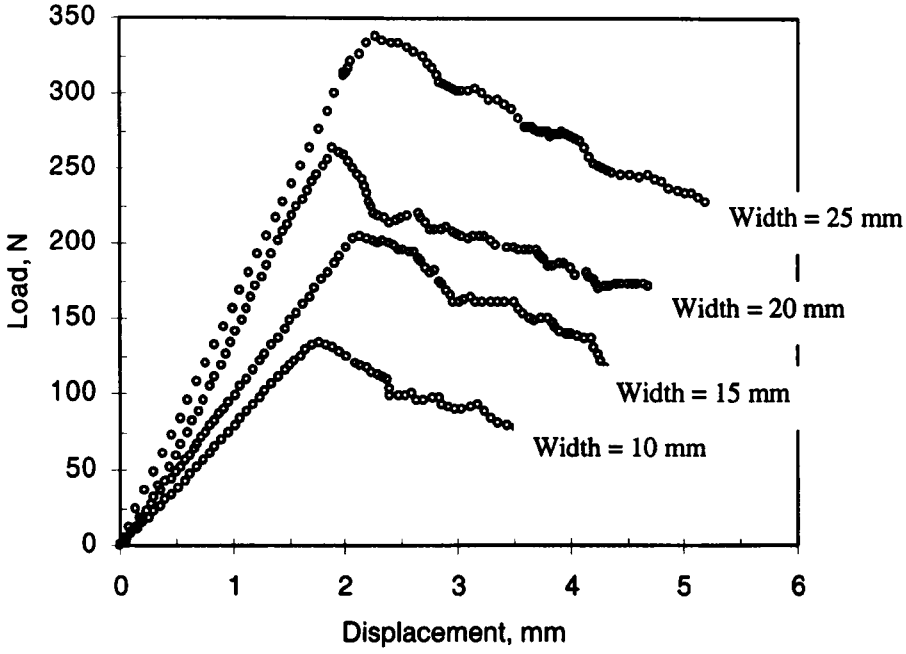

Figure 6.2.3 Load-displacement records following CNFS tests on specimens with different widths.

From the figure, it is clear that the load-displacement response of specimens with different widths is essentially the same. As expected, the load at fracture initiation increases with increasing specimen width and the slopes of the crack propagation portions of the load-displacement responses are similar. The average interfacial fracture toughness calculated following these CNFS tests are presented in Fig. 6.2.4. The result shows that the toughness is not significantly affected by the change in specimen width and also the scatter of the data does not vary significantly between specimens of different width. This suggests that the toughness measurements made from these CNFS tests are an intrinsic value of the interfacial fracture toughness of the sandwich structure. Here, the error bars indicate standard deviation and have the same meaning in all the histograms within

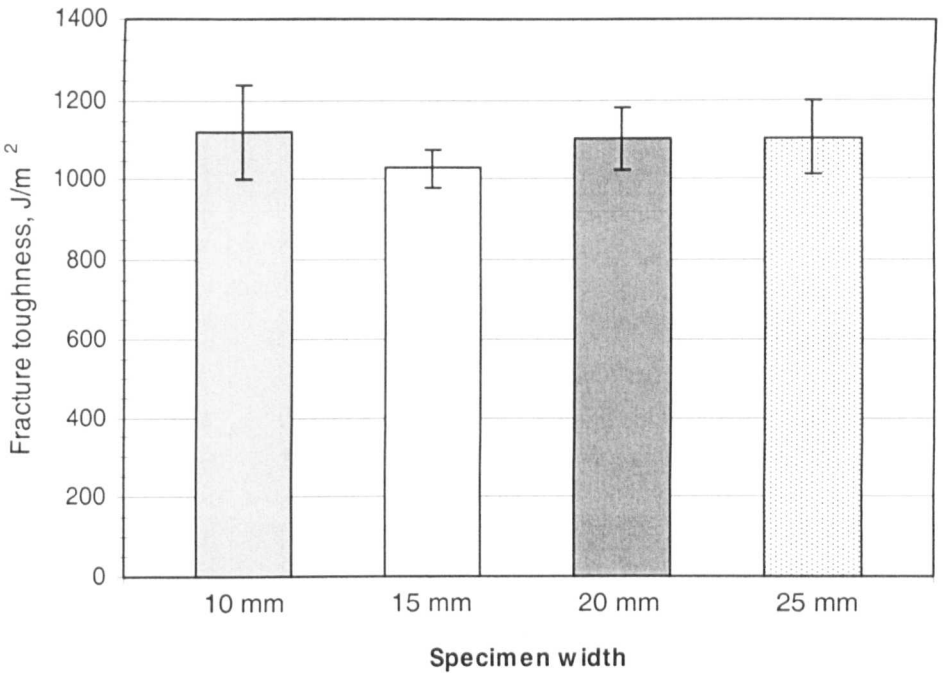

Figure 6.2.4 Influence of CNFS specimen width on interfacial fracture toughness following CNFS tests on Structure G.

6.2.4 Comparison of the Interfacial Fracture Toughness Values Obtained Using the CNFS and MTPB Geometries

To further investigate the reliability of the CNFS geometry, interfacial fracture tests were conducted on Structures A to F using the CNFS and the MTPB geometries. These structures were all based on a Nomex® honeycomb core (density 80 kg/m^3). The cores in Structures A to C were reinforced by glass/epoxy face-sheets, whereas the cores in Structures D to F were reinforced by carbon fibre/epoxy facings, Fig. 4.2.1. The average fracture toughness values for these sandwich systems are presented in Fig.6.2.5. In all cases, the fracture toughness values were calculated using the compliance calibration

technique. Furthermore, these toughness values are in good agreement with those reported previously for the same sandwich systems [2].

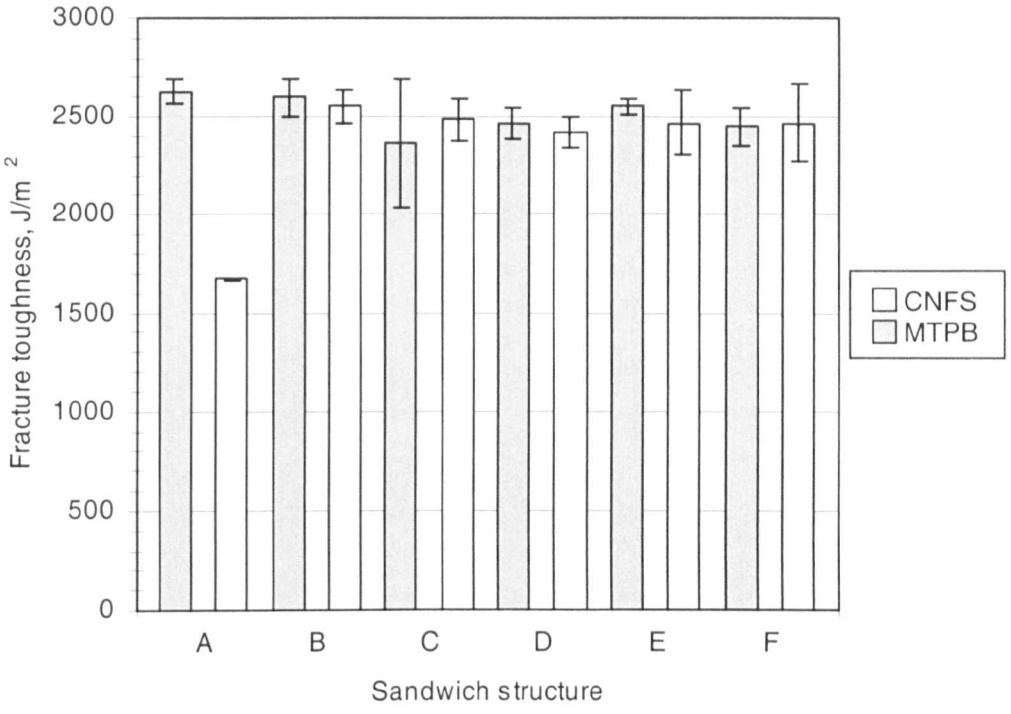

Figure 6.2.5 Interfacial fracture toughness of Structures A-F following CNFS and MTPB tests.

In all majority of cases, the fracture toughness values obtained following the CNFS and MTPB tests were in good agreement. An inspection of the fracture surfaces confirmed that in all cases, crack propagation occurred within the core material, parallel to the face-sheet/core interface, Figs 6.2.6 and 6.2.7. This explains the similarity of the fracture toughness data between Structures A to F. However, CNFS tests on Structure A yielded significantly lower toughness values in comparison to the other systems. This

technique. Furthermore, these toughness values are in good agreement with those reported previously for the same sandwich systems [2].

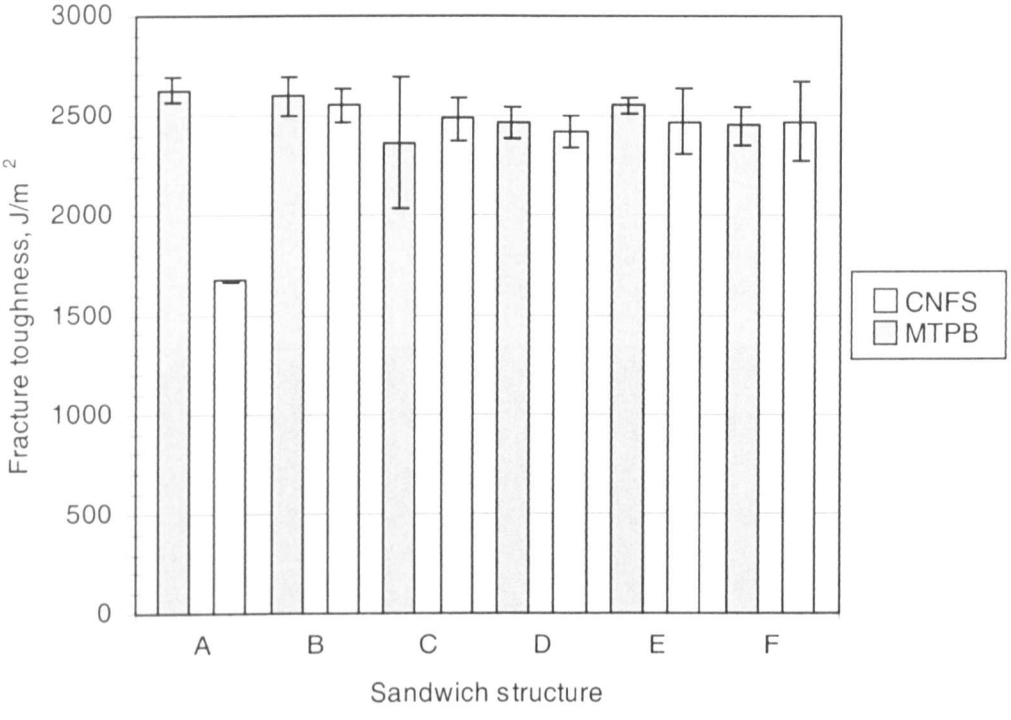

Figure 6.2.5 Interfacial fracture toughness of Structures A-F following CNFS and MTPB tests.

In all majority of cases, the fracture toughness values obtained following the CNFS and MTPB tests were in good agreement. An inspection of the fracture surfaces confirmed that in all cases, crack propagation occurred within the core material, parallel to the face-sheet/core interface, Figs 6.2.6 and 6.2.7. This explains the similarity of the fracture toughness data between Structures A to F. However, CNFS tests on Structure A yielded significantly lower toughness values in comparison to the other systems. This

unexpected value was thought to be a consequence of a defective panel, from which the CNFS specimens were taken. Additionally, the fracture toughness values obtained following the CNFS tests were slightly lower than those determined following the MTPB tests. This is in accordance with the predictions made from the finite element analyses where the MTPB specimen was shown to exhibit a slightly larger amount of Mode II loading in comparison to the CNFS geometry.

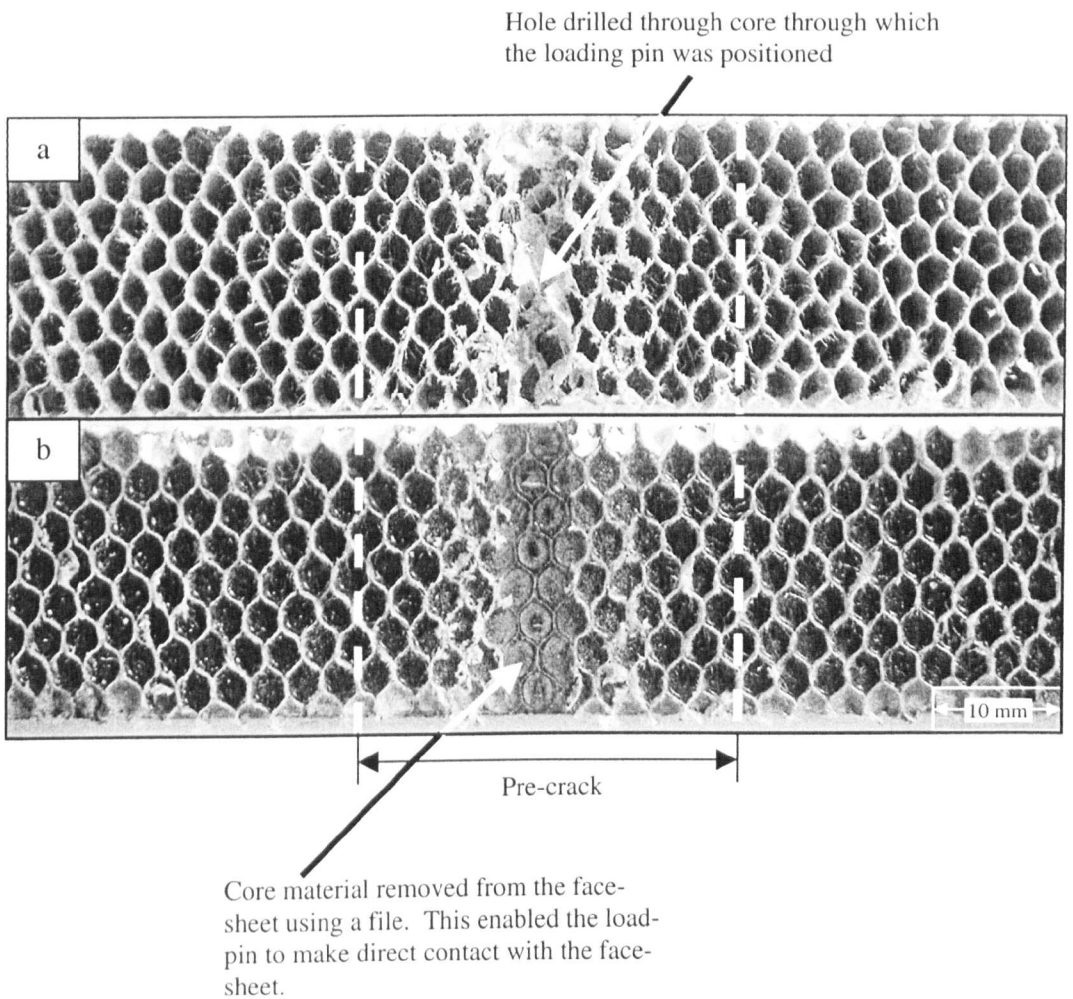

Figure 6.2.6 Fracture surfaces of a CNFS specimen from Structure A, (a) core surface, (b) face-sheet surface.

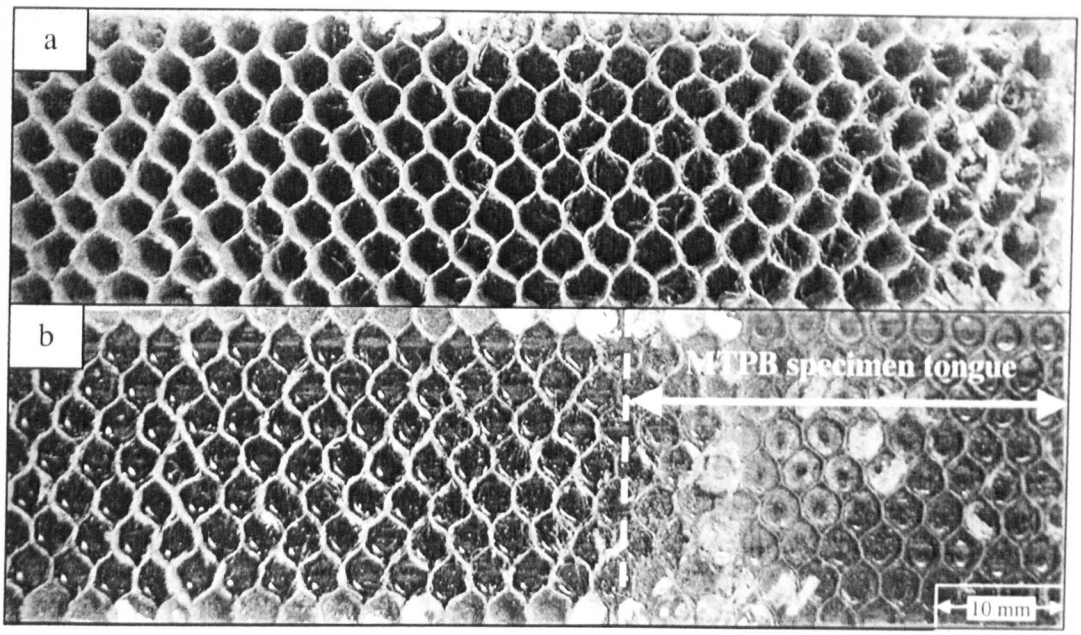

Figure 6.2.7 Fracture surfaces of a MTPB specimen from Structure A, (a) core surface, (b) face-sheet surface.

6.2.5 Summary of Test Method Development

The ASPT and CNFS test geometries were designed to undertake interfacial fracture tests on sandwich structures based on thin facings. Preliminary CNFS tests on Structure G demonstrated that this test was the most appropriate method for characterising the properties of thin-skinned sandwich systems. Additionally, fracture toughness values calculated using the compliance calibration and the crack length extension data reduction techniques were in good agreement. Furthermore, the width of CNFS specimens was found to have little effect on the calculated fracture toughness values. This suggests that the toughness values are intrinsic material properties and not dependent on the dimensions of the CNFS specimen. Finally, the interfacial fracture toughness of a range

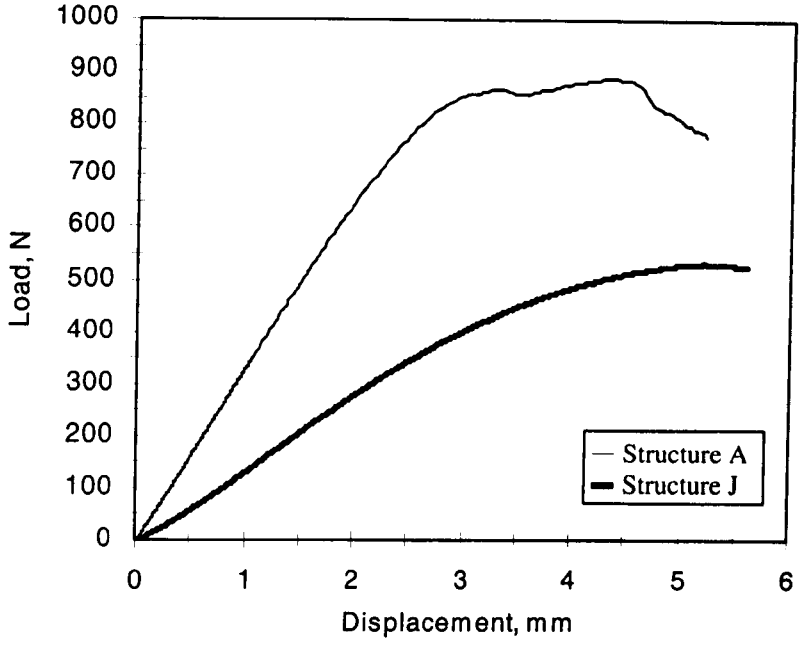

Figure 6.3.1 Load-displacement response following CNFS tests on Structures A and J.

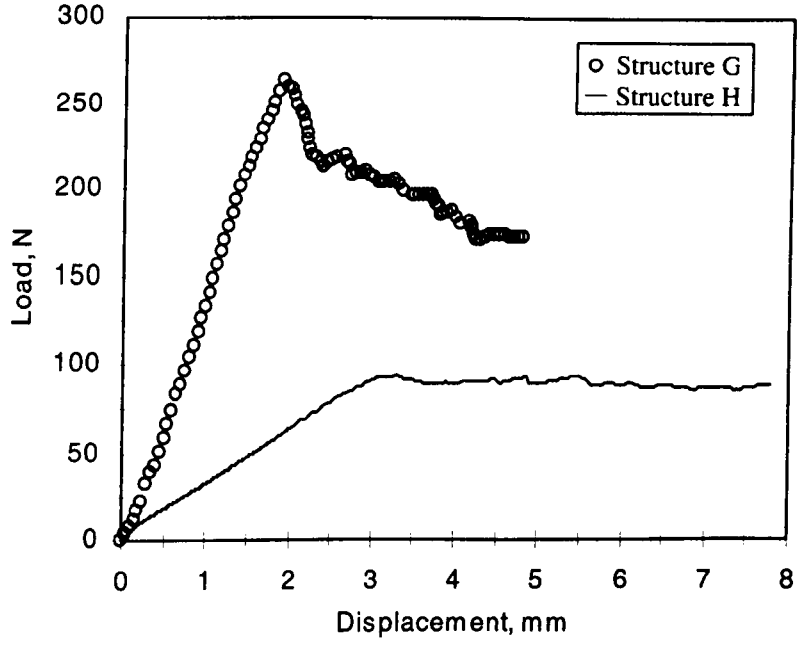

Figure 6.3.2 Load-displacement response following CNFS tests on Structures G and H.

The CNFS load-displacement traces for Systems A to H were essentially linear. In each case, a residual displacement of less than 0.5 mm remained at the end of the test. This permanent displacement was thought to be due to core deformation during the tests. Furthermore, in most cases crack propagation was accompanied by a reduction in the measured load, which in turn resulted in an increase in specimen compliance with increasing crack length. However, the presence of fibre bridging during crack growth in Structure H caused the fracture propagation load to remain constant, as illustrated in Fig. 6.3.2. Cartié *et al* [3] observed a similar behaviour in the load-displacement response of CFRP double cantilever beam specimens containing through-thickness reinforcing Z-Fibres®. In this instance, the propagating crack was bridged by the Z-Fibres® resulting in a constant crack propagation load. Furthermore, Cantwell *et al* [4] reported fibre bridging in a balsa-based sandwich beam, similar to Structure H in which the 0° fibres of the composite face-sheet were bonded directly to the core material during the manufacturing process. Thus, it is likely that the positioning of the 0° fibres on the core material during the manufacture of Structure H is the reason for the occurrence of the fibre bridging.

CNFS tests on Structure J resulted in significant plastic deformation within the linear PVC core material, an effect that is thought to be the reason for the non-linear loading response observed in this specimen, Fig. 6.3.1. Here, the unloading curve of the specimen was non-linear, followed by a residual displacement of approximately 2.5 mm. These observations suggest that the core material underwent large-scale yielding during the course of the CNFS test.

Crack propagation in CNFS specimens from Structures I, K and Structures L to P was unstable. Here, the loading curves for each specimen were linear, Figs. 6.3.3 and 6.3.4.

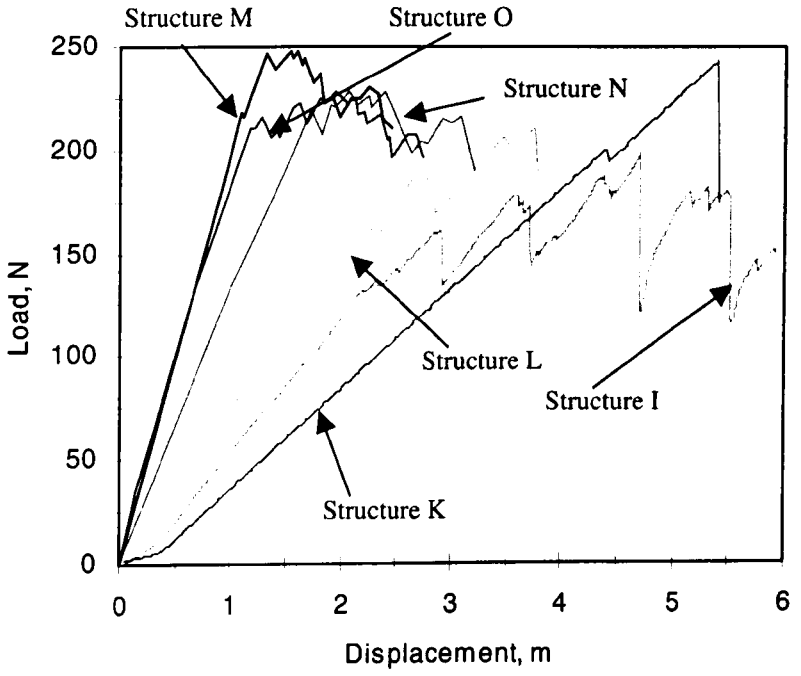

Figure 6.3.3 Load-displacement response following CNFS tests on Structures I to O.

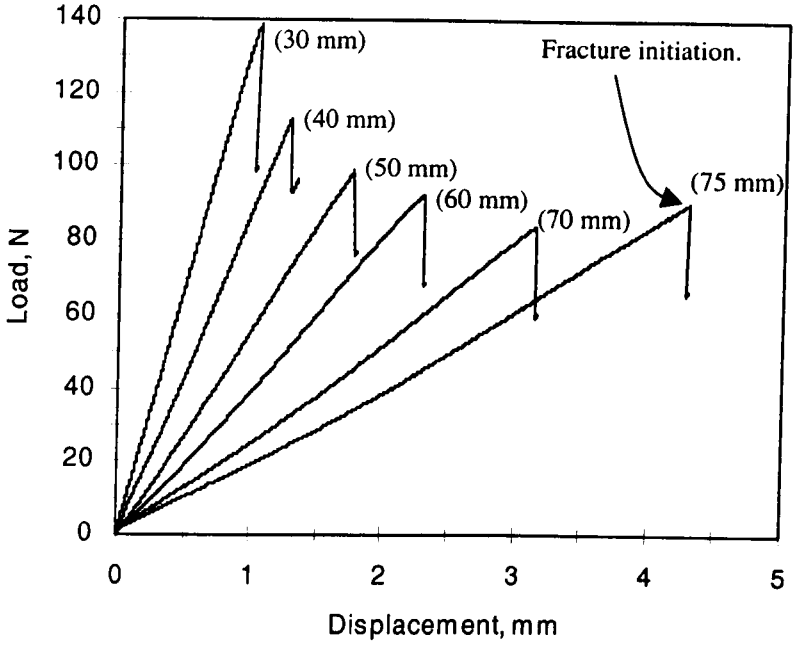

Figure 6.3.4 Load-displacement response following CNFS tests on Structure P. Numbers in parenthesis denote specimen pre-crack length.

From Figs. 6.3.3 and 6.3.4, it is clear that in all cases fracture initiation is well defined, corresponding to a sudden decrease in load. Subsequent crack growth in CNFS specimens from Systems I, and Structures L to O occurred in a stick-slip manner, resulting in the jagged crack propagation traces shown in Fig. 6.3.3. Crack propagation in Structure P, which occurred in the linear PVC core material, was extremely unstable, making it very difficult to monitor crack extension. Similar observations were reported by Prasad and Carlsson following DCB tests on a sandwich system based on the same core material [5]. Therefore, in order to generate a sufficient number of data points to calculate the fracture toughness values using the compliance calibration procedure, a series of CNFS specimens were prepared with different pre-crack lengths. Each

specimen was then loaded until a natural crack initiated from the pre-crack, yielding a range of critical load values (load at fracture initiation) as shown in Fig. 6.3.4.

The reason for the unstable crack growth observed in the CNFS specimens from structures K and Structures L to P is likely to be the plastic zone that develops around the crack-tip as the specimens are loaded [6]. In these tests, crack propagation occurred within the PVC core material. The high ductility of these foams enables a large plastic zone to develop at the crack-tip prior to fracture initiation. Subsequently, by the time fracture initiation occurs, the large amount of strain energy stored in the specimen is released, resulting in a large and sudden increase in crack length. Crack propagation in Structure I occurred at the face-sheet/core interface. Here, the crack was observed to propagate from cell to cell along the surface of the aluminium honeycomb core. This explains the observed unstable crack growth in this specimen.

6.3.2 Variation of the CNFS Specimen Compliance with Crack Length

Following each CNFS test, the specimen compliance was recorded as a function of crack length. A selection of typical compliance versus crack length curves is presented in Fig. 6.3.5. In all cases, the specimen compliance appears to have a finite value at zero crack length, which corresponds to the compliance of the uncracked part of the sample. Previous workers [7-8] have also reported this trend in specimen compliance during interfacial fracture tests on sandwich laminates using different specimen geometries.

Having established a relationship between specimen compliance and crack length, the constants, C_o, k and Δ, used in the two data reduction techniques were evaluated following the procedure outlined in Sections 3.5.2 and 4.3.4.

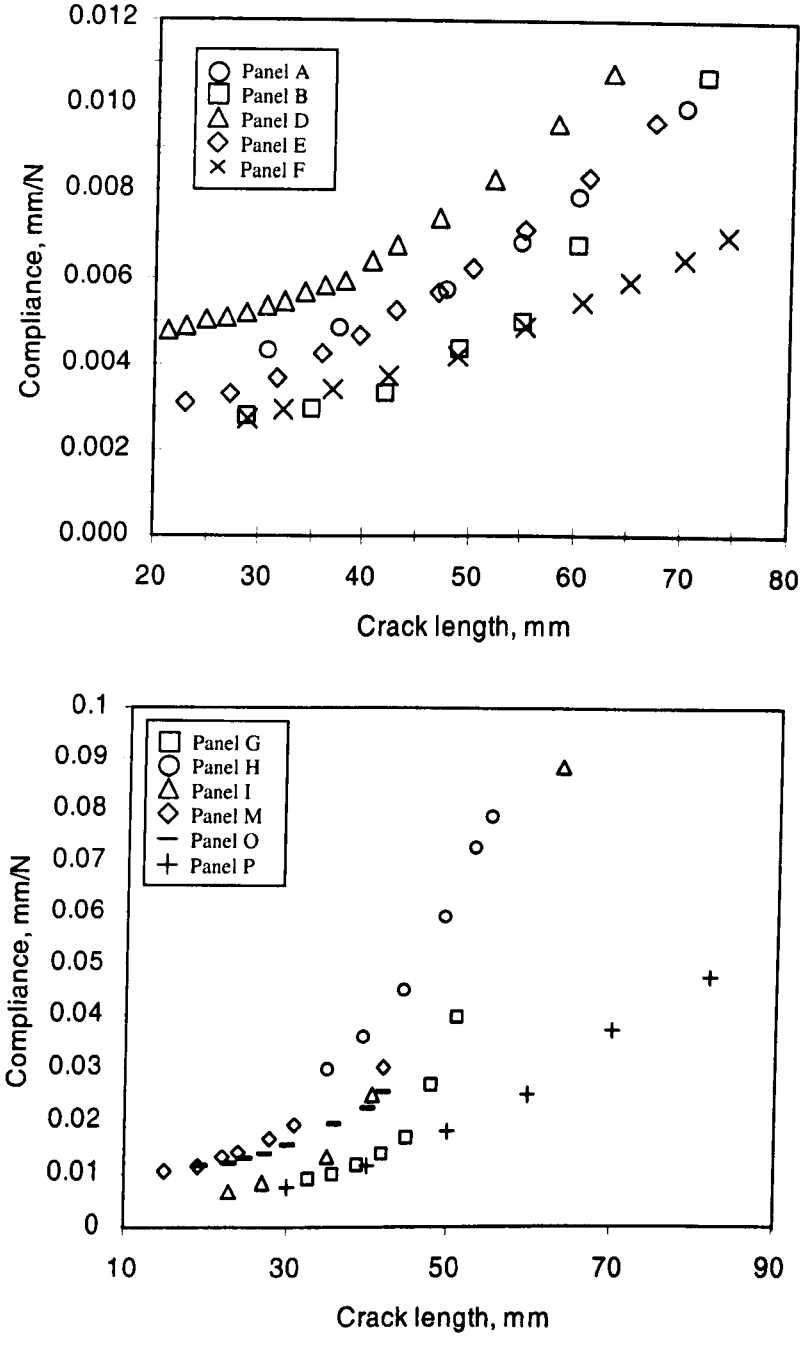

Figure 6.3.5 Examples of compliance vs. crack length data following CNFS tests on Structures A to P.

By calculating the crack length extension factor, Δ, following CNFS tests on Structures A to F, it was found that this term was sensitive to the thickness of the face-sheets of these sandwich specimens. Here, the value of Δ was found to increase with increasing face-sheet thickness, as shown in Table 6.3.1.

CNFS test specimen	**Face-sheet thickness, mm**	Δ **mm**	C_o **(mm/N) $\times 10^{-3}$**	k **($N^{-1}mm^{-2}$) $\times 10^{-8}$**
Structure D	0.5	3.8	4.62	2.53
Structure E	1.0	11.8	3.12	2.29
Structure F	1.3	24.2	2.58	1.34

Table 6.3.1 The effect of face-sheet thickness on the crack length extension factor, and the compliance calibration constants 'C_o' and 'k' following CNFS tests on Structures D to F.

An increase in face-sheet thickness results in an increase in the flexural rigidity of the facings. Figure 6.3.6 shows examples of traces of the cube root of compliance versus crack length following CNFS tests on Structures D to F. Here, the gradient of the lines is inversely proportional to the flexural rigidity of the face-sheet to which the load is applied. Consequently, an increase in face-sheet thickness results in a reduction in the gradient of the lines, resulting in an increase in the crack length extension factor, as

illustrated in Fig. 6.3.6. Furthermore, the trend indicated in Fig. 6.3.6 was also predicted by the FE analyses conducted herein, Section 5.6.

Following the compliance calibration data reduction technique, the constants C_o and k were determined from a plot of the compliance versus the cube of the crack length. Figure 6.3.7 shows an example of these graphs following CNFS tests on Structures D to F. As in the case of the crack length extension factor, the constants 'C_o' and 'k' were found to be sensitive to the thickness of the face-sheets. Here, an increase in face-sheet thickness resulted in a decrease in the values of 'C_o' and 'k', as illustrated in Table 6.3.1 and Fig. 6.3.7.

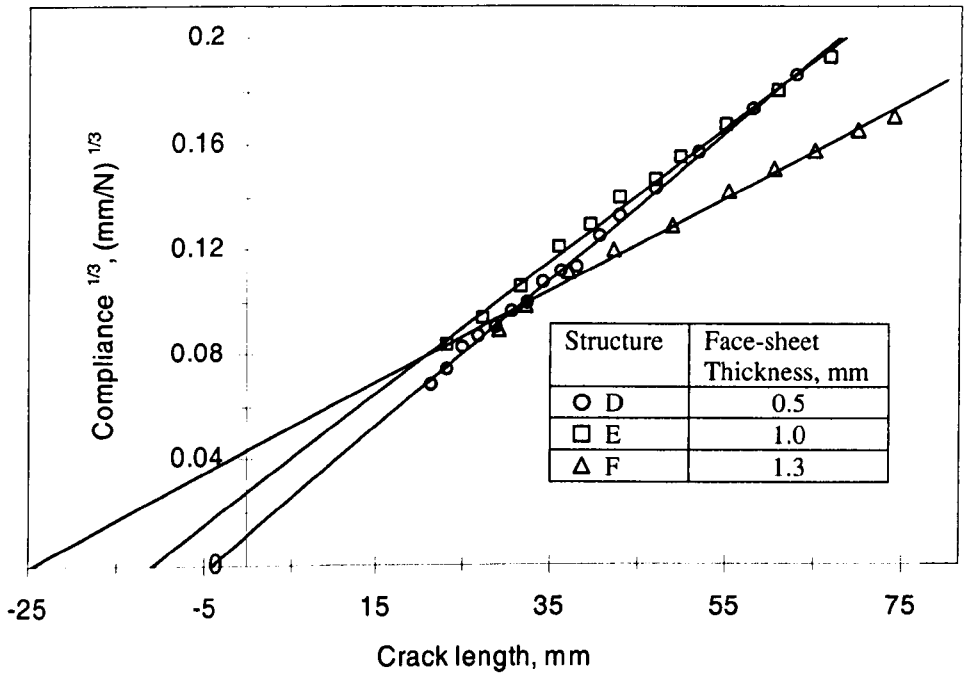

Figure 6.3.6 Examples of the cube root of compliance vs. crack length graphs for determining 'Δ' following CNFS tests on Structures D to F.

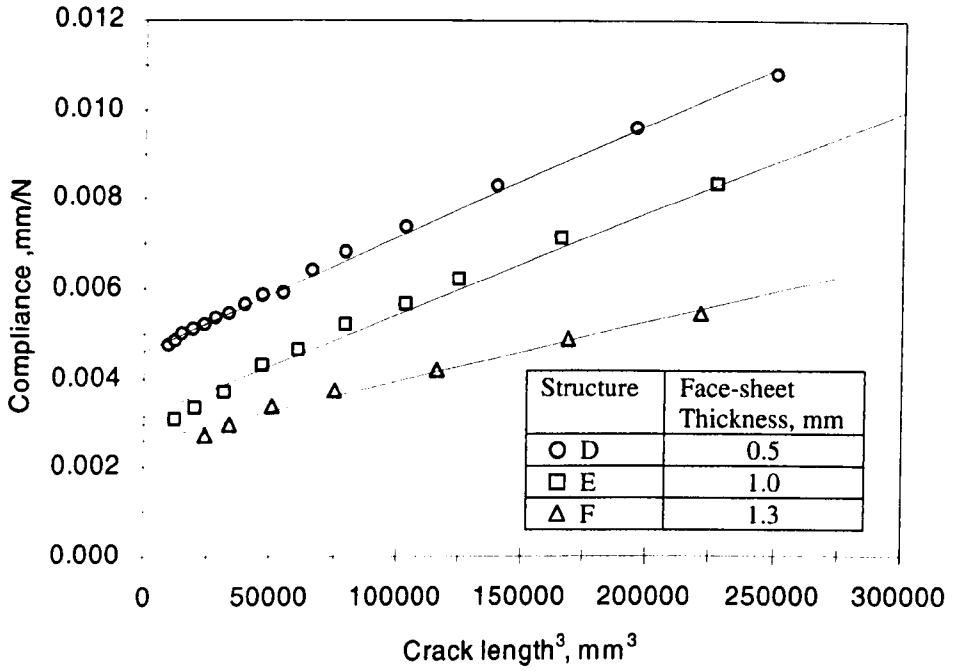

Figure 6.3.7 Examples of compliance vs. the cube of crack length plots for determining 'C_o' and 'k' following CNFS tests on Structures D to F.

As the thickness and therefore the flexural rigidity of the face-sheets is increased, the apparent compliance of a specimen with no pre-crack, 'C_o', decreases. This is confirmed by the graphs shown in Fig. 6.3.7. Furthermore, the figure shows that the gradient of the lines, 'k', decreases as the face-sheet thickness increases. This was expected since 'k' is inversely proportional to the flexural rigidity of the facings.

Thus, using the compliance calibration procedure and the crack length extension factor following a fracture test, the interfacial fracture toughness was calculated. Table 6.3.2 presents an example of the data reduction technique used to calculate the fracture toughness following CNFS tests on Structure P.

a mm	P N	δ mm	k $N^{-1}mm^{-2} \times 10^{-8}$	C_o mm/N	Δ mm	G_c^1 J/m^2	G_c^2 J/m^2
30	140	0.71	10.2	0.0036	14	108	136
40	110	1.24	10.2	0.0036	14	119	152
50	99	1.77	10.2	0.0036	14	150	165
60	93	2.3	10.2	0.0036	14	191	174
70	84	3.14	10.2	0.0036	14	212	189
75	90	4.3	10.2	0.0036	14	279	261
Average interfacial fracture toughness, J/m^2						**177**	**179**

[1] G_C calculated from the compliance calibration technique [2] G_C calculated from the crack length extension factor method.

Table 6.3.2 Example of the crack length extension factor technique and the compliance calibration method used to calculate interfacial fracture toughness values following the CNFS tests. The specimen was a GFRP/PVC foam sandwich (Structure P).

This example illustrates the close agreement between the two data reduction methods used to calculate the interlaminar fracture toughness following a CNFS test.

6.3.3 Interfacial Fracture Toughness of Structures A to F

The interfacial fracture toughness of sandwich structures A to F were reported in the first section of this chapter. Reiterating the findings from the CNFS tests on these panels, Structures A to F were all found to offer fracture toughness values in the region of 2500 J/m^2. Here, crack propagation occurred within the Nomex core material in each specimen, which explains the similar toughness values obtained following tests on these

systems. During a round-robin study, Gower *et al* conducted CNFS tests on the same structures and calculated an average interfacial fracture toughness using the areas method [2]. The resulting toughness values were reported in the range of 2700 J/m^2, approximately 8% higher than those measured here for the same systems. It is probable that the observed disparity between the two sets of average values for these systems reflects the differences in the calculation methods used. As indicated by Fig. 4.3.9, the areas method uses the entire area enclosed by the load-displacement response from a test, whereas the global energy approaches use compliance values at various stages of crack propagation as illustrated in Fig. 4.3.7. The latter technique assumes that at any stage of the test, specimen unloading will be linear. In reality this is not exactly the case, as some yielding will inevitably occur in the specimen. Consequently, the areas method will include any energy absorbed due to yielding and other non-linear effects (as it uses the area encompassed by the load-displacement response to calculate a fracture toughness), resulting in an overestimation of the average fracture toughness, as illustrated in the case of Structures A to F. Indeed, other investigators have reported the areas method to yield higher fracture toughness values than the LEFM based approaches [9].

6.3.4 Interfacial Fracture Toughness of Structures G to K

Structure G offered an average fracture toughness of approximately 1100 J/m^2. CNFS tests on this structure resulted in interlaminar crack growth between the 0° and 90° plies of the unidirectional glass fibre/epoxy face-sheets. The interfacial fracture toughness of Structure H was found to increase with crack length, as illustrated in the R-curve for this

system, Fig. 6.3.8. Here, fracture occurred within the unidirectional glass/epoxy face-sheets and the glass fibres were observed to bridge the propagating crack, as illustrated in Fig. 6.3.9. These bridging fibres provide an indirect closure traction to the crack faces, which serves to increase the critical load required to extend the crack, is thought to be the cause of the observed increase in toughness with crack length. A Similar increase in toughness with crack length was reported following fracture tests on the same sandwich system using a different specimen geometry [8]. The average toughness for this system was approximately 1100 J/m^2, which is in reasonable agreement with previously reported toughness values for this system [7-10].

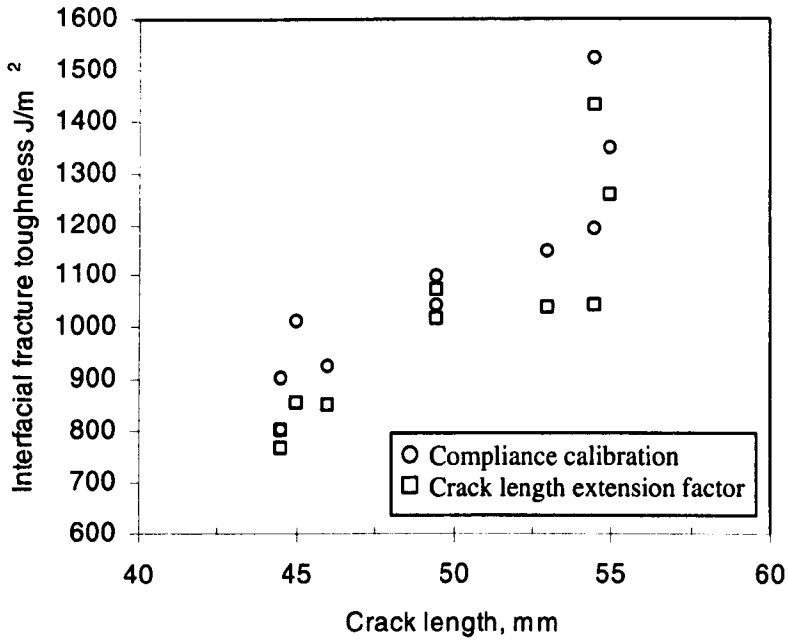

Figure 6.3.8 R-curve for Structure H. The interfacial fracture toughness values were calculated using the crack length extension factor technique and the compliance calibration method.

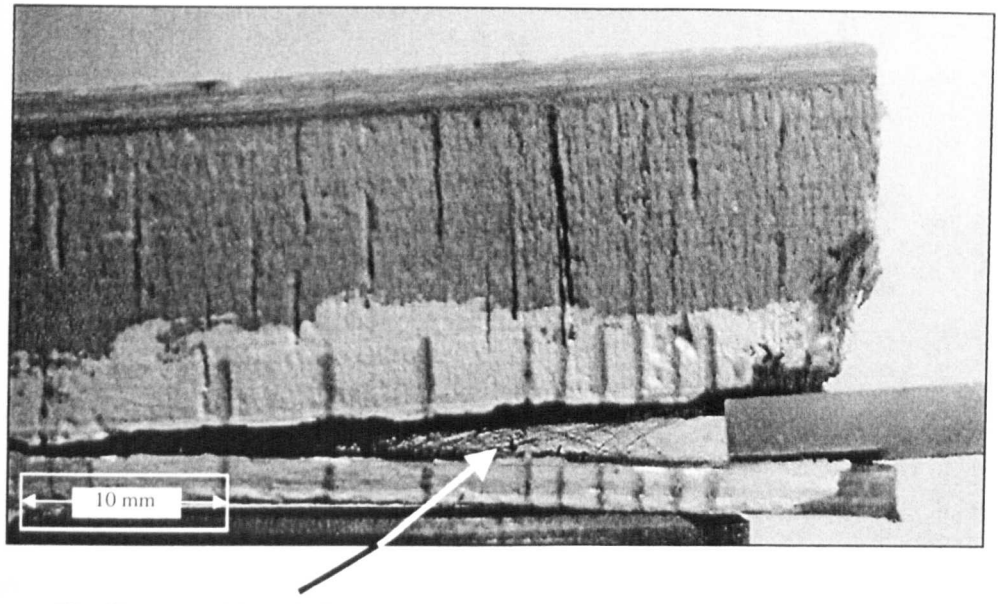

Figure 6.3.9 A sectioned CNFS specimen of Structure H with one half of the specimen removed to highlight the fibres bridging the crack.

The average fracture toughness of Structure I was found to be 1050 J/m^2, Fig. 6.3.10, which is similar to previously determined values of toughness for the same sandwich system using the MTPB specimen geometry [9]. An inspection of the fracture surfaces confirmed that crack growth occurred at the face-sheet/core interface. Here, an imprint of the aluminium honeycomb core is visible on the surface of the face-sheet, as shown in the micrograph in Fig. 6.3.11. Additionally, the resin used to bond the facings to the core has adhered to the cell walls of the honeycomb, as illustrated in the micrograph.

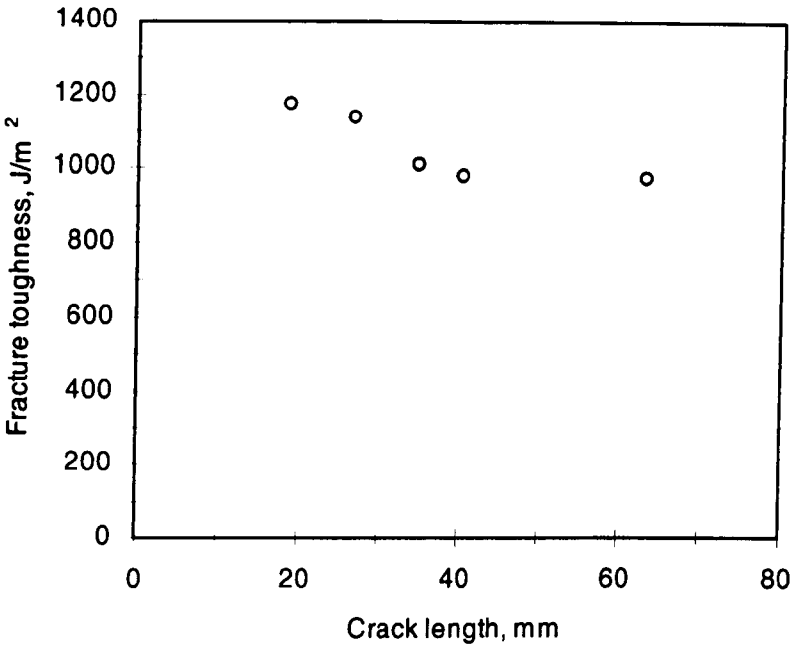

Figure 6.3.10 Interfacial fracture toughness values for Structure I, calculated using the crack length extension factor.

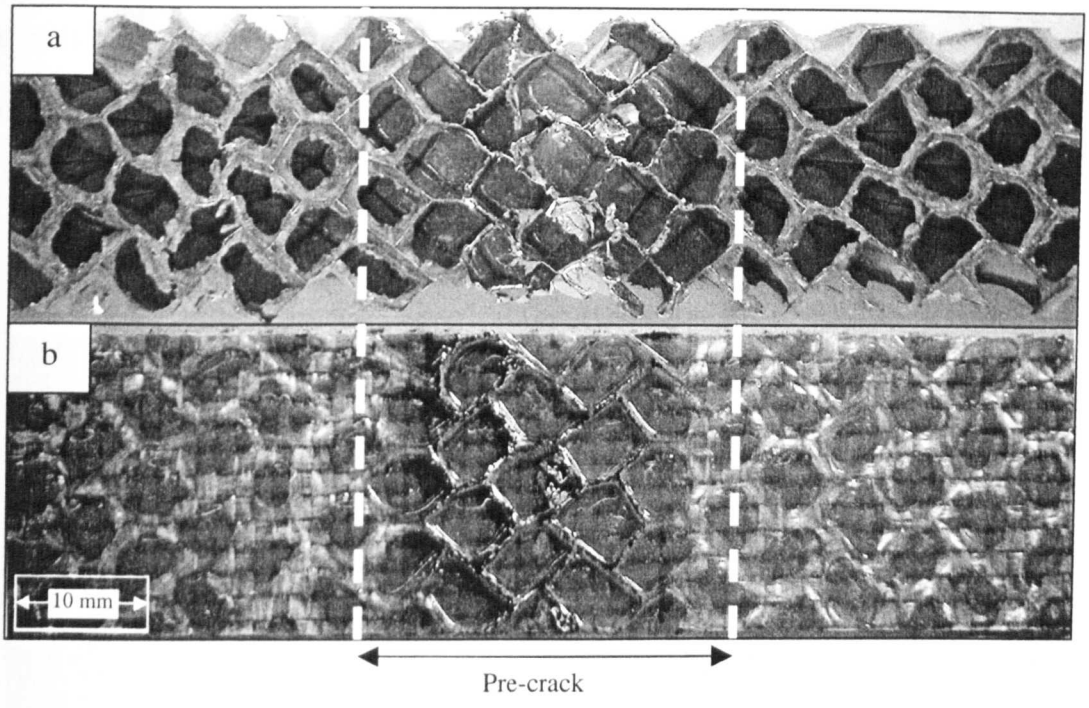

Figure 6.3.11 Fracture surfaces of a CNFS specimen from Structure I (a) the resin material has remained on the honeycomb cell walls (b) the imprint of the honeycomb is visible on the fracture surface of the face-sheet.

As a result of the highly non-linear CNFS load-displacement response of Structure J, it was not possible to calculate a fracture toughness using the LEFM-based techniques. However, the interfacial fracture toughness of this system was characterised using the *J* integral method, following the procedure outlined in Section 4.5. The findings from this procedure will be discussed later in Section 6.6.

An inspection of the fracture surfaces following CNFS tests on Structure K confirmed that crack propagation had occurred through the crosslinked PVC core material, parallel to the face-sheet/core interface, as shown in Fig. 6.3.12. Here, the areas method was used

to calculate the interfacial fracture toughness, the average value of which was 460 J/m^2. This value is in good agreement with fracture toughness values reported previously following tests on the same sandwich system [11].

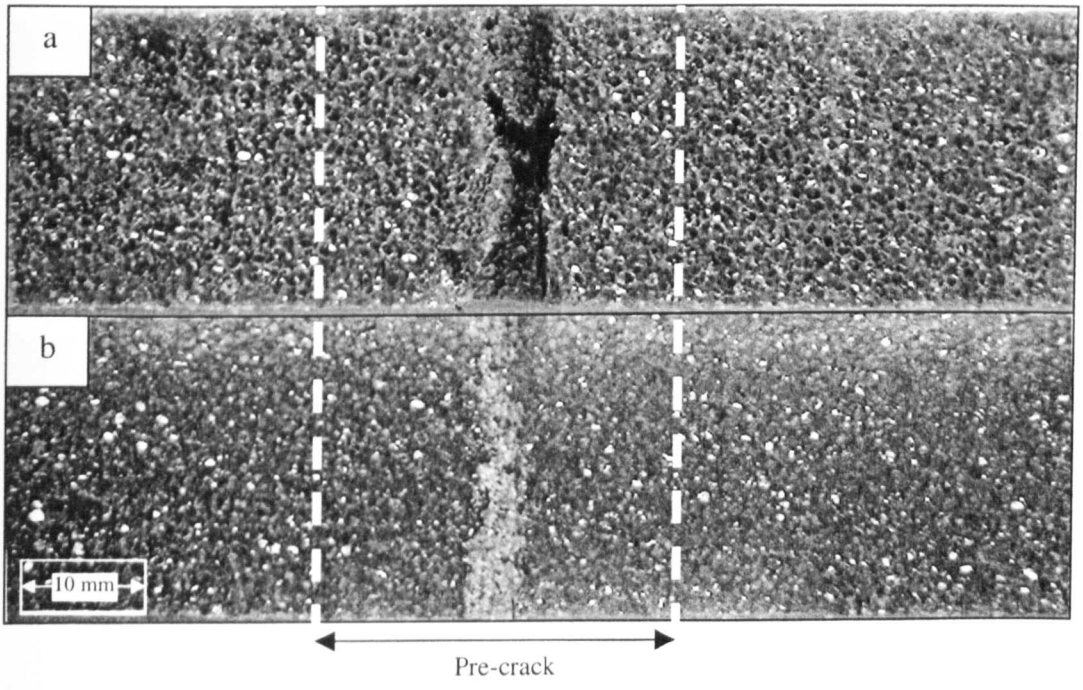

Figure 6.3.12 (a) Fracture surface of the crosslinked PVC core material in Structure K (b) fracture surface of the face-sheet showing the residual core material.

6.3.5 Interfacial Fracture Toughness of Structures L to P

CNFS tests on Structures L to O were all conducted on the interface between the CFRP facings and the PVC/PUR foam illustrated in Fig. 4.2.2. In each case, crack propagation was observed to grow both through the core material and at the face-sheet/core interface along the woven glass fibre interlayer as indicated in Fig. 6.3.13. The micrograph

presented in Fig. 6.3.13 shows the fracture surfaces following CNFS tests on Structure N, which was typical of the fracture surfaces generated from CNFS tests on Systems L to O.

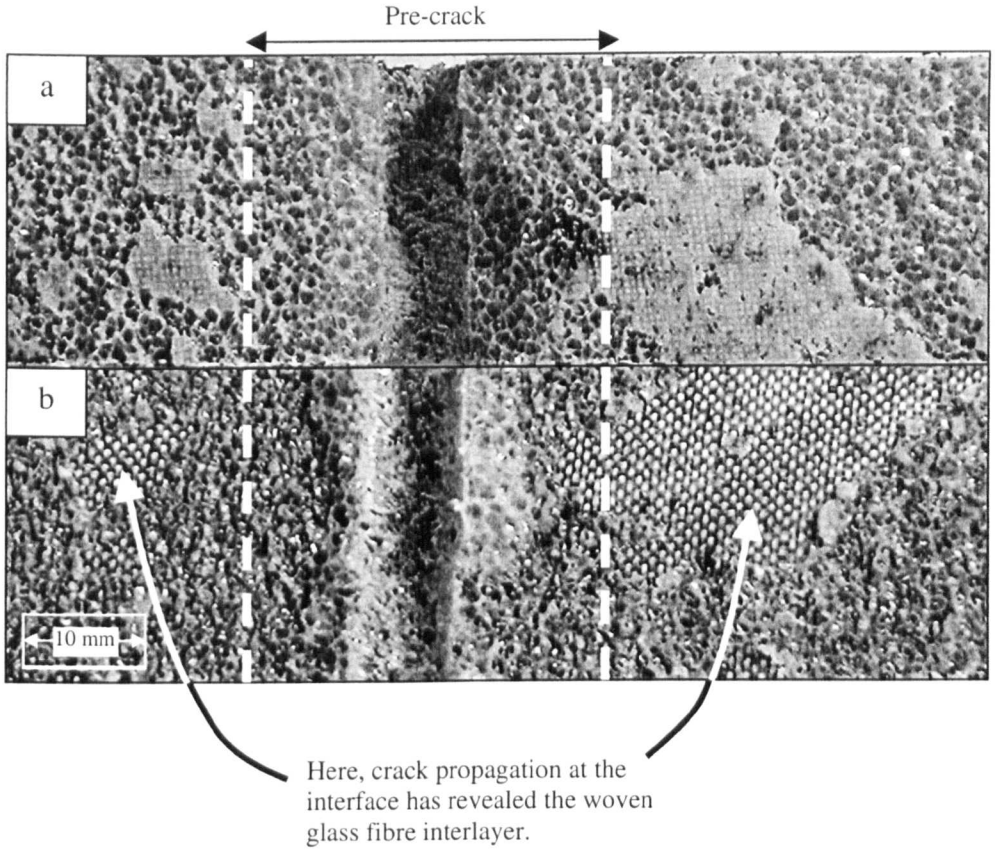

Figure 6.3.13 Fracture surfaces following a CNFS test on Structure N, (a) the upper surface of the core material showing the imprint of the woven GFRP interlayer where crack propagation occurred at the interface, (b) the face-sheet fracture surface, containing patches of core material.

This mixed form of fracture is thought to be due to the heterogeneity of the interfacial bond, where crack propagation at the interface corresponds to weaker areas of the bond. The fracture toughness of Structure L was calculated using the areas method, because

insufficient data points were recorded for the successful application of the global energy techniques. The average interfacial fracture toughness for this system was approximately 650 J/m^2. Figure 6.3.14 presents the interfacial fracture toughness values following the CNFS tests on Structures M to O.

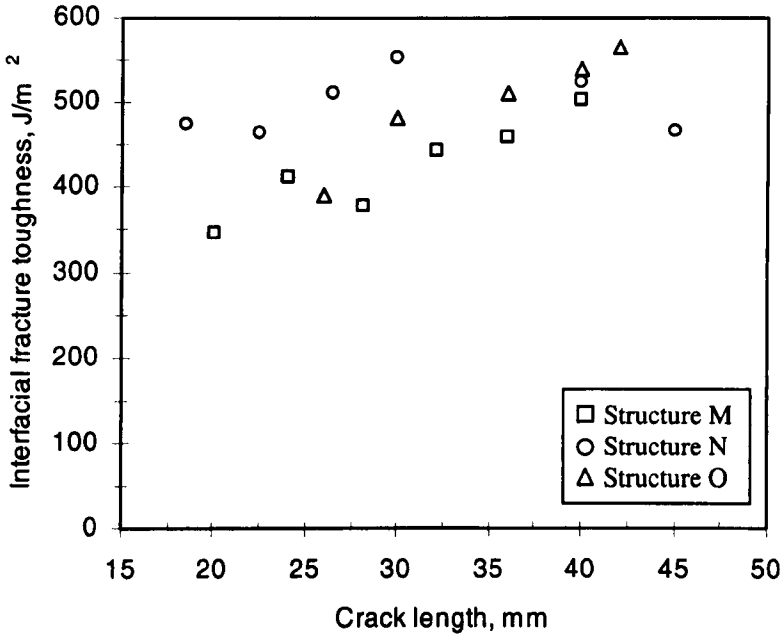

Figure 6.3.14 Interfacial fracture toughness of Structures M to O. Toughness values calculated using the compliance calibration technique.

The average interfacial fracture toughness of Structure M was approximately 500 J/m^2, although the scatter of the data is high, an effect that may be due to the apparent heterogeneity of the face-sheet/core bond. Also, the increasing in fracture toughness with increasing crack length corresponds to the predictions from the FE analyses of a CNFS specimen with a crack positioned in the core material. Here, within the crack length ranges used in this test, the Mode II loading in the specimen will increase with crack

length. Furthermore, the Mode I fracture toughness of the PVC foam material used in Structures L to O has been reported to be to 711 J/m^2 [11], which is significantly higher than the average interfacial fracture toughness measured on these systems. This discrepancy is probably due to the fact that crack propagation occurred at the face-sheet/core interface, as well as within the core material.

Structure P offered the lowest interfacial fracture toughness of all the sandwich system interfaces tested. Here, the average toughness was found to be 167 J/m^2. In this sandwich structure, crack growth occurred entirely within the crosslinked PVC foam core, parallel to the face-sheet/core interface as illustrated in Fig. 6.3.15.

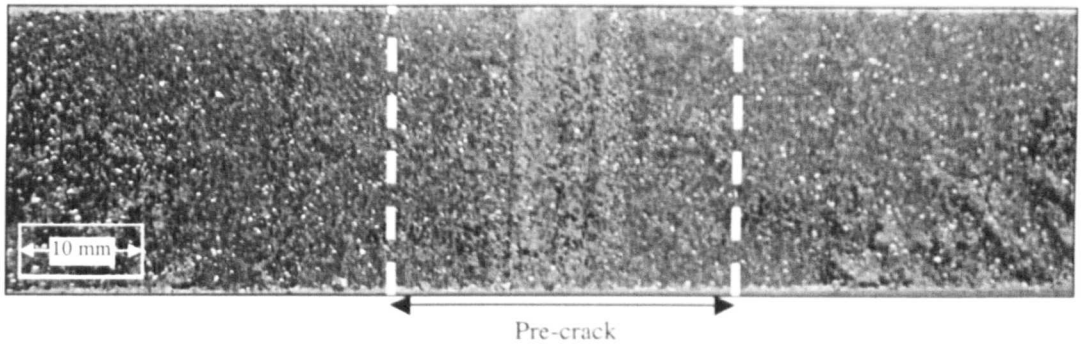

Figure 6.3.15 Fracture surface of the face-sheet material from a CNFS specimen of Structure P.

The fracture toughness of the PVC foam used in Structure P has been reported to be approximately 179 J/m^2 [11], which is in reasonable agreement with the average interfacial fracture toughness measured here. Furthermore, the fracture toughness of PVC foams has been shown to decline with decreasing density [12,13]. This partly explains the low fracture toughness values of Structure P relative to Structures K and L to

O, which were manufactured from PVC based foams with higher densities than that used for Structure P.

6.3.6 Summary of the Interfacial Fracture Toughness Characteristics of Structures A to P

Table 6.3.3 presents the average interfacial fracture toughness of Structures A to P following CNFS tests. The reported toughness data in the table represents average values from four CNFS tests on each structure, calculated using the compliance calibration technique. Where available, corresponding fracture toughness values are quoted from the literature for similar sandwich systems.

Sandwich Structure	Component materials		Crack location	Fracture toughness (CNFS tests)	Fracture toughness (Literature)
	Face-sheet	Core		J/m^2	J/m^2
A	[0°/90°] UD Glass/epoxy	Nomex®	Core	1600 (23)[1]	3073 [2]
B	[0°/90°] UD glass/epoxy	Nomex®	Core	2587 (200)	3068 [2]
C	[0°/90°] UD glass/epoxy	Nomex®	Core	2473 (187)	4261 [2]
D	[0°/90°] UD carbon/epoxy	Nomex®	Core	2423 (190)	2886 [2]
E	[0°/90°] UD carbon/epoxy	Nomex®	Core	2456 (256)	2445 [2]
F	[0°/90°] UD carbon/epoxy	Nomex®	Core	2482 (367)	2877 [2]
G	[0°/90°] UD glass/epoxy	Glass/PMI	Face-sheet	1105 (116)	-
H	[0°/+45°/-45°] UD glass/polyester	Balsa	Face-sheet[2]	1098 (216)	1130 [8]
I	[0°/90°] woven glass/polyester	Al honeycomb	Interface	1053 (95)	1000 [9]
J	[0°/90°] CSM/UD glass/polyester	R63.80	Core	Not calculated	1100 [8]
K	[0°/90°] CSM/UD glass/polyester	H80	Core	460 (32)	510 [11]
L	[0°/90°] woven carbon/epoxy	C70.130	Core/interface	650 (103)	711 [11][3]
M	[0°/90°] woven carbon/epoxy	C70.130	Core/interface	499 (37)	711 [11][3]
N	[0°/90°] woven carbon/epoxy	C70.130	Core/interface	498 (68)	711 [11][3]
O	[0°/90°] woven carbon/epoxy	C70.130	Core/interface	423 (57)	711 [11][3]
P	[±45°] woven glass/polyester	Crosslinked PVC (75 kg/m^3)	Core	167 (12)	179 [11][3]

[1] Numbers in parenthesis denote standard deviations, [2] Crack growth bridged by fibres, [3] Fracture toughness values from Mode I tests on the corresponding core material.

Table 6.3.3 Summary of the face-sheet/core fracture toughness of Structures A to P. In all cases a comparison is made with fracture data reported in the literature.

From the summary of the CNFS fracture toughness data in Table 6.3.3, it is clear that the Nomex® honeycomb-based systems (A-F) offer the highest toughness values. Here,

crack growth occurred within the Nomex® honeycomb core material. The Nomex® material is reinforced with aramid fibres, which bridge the propagating crack and this mechanism is thought to be the reason for the high fracture toughness values offered by these systems. Structures G to I offered intermediate toughness values relative to those offered by the other structures. These toughness values are in good agreement with fracture toughness values reported previously following tests on the same systems [2,8,9,11]. The interfacial fracture toughness values calculated following CNFS tests on Structures L to O were smaller than the Mode I fracture toughness of the core material used in the manufacture of these structures. This was due to the fact that crack growth during the CNFS tests occurred both at the face-sheet/core interface, as well as in the core material. Finally, Structure P offered the lowest fracture toughness of all the sandwich systems tested. This is in part due to the fact foam used in Structure P having the lowest density of all the foams used in the sandwich systems studied here. The interfacial fracture toughness of Structure P compared reasonably well with corresponding toughness values reported in the literature [11].

6.4 MTPB Interfacial Fracture Toughness Tests – Sandwich Systems A to F and L to R

The MTPB test geometry was also used to conduct fracture tests on Structures A to F and L to R to offer a comparison with the fracture data determined using the CNFS test geometry. Furthermore, the CNFS test geometry was not suitable for testing Structures Q

and R, due to the high flexural rigidity of the face-sheets in these two systems. Therefore, the MTPB geometry was used to perform interfacial fracture tests on these structures.

6.4.1 Load-Displacement Response

The load-displacement traces resulting from the MTPB tests are presented in two groups, with the specimens that exhibited stable crack propagation presented in one group (Fig. 6.4.1) and those which exhibited unstable crack growth shown in the other group, Fig. 6.4.2.

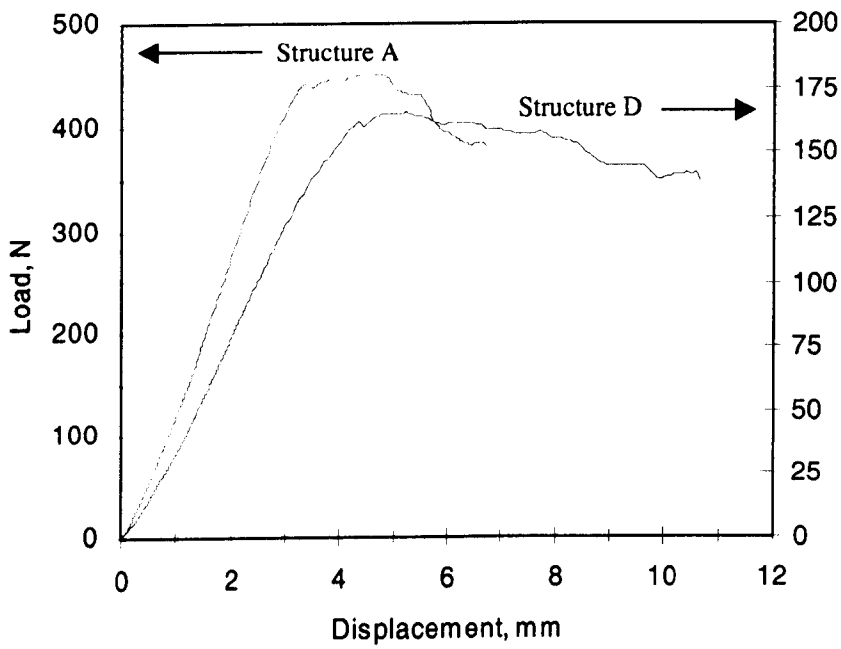

Figure 6.4.1 Load-displacement response from MTPB tests on Structures A and D.

The MTPB load-displacement traces for Structures A to F were essentially linear. In each case crack propagation was stable and a residual displacement of less than 0.5 mm

remained at the end of the test. As in the case of the CNFS test, this resudual displacement was attributed to deformation within the core material during the MTPB test. Since the load-displacement traces of Structures A to F were similar, Structures A and D are used to represent the response of all these systems as shown in Fig. 6.4.1.

Crack propagation in MTPB specimens from Structures L to R was unstable. Here, the loading curves for each specimen were linear as shown in Fig. 6.4.2.

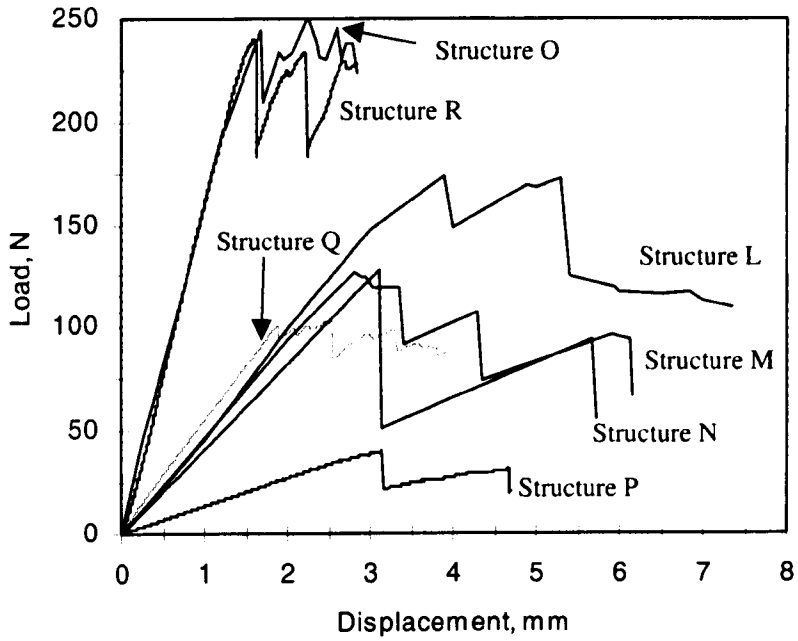

Figure 6.4.2 Load-displacement response following MTPB tests on Structures L to R.

The upper face-sheet/core interface as indicated in Fig. 4.2.2 of Structures L to O was tested using the MTPB geometry. Crack growth in Structures L and M occurred between the CFRP interlayer and the Kevlar®/epoxy face-sheets and was accompanied by fibre bridging. Here, unstable crack growth corresponded to the bridging fibres being pulled

from the fracture surfaces. The unstable crack propagation exhibited by Structures N and R was attributed to the cracks growing through the PVC foam core material.

6.4.2 Variation of Specimen Compliance with Crack Length

The same data reduction procedures to those used with the CNFS tests were used to calculate the fracture toughness values following MTPB tests on Structures A to F and Structures L to R. Examples of typical compliance versus crack length curves obtained following these tests are presented in Fig. 6.4.3.

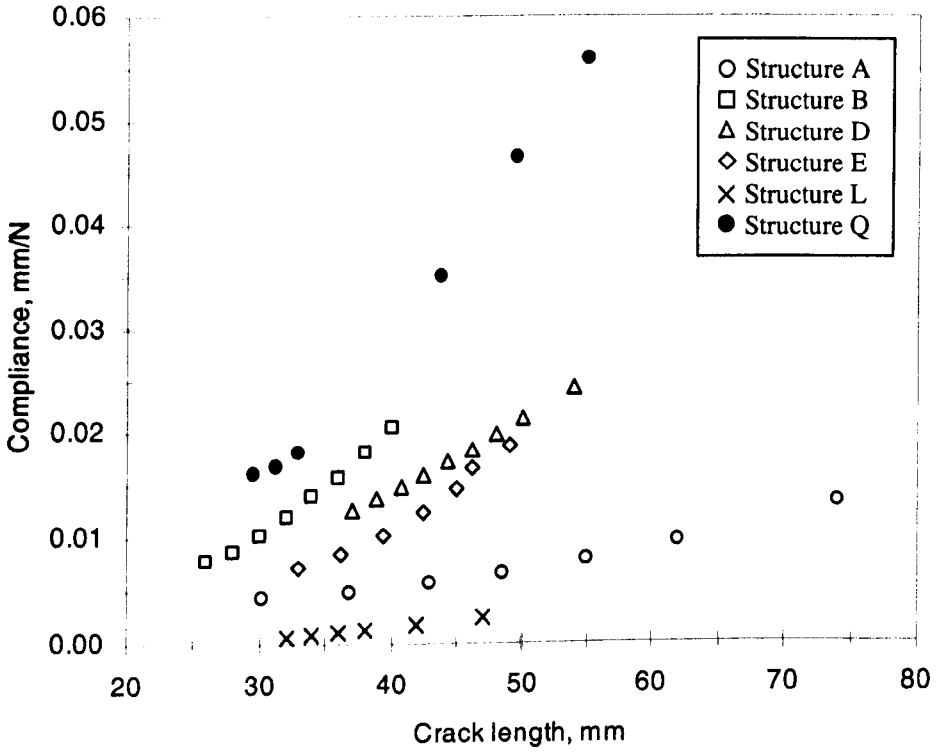

Figure 6.4.3 Examples of compliance vs. crack length data following MTPB tests on the structures indicated in the legend.

Again following the procedures detailed in Sections 3.5.2 and 4.3.4, the appropriate curves were plotted to calculate the constants in the crack length extension method and the compliance calibration technique. Furthermore, in agreement with the findings from the CNFS tests and the finite element models, the crack length extension factor was found to have a positive relationship with face-sheet thickness. Figure 6.4.4 presents the cube root of compliance versus crack length curves from MTPB tests on Structures P to R which differ only in the thickness of the face-sheet used in the sandwiches.

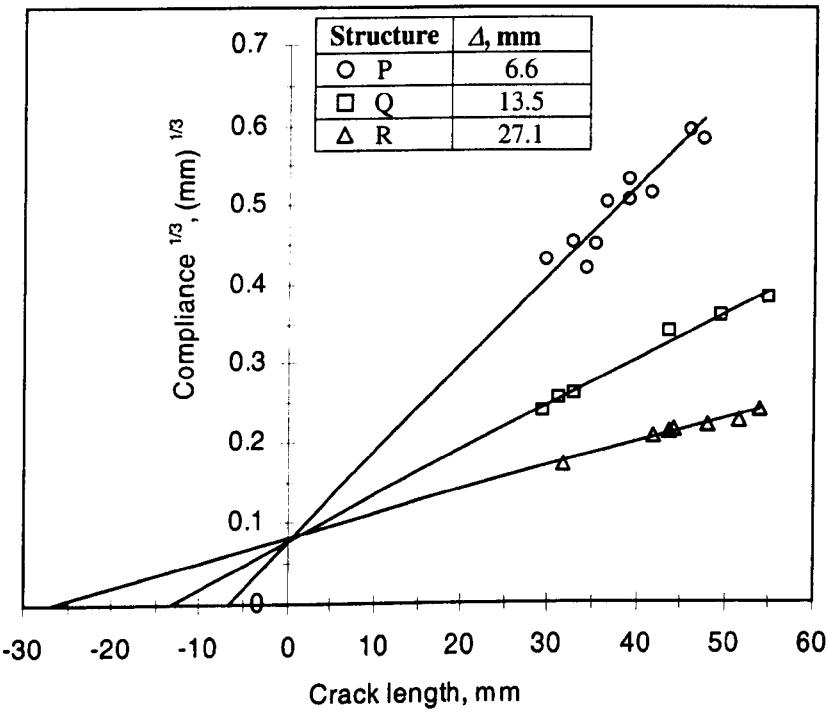

Figure 6.4.4 Examples of the cubed root compliance vs. crack length curves following MTPB tests on Structures P to R.

As expected, the compliance calibration technique constants, C_o and k, decreased with increasing face-sheet thickness as illustrated in Fig. 6.4.5. A summary of this study is given in Table 6.4.1.

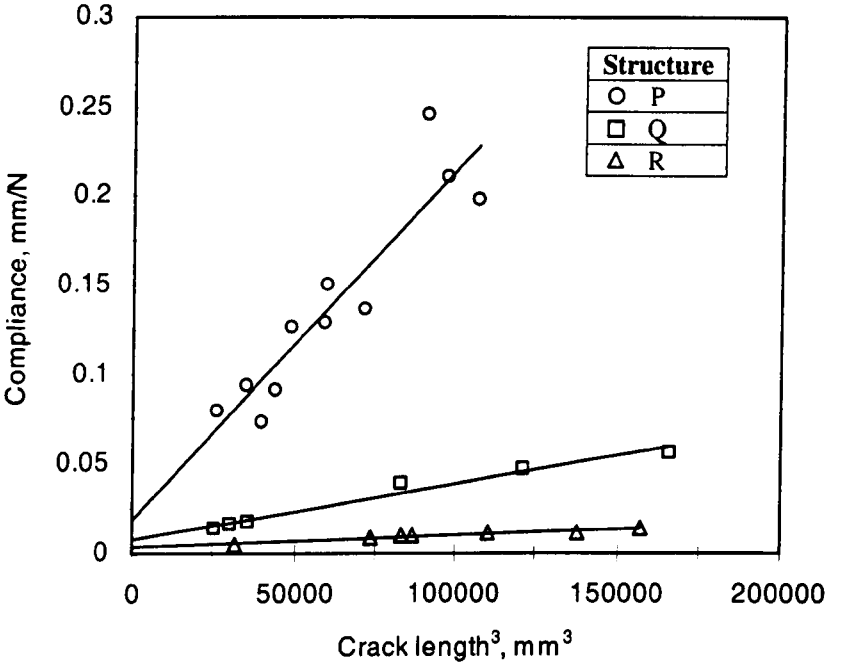

Figure 6.4.5 Examples of compliance vs. the cube of crack length plots for determining 'C_o' and 'k' following MTPB tests on Structures P to R.

MTPB test specimen	Face-sheet thickness, mm	Δ (Experimental) mm	Δ (Numerical) mm	C_o mm/N × 10^{-2}	k $N^{-1}mm^{-2}$ × 10^{-8}
P	1	6.6	7.1	1.82	195
Q	2	13.5	12.1	0.81	31
R	4	27.1	26.9	0.38	6.5

Table 6.4.1 The effect of face-sheet thickness on the crack length extension factor and the compliance calibration constants following MTPB tests on Structures P to R.

The measured values of the crack length extension factor are compared in Table 6.4.1 with those predicted by the FE analyses and the two sets of results are in good agreement.

Having determined the crack length extension factor and the compliance calibration constants associated with each test, the interfacial fracture toughness was calculated. Table 6.4.2 presents an example of the interfacial fracture toughness of Structure B calculated using both techniques.

a mm	P N	δ mm	k $N^{-1}mm^{-2} \times 10^{-8}$	C_o mm/N	Δ mm	G_c^1 J/m^2	G_c^2 J/m^2
26	450	3.5	27.7	0.0028	9.44	2651	2212
28	448	3.8	27.7	0.0028	9.44	2435	2395
30	419	4.3	27.7	0.0028	9.44	2467	2542
32	403	4.8	27.7	0.0028	9.44	2566	2713
34	369	5.1	27.7	0.0028	9.44	2432	2626
36	350	5.4	27.7	0.0028	9.44	2352	2561
38	332	6.0	27.7	0.0028	9.44	2380	2623
40	318	6.5	27.7	0.0028	9.44	2382	2640
Average interfacial fracture toughness, J/m^2						**2458**	**2539**

[1] G_C calculated from the compliance calibration technique [2] G_C calculated from the crack length extension factor method.

Table 6.4.2 Example of the crack length extension factor technique and the compliance calibration method used to calculate interfacial fracture toughness values following the MTPB tests. The specimen was a UD glass fibre/Nomex® sandwich (Structure B).

Echoing the findings from the CNFS tests, the two data reduction techniques yield very similar interfacial fracture toughness values.

6.4.3 Interfacial Fracture Toughness of Structures A to F

The interfacial fracture toughness of sandwich structures A to F were reported in the first section of this chapter. Reiterating the findings, all of these Structures were found to offer fracture toughness values close to 2500 J/m^2. Here, crack propagation occurred within the Nomex core material in each specimen, which explains the similar toughness values reported for these systems.

6.4.4 Interfacial Fracture Toughness of Structures L to O

MTPB tests were conducted on Structures L and M in which the Kevlar® face-sheet/core interface indicated in Fig. 4.2.2 was debonded. Additionally, the upper CFRP face-sheet/core interface of Structures N and O were tested, Fig. 4.2.2. In the case of the first two structures, crack propagation occurred between the Kevlar® facings and the CFRP interlayer. Kevlar® fibres were observed to bridge the propagating crack during these MTPB tests. An inspection of the fracture surfaces revealed that Kevlar® fibres remained bonded to the interlayer surface as shown in Fig. 6.4.6.

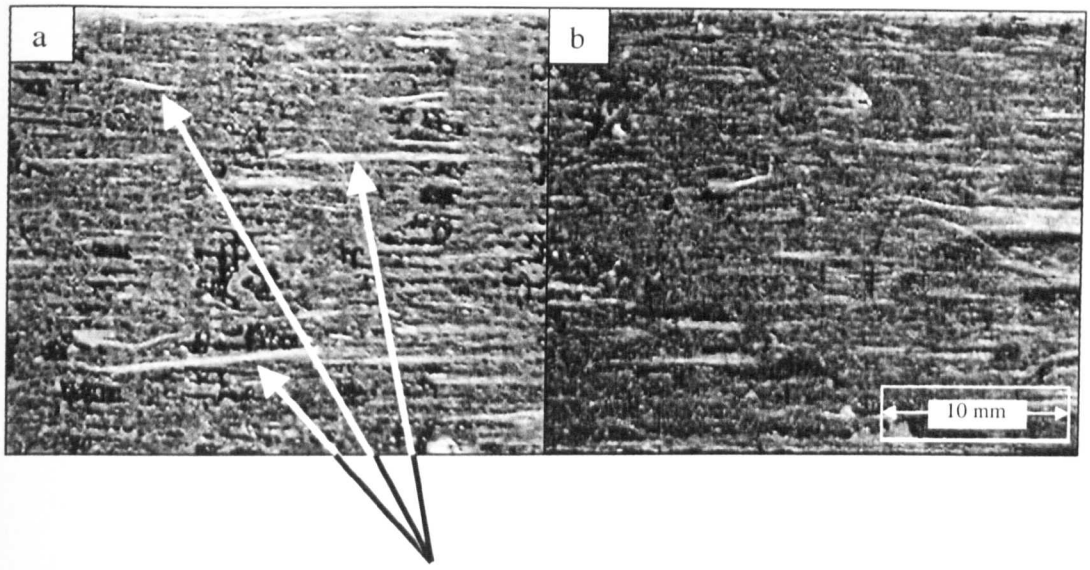

Figure 6.4.6 Fracture Surfaces following of Structure M following an MTPB test, (a) Kevlar fibres have remained bonded to the woven fabric carbon interlayer, (b) fracture surface of the Kevlar reinforced face-sheet, showing areas where the unidirectional fibres have been detached.

The interfacial fracture toughness calculated following MTPB tests on Structures L and M are presented in Figure 6.4.7. The scatter in the data is attributed to the difference in the extent of fibre bridging between different specimens. The average toughness values for Systems L and M were 1200 and 860 J/m^2 respectively.

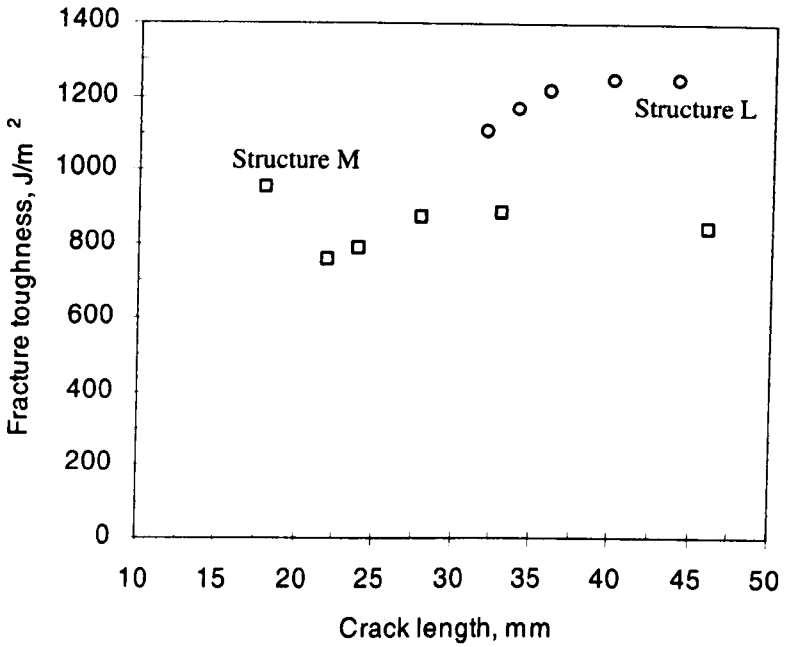

Figure 6.4.7 Interfacial fracture toughness data following MTPB tests on Structures L and M.

Crack propagation during MTPB tests on Structures N and O occurred within the PVC/PUR foam core material, as illustrated in the micrographs in Fig. 6.4.8. The average fracture toughness calculated for these two systems were in good agreement, at approximately 700 J/m^2. This value is similar to previously-reported Mode I fracture toughness values on the foam system used in these sandwich systems. [11].

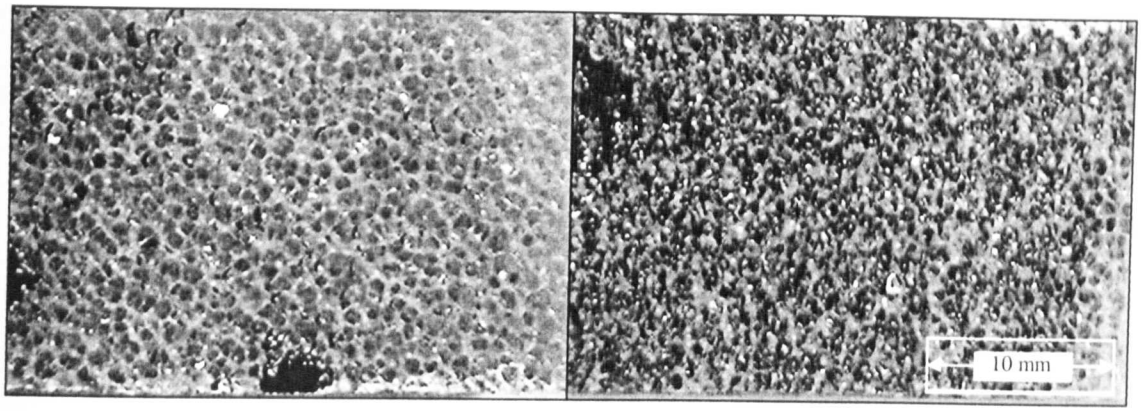

Figure 6.4.8 Fracture surfaces following an MTPB test on Structure N, (a) Foam core fracture surface, (b) Face-sheet fracture surface. The foam material is clearly visible on this surface.

6.4.5 Interfacial Fracture Toughness of Structures P to R

The average fracture toughness values calculated following MTPB tests on Structures P to R are presented in Fig. 6.4.9. There is clearly a significant variation in toughness between the different structures, which was unexpected as crack growth in all cases occurred within the crosslinked PVC foam material. However, an inspection of the face-sheet fracture surfaces revealed that crack propagation had occurred closer to the face-sheet/core interface in Structures P and Q in comparison to Structure R. This is probably due to the action of the resin layer on the surface of the PVC core material during the lay-up process of theses systems. It is thought more of the adhesive resin used to bond the face-sheets to the core will have penetrated further into the core material for the structures with the thicker face-sheets, providing a greater amount of mechanical bonding with the core material.

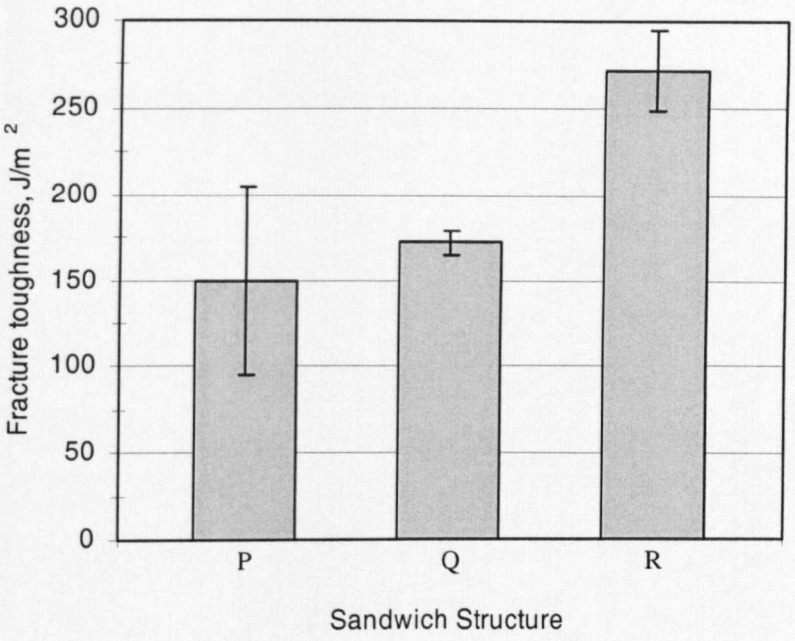

Figure 6.4.9 Average interfacial fracture toughness values following MTPB tests on Structures P to R.

Furthermore, the scatter in the fracture toughness values following MTPB tests on Structure P are very high, which was probably due to the variation in the toughness of the face-sheet/core bond, although this average value is in moderate agreement with the fracture toughness determined following CNFS tests on Structure P.

6.4.6 Summary of The Interfacial Fracture Toughness Tests on Structures A to F and Structures L to R

Table 6.4.3 presents the average interfacial fracture toughness of the structures tested using the MTPB geometry. The reported toughness data in the table represents average

values from four MTPB tests on each structure. Where available, corresponding fracture toughness values are quoted from the literature for similar sandwich systems.

Sandwich Structure	Component materials		Crack location	Fracture toughness (MTPB tests)	Fracture toughness (Literature)
	Face-sheet	Core		J/m^2	J/m^2
A	[0°/90°] UD Glass/epoxy	Nomex®	Core	2610 (190)1	2794 [2]
B	[0°/90°] UD glass/epoxy	Nomex®	Core	2598 (211)	2679 [2]
C	[0°/90°] UD glass/epoxy	Nomex®	Core	2352 (698)	2360 [2]
D	[0°/90°] UD carbon/epoxy	Nomex®	Core	2487 (192)	2787 [2]
E	[0°/90°] UD carbon/epoxy	Nomex®	Core	2554 (104)	2807 [2]
F	[0°/90°] UD carbon/epoxy	Nomex®	Core	2476 (247)	2732 [2]
L	UD Kevlar®/epoxy	C70.130	Core/interface	1200 (97)	
M	UD Kevlar®/epoxy	C70.130	Core/interface	900 (74)	
N	[0°/90°] woven carbon/epoxy	C70.130	Core/interface	704 (25)	711 [11][3]
O	[0°/90°] woven carbon/epoxy	C70.130	Core/interface	697 (30)	711 [11][3]
P	[±45°] woven glass/polyester	Crosslinked PVC (75 kg/m^3)	Core	153 (54)	179 [11][3]
Q	[±45°] woven glass/polyester	Crosslinked PVC (75 kg/m^3)	Core	172 (7)	179 [11][3]
R	[±45°] woven glass/polyester	Crosslinked PVC (75 kg/m^3)	Core	272 (23)	179 [11][3]

[1] Numbers in parenthesis denote standard deviation, [2] Crack growth bridged by fibres, [3] Fracture toughness values from Mode I tests of the corresponding core material.

Table 6.4.3 Summary of the face-sheet/core fracture toughness of Structures A to F and L to R. When available, a comparison is made with fracture data reported in the literature.

Again, the Nomex®-based sandwich structures offered the highest fracture energies, which, in the majority of cases, were in good agreement with the toughness values

calculated via CNFS tests on these structures. Structures L and M offered moderate fracture toughness values. Here, it is likely that the occurrence of fibre bridging enhanced these values. Crack growth in Structures N and O occurred within the PVC/PUR foam core. The subsequent toughness values following MTPB tests on Structure N and O were found to compare closely with previously published Mode I toughness values measured on the same core material [11], which gives confidence in the toughness data reported here. Echoing the findings from the CNFS tests, the specimens in which crack growth occurred in a foam core material offered the lowest fracture toughness values. Furthermore, in accordance with previous findings [12,13], the fracture toughness values of the foam core systems reported here, appear to be directly proportional to the density of the foam through which crack growth occurred. The tests conducted on the crosslinked PVC-based structures with different face-sheet thicknesses (Structures P to R) have shown that even though crack growth occurred within the core material, the resulting fracture toughness will be a function of the of the mechanical bonding created at the interface, in addition to the toughness of the material through which the cracks grow.

6.5 Effect of Temperature and Crosshead Displacement Rate on the Interfacial Fracture Toughness of PVC Foam-based Sandwich Structures

6.5.1 Effect of Crosshead Displacement Rate on Fracture Toughness

Typical load-displacement records following TPBS tests on Structure Q at five different crosshead displacement rates are presented in Figs. 6.5.1 and 6.5.2.

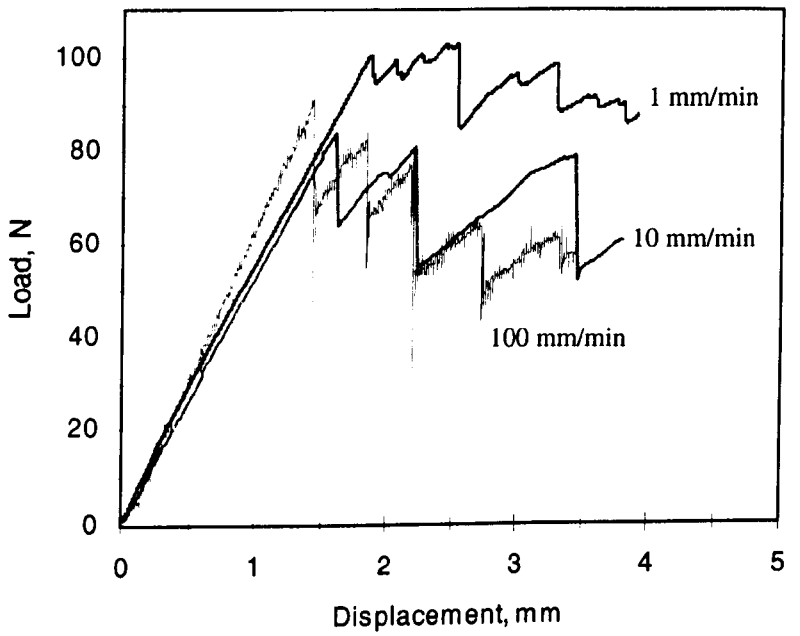

Figure 6.5.1 Load-displacement response of Structure Q following MTPB tests at 1, 10 and 100 mm/min.

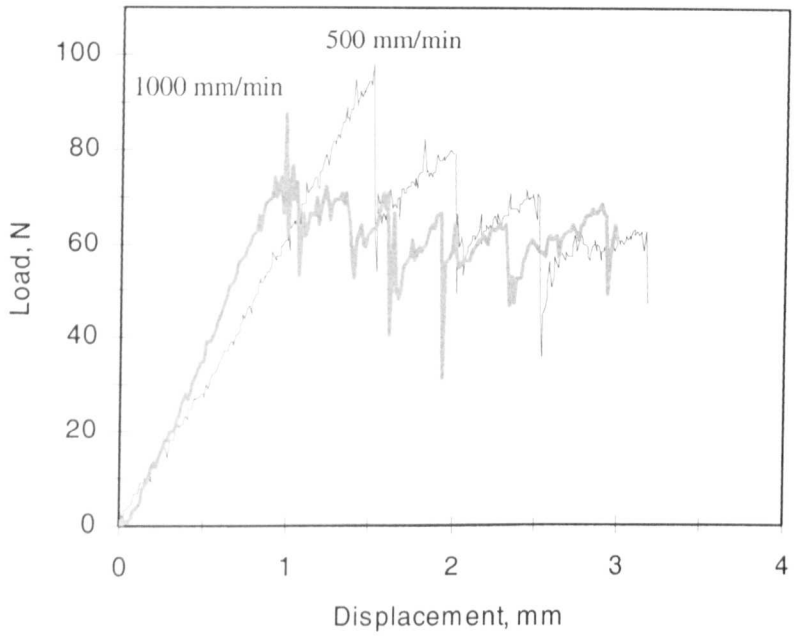

Figure 6.5.2 Load-displacement response of Structure Q following MTPB tests at 500 and 1000mm/min.

The load-displacement responses are similar at the five crosshead displacement rates, although the critical load at fracture initiation decreased slightly with increasing crosshead displacement rate. Crack propagation was too rapid to monitor optically at higher displacement rates, therefore the areas method was used throughout to calculate fracture toughness values for these samples. The average fracture toughness values following these tests are presented as a function of displacement rate, Fig. 6.5.3. The figure shows that the fracture toughness suffered a significant decrease from 180 J/m^2 at 1 mm/min to 103 J/m^2 at 1000 mm/min. Previous investigations into the effect of displacement rate on the fracture toughness of the foam core used in Structure Q have also reported a decrease in toughness with increasing crosshead displacement rate [14-

16]. As crack growth occurred within the core material in all tests, it is believed that the decrease in fracture toughness with increasing displacement rate reported here is a consequence of the visco-elastic properties of the PVC foam. Furthermore, this result suggests that care should be taken when selecting materials for use in sandwich components which may be subjected to dynamic loads during operational service.

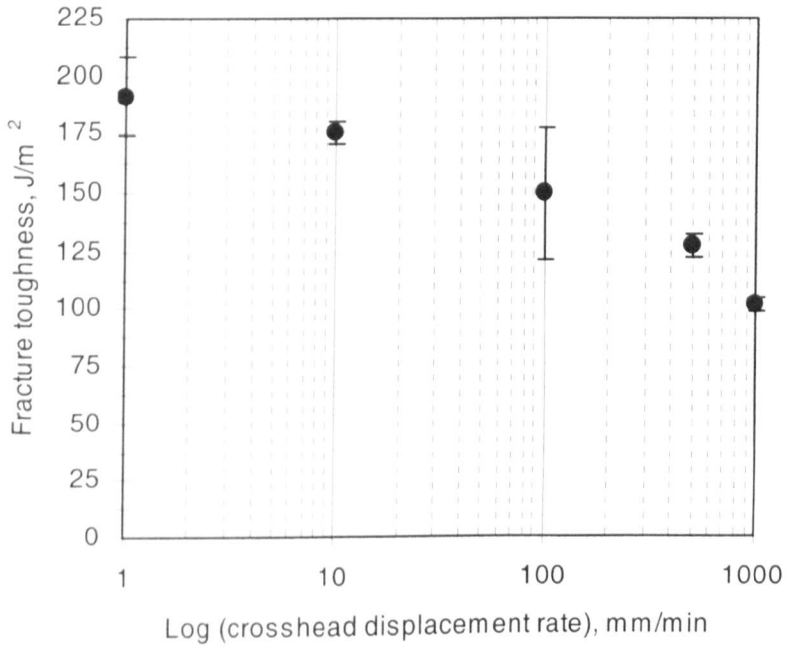

Figure 6.5.3 Influence of crosshead displacement rate on interfacial fracture toughness following TPBS tests on Structure Q.

6.5.2 Effect of Temperature on Fracture Toughness

The load-displacement response at a range of temperatures following MTPB tests on Structure R is shown in Fig. 6.5.4. It can be seen that the test temperature does not significantly affect the mode of crack propagation. However, an increase in the test

temperature to 40°C did result in a more stable mode of crack growth. Furthermore, crack propagation occurred within the core material in each case. The temperature chamber used to conduct the MTPB tests prevented monitoring of crack advance, therefore, the areas method was used to calculate an average interfacial fracture toughness in each test.

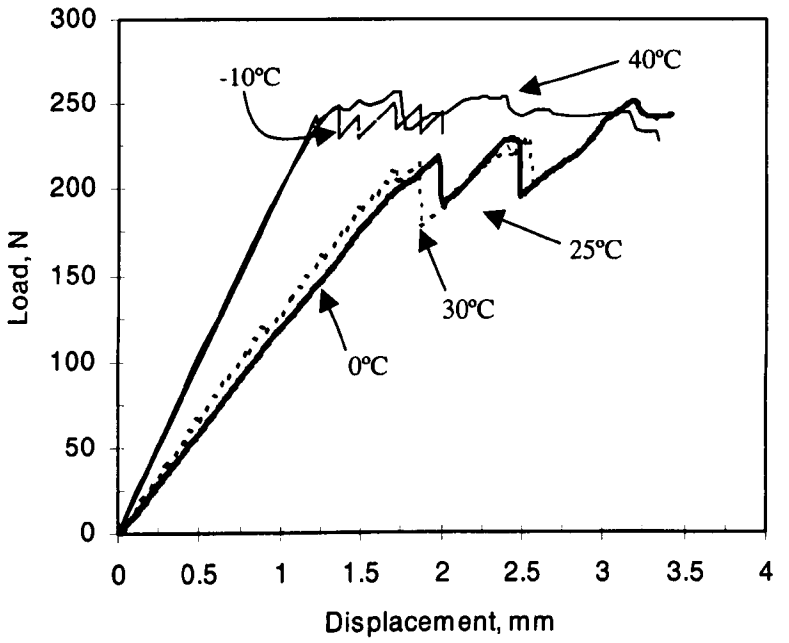

Figure 6.5.4 Load-displacement records following MTPB tests on Structure R at different temperatures.

The fracture toughness values determined from these tests shows a positive relationship between G_c and temperature, although a slight decrease in G_c was measured from 30° to 40°C, Fig. 6.5.5. This is likely to be due to the fact that the highest temperature used in this study approached the glass transition temperature of the PVC foam. This increase in

fracture toughness at elevated temperatures corresponds to the reduction in G_c at higher loading rates, which appears to support the contention that the observed sensitivity of the interfacial fracture toughness of this sandwich system is a consequence of the visco-elastic properties of the core material.

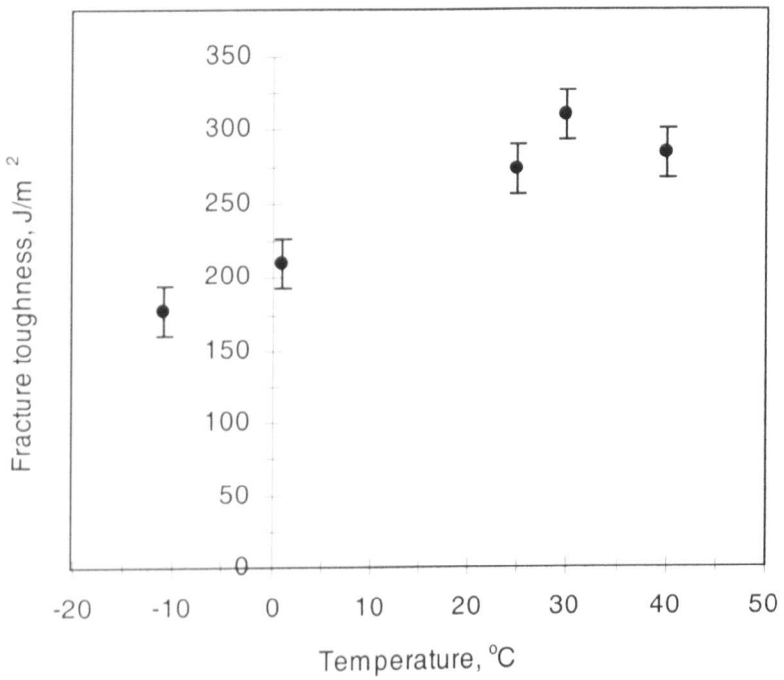

Figure 6.5.5 Effect of temperature on interfacial fracture toughness following MTPB tests on Structure R.

Again, these findings suggest that care should be taken when selecting materials for sandwich components, which may have to withstand a certain range of temperatures during the operational service of the construction.

6.6 J-Integral Estimation

6.6.1 Equivalence of J_c to G_c

For fracture specimens that respond in a linear elastic manner during a test, the J integral measured at fracture initiation is equal to the fracture toughness, G_c. In this instance the following equality holds true:

$$J_C = G_C \therefore \frac{1}{B}\frac{dU}{da} = \frac{P^2}{2B}\frac{dC}{da} \tag{6.6.1}$$

Thus, CNFS tests on Panels I and P, which responded linearly during the tests, were conducted to estimate both G_c and J_c, enabling a comparison between the two values. Five CNFS specimens from Structure I, each with a different pre-crack length, were tested until fracture initiation. The values of P_c measured from each test are given in Table 6.6.1.

Pre-crack length mm	P_C, N
19	223
27	180
35	165
41	140
63	120

Table 6.6.1 Critical load for different pre-crack lengths following CNFS tests on Structure I.

Here, the J-integral was calculated via the constant load method, enabling J to be determined from plotting the stored elastic strain energy versus crack length for a range of load values as shown in Fig. 6.6.1. The J values were then plotted as a function of

load, Fig. 6.6.2, and using a power law relationship between J and load values of J corresponding to the critical loads to cause fracture, J_c, were determined for each crack length. Additionally, the crack length extension factor method was used to calculate G_c. Figure 6.6.3 compares the fracture toughness with the critical J integral. The agreement between the two values is good for the smallest three crack lengths and are significantly different for the two largest crack lengths. This is probably due to the assumed power law relationship between J and load, where the values of J_c are estimated by extrapolating the curve. Furthermore, the response of the specimen may vary slightly from linear elastic behaviour.

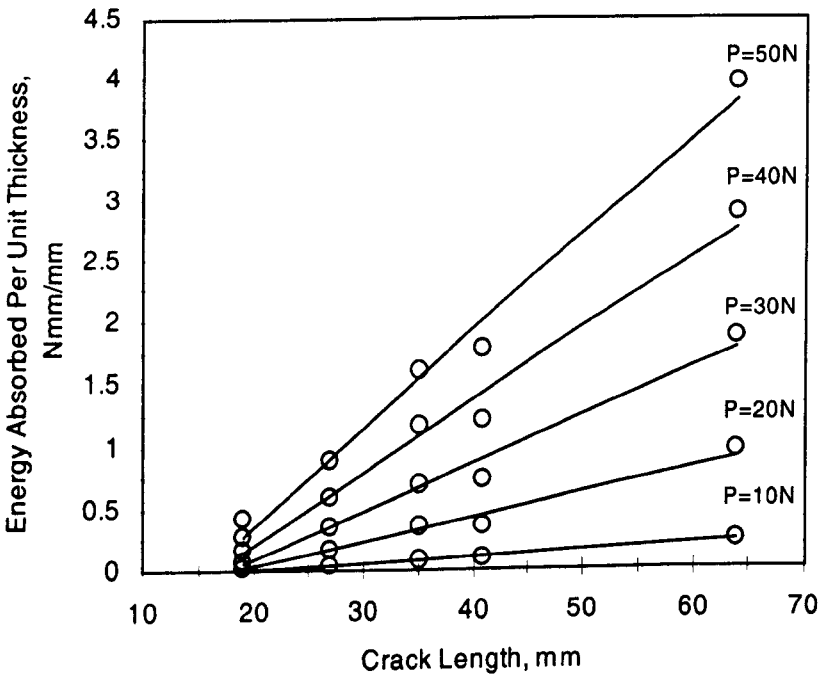

Figure 6.6.1 The linear relationship between the stored elastic strain energy and crack length at a range of loads. The J integral taken as the gradient of the lines.

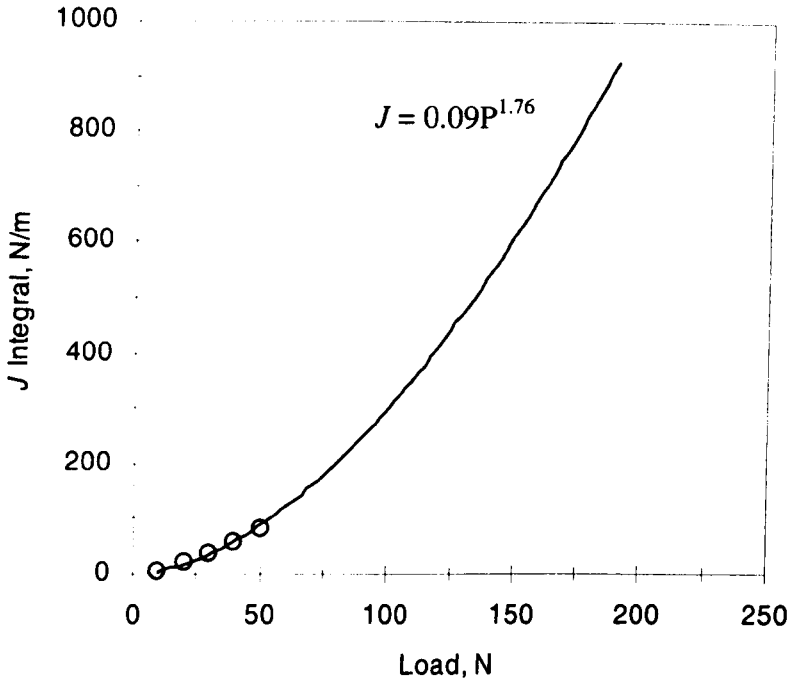

Figure 6.6.2 The *J* integral plotted as a function of load. Here a power law relationship is assumed.

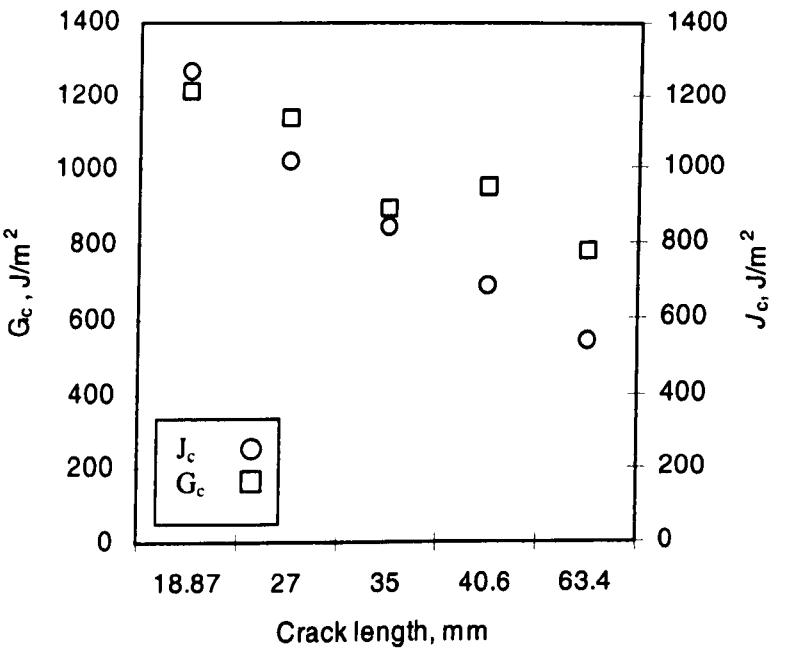

Figure 6.6.3 Comparison of G_c with J_c following CNFS tests on Structure I.

Following CNFS tests on Structure P, the interfacial fracture toughness and the J integral were calculated. Figures 6.6.4 and 6.6.5 show the data used to calculate the J integral. Using the values of load at fracture initiation for different crack lengths, a series of values of J_c were calculated using Fig. 6.6.5. The average value of J_c was 184 J/m^2, approximately 10% greater than the average fracture toughness value calculated using the crack length extension factor. Again, this moderate difference is thought to be due to extrapolation method used to estimate J_c for a given load and because the CNFS specimens may undergo a slight amount of yielding during the tests.

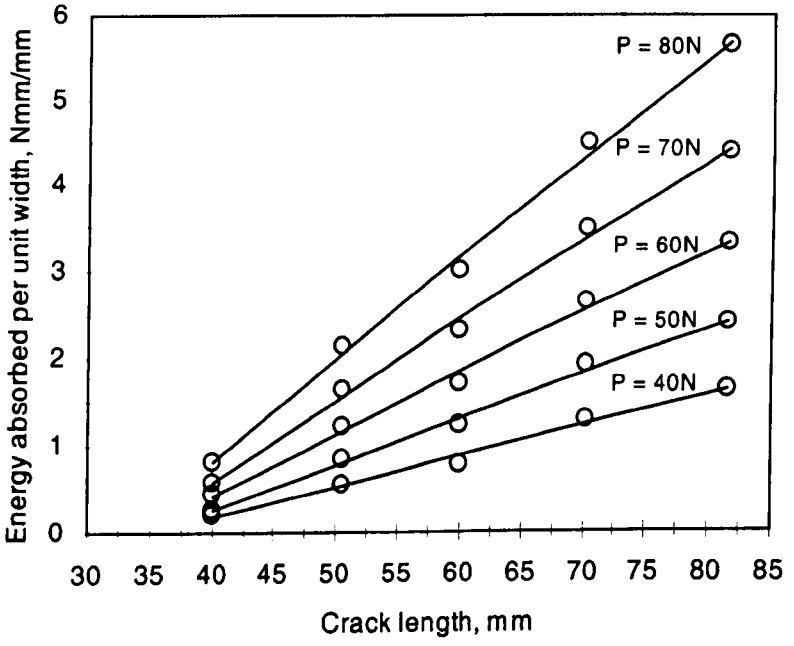

Figure 6.6.4 The linear relationship between the stored elastic strain energy and crack length at a range of loads. CNFS tests on Structure P.

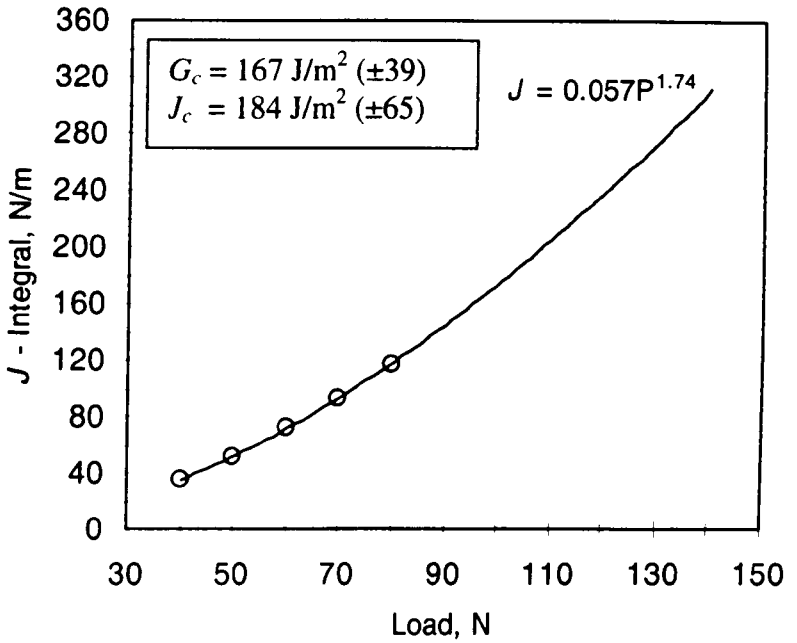

Figure 6.6.5 The J integral plotted as a function of load. Following CNFS tests on Structure P.

The preliminary tests on Structures I and P have shown that the J integral test procedure can provide values of J_c that are in moderate agreement with the fracture toughness values calculated using LEFM-based techniques. This demonstrates that the J integral should be a valid criterion for crack growth in the beam-type sandwich specimens investigated herein.

6.6.2 *J*-Integral Estimation – CNFS Tests on Structure J

The J-integral estimation data from CNFS tests on Panel J are presented in Figures 6.6.6 and 6.6.7. Here again, the constant load method was used for the J-integral estimation, and a value of J_c was extrapolated according to the average critical load observed during

CNFS tests on this panel (330N ±20N). This value was compared with an average fracture toughness value reported previously for the same sandwich system following MTPB tests [8]. The result shows good agreement between J_c from CNFS tests and G_c from MTPB tests for Panel J.

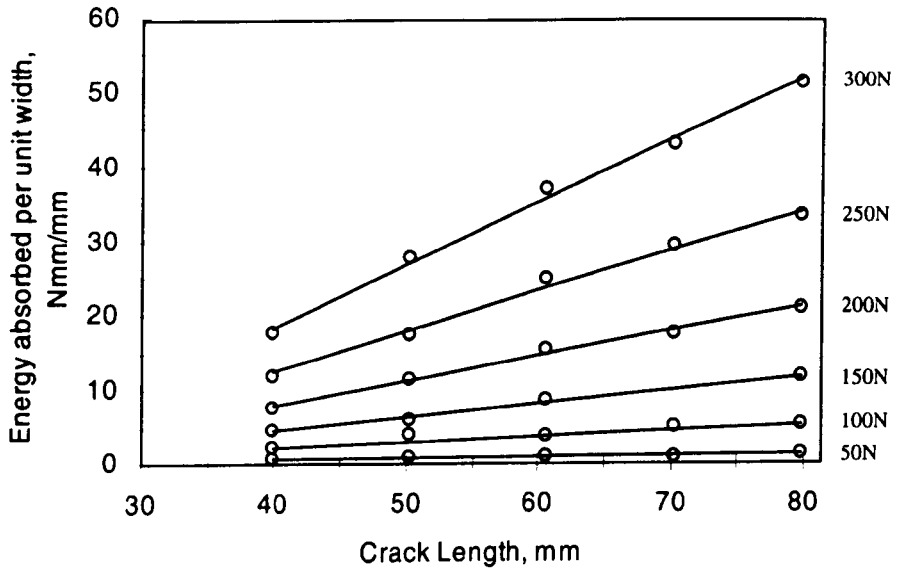

Figure 6.6.6 The linear relationship between the stored elastic strain energy and crack length at a range of loads. CNFS tests on Structure J.

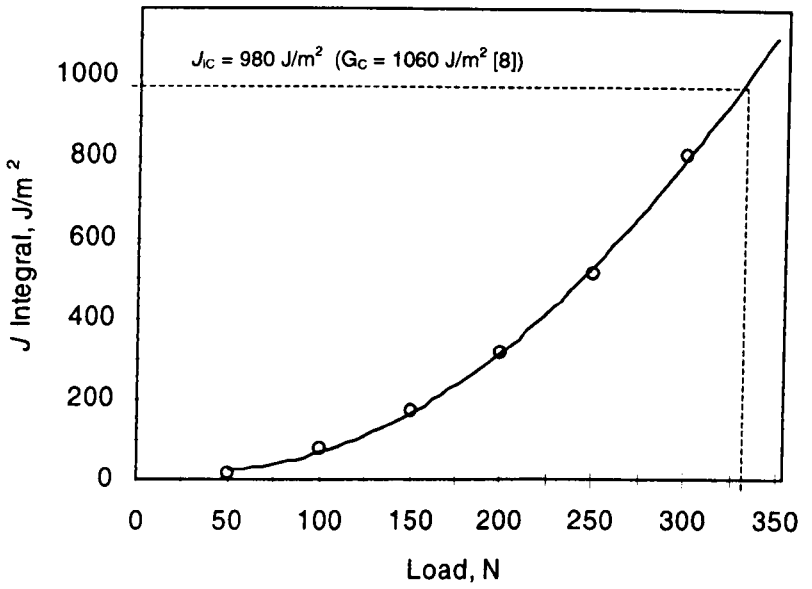

Figure 6.6.7 The *J* integral plotted as a function of load. Following CNFS tests on Structure J.

6.6.3 Summary of *J* Integral Testing

The tests outlined in this section have suggested that the *J*-integral can be used as a fracture criterion for sandwich specimens that do not adhere to LEFM. Initial tests illustrated that J_c is reasonably comparable to G_c for the samples tested here that exhibited a linear elastic response during CNFS tests. The J integral was also determined following CNFS tests on Structure J, during which yielding occurred within the linear PVC core material. A comparison of J_c of this system with fracture toughness values from the literature for the same structure showed good agreement. It is noted, however, that in the case of Panel J, the *J*-integral does not provide an actual fracture toughness. As stated previously [17], for specimens that do not comply with LEFM, the *J*-integral should be considered as a quantity that is characteristic of the displacement field

surrounding a crack-tip. This statement implies that the *J*-integral is therefore characteristic of the strain energy stored within a specimen, and thus a fracture toughness can be inferred from the *J*-integral values, as demonstrated from the tests conducted on Structure J.

6.7 Summary of Experimental Findings

A series of investigations were undertaken with the primary aim of characterising the face-sheet/core interface of sandwich structures representative of those used in the marine and aerospace industries. Initially, a test geometry, the centre notch flexure specimen, was designed specifically for conducting face-sheet peel tests on sandwich laminates based on thin facings. Subsequent tests conducted on a range of sandwich systems highlighted the suitability of this test geometry for conducting the peel tests. The Nomex® honeycomb-based systems were found to offer the highest interfacial fracture toughness, in comparison to those structures based on a crosslinked PVC foam core which offered the lowest fracture energies. A comparison of the interfacial fracture toughness determined for a number of the structures investigated here, showed good agreement with data available in the literature. This lent some confidence to the reliability of the fracture test methods used herein. Furthermore, following MTPB tests on Structure Q and R, the interfacial fracture toughness of these systems was found to be moderately rate sensitive. The *J* integral was used as an alternative fracture criterion to

the LEFM-based criteria and a series of tests demonstrated that J integral can be applied to the beam-type sandwich specimens investigated within.

6.8 References

[1]. Liechti, K.M. and Marton, B, Submitted to Experimental Mechanics, 2001.

[2]. Gower M.R.L., Sims G.D., Ratcliffe J. and Cantwell W.J., Institute of Mechanical Engineers, UK, Paper C548/015/99, pp99-110.

[3]. Cartie D.D.R. and Partridge I.K., Proc. Sixth International Conference - Deformation and Fracture of Composites, Institute of Materials Science, 2001, pp49-55.

[4]. Cantwell W.J., Scudamore R., Ratcliffe J. and Davies P., Composites Science and Technology, Vol.59, 1999, pp2079-2085.

[5]. Prasad, S. and Carlsson, L.A., Engineering Fracture Mechanics, Vol.47, 1994, pp825-841.

[6]. Kinloch, A.J., Young, R.J., Fracture behaviour of polymers, Applied Science Publishers LTD, 1983.

[7]. Carlsson, L.A., Sendlein L.S. and Merry S.L., Journal of Composite Materials, Vol.25, 1991, pp101-116.

[8]. Scudamore, R., Ph.D Thesis, University of Liverpool, UK, 2000.

[9]. Cantwell, W.J. and Davies, P., Applied Composite Materials, Vol.3, 1996, pp407-420.

[10]. Carlsson L.A., Sendlein L.S. and Merry S.L., First International Conference on Sandwich Construction, 1989, pp571-575.

[11]. Cantwell W.J., Fracture Properties of Foams and Balsa, University of Liverpool Report for Airex, Switzerland, 1996.

[12]. Zenkert D., Composite Structures, Vol.17, 1991, pp331-350.

[13]. Li X., and Carlsson L.A., Journal of Sandwich Structures and Materials, Vol.1, 1999, pp60-75.

[14]. Zenkert D. and Backlund J., Composites Science and Technology, Vol.34, 1989, pp225-242.

[15]. Danielsson M., and Olsson, K-A., Proc. Third International Conference on Sandwich Construction, Vol.2, 1995 pp535-544.

[16]. Cantwell W.J., The Influence of Loading Rate on The Fracture Toughness of Foam Materials, University of Liverpool Report for Airex, Switzerland.

[17]. Begley J.A., Landes J.D., Progress in Flaw Growth and Fracture Toughness Testing, ASTM STP 536, 1973, pp246-263.

7. CONCLUSIONS

7.1 General Summary

Having conducted a search of the literature, a number of issues requiring further attention were identified. The major gap was found to be the characterisation of the face-sheet/core interface strength of sandwich laminates comprised of thin face-sheets. This led to the formation of the objectives outlined at the end of Chapter 2. The success with which these objectives were realised, in addition to the findings from the experimental and numerical modelling investigations are the subject of the following summary.

- The research was initiated by designing a test configuration, which enabled the characterisation of the face-sheet/core fracture toughness of sandwich laminates with thin facings. The resulting test configuration, the centre notch flexure sandwich (CNFS) specimen, was used to determine the face-sheet/core fracture toughness of a wide range of sandwich laminates. The fracture toughness data obtained was compared to data from an alternative test, and were found to provide consistent toughness values. Furthermore, the fracture toughness data determined following CNFS tests gave similar values to those reported in the literature for the same sandwich systems and constituent materials.

- A series of analyses were conducted using the finite element method, with the primary objective being to determine that crack-tip loading conditions of the newly

developed test configuration. Additionally, two existing sandwich fracture test configurations were analysed to predict their crack-tip loading conditions. The analyses predicted that all three configurations would offer highly Mode I dominated loading for sandwich laminates comprised of low modulus core materials and when crack growth occurred in the core material. However, when the crack location was changed to within the face-sheet material, the Mode II loading component was predicted to increase. This effect was only moderate in the CNFS specimen. The MTPB and SCSB were the most sensitive to a change in crack location. The reliability of these findings was judged by analysing geometries for which mode ratio values were available in the literature. The agreement between the analyses here and those from previous work was found to be good, providing assurance as to the accuracy of the analyses detailed here. Furthermore, it was found that in all three test geometries, the Mode II component of loading will increase as the modulus of the core increases; this was true for a crack situated either within the core material and the face-sheet. However, for majority of sandwich constructions, the loading remained Mode I dominated.

In general, the analyses predicted the crack-tip loading conditions in all three specimens to remain reasonably constant with crack length. Moreover, the three test configurations were predicted to provide similar values of mixed-mode loading for the case where crack growth occurs within the core material.

- The interfacial fracture toughness of a wide range of sandwich laminates was determined using the CNFS and MTPB configurations. Nomex® honeycomb based sandwich specimens exhibited a fracture toughness far superior to the balsa and

foam-based structures. Fracture toughness values from linear PVC foam-based structures were found to offer the highest fracture energies of the foam-based systems tested within. Conversely, the crosslinked PVC foam-based sandwich systems gave the lowest interfacial fracture toughness of all the systems tested.

- The *J* integral was used as a fracture criterion to characterise the face-sheet/core interface of three sandwich systems. Here, values of *Jc* calculated following CNFS tests on two sandwich systems which responded in a linear elastic manner were in reasonable agreement with the corresponding fracture toughness values, *Gc*. Furthermore, the *J* integral values determined from a system which exhibited significant yielding during CNFS tests were found to be similar to toughness values of this system reported in the literature. From these findings, it is suggested that the *J* integral can be applied as a fracture criterion for the sandwich specimens investigated within.
- The fracture toughness of a crosslinked PVC foam-based sandwich structure was found to be sensitive to temperature and crosshead-displacement rate, as would be expected. These preliminary findings confirm that these parameters must be considered when selecting a sandwich structure for a specific application.
- By considering the loaded tongues of the MTPB and SCSB specimens as end-loaded cantilever beams, a criterion for the selection of the CNFS geometry can be formulated. From simple beam theory the displacement and bending stress induced in the tongues can be expressed as:

$$\delta = \frac{4Pa^3}{Bh^3E}$$
$$\sigma = \frac{6aP}{Bh^2} \qquad (7.1.1)$$

where δ is the load-point displacement of the tongue, P is the applied load, a is the crack length, E is the Young's modulus, h is the tongue thickness and B is the specimen width (Section 3.3). Combining the two equations above yields an expression for the bending stress, σ, in terms obtained the fracture tests, such that:

$$\sigma = \frac{3\delta hE}{4a^2} \qquad (7.1.2)$$

Thus, the CNFS geometry should be proposed for use when the bending stress approaches the failure stress of the constituent material of the loaded tongue.

In summary, the research conducted here has provided an advancement in face-sheet/core fracture toughness characterisation of sandwich structures, through the development of a novel test configuration which has the potential to rival the existing climbing drum peel technique. The fracture toughness of a wide range of sandwich constructions has been determined. Furthermore, the typical mixed-mode loading conditions of three flexural sandwich beam tests have been predicted with reasonable confidence. Finally, an alternative fracture criterion has been applied to characterise the fracture strength of specimens that exhibit significant yielding within the low-modulus core material during a test.

7.2 Further Work

As a direct consequence of the research detailed here, there are a number of considerations, which may be of interest for future workers in this field.

- The CNFS configuration developed as part of this research, proved to be a valuable tool for testing thin-skinned sandwich laminates. However, the test requires further investigation, with respect to studies such as the effect of pre-crack manufacture and length and specimen span on the measured fracture toughness. Furthermore, it would be useful to conduct a further round robin exercise, in order to test the reliability of the configuration from a number of independent laboratories.
- A number of the shipyard grade sandwich structures exhibited very low interfacial toughness values. An inspection of the fracture surface of these specimens revealed that very little mechanical bonding had been developed at the face-sheet/core interface. Infact, in some instances the surface of the core materials was very smooth (Structure N, Fig. 6.3.13). Clearly, further investigations into the development of a good mechanical bond between unidirectional face-sheets and these foams is required, taking into consideration issues such as adhesive viscosity and surface preparation.
- The finite element models constructed here could be adapted for alternative uses. An example is the requirement to understand the dynamic mode response of sandwich fracture beams subjected to impact strain rates. The FEA could be used

in conjunction with an eigenvalue technique, which would predict the dynamic mode response of these specimens. This information would prove useful, on the basis that data analysis of such specimens is based on beam theory, assumptions from which do not hold if the dynamic mode response is higher than one.

- The *J* integral testing initiated here is in need of further validation. Within the scope of this work, only three sandwich structure types were applied to this type of testing. With materials such as high-ductile linear PVC foams being made available, it is likely that alternatives to LEFM will be required. The *J* integral thus far has proved to be a good candidate.
- A further analysis is required to formulate a criterion to determine the conditions in which the CNFS specimen should be used. The brief analysis presented in the previous section should be extended to complete this task.
- The final consideration is likely the most pertinent issue with respect to characterising face-sheet/core fracture toughness, that being variation in bond quality due to incompatible materials and manufacture. Findings from this research have found that fracture toughness values can vary to above 50% of the mean value. Indeed, some of the blame must lay with the experimentalist, but there can be little doubt that inconsistent manufacturing (particularly within the marine industry) is a major contributor to the observed scatter in the fracture data. It is suggested, therefore, that statistical techniques should be investigated to manage the scatter of the data. Techniques such as Weibull analysis are available for materials which display apparent random failure strengths, such a ceramics. These techniques are useful in that they provide the user of the material with a

'characteristic' property, at which a quantifiable probability of survival can be assigned. This kind of analysis may prove useful in the characterisation of properties such as face-sheet/core interface toughness.

APPENDIX A

The purpose of this appendix is to provide an overview of the computing facilities used to perform the finite element analyses detailed in this thesis. The following provides the facilities used during the research programme, which was conducted at the University of Liverpool.

- The commercial code ABAQUS implicit version 4.6 was used to undertake the finite element analyses.
- The database input file containing the code necessary to conduct the analysis was written on a PC using a standard word processor. This file was saved as a .inp file.
- The University of Liverpool Compute Intensive Service (CIA) was used to run the analyses. This facility was accessed using a Sun Spark 10 workstation. The database input file was transferred from the university managed network to the CIA via an FTP remote login link.
- Solution time for a typical geometrically non-linear analysis conducted within (200000 degrees of freedom) was approximately 20 minutes.
- The disk space required to store the results data created from a typical analysis was 1 GByte.

An example input file is given in the remainder of this appendix. The analysis is of a SCSB test on Structure Q, containing a crack within the core material of length 60 mm and loaded to 50 N.

```
*HEADING
**DATE                          20/5/2001
**MODELLER                      J. RATCLIFFE
**MODEL NAME                    core2.inp
**DESCRIPTION                   scb MODEL OF IQBP SPEC
**                  2-D PLAIN STRAIN, GEOMETRICALLY NON-LINEAR
**                  LINEAR ELASTIC ANALYSIS
**CRACK TIP ELEMENT LENGTH      0.01 mm
**CRACK LENGTH                  60 mm
**
***** CORE NODE AND ELEMENT SPECIFICATION**************
**
*RESTART,WRITE,FREQUENCY=2000
**
**CRACK TIP NODES********
**
*NODE
1,59.97,31.97
1201,59.97,32.
2401,59.97,32.03
38401,60.03,32.03
37201,60.03,32.
199201,60.03,32.
189001,60.03,31.97
18001,60.,31.97
19201,60.,32.
**
**OUTER CRACK TIP NODES********
**
21,59.,31.
2421,59.,33.
38421,61.,33.
37221,61.,32.
199221,61.,32.
198021,61.,31.
18021,60.,31.
**
**left and right hand nodes**
**
```

```
41,49.,31.
2441,49.,33.
101,0.,31
2501,0.,33
198041,71.,31.
199241,71.,32
37241,71.,32.
38441,71.,33.
198071,95.,31.
199271,95.,32
37271,95.,32.
38471,95.,33.
37301,120.,32
38501,120.,33.
**
**node genration**
**
*NGEN,NSET=C1
1,1201,200
*NGEN,NSET=C2
18001,19201,200
*NGEN,NSET=C3
198001,199201,200
*NGEN,NSET=C4
1201,2401,200
*NGEN,NSET=C5
37201,38401,200
*NGEN,NSET=C6
2401,38401,3000
*NGEN,NSET=C7
1,18001,3000
*NGEN,NSET=C8
18001,198001,30000
*NGEN,NSET=C9
18021,198021,30000
*NGEN,NSET=C10
21,18021,3000
*NGEN,NSET=C11
21,2421,200
*NGEN,NSET=C12
2421,38421,3000
*NGEN,NSET=C13
37221,38421,200
*NGEN,NSET=C14
198021,199221,200
*NGEN,NSET=C15
```

```
37241,38441,200
*NGEN,NSET=C16
198041,199241,200
*NGEN,NSET=C17
37271,38471,200
*NGEN,NSET=C18
198071,199271,200
*NGEN,NSET=C19
37301,38501,200
*NGEN,NSET=C20
41,2441,200
*NGEN,NSET=C21
101,2501,200
*NSET,NSET=TIPL
C1
C4
****CRACK TIP NODES GENERATION****
**
*NFILL
C1,C2,6,3000
C2,C3,6,30000
C4,C5,12,3000
**
****OUTER CRACK TIP NODES GENERATION****
**
*NFILL,BIAS=0.84
C3,C14,20,1
C5,C13,20,1
C6,C12,20,1
TIPL,C11,20,1
C7,C10,20,1
C8,C9,20,1
**
****BULK MESH NODE GENERATION****
**
*NFILL,BIAS=0.943
C13,C15,20,1
C14,C16,20,1
C11,C20,20,1
*NFILL
C15,C17,30,1
C16,C18,30,1
C17,C19,30,1
C20,C21,60,1
**
********ELEMENT SPECIFICATION********
```

```
*ELEMENT,TYPE=CPE8R
1,1,401,6401,6001,201,3401,6201,3001
*ELEMENT,TYPE=CPE8R
11,1201,1601,7601,7201,1401,4601,7401,4201
*ELEMENT,TYPE=CPE8R
30,18001,18401,78401,78001,18201,48401,78201,48001
*ELEMENT,TYPE=CPE8R
40,37201,37601,37603,37203,37401,37602,37403,37202
**200,1,2,8002,8001
*ELEMENT,TYPE=CPE8R
100,2401,8401,8403,2403,5401,8402,5403,2402
**300,40001,40002,90002,90001
*ELEMENT,TYPE=CPE8R
200,1,3,403,401,2,203,402,201
**400,290001,290002,290202,290201
*ELEMENT,TYPE=CPE8R
300,1,3,6003,6001,2,3003,6002,3001
**500,81001,81002,81202,81201
*ELEMENT,TYPE=CPE8R
400,18001,18003,78003,78001,18002,48003,78002,48001
*ELEMENT,TYPE=CPE8R
500,198001,198401,198403,198003,198201,198402,198203,198002
*ELEMENT,TYPE=CPE8R
600,37221,37621,37623,37223,37421,37622,37423,37222
**1200,290012,290013,290213,290212
*ELEMENT,TYPE=CPE8R
1000,198021,198421,198423,198023,198221,198422,198223,198022
**1800,81012,81013,81213,81212
*ELEMENT,TYPE=CPE8R
3000,21,23,423,421,22,223,422,221
*ELGEN,ELSET=CORE
1,3,400,1,3,6000,3
11,3,400,1,6,6000,3
30,3,400,1,3,60000,3
40,3,400,1,10,2,3
100,6,6000,1,10,2,6
200,10,2,1,6,400,10
300,10,2,1,3,6000,10
400,10,2,1,3,60000,10
500,3,400,1,10,2,3
600,3,400,1,40,2,3
1000,3,400,1,25,2,3
3000,40,2,1,6,400,40
**
****CORE REMAINDER****
**
```

```
*NODE
200000,59.,3.
217000,59.,31.
200020,49.,3.
217020,49.,31.
200080,0.,3.
217080,0.,31.
440000,61.,3.
457000,61.,31.
440020,71.,3.
457020,71.,31.
440050,95.,3.
457050,95.,31.
*NGEN,NSET=CC1
440050,457050,100
*NGEN,NSET=CC2
440020,457020,100
*NGEN,NSET=CC3
440000,457000,100
*NGEN,NSET=CC4
200000,217000,100
*NGEN,NSET=CC5
200020,217020,100
*NGEN,NSET=CC6
200080,217080,100
*NFILL,BIAS=0.943
CC3,CC2,20,1
CC4,CC5,20,1
*NFILL
CC2,CC1,30,1
CC4,CC3,12,20000
CC5,CC6,60,1
*ELEMENT,TYPE=CPE8R
4000,200000,200200,200202,200002,200100,200201,200102,200001
*ELEMENT,TYPE=CPE8R
14000,200000,240000,240200,200200,220000,240100,220200,200100
*ELEMENT,TYPE=CPE8R
24000,440000,440002,440202,440200,440001,440102,440201,440100
*ELGEN,ELSET=CORE
4000,85,200,1,40,2,85
14000,6,40000,1,85,200,6
24000,25,2,1,85,200,25
**
****TOP SKIN****
**
*NODE
```

```
500000,59.,33.
501800,59.,36.
500020,49.,33.
501820,49.,36.
500080,0.,33.
501880,0.,36.
524000,61.,33.
525800,61.,36
524020,71.,33.
525820,71.,36.
524050,95.,33.
525850,95.,36.
524080,120.,33.
525880,120.,36.
*NGEN,NSET=T1
524080,525880,100
*NGEN,NSET=T2
524050,525850,100
*NGEN,NSET=T3
524020,525820,100
*NGEN,NSET=T4
524000,525800,100
*NGEN,NSET=T5
500000,501800,100
*NGEN,NSET=T6
500020,501820,100
*NGEN,NSET=T7
500080,501880,100
*NFILL,BIAS=0.943
T4,T3,20,1
T5,T6,20,1
*NFILL
T2,T1,30,1
T3,T2,30,1
T5,T4,12,2000
T6,T7,60,1
*ELEMENT,TYPE=CPE8R
30000,500000,500200,500202,500002,500100,500201,500102,500001
*ELEMENT,TYPE=CPE8R
40000,500000,504000,504200,500200,502000,504100,502200,500100
*ELEMENT,TYPE=CPE8R
50000,524000,524002,524202,524200,524001,524102,524201,524100
*ELGEN,ELSET=TSKIN
30000,9,200,1,40,2,9
40000,6,4000,1,9,200,6
50000,40,2,1,9,200,40
```

```
**
****BOTTOM SKIN****
**
*NODE
800000,59.,0.
801800,59.,3.
800020,49.,0.
801820,49.,3.
800080,0.,0.
801880,0.,3.
824000,61.,0.
825800,61.,3.
824020,71.,0.
825820,71.,3.
824050,95.,0
825850,95.,3.
*NGEN,NSET=B1
824050,825850,100
*NGEN,NSET=B2
824020,825820,100
*NGEN,NSET=B3
824000,825800,100
*NGEN,NSET=B4
800000,801800,100
*NGEN,NSET=B5
800020,801820,100
*NGEN,NSET=B6
800080,801880,100
*NFILL,BIAS=0.943
B3,B2,20,1
B4,B5,20,1
*NFILL
B2,B1,30,1
B4,B3,12,2000
B5,B6,60,1
*ELEMENT,TYPE=CPE8R
60000,800000,800200,800202,800002,800100,800201,800102,800001
*ELEMENT,TYPE=CPE8R
70000,800000,804000,804200,800200,802000,804100,802200,800100
*ELEMENT,TYPE=CPE8R
80000,824000,824002,824202,824200,824001,824102,824201,824100
*ELGEN,ELSET=BSKIN
30000,9,200,1,40,2,9
40000,6,4000,1,9,200,6
50000,40,2,1,9,200,40
**
```

```
****REFERENCES FOR RIGID SURFACES****
**
*ELSET,ELSET=RESB,GENERATE
699,717,1
*NODE
1000000,120.,26.9
1000002,120.,31.9
1000007,115.,26.9
*NGEN,LINE=C
1000002,1000007,1,1000000,,,,0,0,1
*ELEMENT,TYPE=R2D2,ELSET=PIN
2000000,1000002,1000003
*ELGEN,ELSET=PIN
2000000,5
*RIGID BODY,ELSET=PIN,REF NODE=1000000
*SURFACE DEFINITION,NAME=LPIN
PIN,SNEG
*SURFACE DEFINITION,NAME=ASURF1
RESB,S4
*CONTACT PAIR,INTERACTION,NAME=NFRIC1
ASURF1,LPIN
*SURFACE INTERACTION,NAME=NFRIC1
26.
*NORMAL,TYPE=CONTACT SURFACE
LPIN,1000002,0.,1.,0
**
****NODE SETS FOR MPCS AND BOUNDARY CONDITIONS****
**
*NSET,NSET=CORET,GENERATE
2421,2501,1
2421,38421,3000
38421,38501,1
*NSET,NSET=COREM,GENERATE
21,101,1
21,18021,3000
18021,198021,30000
198021,198071,1
*NSET,NSET=COREN,GENERATE
217000,217080,1
217000,457000,20000
457000,457050,1
*NSET,NSET=COREB,GENERATE
200000,200080,1
200000,440000,20000
440000,440050,1
*NSET,NSET=TSKINB,GENERATE
```

```
500000,500080,1
500000,524000,2000
524000,524080,1
*NSET,NSET=BSKINT,GENERATE
801800,801880,1
801800,825800,2000
825800,825850,1
*NSET,NSET=CLAMP
800080
501880
**
********MATERIAL PROPERTY DEFINITION********
**
*SOLID SECTION,MATERIAL=PVC,ELSET=CORE
26.
*MATERIAL,NAME=PVC
*ELASTIC
50.,0.3
*SOLID SECTION,MATERIAL=TWOVEN,ELSET=TSKIN
26.
*MATERIAL,NAME=TWOVEN
*ELASTIC,TYPE=ENGINEERING CONSTANTS
11000.,4140.,11000.,0.26,0.26,0.24,4140.,4000.
4140.
*SOLID SECTION,MATERIAL=BWOVEN,ELSET=BSKIN
26.
*MATERIAL,NAME=BWOVEN
*ELASTIC,TYPE=ENGINEERING CONSTANTS
11000.,4140.,11000.,0.26,0.26,0.24,4140.,4000.
4140.
*BOUNDARY
CLAMP,ENCASTRE
9000000,1,2
9000000,1,2
1000000,1
1000000,6
*EQUATION
3
22201,1,1.0,49201,1,-1.0,9000000,1,-1.0
*EQUATION
3
22201,2,1.0,49201,2,-1.0,9000000,2,-1.0
*EQUATION
3
25201,1,1.0,79201,1,-1.0,9000000,1,-1.0
*EQUATION
```

```
3
25201,2,1.0,79201,2,-1.0,9000000,2,-1.0
*MPC
TIE,TSKINB,CORET
*MPC
TIE,COREM,COREN
*MPC
TIE,COREB,BSKINT
**
****STEP1 TO MOVE THE LOAD PIN TO MAKE INITIAL CONTACT WITH SCB
TONGUE****
**
*STEP,INC=2000,AMPLITUDE=RAMP
*STATIC
0.05,1.0, ,0.1
*BOUNDARY
1000000,2,,0.11
*PRINT CONTACT=YES
*CONTACT PRINT,FREQUENCY=1,SLAVE=ASURF1
*CONTACT FILE,FREQUENCY=1,SLAVE=ASURF1
*NODE PRINT,FREQUENCT=2000
U
RF
*EL PRINT,POSITION=AVERAGED AT NODES,FREQUENCY=2000
S
E
ENER
PE
*NODE FILE,FREQUENCY=2000
U
RF
*EL FILE,POSITION=AVERAGED AT NODES,FREQUENCY=2000
S
E
ENER
PE
*MONITOR,NODE=1000000,DOF=2
*END STEP
**
****APPLY 50N LOAD TO THE LOAD PIN****
**
*STEP,NLGEOM,INC=2000
*STATIC
*BOUNDARY,OP=NEW
CLAMP,1,2
1000000,1
```

```
1000000,6
9000000,1,2
9000001,1,2
*CLOAD
1000000,2,50
*PRINT CONTACT=YES
*CONTACT PRINT,FREQUENCY=1,SLAVE=ASURF1
*CONTACT FILE,FREQUENCY=1,SLAVE=ASURF1
*NODE PRINT,FREQUENCY=2000
U
RF
*EL PRINT,POSITION=AVERAGED AT NODES,FREQUENCY=2000
S
E
ENER
PE
*NODE FILE,FREQUENCY=2000
U
RF
*EL FILE,POSITION=AVERAGED AT NODES,FREQUENCY=2000
S
E
ENER
PE
*MONITOR,NODE=1000000,DOF=2
*END STEP
```